QUENCH CORRECTION IN LIQUID SCINTILLATION COUNTING

A thesis submitted to the Council for National Academic Awards in partial fulfilment of the degree of Doctor of Philosophy.

I. LILLEY

Department of Physical Sciences

Trent Polytechnic, Nottingham.

June 1987

Abstract

QUENCH CORRECTION IN LIQUID SCINTILLATION COUNTING

I. Lilley

Quench correction in liquid scintillation counting has been
investigated. A detailed comparison of the curve fitting
routines compatible with a microcomputer has been made for
the quench calibration curve and concludes that a cubic
spline with natural end conditions is most suitable. The
effect of colour/chemical quenching on the calibration
curve and the choice of regions for dual and triple radio-
nuclide counting is studied.

A new computer simulation of the LS counter has been
created and proven to be a useful tool in LS counting.
Modelling of the LSC has led to the invention of several
novel quench correction techniques which are independent of
colour and/or chemical quench for homogeneous solutions. A
fully worked example of the use of one of the techniques
(the SumDiff quench correction method) is presented. The
successful application and modular design of the simulation
has established a LS research program from which future
discoveries are anticipated.

ACKNOWLEDGEMENTS

CONTENTS

Chapter 4

Chapter 1

INTRODUCTION

Since the discovery that organic solutions could be induced to fluoresce upon excitation by nuclear radiations the development of materials and methods for liquid scintillation counting (LSC) has been rapid. LSC is now well established for the counting of low energy β-emitting isotopes such as ^{3}H and ^{14}C.

With any assay of a radioisotope the knowledge of the activity is essential. This thesis deals with specific aspects of activity determination which have been difficult in the past but receive a novel treatment given modern electronics and computer technology.

1.1   Liquid Scintillation Counting Theory

Theoretical work important to the understanding of LSC can
be divided   into   that   dealing   with   the   basic   physical
processes at work in a LS counter and that dealing with the
global   properties   of   the   LSC   system,   i.e.   into   the
microscopic   and the macroscopic.   Topics of the prior type
of work   are   typified   by   the   photophysics   of   aromatic
molecules and   mechanisms   of   molecular   energy   transfer,
whereas topics of the latter are typified by LSC simulation
models and techniques of radioactive assay.

1.1.1 Basic Physical Processes in LSC

Nuclear radiations interact with the molecules of organic solutions in many ways. Along the track of a nuclear particle large numbers of molecules are given energy and form ions, excited molecules, free radicals and secondary particles. The concentrations of these excited and ionised molecules in the wake of the ionising radiation determines the types of secondary processes (chemical and physical) that may occur. Neutralisation, excimer production, X-ray emission, fluorescence, phosphorescence, and excitation energy migration are examples of such processes. In liquid solutions these secondary reactions occur in or near the track of the particle where the concentration of the reactants is the highest. The probability of these secondary reactions is related to the concentration of the reactants which in turn is related to the specific ionisation of the exciting particle. A certain fraction of the ions and excited molecules produced in the organic solution leads to luminescence. The creation and detection of this luminescence forms the basis of liquid scintillation counting. The photo-production process is dependent on the efficient conversion of nuclear energy into optical energy. The photo detection processes then depend on the efficiency of photon collection and their conversion into electrical energy.

3

The photo-production process (after Birks)[14] in a liquid scintillator solution XYZ where X is the solvent, Y is the primary scintillator and Z is the secondary scintillator (if present), consists of: (a) radiation physical processes; (b) internal conversion processes; (c) solvent excitation migration and solvent-solute energy transfer processes; (d) the primary to secondary solute-solute energy transfer process; and (e) solute fluorescence.

(a) Radiation physical processes are those in which the particle energy is converted into molecular ionisation energy or otherwise dissipated. They are comprised of:

$$(1) \quad {}^{1}X + E \longrightarrow {}^{1}X^{**}$$

$$(2) \quad {}^{1}X + E \longrightarrow {}^{3}X^{**}$$

$$(3) \quad {}^{1}X + E \longrightarrow \sigma^{**}$$

$$(4) \quad {}^{1}X + E \longrightarrow {}^{2}X^{+} + e^{-}$$

$$(5) \quad {}^{1}X + E \longrightarrow F^{+} + F^{-}$$
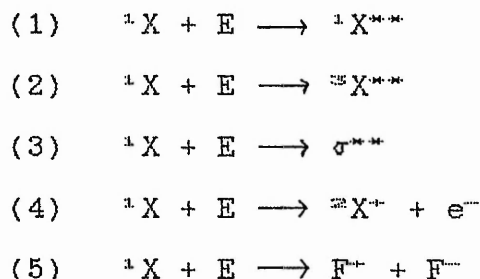
where

$\quad {}^{1}X$ = ground state molecule

$\quad {}^{1}X^{**}$ = excited singlet π-electronic state molecule

$\quad {}^{3}X^{**}$ = excited triplet π-electronic state molecule

$\quad \sigma^{**}$ = excited σ-electronic state

$\quad {}^{2}X^{+}$ = molecular ion

F^{+} and F^{-} = free radicals

$\quad e^{-}$ = slow electron

4

The slow electrons from (4) can produce further reactions:

$$(6) \quad {}^{2}X^{+} + e^{-} \longrightarrow {}^{1}X^{**}$$

$$(7) \quad {}^{2}X^{+} + e^{-} \longrightarrow {}^{3}X^{**}$$

$$(8) \quad {}^{2}X^{+} + e^{-} \longrightarrow \sigma^{**}$$

$$(9) \quad {}^{1}X + e^{-} \longrightarrow {}^{2}X^{-}$$

$$(10) \quad F^{+} + e^{-} \longrightarrow F$$
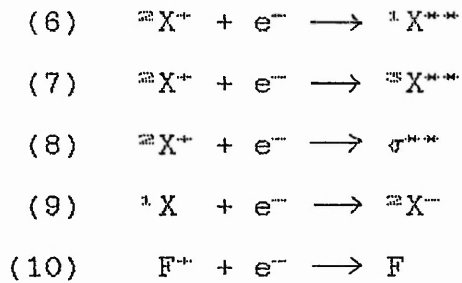
and the ions from (4) and (9) can produce the reactions:

$$(11) \quad {}^{2}X^{+} + {}^{2}X^{-} \longrightarrow {}^{1}D^{**}$$

$$(12) \quad {}^{2}X^{+} + {}^{2}X^{-} \longrightarrow {}^{3}D^{**}$$

$$(13) \quad {}^{2}X^{1} + {}^{1}X \longrightarrow {}^{2}D^{+}$$

$$(14) \quad {}^{2}D^{+} + e^{-} \longrightarrow {}^{1}D^{**}$$

$$(15) \quad {}^{2}D^{+} + e^{-} \longrightarrow {}^{3}D^{**}$$
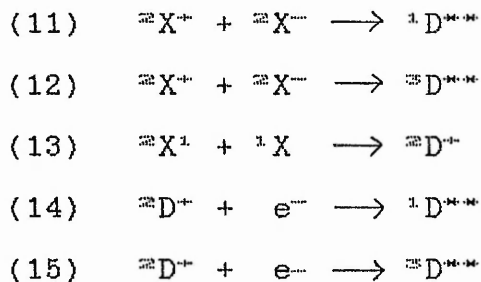
where $^{1}D^{**}$ is a singlet state excited dimer (or excimer)[16,21,24,38], $^{3}D^{**}$ is a triplet state excimer and $^{2}D^{+}$ is a dimer cation.[6]

Processes (1), (6), (11) and (14) yield $^{1}X^{**}$ and $^{1}D^{**}$ the scintillation emission of which occurs within a few nanoseconds (and is known as the fast scintillation component); and processes (2), (7), (12) and (15) yield $^{3}X^{**}$ and $^{3}D^{**}$ - the resulting emission from which occurs over a few microseconds (and is known as the slow scintillation component).[13,107]

5

(b) Internal conversion processes are radiationless transitions between states of the same multiplicity e.g. ($S_n \longrightarrow S_0$, $S_n \longrightarrow S_{n-1}$, or $T_n \longrightarrow T_1$). These processes compete with intersystem crossing (radiationless transitions between states of different multiplicity), vibrational relaxation, excimer formation, and solute-solute energy transfer. The main processes that occur in aromatic molecules after excitation are (Fig. F1.1):

(16) $S_n \longrightarrow S_{n-1}$ internal conversion

(17) $S_1 \longrightarrow S_0$ fluorescence

(18) $S_1 \longrightarrow S_0$ internal conversion

(19) $S_1 \longrightarrow T_1$ intersystem crossing

(20) $T_n \longrightarrow T_{n-1}$ internal conversion

(21) $T_1 \longrightarrow S_0$ phosphorescence

(22) $T_1 \longrightarrow S_0$ intersystem crossing

(23) $S_n \longrightarrow S_0$ internal conversion

where $S_0 \ldots S_n$ and $T_1 \ldots T_n$ are the singlet and triplet π-electron excited state manifolds

and $S_0 = {}^1X$, $S_1 = {}^1X^*$, $S_{n\,(n>1)} = {}^1X^{**}$, $T_1 = {}^3X^*$, $T_{n\,(n>1)} = {}^3X^{**}$.

(c) Two theories are currently being debated regarding the actual solvent-solvent excitation migration process. One theory[15,24,98] involves the formation of solvent excimers which upon dissociation find the excitation energy on the previously unexcited solvent molecule. This excimer forming and breaking is fast ($\approx 10^{-11}$s)[117] compared to the fluorescence emission time thereby allowing the energy to migrate through the solution:

6

$$^1X_{aa}^* + {}^1X_{b} \rightleftharpoons {}^1D_{aab}^* \rightleftharpoons {}^1X_{a} + {}^1X_{b}^* \qquad \text{mechanism (A)}$$

$$^1X_{b}^* + {}^1X_{c} \rightleftharpoons {}^1D_{bc}^* \rightleftharpoons {}^1X_{b} + {}^1X_{c}^* \qquad \text{,etc}$$
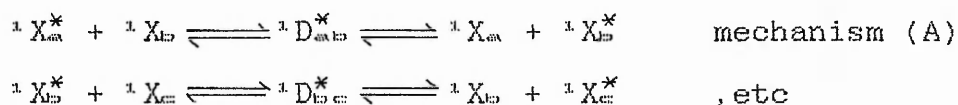
Accordingly, the processes leading to the formation, dissociation and fluorescence of excimers are:

(24) $^1D^{**}$ formation $\qquad ^1X^{**} + {}^1X \longrightarrow {}^1D^{**}$

(25) $^1D^{**}$ dissociation $\qquad ^1D^{**} \longrightarrow {}^1X^{**} + {}^1X$

(26) $^1D^{**}$ dissociation $\qquad ^1D^{**} \longrightarrow {}^3X^{**} + {}^1X$

(27) $^1D^{**}$ dissociation $\qquad ^1D^{**} \longrightarrow 2{}^1X$

(28) $^1D^{**}$ internal conversion $^1D^{**} \longrightarrow {}^1D^{*}$

(29) $^1D^{*}$ formation $\qquad ^1X^{*} + {}^1X \longrightarrow {}^1D^{*}$

(30) $^1D^{*}$ dissociation $\qquad ^1D^{*} \longrightarrow {}^1X^{*} + {}^1X$

(31) Excimer fluorescence $\qquad ^1D^{*} \longrightarrow 2{}^1X$

(32) $^1D^{*}$ dissociation $\qquad ^1D^{*} \longrightarrow {}^3X^{*} + {}^1X$

(33) $^1D^{*}$ dissociation $\qquad ^1D^{*} \longrightarrow 2{}^1X$
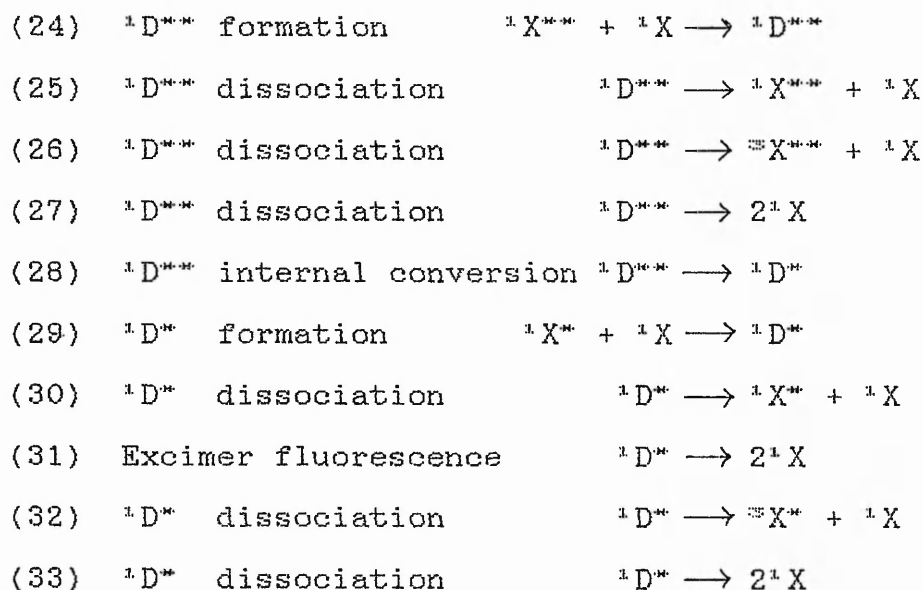
where $2{}^1X$, $^1D^{*}$, $^1D^{**}$ are the ground state, first excited singlet state and higher excited singlet state excimers. $^3D^{*}$ and $^3D^{**}$ are normally dissociated. These processes are summarised in Fig. F1.2.

A second theory proposed by Furst and Kallmann[94,95] and Voltz[100] of the energy transfer between solvent molecules involves energy migration between adjacent solvent molecules:

$$X_m^* + X_b \rightleftharpoons X_a + X_b^* \qquad \text{mechanism (B)}$$

$$X_b^* + X_c \rightleftharpoons X_b + X_c^*, \qquad \text{etc}$$
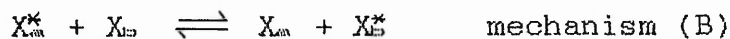
Laustriat and Voltz and Klein[117] also propose a further energy transfer via a similar resonant process for higher excitation states:

$$X_m^* {}^* + X_b \rightleftharpoons X_a + X_b^* {}^* \qquad \text{mechanism (C)}$$
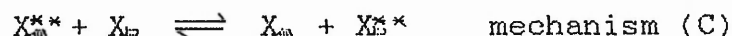
Also, Voltz[179] has given a description of energy migration encompassing diffusion, resonance type energy transfer and excimer type energy transfer.

Together, these mechanisms explain the observed evidence of energy transfer between solvent molecules.[116,179] Evidence of diffusion playing a role in solvent-solvent energy transfer has been obtained by the introduction of diluters (e.g. cyclohexane) to scintillator solvents.[95] The diluters do not participate in the energy transfer process either as an energy quencher or as a transfer medium and the result is that energy transfer efficiency decreases. This is due to the increased solvent separation and implies that solvent-solvent energy transfer is in part diffusion controlled. Evidence of the existence of excimer formation and their importance in the scintillation process has been given by Birks.[13,21,20] Evidence for mechanism (B) has been supplied by Voltz et al for the lowest excited energy states in a study of energy transfer and quenching in various liquid scintillators excited by UV light[117], and by

Voltz[179], Laor[177] and Kallmann-Oster[117] for mechanism (C).

According to Horrocks[93] it is unlikely that contact will be made with solute molecules, which are present in concentrations of about 5 to 10 g l^{-1}, as energy is passed between solvent molecules. The energy is, however, quantitatively transferred from solvent molecules to solute molecules. The transfer is non radiative since solvent emission has a decay time of approximately 30×10^{-9}s whereas the observed solvent-solvent transfer occurs in 10^{-11}s. Nor is it diffusion controlled which occurs in approximately 10^{-4}s. The energy transfer occurs by Forster type resonance transfer process. The strength of the interaction is related to the degree of overlap of the fluorescence spectrum of the solvent and the absorption spectrum of the solute and the distance over which the transfer takes place is related to the extinction coefficient of the solute molecules over the region of the overlap of the two spectra. The Forster radius, R_o, which is defined as the distance between solute molecule and solvent molecule such that the probability of transfer is equal to the probability of all other processes of energy release by the solvent, has been calculated to be 2-3nm for many organic molecules used in LSC.[93] This contrasts with the 0.6nm approximate collision distance. Experimental support for the evidence of Forster type resonance transfer being the mechanism for energy transfer between solvents and solutes in LSC has been obtained by Voltz.[117]

9

This view of solvent-solute energy transfer is not universally accepted and evidence that supports collisional solvent-solute energy transfer has been presented by Birks et al[23] in a comparison between the rates of solvent-solute energy transfer using fluors and quenchers as the solute. However, the solvent-solute interaction is more complex for fluors than for quenchers because of the importance of the $S_n \longleftarrow S_0$ transition dipole moments and because of competing backprocesses such as $F_n + S_0 \longrightarrow F_0 + S_n$ · (as opposed to $F_n \longrightarrow F_1$ and fluorescence) whereas solvent-quencher energy transfer often involves the formation of charge transfer complexes resulting from molecular collisions. More experimantal data is necessary to remove the uncertainties surrounding energy trapping by fluorescent solutes.

(d) Energy may also be transferred between solute molecules. Low solute concentrations make diffusion controlled energy transfer improbable and result in fluorescence being the most probable energy transfer process.[24] There is also some long-range dipole-dipole interaction between like solutes which is monoenergetic and involves the same energy levels of each solute. Energy transfer between unlike solutes is also monoenergetic but is usually accompanied by vibrational relaxation in the acceptor molecule.[13,24]

(e) Fluorescence is a spin allowed radiative transition between states of the same multiplicity. It usually occurs between the first excited state (S_1) and the ground state of the molecule over a time of $10^{-10} - 10^{-11}$ s and is not monoenergetic. The energies of the photons correspond to the energy difference between the zero vibrational level of the S_1 state and the many vibrational levels of the ground state (S_0). The fluorescence spectrum reflects the probability of the transitions between S_1 and the vibrational levels of the ground state. Spin forbidden transitions between states of different multiplicity describe phosphorescence. Phosphorescence is not usually observed in LSC due to its long lifetime ($>10^{-3}$ s) which renders it susceptible to quenching or other triplet energy transfers.

The photodetection process can be subdivided into the photon collection process and the photoelectric conversion process. Photon collection includes the passage of photons through the LS cocktail, the vial and the counting chamber.

Since the common scintillator solutes emit photons of energy corresonding to the wavelengths between 300 and 600nm it is required that the LS cocktail and the vial be transparent over that region. If the LS solution is not transparent over that region then self absorption is said to occur. Self absorption is present to some extent in most LS solutions and is a feature of both the primary and

secondary solutes. It is dependent on the overlap between the emission and absorption spectra of the solute, the molar extinction coefficient and the concentration of the solute. Also an important factor in the amount of self absorption is the path length for the photons before they escape from the LS solution.

In addition to the solvent and solute other materials forming the sample in the LS solution may have an absorption band which overlaps the solute emission spectrum. If this is the case then colour quenching is said to occur[*]. Colour quenching is dependent on the absorptivity and concentration of the quenching molecule, and on the path length which the photons must travel before escaping the solution. It can be seen that self absorption may be regarded as a particular case of colour quenching. Further sources of photon losses in the LS cocktail arise at the cocktail-air interface and the cocktail-vial interfaces. These are the result of reflections which cause the reflected photons to undergo the chances of self-absorption and colour quenching within the LS cocktail once more. The probability of photon reflection is dependent on the difference between the refractive indices of the two materials forming the interface according to Fresnel's equations. It is greater for greater differences and hence is greater for the liquid-air interface than for the liquid-vial interface.

[*] Refer to section 1.3.4a

As with the LS cocktail, photons may be absorbed or reflected in the vial. Absorption constitutes another form of colour quenching, but since the vial path lengths traversed by the majority of photons from a single event are approximately equal (assuming uniform wall thickness) the resulting effect resembles chemical quenching[*].[43] Reflection at the vial-air interface may ultimately result in the photon re-entering the LS cocktail or in the photon taking a path leading to total internal reflection in the vial wall and subsequent absorption in the vial, the vial cap or the vial base.

The fate of photons once they have left the vial is largely machine dependent. Usually, counting chambers consist of highly polished reflectors which fit closely to the vial and the face of the photomultiplier detector in an attempt to minimise both scintillation-photon loss and ambient light input. Although oils and greases have been used in the past as optical couplers between the vial and the PMT face, most current LSC's use reflective air-filled chambers. With these chambers, photons may be lost through absorption by the reflecting materials or on reaching the PMT face may be reflected back into the chamber and/or vial. These photon pathways are summarised together with the photon collection processes in the cocktail and vial in Fig. F1.3.[45]

[*] Refer to section 1.3.4a

13

The final stages of the photodetection process - the conversion of signal photons into an electrical pulse - occurs within the photomultiplier tubes (PMT) of the LSC. There are three main parts of a PMT which are critical in the determination of its efficiency and response. These are (a) the photocathode, which converts the photons into a number of electrons defined by the wavelength of the photons, the number of photons, the quantum efficiency of the photocathode, and the geometry and type of material of the photocathode; (b) the dynodes, which multiply the number of electrons by means of secondary emission; and (c) the anode, which collects electrons from the dynodes and converts them into a pulse of amplitude proportional to their number.

The conversion of photons into electrons (photoemission) consists of photon absorption and transfer of its energy to an electron in the photocathode material, migration of the electron to the surface of the photocathode, and, escape of the electron into the vacuum by overcoming the potential barrier (work function) of the photocathode. The theory for photoemission stems from Einstein's photoelectric effect equation:

$$E = h\nu - \phi = \tfrac{1}{2}mv^2$$

where E = kinetic energy of the emitted electron

h = Plancks constant

ν = frequency of incident photon

ϕ = work function of photocathode material

14

Experimental evidence supporting this quantum theory of photoemission has been given by Sommer and Brady among others.[44] Ideal photocathodes have quantum efficiencies of 100%, i.e. every incident photon releases a photoelectron. Practical photoemitters have less than 100% quantum efficiency because of energy losses due to photon reflection or transmission, due to electron scattering and photon scattering of photoelectrons as they migrate to the surface, and due to prevention of photoelectron release by the potential barrier. Quantum efficiencies of the alkali metals in the visible region are only 0.1% but deliberate modification of the energy band structures of semi-conductors has led to negative electron affinity materials[44,162] which allow greater photocathode thickness and produce greater photoelectron escape depths and has resulted in quantum efficiencies up to 26%.

The photoelectrons are accelerated and focused by potential differences between the photocathode and first dynode and the field created by the focusing electrodes. The first dynode collection efficiency ranges from 85% to 98%.[44] The efficiency is less than 100% because some photoelectrons are released with velocities that cause imperfect focussing. Those electrons which do strike the first dynode have enough kinetic energy to produce a number of secondary electrons. The physical processes involved in secondary emission are similar to those in the production of photoelectrons at the photocathode except that electrons rather than photons comprise the incident particle. Three

steps can occur:

   (i)   incident electrons excite electrons in the
         dynode material

  (ii)   some of the excited electrons move to the
         surface, and,

 (iii)   those electrons with energy greater than the
         surface barrier are emitted.

The   secondary electrons that escape from the first dynode
are accelerated by a p.d. to the next dynode and the same
processes occur again.

The secondary emission yield is defined   as   the   average
number of secondary electrons emitted per number of primary
electrons incident on the surface. The yield is dependent
on the primary electron energy (and hence on the PMT
operating voltage) and a theory for the dependence has been
given by Simon and Williams[1,2] for GaP:Cs dynodes which is
corroborated by experimental data.[44]   The statistical
variations in the yield are most significant for the first
and second dynodes. This is because after the first two
dynodes the number of secondary electrons will not be
enough to affect the final gain of the PMTube.   The
variations in the yield in the first two dynodes may, in
some circumstances, result in loss of counts in LSC.[93]

The anode collects the electrons leaving the last dynode.
Its response is limited by its current capacity. If the
number of electrons is too great a space charge builds up
between the last dynode and the anode leading to nonlinear

16

response at high currents. (This may be caused by high count rates and/or high energy radionuclides). The electron collection by the anode produces a voltage which is converted into a voltage pulse through a capacitor. The amplitude of the pulse is proportional to the number of electrons collected at the anode, which are proportional to the number of photoelectrons[a], which are proportional to the number of photons[a], which are proportional [b] to the energy of the original ionising particle in the LS cocktail.

This proportionality may vary from sample to sample due to interference with the energy transfer process, namely quenching. The major aim of the project is to devise a method which takes account of the type of quenching in each sample with particular reference to chemical and colour quenching. A detailed explanation of the quenching process is given in 1.3.4(a).

[a] if numbers not small, [b] only approximately[1,2,3]

1.1.2   <u>Macroscopic Properties of LSC systems</u>

Theories and techniques associated with the properties of LSC systems have been developed from observations of the variations of these properties (such as counting efficiency or pulse height spectrum channels ratios) under different counting conditions. The developments in theoretical techniques have been dependent on the progress made by LSC equipment manufacturers - an example being the use of spectrum parameters for quench correction, as demonstrated by Ring et al[192], which was impracticable before the advent of LSC's with integral multi-channel pulse height analysers. Of course, many of the equipment improvements have been directed towards user convenience and these, along with the technical advances, are summarised in section 1.2.

The primary function of a LSC system is to estimate the true disintegration rate (DPM) of a radioisotope. The theoretical techniques used to accomplish this function essentially rely on the estimation of just two variables - the apparent sample activity (CPM) and the efficiency (E) with which the sample was counted. The true rate is then given by the expression DPM = CPM/E. If the counting efficiency remained constant for all samples then the variations in the calculated DPM would depend only on variations in the sample activity resulting from the random nature of radioactive decay, from the decay rate of the radioisotope and possibly from external chemical and

physical influences on the radioactive decay process.[49] The latter source of variation is negligible in LSC and the former two sources can usually be satisfactorily overcome. It is unfortunately the case, however, that the efficiency is not constant for all samples.

As a prerequisite for the determination of counting efficiency reference must be made to a standard. This may be an internal standard[73], an external standard[81], or a quenched sample or series of samples, all of known activity. The choice of standardisation is often related to quench correction (section 1.3) although no single method is capable of correcting for all the sources of efficiency variation.

LSC efficiency varies with the type of nuclear radiation, the type of chemical constituents in the sample and their relative proportions, scintillation detector performance, and, the method of counting. The variation in the counting efficiency with the nature of the ionising particle is related to the specific ionisation of the particle and has been reported by numerous workers.[8,9,17,27,93,101,160,172] The composition of the solution (solvent, solutes and quenching materials) may affect the scintillation efficiency which in turn affects the detection efficiency or may affect the detection efficiency directly hence affecting the counting efficiency – these changes being different for different types of quencher. For example, chemical quenching (which is the scavenging of LS solvent

excitation energy by impurities or added samples in competition with the fluorescent solutes) and colour quenching (which is the molecular absorption of the fluorescent solutes' emissions) give rise to changes in the measured pulse height spectrum as shown in Fig. F1.4.[128] Correlation of the counting efficiency with the _amount_ of quench but independent of the _type_ of quench has been a goal of LSC for many years. The most recent quench indicating parameters to be used, such as H[#][84], SIE[132] and ESP[112] all fail in this respect. A typical plot of efficiency vs SIE even with AEC is shown in Fig. F1.5. Quenching is considered further in section 1.3.

Detector performance variables are shared between the PMTubes and the electronic analyser circuitry. LSC stability is one of them and has been studied by Galloway[79] and Crookes & Lilley[37]. Although it can be a source of efficiency variation it is usually small enough to be neglected. PMT response and performance may by affected by temperature[123,127,153,166,187], by ageing of the glass face plate[100], by external magnetic and electric fields[44], by ambient light levels and by vibration or shock. Any such changes in the PMT response will be reflected in the counting efficiency. Dead time (especially with intense sources) and spectral matching of PMT to the fluorescent species may also affect the efficiency. So too will changes in the electronic thresholds and pulse height analyser discriminators of the analyser circuitry. Geometry is often an important aspect in the determination

of activities of radionuclides and LSC is no exception. The effects of relative changes in sample and external standard position on the counting efficiency and of variations in sample volume on the external standard counting efficiency, and other 'volume effects' has been investigated by numerous workers.[10,38,48,59,64,87,137,154,168,149]

Despite such a list of possible sources of error reliable counts are obtained from LSC's. This is because the magnitudes of the variations are small in everyday applications. The major sources of error in efficiency determination are usually (a) quenching and (b) the method of counting employed.

The method of counting can affect the counting efficiency in many ways even under conditions of constant quench. Most LS counters employ two photomultiplier tubes and a coincidence counting system although there are some single tube counters.[148] Coincidence counting provides a marked reduction of background count rates due to the randomly generated pulses in each PMT as a result of thermal noise and spurious light sources (e.g. chemiluminescence). This advantage must be balanced against the main disadvantage of coincident systems which is an inherently lower counting efficiency, especially for low energy isotopes. This is due to the requirement of at least one photon being detected at each PMT in a coincident system whereas a single photon may suffice in a non-coincident system. In

practice, the reduction in efficiency is not excessive and even theoretically the difference is only about 6% for an average energy tritium ß-particle for PMT's operating with a 30% quantum efficiency.[62]

Also, with two PMT's there are alternatives to the way the PMT pulses can be handled which can result in changes to the measured counting efficiency. One of the PMTubes may be utilised for pulse height analysis with the other acting as a coincidence monitor only.[79] This technique has been superceded by pulse summation prior to pulse height analysis which gives increased resolution between events of different energy and a slight improvement in counting efficiency for low energy emitters by increasing the number of coincident events capable of passing low level noise thresholds. The only other 'front end' pulse handling technique to have been proposed (by Laney[112]), is lesser pulse height analysis, which represents an attempt to minimise crosstalk.[114] Further work by Laney in this area shows the information value inherent in the individual PMT signals.[113] Although concentrating on the rejection of background, two-parameter pulse height spectra of colour and chemically quenched ^{14}C samples were presented. These results are reproduced in Fig. F1.6. The conclusion that the two-parameter pulse height analysis can distinguish between colour and chemically quenched samples is drawn by Laney but no methods to attempt to quantify the differences are proposed. This subject of 'front end' pulse handling and pulse information value in relationship to quench

correction has been largely neglected in LSC. It forms however an integral part of this thesis and is discussed at length in chapter 3.

The recorded counting efficiency can be substantially altered by the method of analysing the coincidence-gated pulses. Most modern machines now have integral Multichannel analysers (MCA) for pulse height storage and microprocessors/microcomputers for spectral analysis. They allow user selection of regions of interest, or pulse height windows, and thus are prone to reduced counting efficiency resulting from poor choice of counting regions.

Assumptions of constant quench are almost always invalid and thus in addition to the above sources of efficiency variation there are those resulting from the various types of quench. Indeed, the need to correct for quench has been responsible for most of the methodological developments over the past two decades. The developments are detailed in the section on quenching (1.3).

The determination of the true disintegration rate is not the only function of a LSC system. LSC's may be used to provide relative counts only, or assess the purity of radiolabelled materials irrespective of the total count[140], or to check for chemiluminescence, or perhaps perform radioisotope identification - a task which is gradually becoming more feasible owing to improvements in LSC resolution.

1.1.3 Theoretical Modelling of the LSC

For whichever mode of operation, correct use of the LSC requires an understanding not only of all the separate processes at work but also of how they interrelate. To achieve such an understanding a systems rather than an analytic approach is necessary. Theoretical work which has been conducted with a view to predicting the global properties of LSC's has been tackled by few authors. Kaczmarczyk[103] has presented a detailed model of chemical quenching at the spectral level but has not included any optical considerations such as PMTube response or even colour quenching. A one dimensional and simple three dimensional model of a LSC has been proposed by ten Haaf.[176,177] The first model qualitatively explains the broader pulse height spectrum obtained with colour quenched samples rather than with chemically quenched samples[126] by suggesting that light produced in different parts of a sample will take paths (to the detectors) of different length. The second model represents an improvement by extending the analysis to cover a three dimensional (3D) cylinder of scintillation material but still suffers from many drawbacks: the vial base and top are assumed to be perfect mirrors; no allowance is made for the spectral nature of light emission or absorption; the pulse height and β-energy relationship is assumed to be linear; all statistical fluctuations are ignored; and the scintillator is surrounded by perfect detectors. A more detailed model has been created by Malcolm and Stanley[120,121,171] using a

stochastic approach which accumulates "counts" resulting from events considered at the photon level. For my model to be useful as a predicitive tool it must be able to closely reproduce known experimental data and it was the approach used by Stanley and Malcolm that best simulated the properties of an LSC system. Work for this model commenced in 1972 and although still under development was first presented at the International Symposium on LSC in 1973.[120] It is summarised below but a full description may be found in the aforementioned references.

The model simulated a two PMT coincidence LSC by computer generation of a ß-event of random energy, according to the Fermi distribution of the isotope, at a random 3D position within the solution in an idealised vial. This energy was then converted to an appropriate number of photons of random wavelength (following the fluorescence spectrum of the phosphor solution), which were assigned random directions in 3D. Each of these photons was traced to its extinction through the solution and vial (which was assumed to be optically continuous) and up to the PMTube, although the actual geometry of the vial was greatly simplified and any counting chamber effects were bundled with the PMT response. See Fig. F1.7.

Colour quench was simulated by calculating the absorbance of the solution for each photon according to its wavelength and an experimentally obtained absorption spectrum, and escape distance with the probability of absorption

following the Beer-Bouguer Law. Self (colour) quenching by the fluor was also modelled.

PMT response was simulated in a probabalistic fashion according to the photocathode quantum efficiency and wavelength of the incident photon. This response was scaled according to the point at which the photon left the vial. This approach was taken to avoid the further complicated geometrical analysis required to trace photons through the counting chamber.

Once all the available energy was exhausted in terms of photon production and these photons traced, the number of photoelectrons at each PMTube represented the pulse amplitude for each PMT. These were coincidence selected to produce summed and lesser pulse height spectra.

The model was subject to the following additional assumptions and restrictions:

  (i)   ß-particle path lengths were zero (only ^{3}H and ^{14}C modelled)

  (ii) isotopes followed the theoretical distribution

  (iii) only one ß-event was processed at any one time (no dead time losses and no time dimension in the model)

  (iv) scintillation efficiency variation with energy followed the results given by Horrocks[9][9]

  (v)   chemical quench was independent of energy of the ß-particle

(vi)   vial and solution were optically continuous, and were in the form of a perfect cylinder

(vii)   optical dispersion and polarization-related phenomenon were negligible with Snells Law dictating photon behaviour at interfaces

(viii) vial cap and vial base were perfect absorbers.

Despite these restrictions, the matching of modelled ^{3}H and ^{14}C colour or chemically quenched sample counting efficiencies with their experimantally obtained counter-parts was achieved with some degree of success and Malcolm and Stanley were able to conclude that the model's behaviour was in accordance with that observed in the laboratory.[121,171]

1.2   Liquid Scintillation Counting Materials and Equipment

The materials and equipment used in LSC may be be split
into hardware and 'wetware'. Wetware includes the
solvents, solutes, cocktails and nuclear labelled compounds
that are available for LSC. The variety of nuclear
labelled compounds is as endless as that of unlabelled
compounds even when only considering the commonly used
isotopes (^{3}H, ^{14}C, ^{32}P) and no attempt is made to
categorise them. Liquid scintillation solvents are
typified by molecules that have low energy levels and
nonbinding π-electrons, which require little excitation.
Many such candidates have been investigated by Birks[15,16],
Hayes[75], Horrocks[93,99], Klevans[107], Laustriat et al[117],
Lawson et al[118], Skarstad et al[163], Oster[133],
Parmentier[136], Skerbele[164] and Voltz[179]. Fluorescent
solutes have been studied by many workers including
Berlman[12], Birks[15,26], Furst et al[56,57], Gershuni[61],
Gusten[66], Hayes[74], Horrocks[90,96,97], Kallman[105,106],
Kowalski[111], Painter[139], Scales[157], Scoggins[160], Ware[183]
and Wirth[184]. Also, various aspects of solute-solvent
systems and LS cocktails (i.e. solute-solvent and
emulsifiers and/or solubilisers) have been reported by
Benakis[11], Farmer[49], Gebicki[60], Langenscheidt[116], Nibeck[127]
and Spolders[167] and Stanley[170].

A detailed review of the developments in LSC hardware from
1950 to 1971 has been given by Rapkin.[148]   Stanley has
reviewed the developments in LSC generally[170] (including

28

hardware features) for the period 1964 to 1979. A more recent study of modern LSC's has been conducted by Price.[147] Since that time few major changes in LSC design have occurred.

1.3   Liquid Scintillation Counting Problems

1.3.1   Sample Preparation

Sample preparation for LSC depends on the nature of the sample to be counted and may be a very simple or very complicated procedure. The counting of aqueous, gaseous or heterogeneous sample in the aromatic organic solvents used in LSC present special problems.

General reviews of sample preparation techniques have been given by Parmentier and ten Haaf[138] and Horrocks[93] and collections of sample preparation papers can be found in "Liquid Scintillation Counting" vol. 2, "Liquid Scintillation Counting" vol. 4, "Liquid Scintillation Counting" vol. 5, "Liquid Scintillation Science and Technology" and "Liquid Scintillation Counting Recent Applications and Developments".

The labelled materials and quenching agents in this thesis have been chosen to facilitate sample preparation, although it is recognised that for the majority of LSC users this is not possible.

1.3.2   Counting Vials

There are several types of vials available commercially. These include low cost soda lime glass, low background glass (borosilicate glass low in ^{40}K), quartz, polythene, nylon and teflon. The choice of vial depends on cost, background rate requirements, U.V. transmission requirements, re-usability, solvent absorption characteristics and solute asorption characteristics. Problems arising from poor choice of vial can include vial "wall effects"[99,134,126,132] due to solvent and solute permeability, background count rate[31,32,136] variations, efficiency variations due to vials of variable thickness and geometry[93], photoluminescence[128] and sample leakage.[119]

A very useful review of choice of counting vials with 85 further references has been given by Painter in "Liquid Scintillation Counting - Recent Developments".[134]

1.3.3   Background

There are many sources of background counts in LSC all of which may impair DPM determinations especially with samples of low activity. A good discussion of background is given by Horrocks in chapter 9 of "Applications of Liquid Scintillation Counting" with a table which neatly summarises the various sources of background.

Other references include those of Noakes[130] and Hartley and Church[70] and Calf and Polach[33] who each concentrate on low level counting and ^{14}C dating, Laney[114] who proposes a method to reduce the crosstalk component of background with various types of aqueous solutions in several different vials and cocktails and Scales[167], Alessio et al[1,2] and Horrocks[71] who have each studied the effect of quenching on LSC background.

1.3.4   Quenching and Quench Correction

(a) Quenching

Quenching is any energy transfer process which interferes with the efficient conversion of the ionising radiation into a measurable electron pulse. As explained in section 1.1, the LSC process may be held as a logical series of subprocesses. Each subprocess is susceptible to quenching (see Fig. F1.8).

Nuclear quenching, in the case of β^- emitters such as ^{3}H and ^{14}C, is inherent to the nuclear decay process. The available nuclear energy after disintegration is shared by the β-particle and an antineutrino[1,50] and the energy that is carried away by the antineutrino is lost to the LSC (since the probability of interaction is negligible).

Ionisation quenching covers those processes by which the β-particle energy is dissipated through the solution and/or vial via mechanisms that do not lead to the formation of excited π-electronic states of the solvent. Strictly speaking, the term should also exclude excitation of the solvent to σ-excited states but since these are wasteful states so far as energy transfer to the fluorescent solute is concerned, I include them here. (Processes (3), (5), (8) and (10) of section 1.1.1, pages 4 and 5). Not restricitng attention to β^- emitters alone, Birks[1,9] investigated the scintillation response of anthracene and proposed a theory to relate the specific scintillation

response, dL/dr, with the specific particle energy loss dE/dr:

$$(dL/dr) = \frac{S(dE/dr)}{1 + kB(dE/dr)} \quad ,$$

where   S = dL/dE = scintillation yield

BdE/dr = concentration of ionising events

k = relative rate constant (for equations giving ionisation)

This theory has been experimentally supported by several workers.[13,62,63] The effect of ionisation quenching is to make the response of the scintillator non-linear with particle energy type.[64,93]

Chemical quenching (also known as impurity quenching) has been defined by Neary and Budd[120] as

"any process, active within the sample, which reduces the energy transfer efficiency of some member or members of the set of compounds essential to the scintillation process"

and by Peng[140] and Gibson[64] as a decrease in the fluorescence quantum yield caused by the presence of non-fluorescent molecules which compete with fluor molecules for the excitation energy of solvent molecules. The essential points of the definitions are (a) the assumed existence of excited solvents capable of transferring energy to the solutes and (b) the possible presence of

materials in solution apart from the solvent and solute - whether as impurities (eg O_2) or as a labelled sample. Chemical quenching thus covers all those processes by which energy is taken from excited solvents but which does not result in photon emission. Gibson and Gale[49] have shown that the relative chemical quenching factor (which is the ratio of available fluorescence to actual fluorescence from a quenched solution) is independent of energy. Mechanisms of chemical, or impurity, quenching have been presented by Birks[14,20] and Laustriat et al[117] amongst others.

Colour quenching is the absorption of the fluorescent radiation by substances which have an absorption band within the emission spectrum of the liquid scintillation fluors. Colour quenching is a function of the absorptivity and concentration of the quenchers and also of the path length the photon must traverse in order to escape the solution. It is this latter feature of colour quenching that affects the counting efficiency and pulse height spectra in a way that is quite different to chemical quenching (see Fig. F1.4). Simple models to explain the differnces have been given by ten Haaf[175,177] and Neary & Budd.[128]

Optical quenching is the loss of photons on leaving the scintillation solution prior to interaction with the photocathode of the PMTubes. It includes photon absorption in the vial material (glass or plastic), the vial base, the vial cap, the counting chamber reflectors, the PMTube

faceplate, and any dirt or condensation that may be present. It also includes direct photon escape through the narrow gaps around the vial in the counting chamber. These effects are normally small but are not negligible. Stanley[77] has shown, for instance, that around 9% of all photons are lost through the annular gaps around the vial although many of the other instrument design-dependent losses remain unquantified (at least publicly).

The quantum efficiency of a photocathode is defined as the probability that a photoelectron is released per incident photon. It depends on the wavelength of the incident photon as shown in Fig. F1.10 for an RCA 4501/V3 PMTube. Photoelectric emission involves three stages. Firstly, the photon must be absorbed and its energy transferred to an electron; secondly, the electrons must move to the material-vacuum surface; and thirdly, the electron must escape past the surface potential barrier. As explained in section 1.1.1 energy losses or quantum quenching may occur at each stage and so reduce the quantum efficiency to well below 100%.

PMTube quenching covers losses of energy due to imperfect focussing of photoelectrons between the photocathode to the first dynode and between successive dynodes and losses encountered in secondary emission. These losses seldom contribute to a reduction in the recorded counting efficiency under normal operating conditions but do alter the shape of the pulse height spectrum.[93]

Electronic quenching is the reduction in height or loss of the PMTube pulses due to electronic thresholds (and discriminators) of the counting system, and may affect the counting efficiency and/or the shape of the pulse height spectrum.

In this scheme of quenching in the LSC process it is assumed throughout that the LS solution is homogeneous. This is not always the case. Many samples are counted in LSC 'cocktails' containing emulsifiers or solubilisers such as Triton X-100, in solid gels, or on solid supports immersed in scintillator solutions. With such mixtures, ß-particles can be lost in nonscintillating micelles of an emulsion, in particles in a gel, in the solid supports or in the vial walls. Apart from the vial wall effect[132] such energy losses are difficult to assess and no method of quench correction can currently be applied irrespective of the phase of the sample, although phase changes during counting may be flagged.[48,131] To avoid the compounded problems of mixed colour and chemical quenching in heterogenous systems Ewer and Harding suggest the incorporation of the whole sample in the micellar phase where possible. Further references concerning the counting of heterogenous samples may be found in the bibliography.

(b) Quench Correction

Quenching can cause gross changes in counting efficiency and thus must be monitored to enable the count to be corrected. This task, quench correction, is complicated by the different types of quenching that may be present. Many attempts have been made to achieve quench correction but none can be applied uncritically. They are listed below:

(i)   Internal Standard[38,73,137,168]

(ii)   Samples Channel Ratio (SCR)[7,29]

(iii)   External Standard Count (ESC)[41,51,72,81]

(iv)   External Standard Channel Ratio (ESCR)[*]

(v)   Relative Pulse Height (RPH)[73,112] Methods
        – H[*], SIE, ESP

(vi)   Balance point counting[4]

(vii)   Gain Overrestoration[102,181,182]

(viii) Double Count Channels[149]

(ix)   Efficiency stick[42]

(x)   Optical filter[92]

(xi)   Optical absorbancy[39,76,77,184,188]

(xii)   Extrapolation[141,142,143]

(xiii) Double channels ratio[50]

(xiv)   Tracer[166]

[*] no known reference except Horrocks says it was a commercial feature on Beckman LS200 in 1965

The Internal Standard (IS) technique involves the addition of a known amount of the labelling nuclide to the sample. The added activity should be high in relation to the sample activity to reduce the uncertainty in the efficiency determination. The efficiency determination is based on the subtraction of the sample count from the sample + standard count, and division of the resultant standard count rate by its known activity. The standard and sample should be chemically similar and the standard should not introduce large changes in quench. If this is possible, the method has the advantage that it eliminates the necessity to count a series of quenched standards. However, recovery of the sample may be impossible and samples cannot be recounted. Opening of vials taken from refrigerated systems leads to condensation of moisture in the vial (and water is a strong quencher). The technique cannot be applied to heterogeneous samples unless the standard goes into the same phase as the sample or is of the same form as the sample on a solid support. The technique is difficult to apply to dual label assays in presence of the above drawbacks and is difficult to automate. Also it is prone to operator error and repeated use can cause a gradual increase in the background. These disadvantages have led to the reduced use of the IS technique.

The SCR method of quench correction gives a measurement in the change in the differential pulse height spectrum with the amount of quench. It is based on the ratio of counts belonging to the two fixed pulse height channels/windows. The method has the advantages that no additions must be made to the sample and recounts are possible. However its accuracy is limited by the activity of the sample and by working with fractions of the total count - especially in the prescence of high quenching. The method requires the production of a standard quench curve - i.e. a series of known activity samples with increasing amounts of quench similar to the samples to be measured are counted and the efficiency vs SCR for each are plotted. Unknown sample efficiencies are then interpolated from this curve. The dynamic range of the method is dependent on the discriminator settings which define the two channels. The low discriminator rejects low level background noise and the high level discriminator is set to just include the maximum energy possible for the sample isotope. The middle discriminator determines the relative channel widths. If it is set low then the dynamic range is increased at the expense of the low quench sensitivity and if it is set high then the dynamic range is poor. Another feature of the SCR method is the generation of widely different calibration curves for colour and chemical quenchers.[177]

Automatic external γ-standards are the most commonly used standards for quench correction. They are convenient and easy to use and can have a wide dynamic range. Half-life

and availability considerations have mainly limited the standards used to ^{133}Ba, ^{137}Cs and ^{226}Ra. The samples are exposed to such standards by means of a shutter or by moving the standard close to the vial. The former method requires higher activity sources and greater shielding and the latter requires reproducible positioning. The γ-rays interact with the sample, the processes of Compton scattering and internal conversion and provide an energy continuum of electrons.

One method of quench correction which utilises external γ-ray standards is the External Standard Count (ESC). It involves the counting of a quenched series of known activity samples without and then with the presence of the external standard. If part of the sample counts are within the external standard count channel the external standard count is corrected. A calibration curve of efficiency vs external standard count is thus prepared. Samples with unknown quench levels are then counted with and without the external standard and the calibration curve is used to give the sample counting efficiency. There are various limitations to this method which may include sample volume dependency, a dependency on the sample to external standard relative position, half-life of the γ-source and changes in electron density from sample to sample. The ESC method is insensitive to the colour to chemical quench ratio whereas the sample count is not.

Another method is the ESCR which is equivalent to the SCR method mentioned above with the exception that the external standard is used to produce the efficiency vs quench calibration curve. ESCR represents an improvement over ESC since taking a ratio of counts reduces errors associated with sample volume, source half-life, sample electron density and source positioning. ESCR is insensitive to the colour to chemical quench ratio for appropriately chosen counting channels. As with the SCR method the ESCR method necessitates a compromise between high resolution (narrow window) and wide dynamic range (wide windows) and ESCR cannot be applied after phase separation.[93]

Improvements in instrumentation have enabled pulse height spectrum storage through the incorporation of analogue to digital converters (ADC) and MCAs in LSCs and has led to several recent developments in quench correction methods. These methods involve analysis of either the whole spectrum or of local spectrum features. The first of these is the $H^{\#}$ number method. The $H^{\#}$ number is the difference in the location of the inflection point of the Compton edge of a ^{137}Cs external standard for unquenched and experimental samples after logarithmic amplification of the summed PMTube pulses. It is thus a ratio of the quenched Compton edge pulse height relative to an unquenched Compton edge pulse height. A second method the SIE, uses the mean summed-pulse height of the external standard spectrum relative to the mean summed-pulse height of an unquenched external standard spectrum (although not quite all the

42

spectrum is used for the computation due to wall effect discriminator). A third and similar quench indicating parameter (QIP) is the ESP. The ESP value of a sample is the mean lesser pulse height of an unquenched external standard spectrum divided by the mean lesser pulse height spectrum obtained with the sample (and with a small correction for the quantum efficiency).

The common feature of these methods, irrespective of the use of lesser or summed spectra, is the concept of relative pulse height (RPH). SIE and H$^{\#}$ are related to the RPH and ESP to the reciprocal of RPH and all three methods have been shown to be linearly related by the expressions[121]:

$$H^{\#} = 225 \log(ESP) - 6.35$$

$$H^{\#} = -475 \log(SIE) - 1391,$$

the log term being present only because of the use of logarithmic amplification in the Beckman LSC and linear amplification in the Packard and Tracor LSCs. All these RPH methods make the problems of channel settings redundant, they have a wide dynamic range, are applicable to multilabel dpm determinations, are insensitive to structured pulse height distributions (e.g. [125]I), can be used with a wide range of sample count rates and are reasonably independent of volume and electron density. They are not, however, suitable for heterogeneous samples and are insensitive to the colour to chemical quench ratio.

The idea of using RPH for quench correction is not restricted to external standards. Reference samples (e.g. ^{14}C ß-emitters) may be used to construct calibration curves which provide a direct relationship with the unknown samples rather than the indirect relationship obtained with the Compton electrons of a scattered external standard γ-ray. The main disadvantage of this is the greater effect that quench has on the efficiency of detection of lower energy isotopes which necessitates longer counting times to provide a reliable measure of the sample based QIP.

The rest of the quench correction methods listed above have not gained general acceptance and popularity for various reasons. Methods (vi), (vii) and (viii) are all designed to produce a constant counting efficiency (and hence not require a calibration curve). Balance point counting achieves this by measuring counts in a middle section of the spectrum. As quenching shifts the spectrum to lower pulse heights the number of counts dropping below the middle section is balanced by the number of counts coming in from above the middle section. The method only works well for small quench changes and high count rate samples. Gain overrestoration involves the changing of amplifier gain in response to a QIP measurement (e.g. ESCR) such that a fraction of the pulses from below a low level discriminator (as set for an unquenched spectrum) are amplified into the counting region. This technique has a limited dynamic range and is restricted to high energy isotopes. The double-count channels method is similar to

44

the balance point method except that the middle section is not counted and the higher and lower sections are. This reduces the efficiency of all the samples to that of the most quenched and thus only uses a fraction of the total count. Descriptions of the other minor methods of quench correction may be found in the literature.

A common failure of many of these quench correction methods is the need to create a calibration curve of counting efficiency vs a quench indicating parameter. Curve fitting in LSC is another possible source of error. It is dealt with in chapter 2.

1.3.5   Dual and Triple Label Counting in LSC

The simultaneous counting of two isotopes using a LSC results in the superpositioning of the pulse height spectra associated with each isotope. Three possible cases arise: (a) no spectral overlap, (b) partial overlap, (c) total (or near total) overlap. An example of case (a) is the dual-label counting of the 5.1 MeV α-emitter ^{239}Pu and the 21 keV ß-emitter ^{241}Pu[74], and no problems are encountered in resolving the counts due to each isotope. Case (c) dual label counting is only feasible if some other feature of the radiation can be utilised to separate the contributions of each spectrum. One such feature may be the respective halflives of the isotopes. The difference in counts when the sample is counted at two different times is used in conjunction with the decay equation to give the activity of each isotope. Other features may be the use of Cerenkov radiation[20] or local pulse height features.[75]

Case (b) is the most common example of practical dual label counting and the ^{14}C-^{3}H dual label is the most common representative of this case. Both isotopes decay by emission of a ß continuum from 0 to 18.6 keV for ^{3}H and 0 to 156 keV for ^{14}C. A window (B) set above the pulse height corresponding to 18.6 keV events will count a fraction of the ^{14}C events and no ^{3}H events. (See Fig. F1.9). A second window (A) spanning the pulse heights from 0 up to window B will count all the ^{3}H events and the remainder of the ^{14}C events. Dual label DPM determination

is achieved by counting similar composition known activity single label ^{14}C samples and ^{3}H samples using the same LSC settings. The single label reference samples provide the efficiency of counting ^{14}C in windows B (E_{BC}) and A (E_{AC}) and the efficiency of counting ^{3}H in window A (E_{AH}), whence the DPMs of the ^{3}H and ^{14}C in dual label samples may be found.

As with single label samples, quenching presents a major problem and quench correction calibration curves must be established for each of the isotopes in each window. ^{14}C – ^{3}H dual label counting has been reported by numerous researchers. Assailly et al[9] investigated the counting of ^{3}H in the presence of ^{14}C using ESC. Everett[46] reports ^{14}C – ^{3}H dual label counting using SIE with AEC (or automatic efficiency correlation) whereas Kolb[107] discusses optimal choice of windows in ^{14}C – ^{3}H counting. Smith & Hodgson[165] examine the effect of quench on the dual label performance of two different LSCs utilising H# and SIE QIPs. Peng[140] and Reuter and Trefny[151] have included ^{14}C – ^{3}H dual labels in their investigations of several dual label sources which also included ^{3}H – ^{125}I, ^{32}P – ^{125}I, ^{32}P – ^{14}C, ^{3}H – ^{32}P and ^{14}C – ^{125}I, and ^{3}H – ^{22}Na and ^{14}C – ^{22}Na respectively. De Filippis[40], also, has reported results of dual label counting of ^{3}H – ^{125}I. An unusual form of dual label counting which utilised "detector ratio" analogue of LSC channels ratio by means of a Geiger-Muller tube and solid scintillation counter has been reported by Gringorten.[67] A more recent technique to compute dual label radionuclide

activity has been presented by De Filippis.[40] The technique employs just one region and is dependent on the relationship between sample based QIP and external standard QIP for each isotope. It requires single isotope sample based QIP and external standard QIP calibration curves. The proportion of counts attributable to each isotope in a dual label sample is then derived from the relative position of the sample data between the calibration curves. The technique is an extension of the isotope contamination detection method proposed by Peng.[140]

LSC pulse height spectra have been accessible for over a decade on commercial machines but the number of channnels open to the user has been limited to two or three. This restricts multi-label counting to dual or triple label counting and is perhaps one of the reasons why triple label counting has been performed rarely. Horrocks[73] reports the triple label counting of ^{3}H, ^{125}I, ^{14}C and the triple label counting of ^{3}H, ^{14}C, ^{36}Cl is reported in chapter 2.

1.3.6   Other Problems

There are a number of other problems that are often encountered in LSC.   These include saturation of the counter due to high count rate samples and/or high energy isotopes[110],   the interference of external standard or ambient   UV   light   induced   photoluminescence[110], bioluminescence[110]   or   chemilumunescence[78,83,104,110,144, 157,174] from reactions in the solution in the vial, static electricity interference[110], temperature effects[174] on the LS solutions and durability of the quenched standards.[82]

Chapter 2

QUENCH CORRECTION PROBLEMS

Accurate quench correction is essential for the true assay
of radioisotopes. Of all the common methods which attempt
to accomplish this task only the internal standard method
does not require the construction of a calibration curve
relating counting efficiency to a quench indicating
parameter (QIP). For the particular case of the SIE
RPH-based technique certain general shapes of curves are
obtained for the different isotopes counted. Since the
correct choice of curve fitting routine is dependent on the
data set a study of curve fitting to LSC calibration data
was made. Another problem area in quench correction
involves the background count rate. For low activity or
highly quenched samples variations in the background with
quench may become significant and thus were investigated.
A problem though not often encountered in quench
correction, and LS counting generally, is the limitations
set by multilabelled radioassay. As an example of this the
SIE RPH technique was extended to perform a $^{3}H/^{14}C/^{36}Cl$
triple label dpm determination. These distinct but
interrelated investigations are detailed below in sections
2.1, 2.2 and 2.3.

A further problem in quench correction involves colour and chemical quenching. The different quenching mechanisms result in the need to produce separate calibration curves for colour, chemically and mixed colour/chemically quenched samples. This major problem is considered in detail in chapter 3.

2.1 Curve Fitting and LSC Calibration Data

2.1.1 Introduction

Modern liquid scintillation counters (LSC's) allow many useful functions, such as batch handling of samples, counting efficiency vs quench calibration and multilabelled radioassay, to be performed automatically. However, the advances in machine design which have led to the provision of such facilities tend to remove the user from the analysis of the basic data which is obtained and the results are presented as a fait accompli. The most important stage in the analysis of results is the generation of the standards' counting efficiency vs quench calibration curves from which the activity of subsequently counted samples can be calculated. This applies whichever parameter is used to indicate the degree of quench in a sample, whether it is based on internal or external standards, $H^{\#}$ $\Theta 4$ numbers or spectral indices[1,2,3], and whether the quenching is colour or chemical in nature.[1,2,4]

Since different curve fitting routines are better matched to some data sets than others, the fitting of curves through efficiency vs quench calibration data should be dependent on the form of the data set for best results. This availability of a choice of curve fitting routines is not provided on commercial liquid scintillation counters with manufacturers choosing one particular procedure, e.g. Packard use double fixed point least squares quadratic

interpolations and Beckman use cubic spline with natural end conditions. This is reasonable with the good and almost equispaced data provided by commercial calibration standards but the more frequently produced inhouse standards are often less regular.

There are a multitude of algorithms to which recourse may be made in order to fit a curve to LSC efficiency vs quench calibration data. Some are very complicated and form part of large data handling packages requiring large computational processing installations. In this work a restriction is made to those algorithms which could be installed in a modern stand-alone counter and/or dedicated microcomputer.

2.1.2   Experimental

(a)   Hardware and Software

All samples were counted with a United Technologies
Packard 300C model liquid scintillation counter and
the data was stored on disk via a 3D GPIB, Series 4000
CBM microcomputer and CBM 4022 disk drive. Data was
obtained on this equipment through use of a BASIC
program which recognised the number of the internal
program commenced by the LSC and began data capture on
identification of the correct batch of samples. Disk
storage of results allowed repeated use of data sets
for comparison purposes.

Post counting analysis was performed by a BASIC and
6502 machine code program offering a menu of curve
fitting routines with screen plotting, screen dumps
and printed output. When fitting to known functions
or exact data the program allowed point by point
comparisons and when fitting to experimental
calibration data it allowed comparisons of the
resulting assayed activities with samples of known
dispensed activity. The types of curve fitting
offered by the program are listed below:

1. Lagrangian Polynomial (using Newtons Method)[179]

2. Piecewise Linear (piecewise polynomials of degree >2 unsuitable)

3. Quadratic Splines (end conditions linear, spline slope ≡ lagrangian quadratic slope, or spline 2nd derivative ≡ lagrangian quadratic 2nd derivative)

4. Cubic Splines (end conditions natural, parabolic, cantilever, Forsythe's, Swartz & Varga's, or spline 2nd dervative ≡ lagrangian cubic 2nd derivatives)[50,146]

5. Tension (Cubic) Spline[50]

6. Stineman Interpolation[173]

7. Bezier Blending

8. Linear least squares polynomials of degree 2, 3, 4 or 5[179]

(b) Sample and Standards Preparation

The standards used to compare the curve fitting routines were either theoretical or real. Theoretical standards were points chosen from functions which resembled typical LSC calibration curves. This facilitated observation of the effects of choosing many differently grouped calibration standards without having to physically produce them. For tritiated hexadecane in Fisons Fisofluor II chemically quenched with chloroform the function $y = 1/120(16/495 * x + 0.51515)^2 \exp(-(16/495 * x + 0.51515))$ was used to approximate the efficiency vs quench curve, with 100%

55

efficiency normalized to 1 and $0 \le SIE(AEC) \le 650$. For the chemically quenched ^{14}C standards supplied by Amersham the function $y = 1.24 - \exp(-x^2/39900)$ for $100 \le SIE(AEC) \le 1000$ was used to approximate the efficiency vs quench curve.

Real standards were prepared by accurately weighing out quantities of a $10^{\cdot}$ g l^{-1} solution of b-PBD in p-Xylene (Fisons 'Scintran' grade), and quantities of CCl$_4$ or disperse Orange-7 as chemical and colour quenchers respectively. Weights were taken to ±0.0002 g. All liquids and glassware were purged of oxygen using a vacuum and freezing degassing technique*. The dye was recrystallised from acetone and dried prior to dissolving in the same batch of b-PBD/p-Xylene solution used throughout the sample preparation.

* refer to section 2.3.2

56

2.1.3   Results and Discussion

The results for the various methods of fitting curves to
LSC eficiency vs quench calibration data are shown in
Tables T2.1 to T2.10. The effect of regular and irregular
spacing of the standards on the SIE axis is investigated.
Tables T2.1 to T2.4 show the results for the theoretical
tritium standards.   The key to the spacing of standards is
given in Fig. F2.1.   In all cases the comparison between
the fitted curve and the standards function was made at
equispaced intervals along the SIE axis from zero to 650.
The use of $\Sigma_i ABS(X_i - Y_i)$ and $\Sigma_i (X_i - Y_i)^{\frac{1}{2}}$, where X_i, Y_i
are the function efficiency values and the curve-fitted
efficiency values respectively, introduces a bias against
least squares or other non-interpolatory routines due to
the coincidence of some of the comparison points with the
interpolated standards points.   This is evidenced by taking
a ratio of the $\Sigma_i ABS(X_i - Y_i)$ for an interpolatory method
(e.g. Stineman) and a least squares method (e.g. Least
squares third order polynomial) (Table T2.3a) for 65 and
650 comparison points.   These ratios are 0.10548 and
0.10100 to 5D respectively for the interpolated region (SIE
150 to 600) of the ^{3}H-efficiency vs SIE function.   Also,
the use of smooth functions to represent data which is
usually scattered can be biased against least squares
methods and to some extent the piecewise methods.   This is
shown by the obvious superiority of the langrangian
polynomial curve fitting routine with the theoretical
standards used.   Tables T2.5 to T2.7 give the results for

57

the theoretical carbon-14 standards and in all cases the comparisons were made at equispaced interval along the SIE axis from 100 to 750.

A brief investigation of the effect of near coincident standards data was made since this is a common occurrence particularly in undergraduate laboratories. The values of $\Sigma_i ABS(X_i - Y_i)$ for curves with near coincident points at low and medium QIP are given in Table T2.8 along with subjective comments on the calibration curves obtained. In practice, such standards would be regarded as poor calibration data.

Some of the routines require the setting of variables to suit the form of the data to be fitted. This is the case for the tension parameter of the tension spline and the weighting coefficient for the least squares fitting and Bezier blending. Unless otherwise stated these were set to unity. The results for Bezier blending are not tabulated because the routine was observed to give much poorer fits than the others. The tension spline proved to be useful in situations where the ordinary splines began to show severe oscillations (setting the tension parameter >1 'pulls out' the oscillations, see Table T2.8). However, in all other situations the tension spline was inferior to the other splines in terms of accuracy and time requirements and so further results are not tabulated.

58

With the function generated calibration data acting as perfect standards Tables T2.1 to T2.3 and T2.4 to T2.7 can be grouped to compare the relative accuracies of the routines. A simple ranking procedure taking the average $\Sigma_i \text{ABS}(X_i - Y_i)$ over the various data groups lists the routines in order of preference as :

Lagrangian polynomial (Newtons Method)

Cubic spline, natural end conditions

Cubic spline, Swartz end conditions

Cubic spline, L" = S" end conditions

Cubic spline, Forsythe end conditions

Cubic spline, parabolic end conditions

Quadratic spline, S' = L' end conditions

Quadratic spline, linear end conditions

Least squares 4° ploynomial

Stineman

Least squares 3° polynomial

Piecewise linear

To extend the study using theoretical standards the standards could be made more similar to experimentally obtained standards by superimposing random scatter on the function generated data. This would allow a comparison of the routines under conditions of different count precision. Repeated counting of real standards over different count times would also achieve a similar result however.

Tables T2.9 and T2.10 give the results for the real standards and samples prepared experimentally. Those entries marked X were not computed because of the observed occurrence of grossly inaccurate results. Chemically quenched and colour quenched tritium standards and/or samples of known activity range from SIE of 685 down to an SIE of 130 corresponding to ^{3}H detection efficiencies of approximately 55% to 0.1%. The carbon-14 samples were taken only from the region of rapid change of the efficiency curve gradient and the region of very high quench, SIE < 500 (Fig. F2.1). The calculation of the error bounds associated with each curve-generated dpm value is based on the errors in the count, the SIE and the dispensed DPM of the standards used for calibration curve production and the errors in the count and the SIE of the samples (of supposedly unknown activity). The experimental procedure used resulted in error bounds of ±0.06% and ±0.02% for the dispensed DPMs of ^{3}H and ^{14}C respectively with the manufacturers absolute uncertainties of ±3% and ±1.5% being constant throughout the samples. The errors associated with the standards and samples counts are related to the magnitude of the counts accumulated by the expression $\sigma \approx \sqrt{COUNT}$ with the % deviation automatically calculated and printed by the Packard 300C. The SIE values were assumed to be correct to the nearest integer value (error range of ±0.5, and letting $3\sigma \approx 100\%$ of range then $\sigma \approx 0.17$ for SIE number probability constant from X - 0.5 to X + 0.5), but the effect of this error on the efficiency value is dependent on the slope/form of the calibration

60

curve. The efficiency error e $\approx$ q(dE/dQ), where q is the error in the SIE value and dE/dQ is the rate of change of efficiency with respect to SIE at an SIE value of Q, Fig. F2.1 These errors are all combined using the expression:

Fractional dpm$_{unknown}$ error, d$_u$ = {(%dev$_{unk}$/100)^2 + (%dev$_{stds}$/100)^2 + (%DPM$_{error}$/100)^2 + 2 x (%(SIE x slope$_{error}$)/100)^2}$^{1/2}$

The listed values of average % difference refer to the difference between the dispensed dpms and calculated dpms.

Selection of the best curve fitting routine for LSC efficiency vs quench calibration data depends on the judgement criteria used. For example, if the resultant curve is to be smooth (with continuous first derivatives) then piecewise linear fitting is ruled out. Calibration curves are normally based on ten reasonably well spaced real standards, and so the results of the routines used for assay of real samples (Tables T2.9 and T2.11) are taken to be the final judgement criteria.

2.1.4 Conclusions

It may be concluded that cubic spline interpolation with natural end conditions is the best of the LSC efficiency vs quench curve fitting routines tested, but also noted that cubic splines with Forsythe's or parabolic end conditions and Stineman interpolation give good results for tritium and carbon-14 efficiency curve respectively. This assertion follows from the rankings of the routines (see Table T2.11). Indeed, Stineman interpolation has an additional advantage of being more robust and better at fitting curves with sharply changing gradients, i.e. ^{14}C and more energetic ß-sources.

The superior performance of the Lagrangian in the theoretical standards is not maintained in the practical situation. The introduction of noise into the system causes oscillations to occur to some extent in the splines but is excessive in the lagrangian and even within the high accuracy of the standards produced it is inferior to piecewise linear.

The currently used LSC machine routines are therefore found to be acceptable, but it should be emphasised that if calibration standards are poorly spaced the curve fitting by interpolation introduces large errors (even with perfect standards) and visual display of the resultant calibration curve is essential unless some mechanism for rejecting the fit is triggered. This may be accomplished by setting a

data spacing tolerance limit or switching to a generally less accurate but more universally applicable least squares fitting routine as a back-up.

2.2   The Effect of Quench on Background

2.2.1   Introduction

The effects of quenching on the recorded background count have been studied previously by Alessio et al, Scales and Horrocks. In an early study on the effects of colour and chemical quench on background Scales found the background count rate to decrease with the counting efficiency as established by an SCR method after spiking with an internal standard. Conversely, using a non-standard LSC Alessio found the background increased with quench for both ^{3}H and ^{14}C samples. Horrocks has demonstrated and explained these effects by considering the changes to the background pulse height spectrum under conditions of varying quench.

This work complements these studies and assesses the significance of background quenching in routine single ^{3}H, ^{14}C and dual label ^{3}H/^{14}C and triple label ^{3}H/^{14}C/^{36}Cl counting. Owing to the long counting times used in this study a supporting investigation into the detection of drift in LS Counters was performed. In this subsidiary investigation a comparison was made between the Cusum method and Kurtosis as indicators of drift. It is detailed in appendix A.

2.2.2 Experimental

A quenched series of 10 ml samples comprising 10 g l^{-1} butyl-PBD in scintillation grade p-Xylene and varying amounts CCl$_4$ as a chemical quencher was counted in standard 20 ml glass vials using a United Technologies Packard 300C LSC. All liquids and glassware were first purged of air by the technique described in section 2.3.2. The samples were left to temperature stabilize overnight in the refrigerated 300C prior to counting.

SIE with AEC was chosen to monitor the quench level using the integral ^{226}Ra External Standard of the 300C. Counting conditions were set to pre-programmed values of 0 - 19, 0 - 156, 0 - 714, 0 - 12, 12 - 156, 12 - 90 and 90 - 714. This assured compatability with results for single (^{3}H, ^{14}C, ^{36}Cl), dual (^{3}H/^{14}C) and triple (^{3}H/^{14}C/^{36}Cl) label counting using AEC. Results are shown in Table T2.12.

2.2.3   Results and Discussion

The results for the variation in background count rate with quench under normal counting conditions for ^{3}H, ^{14}C and ^{36}Cl single label, ^{3}H/^{14}C dual label and ^{3}H/^{14}C/^{36}Cl triple label are depicted in Figs. F2.2, F2.3 and F2.4 (Table T2.12). The coefficients of the least squares cubic polynomials used to fit and interpolate the data are given in Table T2.13.

Fig. F2.2 shows that the background decreases with increasing quench for all the single windows 0 - 19, 0 - 156, and 0 - 714 when counting using SIE with AEC. Thus use of SIE with AEC avoids the problem of increasing background with increasing quench noted by Alessio et al who used a fixed upper disciminator to select either a ^{3}H or ^{14}C counting window. Figs. F2.3 and F2.4 show the curves obtained for dual label and triple label regions and indicate the presence of a high energy component which is quenched into the windows despite the use of AEC. (AEC is tailored to suit the effects of quench on ^{3}H and ^{14}C β^- type isotopes and not on, say, external standard γ rays). This effect can be better explained by reference to the background pulse height spectra, Fig. F2.5. It is the changing shape with quench of the spectrum relative to the counting regions which explains the background curves obtained.

It would appear generally that background is highly dependent on the counting conditions and the environment and must be fully investigated when low activity and/or highly quenched samples are being used.

2.3   Multilabel DPM Determination - Quenching Limitations

2.3.1   Introductiom

The incorporation of microprocessors and anologue to
digital converters (ADC) into LSCs has led to an expansion
of counting capabilities culminating in the development of
machines capable of spectral analysis. Terminology has
changed to describe the newer techniques (e.g. from windows
to regions of interest) but the underlying processes remain
unchanged. Radioactive decay in the counting vial causes
scintillations to which the PMTubes respond and an
electrical pulse is produced. Usually, two PMTubes are
used and the pulses are coincidence gated. The selected
pulses are then sorted or counted according to one of
numerous criteria. These criteria involve the setting and
scaling of discriminators which are related to the radio-
nuclide's energy to provide information about the total
count and the associated quench. For example, with summed
PMTube pulses the resultant shaped and amplified pulse may
be analysed as being within one of two preset sizes related
to the radionuclide energy. This is the basis of the
sample channels ratio method (described in Chapter 1) and
is simple enough to realise using analogue techniques.
With dual, triple, quadruple and higher label applications
however, the pulse analysis requirements become more
complicated and are best met by digital methods.

The ADCs of the newer counters effectively provide N channels for pulse analysis. These may be 'grouped' to form counting regions (e.g. two for an SCR measurement) and analysed for spectral features such as mean pulse-height. With an SIS type measure of quench a minimum of one counting region is required for single label counting, two for dual label counting, three for triple and so on. Assuming suitable isotopes can be selected, an N-region counter could allow N-label dpm determination. The resultant counts for each region C_i (i=1 to N) can be solved for the dpm contributions d_i (i=1 to N) from the set of simultaneous equations:

$$C_1 = e_{11} d_1 + e_{21} d_2 + e_{31} d_3 + \ldots \ldots e_{N1} d_N$$
$$C_2 = e_{12} d_1 + e_{22} d_2 + e_{32} d_3 + \ldots \ldots e_{N2} d_N$$

.   .

.   .

.   .

$$C_N = e_{1N} d_1 + e_{2N} d_2 + e_{3N} d_3 + \ldots \ldots e_{NN} d_N$$

where e_{ij} (i,j = 1 to N) represent the counting efficiencies for each single isotope in each region (and need to be found by prior counting). The equations may be solved using gaussian elimination with partial pivoting, although pivoting is usually unnecessary since the regions are chosen so that the efficiency matrix is diagonally dominant, (and AEC or AQC type techniques are designed to maintain this situation over a wide quench range).

Currently, commercially produced machines provide up to three counting regions and thus allow single, dual and triple label counting - triple label counting of ^3H, ^{14}C and ^{125}I being recently reported by Horrocks. With these machines, higher label applications require either repeated use of the three output regions by recounting the samples after resetting the region limits or the inspection of the counters ADC output with external apparatus.

The complexity of the analysis and the amount of computation increases with the number of labels and necessitates accurate calibration data. However, the propagation of errors through matrix computations can produce poor results even with good data if the matrix is unstable. In a diagonally dominant matrix the gaussian-reduction coefficients are <1 and so tend to reduce the effects of roundoff errors. This is not necessarily the case in LSC. Referring to Fig. F2.6, visual inspection shows that $e_{11} > e_{21} > e_{31}$, $e_{12} < e_{22} > e_{32}$ and $e_{13} < e_{23} < e_{33}$ and hence that the matrix is diagonally dominant. For a poor choice of counting regions such as (A), (B) and (C) of Fig. F2.5 e_{21} is now greater than e_{11} and diagonal dominance is lost. Thus optimal selection of counting regions gives the additional advantage of reduced computational error propagation.

70

Of course, the total error in the final dpm solutions generally depends much more upon the experimental counting conditions. Utilizing chemically quenched calibration standards to determine colour quenched sample activity would be useless for levels of quench giving rise to significant differences in the e_{1} values for instance.

In this work a multilabel dpm determination for the particular case N=3 for colour and chemically quenched samples has been performed.

2.3.2   Experimental

The materials used in the preparation of the colour quenched series and the chemically quenched series of single label ^{3}H, ^{14}C and ^{36}Cl standards and ^{3}H/^{14}C/^{36}Cl triple label samples were Fisons Scintran grade p-Xylene, butyl-PBD (United Technologies Packard), BDH carbon tetrachloride and disperse orange 7 dye

(NO_2—◯—$N{=}N$—◯(CH_3)(CH_3)—NH_2) which was recrystalised
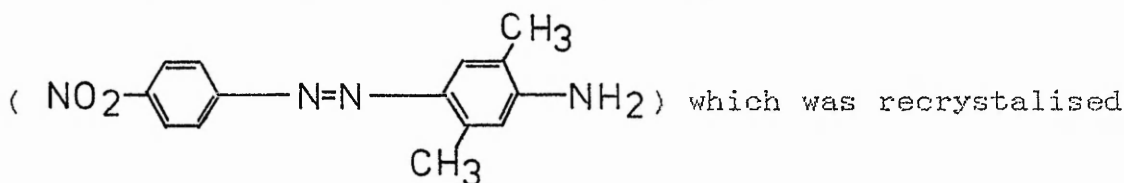
from acetone, Triton-X100, and ^{3}H n-hexadecane (batch 61) standard, ^{14}C n-hexadecane (batch B75) standard and ^{36}Cl as HCl, from Amersham International.

Two 1 litre batches of 10 g l^{-1} b-PBD in p-Xylene were produced and from which a 500 ml solution of 0.225 g of disperse orange 7 dye and the 10 g l^{-1} b-PBD in p-Xylene was made. This solution was used as the colour quencher.

Accurately weighed amounts of the labelled chemicals were measured into separate clean, dry 100 ml twin necked round bottomed flasks. 100 ml of the colour quencher, 100 ml of the chemical quencher (CCl_4) and the remainder of the 10 g l^{-1} b-PBD/p-Xylene were put into clean twin necked round bottomed flasks. All these materials were then purged of oxygen using the following technique. (Fig. F2.7).

Standard 20 ml LSC vials were amended by drilling 9 mm
holes through the centres of the vial caps replacing the
plastic seals with PTFE coated silicon septa (Pierce and
Warriner, Tuf-bond Teflon laminated discs). These were
then placed opened in an air tight container and repeatedly
evacuated with an Edwards model N^o5 vacuum pump and flushed
with nitrogen. These were then held in the container under
slight positive nitrogen pressure. The flasks of the
various cocktail constituents were evacuated and flushed
with nitrogen three times and then frozen by immersion in a
dewar of liquid nitrogen. The flasks were slowly brought
back to room temperature whereupon the gasses which came
out of the solution were drawn off by evacuation and
replaced with nitrogen. The whole procedure was repeated
three times, further cycles not appreciably affecting the
QIP of the material (10 g l^{-1} p-Xylene). Each twin necked
flask was sealed by the use of a Mininert ptfe resealable
septum and glass/ptfe T-valve (Pierce and Warriner). The
resealable septa provided a means for insertion of fine
bore needle tipped stainless steel tubing into the flask
and hence for pumping out the contents, using the
pressurised nitrogen supply, into the amended LSC vials.
This operation was carried out under positive nitrogen
supply and with repeated evacuation and flushing of all
interconnecting parts. Upon completion of the dispensing
of quantities of labelled chemicals, quenchers,
scintillators and solvents the vial caps were replaced
under nitrogen with standard vial caps. This procedure
allowed the addition of colour and/or chemical quencher

from a relatively low quench base.

To minimise the % weighing errors the labelled chemicals were diluted with some of the purged 10 g l^{-1} b-PBD in p-Xylene solution prior to dispensing, (50% Triton-X100/10 g l^{-1} b-PBD in p-Xylene in the case of ^{36}Cl-HCl). At all stages accurate weighings (to ±0.0002 g) were made and the activites of the new and/or diluted solutions were determined. The amended vials were weighed before and after the dispensation of each labelled solution, each quencher and were topped up to ≈ 10 ml total volume (checked by weight) with 10 g l^{-1} b-PBD in p-Xylene. A series of 20 chemically quenched and 20 colour quenched single label standards were prepared for each isotope and a series of 40 chemically quenched and 10 colour quenched triple label standards of various constituent activity ratios were also prepared. In addition, 10 quenched background standards were prepared using CCl$_4$ and b-PBD in p-Xylene only.

The standards were placed in the refrigerated chamber of a Packard 300C model LSC for several hours prior to counting. Samples were counted using AEC until the Packard 300C 2σ% terminators reached 0.2%.

The selection of counting regions for the new nuclides presented a problem. They were programmed manually to be 0-12 KeV for region A, 12-90 KeV for region B and 90-714 KeV for region C. These regions were chosen after obtaining spectra ^{3}H, ^{14}C and ^{36}Cl and background with a NE 4694 MCA and established diagonal dominanace in the efficiency matrix.

Since the 300C is not equipped to automatically produce a triple label assay, all results were stored and analysed externally. This was achieved by echoing the printer output to a series 4000 CBM microcomputer via a 3D GPIB and storing on disk. All counts were quenched-background corrected by reference to a least squares '3 polynomial fit to the quenched series of background standards (see section 2.2). All efficiency vs quench calibration curves for each isotope in each region were generated using cubic spline interpolation with natural end conditions (see section 2.1). The solution of the resulting simultaneous equations was accomplished using gaussian elimination and back substitution.

2.3.3   Results

The calibration curves used for the triple label determination of ^{3}H, ^{14}C and ^{36}Cl are shown in Figs. F2.8, F2.9 and F2.10. Differences arising from the different types of quench become more important as quenching increases becoming notable for SIE values of approximately 500 (equivalent to an H^m of 109). This fact is reflected in the tabulated results for the sample dpm determinations. Referring to Tables T2.17 and T2.18, the use of colour quenched calibration standards with chemically quenched triple label samples produces poor results for SIE values less than approximately 500 and fails for SIE values of approximately 460 whereas the use of chemically quenched calibration standards give satisfactory results down to SIE values of approximately 330.

Tables T2.14 to T2.17 illustrate the effect of varying the ratios of the activity of the labels ^{3}H, ^{14}C and ^{36}Cl. The tritium activity determination is the first to fail in all cases as quench increases, failing for SIE values less than approximately 300 for higher ratios. This is expected and is due to the effect of quenching which reduces the total counting efficiency and reduces the mean energies of the ß-spectra thereby causing an increase in the % of counts of the higher energy radionuclides in the lower counting regions. The effect on the counting matrix is shown graphically for quench levels of X_1 and X_2 in Figs. F2.8, F2.9 and F2.10.

76

For X_1, $e_{11} \approx 50\% > e_{21} \approx 5\% > e_{31} = 0$

$e_{12} \approx 15\% < e_{22} \approx 70\% > e_{32} \approx 15\%$

$e_{13} \approx 5\% < e_{23} \approx 10\% < e_{33} \approx 70\%$

For X_2, $e_{11} \approx 15\% > e_{21} \approx 3\% > e_{31} = 0$

$e_{12} \approx 20\% < e_{22} \approx 55\% > e_{32} \approx 3\%$

$e_{13} \approx 5\% < e_{23} \approx 25\% < e_{33} \approx 55\%$

At X_1 the matrix is diagonally dominant but at X_2 it is not, although the submatrices become so as the gaussian elimination proceeds, indicating good choice of counting regions and reduced computational error propagation. Errors associated with the accuracy of each count, each SIE, and hence each efficiency remain present of course and are combined using the expression (see section 2.1.3):

Fractional efficiency$_{errors}$, $\delta e = \{(\%dev_{stdev}/100)^2 + (\%dpm_{error}/100)^2 + 2 \times (\%(SIE \times slope)_{error}/100)^2\}^{1/2}$

The fractional errors in the counts accumulated in each region (δC_i, i=1 to 3) may be directly determined from the % deviation of each count. These error bounds may be used to determine the confidence limits on the resulting dpm's by application of the expression:

For i,j = 1, 2, 3 :- $\delta(dpm)_i = (\Sigma_{ij}(d(dpm)_i/de_{ij})^2 \delta e_{ij}^2 + \Sigma_i(d(dpm_i)/d(cpm_i))^2 \delta cpm_i^2)^{1/2}$ (1)

and this necessitates differentiation of each dpm expression by each of the e_{ij} and each cpm_i.

Given the matrix equation

$$\begin{bmatrix} e_{11} & e_{12} & e_{13} \\ e_{21} & e_{22} & e_{23} \\ e_{31} & e_{32} & e_{33} \end{bmatrix} \begin{bmatrix} dpm_1 \\ dpm_2 \\ dpm_3 \end{bmatrix} = \begin{bmatrix} cpm_1 \\ cpm_2 \\ cpm_3 \end{bmatrix}$$

gaussian elimination reduces the equation to

$$\begin{bmatrix} e_{11} & e_{12} & e_{13} \\ 0 & (e_{22}-e_{12}.e_{21}/e_{11}) & (e_{23}-e_{13}.e_{21}/e_{11}) \\ 0 & 0 & \begin{array}{c}((e_{33}-e_{13}.e_{31}/e_{11})- \\ (e_{32}-e_{12}.e_{31}/e_{11}).(e_{23}-e_{13}.e_{21}/e_{11}) \\ (e_{22}-e_{13}.e_{21}/e_{11}) \end{array} \end{bmatrix} \begin{bmatrix} dpm_1 \\ dpm_2 \\ dpm_3 \end{bmatrix}$$

$$= \begin{bmatrix} cpm_1 \\ (cpm_2-cpm_1.e_{21}/e_{11}) \\ (cpm_3-cpm_1.e_{31}/e_{11})-(e_{32}-e_{12}.e_{31}/e_{11})(cpm_2-cpm_1.e_{21}/e_{11}) \\ (e_{22}-e_{12}.e_{21}/e_{11}) \end{bmatrix}$$

from which

$$dpm_3 = \frac{(e_{11}cpm_3-e_{31}cpm_1)-(e_{11}e_{32}-e_{12}e_{31})(e_{11}cpm_2-e_{21}cpm_1)/}{(e_{11}e_{33}-e_{13}e_{31})-(e_{11}e_{32}-e_{12}e_{31})(e_{11}e_{23}-e_{13}e_{21})/}$$

$$\frac{(e_{22}e_{11}-e_{12}e_{21})}{(e_{22}e_{11}-e_{12}e_{21})} \qquad -(2)$$

$$dpm_2 = [(e_{11}cpm_2-e_{21}cpm_1)-(e_{11}e_{23}-e_{13}e_{21})(dpm_3)]/$$

$$(e_{22}e_{11}-e_{12}e_{21}) \qquad -(3)$$

$$dpm_1 = [cpm_1-((dpm_2).e_{12}+(dpm_3).e_{13})]/e_{11} \qquad -(4)$$

If it assumed that each e_{ij} has a confidence limit of e_{ij} and each cpm_i has a confidence limit of cpm_i at a certain probability level then the confidence limits on the dpm_i (δdpm_i) may be found using equation (1).

Let $R = (e_{11}cpm_3-e_{31}cpm_1)$; $M = (e_{11}e_{32}-e_{12}e_{31})$

   $S = (e_{11}e_{22}-e_{12}e_{21})$; $P = (e_{11}e_{23}-e_{13}e_{21})$

   $T = (e_{11}cpm_2-e_{21}cpm_1)$; $W = R - ST/Q$

   $Q = (e_{22}e_{11}-e_{12}e_{21})$; $V = M - SP/Q$

So:

$$\frac{d(dpm_3)}{de_{11}} = [V(cpm_3 - S(Q.cpm_3 - T.e_{22})/Q^2 - T.e_{32}/Q) - W(e_{33} - S(Q.e_{23}$$
$$- P.e_{22})/Q^2 - P.e_{32}/Q)]/V^2$$

$$\frac{d(dpm_3)}{de_{12}} = [VT(Q.e_{31} - S.e_{21})/Q^2 - WP(Q.e_{31} - S.e_{21})/Q^2]/V^2$$

$$\frac{d(dpm_3)}{de_{13}} = W(e_{31} - S.e_{21}/Q)/V^2$$

$$\frac{d(dpm_3)}{de_{21}} = [VS(T.e_{12} - Q.cpm_1)/Q^2 - WS(P.e_{12} - Q.e_{13})/Q^2]/V^2$$

$$\frac{d(dpm_3)}{de_{22}} = [V(ST.e_{11}/Q^2) - W(SP.e_{11}/Q^2)]/V^2$$

$$\frac{d(dpm_3)}{de_{23}} = -WS.e_{11}/QV^2$$

$$\frac{d(dpm_3)}{de_{31}} = V(T.e_{12}/Q - cpm_1) - W(S.e_{21}/Q - e_{13}) /V^2$$

$$\frac{d(dpm_3)}{de_{32}} = WP.e_{11}/Q - VT.e_{11}/Q$$

$$\frac{d(dpm_3)}{de_{33}} = -W.e_{11}/V^2$$

$$\frac{d(dpm_3)}{d(cpm_1)} = S.e_{21}/QV - e_{21}/V$$

$$\frac{d(dpm_3)}{d(cpm_2)} = -SQ.e_{11}/V$$

$$\frac{d(dpm_3)}{d(cpm_3)} = e_{11}/V$$

and also, noting that the dpm_3 is not treated as an independent variable,

$$\frac{d(dpm_2)}{de_{11}} = (Qcpm_2 - T.e_{22})/Q^2 - P(\frac{d(dpm_3)}{de_{11}})/Q - (dpm_3).(Q.e_{23} - $$
$$P.e_{22})/Q^2$$

$$\frac{d(dpm_2)}{de_{12}} = -P(Q.\frac{d(dpm_3)}{de_{12}} + (dpm_3.e_{21})/Q$$

$$\frac{d(dpm_2)}{de_{13}} = (e_{21}(dpm_3) - P.\frac{d(dpm_3)}{de_{13}})/Q$$

$$\frac{d(dpm_2)}{de_{21}} = (Q.e_{13} - P.e_{12})(dpm_3)/Q^2 - P.\frac{d(dpm_3)}{de_{21}}/Q - cpm_1$$

79

$$\frac{d(dpm_2)}{de_{22}} = ((dpm_3)e_{11} - Q.\frac{d(dpm_3)}{de_{22}})P/Q^2$$

$$\frac{d(dpm_2)}{de_{23}} = -P(\frac{d(dpm_3)}{de_{23}} + e_{11}(dpm_3))/Q$$

$$\frac{d(dpm_2)}{de_{31}} = -P.\frac{d(dpm_3)}{de_{31}}/Q$$

$$\frac{d(dpm_2)}{de_{32}} = -P.\frac{d(dpm_3)}{de_{32}}/Q$$

$$\frac{d(dpm_2)}{de_{33}} = -P.\frac{d(dpm_3)}{de_{33}}/Q$$

$$\frac{d(dpm_2)}{d(cpm_1)} = -e_{21} - P.\frac{d(dpm_3)}{d(cpm_1)}/Q$$

$$\frac{d(dpm_2)}{d(cpm_2)} = e_{11} - P.\frac{d(dpm_3)}{d(cpm_2)}/Q$$

$$\frac{d(dpm_2)}{d(cpm_3)} = -P.\frac{d(dpm_3)}{d(cpm_3)}/Q$$

and these equations now permit determination of the dpm_1 derivatives:

$$\frac{d(dpm_1)}{de_{11}} = -cpm_1/e_{11}^2 - e_{12}(e_{11}.\frac{d(dpm_2)}{de_{11}}-(dpm_2))/e_{11}^2 - $$
$$e_{13}(e_{11}.\frac{d(dpm_3)}{de_{11}}-(dpm_3))/e_{11}^2$$

$$\frac{d(dpm_1)}{de_{12}} = -(e_{12}.\frac{d(dpm_2)}{de_{12}}+dpm_2+e_{13}.\frac{d(dpm_3)}{de_{12}})/e_{11}$$

$$\frac{d(dpm_1)}{de_{13}} = -(e_{12}.\frac{d(dpm_2)}{de_{13}} + e_{13}.\frac{d(dpm_3)}{de_{13}} + dpm_3)/e_{11}$$

$$\frac{d(dpm_1)}{de_{ij}} = -(e_{12}/e_{11}.\frac{d(dpm_2)}{de_{ij}} + e_{13}/e_{11}.\frac{d(dpm_3)}{de_{ij}} \quad ; \text{ for } i=2,3 \quad j=1,2,3$$

$$\frac{d(dpm_1)}{d(cpm_1)} = 1/e_{11} - e_{12}/e_{11}.\frac{d(dpm_2)}{d(cpm_1)} - e_{13}/e_{11}.\frac{d(dpm_3)}{d(cpm_1)}$$

$$\frac{d(dpm_1)}{d(cpm_i)} = -(e_{12}/e_{11}.\frac{d(dpm_1)}{d(cpm_i)} + e_{13}/e_{11}.\frac{d(dpm_3)}{d(cpm_i)}) \quad ; \text{ for } i=2,3$$

In this work the cpm_i were determined with typical confidence limits of 0.5% and the efficiences with typical confidence limits of 0.4%, 4%, 20% for e_{i1}; i=1,2,3 and 0.5%, 0.2%, 1% for e_{i2}; i=1,2,3 and 0.75%, 0.45%, 0.25% for

$e_{i,j}$; i=1,2,3. Thus with the efficiency matrix

$$\begin{bmatrix} 0.50 & 0.15 & 0.05 \\ 0.05 & 0.70 & 0.15 \\ 0 & 0.10 & 0.75 \end{bmatrix}$$

as an example and cpm_i of $\begin{bmatrix} 10,000 \\ 10,000 \\ 10,000 \end{bmatrix}$ the estimated confidence

limits on the dpm_i become $\delta dpm_1 = 129$, $\delta dpm_2 = 81$, $\delta dpm_3 = 204$ for actual dpms of $dpm_1 = 15,623$, $dpm_2 = 10,616$, $dpm_3 = 11,918$. Comparison of these results with those in Tables T2.14 to T2.17 for dpm ratios of (approx.) 1½:1:1 with light/moderate ranges of quench (equivalent to the efficiency matrix given) largely accounts for the observed scatter.

With unquenched and lightly quenched triple labelled samples there is evidence in Tables T2.14 – 19 that the ^{36}Cl activity is overestimated. (This may be in part due to a systematic error in the 'known' dpm of the ^{36}Cl which was a nonstandard labelled source standardised against a ^{36}Cl standard (suppled by Amersham). The source was of a similar level of quench to the standard.)

It is interesting to note, however, that this situation is not maintained as quenching increases. This may be caused by the AEC although further work would be necessary for verification. If AEC is not selected the calibration curves for ^{3}H, ^{14}C and ^{36}Cl counted in regions 0 – 12 keV, 12 – 90 keV and 90 – 714 keV are substantially altered, see

Fig. F2.11. Examination of the solution matrix for a triple label determination at a quench level of $X_{\cdot}$ shows that

$e_{11} \approx 9\% > 0 \qquad > 0$

$e_{21} \approx 59\% > e_{22} \approx 16\% > 0$

$e_{31} \approx 21\% < e_{32} \approx 61\% > e_{33} \approx 6\%$

and is not diagonally dominant. At first sight the presence of the zero efficiencies may seem advantageous in that no matrix reduction is necessary. However, the backsubstitution process is worsened by the development of coefficients with small denominators. Also, and of greater significance is the larger uncertainties associated with the lower counting efficiencies. It can thus be seen that the AEC feature provides a useful function.

2.3.4   Conclusions

Multilabel dpm determinations using liquid scintillation counting techniques are feasible provided the selection of counting regions is based on a thorough knowledge of the pulse height spectra of the labelling radionuclides.

It remains important to differentiate between colour and chemical quench in multilabel dpm determinations.

AEC type electronic quench compensation remains a useful technique for multilabel dpm determinations.

Chapter 3

SIMULATING THE LSC - I MODEL CONSTRUCTION

This chapter describes the design, development and
implementation of an original simulation of the LSC. The
input data necessary for the correct functioning of the
model was partly researched in the literature and partly
experimentally determined.

A stochastic approach was chosen because of the physically
discontinous nature of the sequence of processes in LSC.
Monte Carlo methods are well established and have been
applied successfully in many branches of Nuclear physics.
Modelling at the photon level gives advantages over
modelling at the spectral level by avoiding the compounding
of complex spectral and geometrical equations, by
encouraging logical program development and by facilitating
independent manual testing of the program. Since the basic
stages of β decay $\longrightarrow$ chemical quenching $\longrightarrow$ fluorescence $\longrightarrow$
colour quenching and photon detection are universally
accepted, parts of this model must be similar to that of
Stanley. However, extensive improvements to the modelled
geometry and modelling of the PMTube response together with
an independently developed program serve to (a) corroborate
the earlier work and (b) provide a closer representation of
a specific LSC. The latter point is important in the
linking of the model to reality for the purposes of
developing new counting techniques.

3.1   The Colour-Chemical Quench Correction Problem

The essential differences between the colour and chemical
quenching effects that are observed in LSC are a
consequence of the geometrical dependence of colour
quenching and geometrical independence of chemical
quenching.   A typical two PMTube LSC is illustrated
schematically in Fig. F3.1.   After certain ß-decay some
energy is ultimately converted into useful photon
production.   Assume that an equal large number of mono-
energetic photons is emitted in each direction (to PMT1 and
PMT2) parallel to the x-axis.   If no colour quencher is
present the pulses at each PMTube will be of equal height.
If a colour quencher is present, however, and the
probability of absorption follows an exponential curve
according to the Beer-Bougouer Law then PMT2 will produce a
smaller pulse than PMT1.   This is generalised in Fig. F3.2
for events of different position x.

In all current LSC machines the two pulses y_1 and y_2 are
either summed or lesser-gated prior to pulse height
analysis and storage.   The net effect is a pulse which is
still dependent on position x as shown in Fig. F3.3, where
$y_s = y_1 + y_2$ for the summed pulses and $y_L = \begin{cases} y_1 & ; \ y_1 < y_2 \\ y_2 & ; \ y_2 < y_1 \end{cases}$ for

"lesser" pulses.   It is evident that y_L varies less with
event position than does y_s.   This explains why lesser
pulse height counting gives calibration curves that are
more alike for colour and chemically quenched samples than

does summed pulse height counting, and also why the resolution is worse (owing to the consistently smaller pulses generated).

This simple analysis indicates two approaches to overcome the colour chemical quench differences:

(a) find a combination, y_c, of pulses y_1 and y_2 which makes y_c independent of x (i.e. conceal the colour quench effect), or

(b) find a new indicator of the event position and use it to indicate the amount of colour quench present (i.e. exaggerate the colour quench effect).

To pursue the simple analysis further let A represent the chemical quench coefficient (where $0 \leq A \leq 1$ and 0=100% quenched; 1=no quench), E be the energy available from the ß-event, and B represent the colour quench coefficient such that

$$y_1 = EAe^{-Bx} \qquad (1)$$

$$\text{and} \qquad y_2 = EAe^{-B(1-x)} \qquad (2)$$

$$\text{Then the sum} \qquad y_s = EA(e^{-Bx} + e^{-B(1-x)}) \qquad (3)$$

$$\text{and the lesser} \qquad y_L = \begin{cases} EAe^{-Bx} & , y_1 < y_2 \\ EAe^{-B(1-x)} & , y_2 < y_1 \end{cases} \qquad (4)$$

These are not the only way that equation (1) and (2) may be combined:

$$\text{e.g. Difference:} \quad y_D = EA(e^{-Bx} - e^{-B(1-x)}) = y_1 - y_2 \qquad (5)$$

$$\text{Product} \quad : \quad y_P = (EA)^2 e^{-B} = y_1 \cdot y_2 \qquad (6)$$

$$\text{Ratio} \quad : \quad y_R = 1/(1 + e^{-B(1-2x)}) = y_1/(y_1 + y_2) \qquad (7)$$

It is noticed immediately that y_r is independent of x and thus is an example of approach (a) whereas y_b, which varies substantially with x (see Fig. F3.1), is an example of approach (b). At first sight the pulse multiplication seems an ideal approach. However, this 1D model is not a very good representation of the processes at work in a LSC. Extension of the model to allow for 2D photon trajectories bounded by a rectangle (Fig. F3.4) shows y_r becomes weakly position dependent. (e.g. Assuming H=1, h=H, r=0.5 and all photons travel by mean path lengths $\overline{L_1}$ or $\overline{L_2}$ then as x varies from 0 to 0.5, $\overline{L_1} + \overline{L_2}$ varies by up to 8.9%. Since $y_b = (EA)^2 e^{-m(\overline{L_1} + \overline{L_2})}$, y_r is shown to be dependent on event position x). Further extension of the model to cover a 3D cylinder of height=1 and radius=0.5 showed that for 1000 randomly positioned events each of 1000 monoenergetic photons emitted in random directions the function $\overline{L_1} + \overline{L_2} = 0.912$ and has a standard deviation of 0.201 and hence represents a worsening of the dependence of y_r on event position. Obviously too much reliance must not be placed on simple models.

Caution must also be exercised in the use of equations (1) to (7). The basic elements of the system in terms of pieces of information rest with the fact that there are two PMTubes. For any given ß event we know a pulse height y_1, from PMT1, and a pulse height y_2 from PMT2, i.e. two pieces of information. Current summed and lesser pulse height techniques are wasteful because only one piece of information is used (y_s or y_L). The approach (b) stated

87

above   is feasible because there is scope for another pulse based   parameter.   The <u>simultaneous</u> use of y_s and y_D is an example.

To accomplish simultaneous   summed   and   differenced   pulse height analysis   experimentally   requires   careful   modification   of the pulse handling   circuit.   Investigation of a large variety of   pulse   handling   techniques   to   optimise selection   of   the   colour-chemical   quench   indicating parameter   becomes time   prohibitive experimentally.   If a reliable   model of the LSC   were developed such constraints would   no longer apply.   A highly detailed model of the LSC has been   developed   and   applied   to   the   colour-chemical quench   correction   problem.   It   is   described   in   the succeeding sections.

3.2   LSC Model Design

3.2.1   Model Geometry

In section 3.1 the geometry dependence of colour quenching was stressed. For this model to approach a good simulation of the LSC the 3D geometry of the whole counting system must be as detailed as possible.   This model is applied specifically to a Packard 300C LSC so far as the counting chamber and PMTubes are concerned although the modular design of the program allows future expansion to cater for alternative counting chamber geometries and materials.

A schematic diagram of the vial and counting chamber geometry used in the model are shown in Fig. F3.5. Dimensions have been chosen in accordance with United Technologies Packard Drawing No. D-5070871 and on measurements made on the standard glass vials used experimentally. The small differences between the vial length and chamber diameter may be adjusted in the model by the incorporation of a z-axis offset. The plane mirrors simulate the slightly curved photon-directing mirrors of the real counting chamber. The vial inner and outer walls are perfect cylinders and are concentric unless otherwise stated and the solution forms a 90° contact angle with the vial inner wall at the meniscus. The cross-hatched PMT faces have the properties of pyrex glass (Corning 7740). The pyrex is of zero thickness so that all non-reflected photons interact with the photocathoode.

The coordinate system adopted in the model is cartesian and the Right Hand axis convention is obeyed. The axes are also illustrated in Fig. F3.5.

3.2.2   The Model Scintillation Detector Processes

In addition to the geometrical constraints of section 3.1 the model is further characterised by the following description:

A ß-event is defined by choosing an event position which is random 3 dimensionally in the volume occupied by the solution. The event position is fixed for ^{3}H and ^{14}C simulated decays for the duration of the photon production and photon tracking stages which result from the ß-decay. The ß-energy, $E_{ß}$, is randomly selected according to the modified Fermi distribution for each particular isotope.

The ß-energy which is released as useful for photon production is determined by application of a scintillation efficiency function and a chemical quench coefficient. The scintillation efficiency is a function of $E_{ß}$ and has been experimentally determined by Horrocks.[90] Malcolm & Stanley have made the point, however, that the data represents the scintillation efficiency as a function of average $E_{ß}$ whereas the model requires the scintillation efficiency as a function of a monoenergetic $E_{ß}$.[121] The chemical quench coefficient is independent of $E_{ß}$ and hence is simulated as a simple multiplicative variable between 0 (fully quenched) and 1 (unquenched).

Photons are generated with random 3D direction vectors and with wavelengths according to the solute fluorescence spectrum. They are also assigned a random electric field vector which is perpendicular to the photon direction vector i.e. they are assumed to be plane polarized. The ß-energy available for photon production, E_p, allows the repeated production of photons with random directions and random wavelengths until E_p is exhausted. If the amount of energy left is between the upper and lower limits of energy for photons of the solute (corresponding to wavelengths of 300 nm and 600 nm in the model) the Monte Carlo decision is based on the truncated fluorescence spectrum. Any residual energy of E_p which is less than that corresponding to a 600 nm photon is assumed lost. All the photon direction vectors start at the ß-event coordinates and the photons are traced in turn until the fate of all is known.

Colour quenching is simulated by assigning to the solution an absorption spectrum and a concentration of the absorbant (or colour quench coefficient). The distance that the photon must travel from the ß-event coordinates to the point of escape from the solution is calculated. The probability of a photon being colour quenched along its path is assumed to follow an exponential distribution according to Beers law. Hence the Monte Carlo decision to quench or transmit a particular photon is based on the exponential

92

distribution defined by:

Prob. of escape $= e^{-acd}$

where a = abs. spectrum prob. $(0 \leq a \leq 1)$

c = colour quench concentration

d = path length of photons

The behaviour of photons at solution-vial interfaces and solution-air interfaces is determined by another Monte Carlo decision. Reflection or refraction is assumed to obey Fresnel's equations:

$$\frac{R_\perp}{E_\perp} = \frac{-Sin(\emptyset - \emptyset')}{Sin(\emptyset + \emptyset')} \quad , \quad \frac{R_{/\!/}}{E_{/\!/}} = \frac{Tan(\emptyset - \emptyset')}{Tan(\emptyset + \emptyset')} \quad ,$$

$$\frac{T_\perp}{E_\perp} = \frac{2Sin\emptyset'Cos\emptyset}{Sin(\emptyset + \emptyset)} \quad , \quad \frac{T_{/\!/}}{E_{/\!/}} = \frac{2Sin\emptyset'Cos\emptyset}{Sin(\emptyset + \emptyset')Cos(\emptyset - \emptyset')} \quad ,$$

where E, R, T, are incident, reflected and transmitted amplitudes of the light electric vector and $\perp$, $/\!/$ are perpendicular or parallel to the plane of incidence. From these equations the reflectances $(R_\perp/E_\perp)^2$, $(R_{/\!/}/E_{/\!/})^2$ may be determined. In the model the total reflectance $(R/E)^2$ of a single photon is assumed to be a weighted average of the parallel and perpendicular reflectances of the photon. These parallel and perpendicular reflectances are computed by resolving the electric vector of the photon into components which are parallel and perpendicular to the plane of incidence (in 3D space). The Monte Carlo decision is thus based on the curve between the 100% $E_{/\!/}$ and 100% $E_\perp$ reflectance vs angle of incidence curves. A simpler method to decide the photon's reflection or refraction

may have been to resolve the electric field vector into the parallel and perpendicular components and then make the photon obey either the 100%E$_{//}$ or the 100%E$_\perp$ curves weighting the choice to a random decision weighted by the electric field vector components. The former method is used in the model and the cumulative result satifies Fresnel's equations and Snell's law. The refractive index, n, is wavelength dependent and is determined by application of a 3 point Cauchy equation at each interface:

$$n = A + B/\lambda^2 + C/\lambda^4$$

where A, B and C = constants

$$\lambda = \text{wavelength}$$

This equation adequately accounts for dispersion in isotropic nonconducting noncolloidal homogeneous materials in the visible region, and is discussed in many standard optics texts.

The new direction vectors of reflected or refracted photons are calculated. If the photon is reflected the point of reflection becomes the new photon origin for the purposes of new path length calculations, colour quenching decisions, and new solution-air or solution-glass interface decisions (or direct loss in the vial base). If refracted it enters a new medium – air or glass. If it enters the air space it will either reach the vial top (and be absorbed) or the vial glass where a new reflection/refraction decision is made. If the photon enters the vial glass it is further traced with

yet more reflection/refraction decisions. These processes are repeated as often as necessary to trace each photon with the model allowing photons to re-enter any medium any number of times.

The path tracing of photons is continued after leaving the vial and entering the air filled counting chamber. Decisions on reflection or absorption at either the cylindrical or plane mirrors are made by a Monte Carlo method using the absorption spectrum of polished aluminium.

At either of the PMTubes photons may be reflected by the glass face-plate or transmitted through it. If transmitted they interact with the photocathode by absorption, reflection or transmission according to the wavelength dependent quantum efficiency of the photocathode. It is incorrect at this stage to continue treating the photons as independent objects. The real world photocathode receives multiphoton pulses as its input signal and integral numbers of photoelectrons are emitted within a time that is short with respect to the resolution time of the PMTube. Thus in the model, as photons arrive at each photocathode they are stored (wavelength and arrival number) until the energy for photon production, E_β, and the whole ß-event is exhausted. On completion of photon tracing for the ß-event the batch of photons at each PMTube are analysed. If all the photons were monoenergetic the

95

number of photoelectrons produced could be determined
from a simple Poisson distribution. However, they are
not monoenergetic and moreover the batch wavelength
spectrum varies from ß-event to ß-event and especially
with low energy emitters. Precise work at this stage
requires the construction of a full binomial
distribution for every event and each PMTube. Owing to
the large time constraints that this would entail an
approximation was developed. In the model a wavelength
is chosen at random from the stored wavelength data.
This choice is naturally weighted according to the
incident batch distribution. All photons in the batch
are assigned the quantum efficiency of the chosen
wavelength and the number of photoelectrons is
determined by a Monte Carlo method based on the
resulting poisson distribution. The poisson
distributions vary from batch to batch and in the long
term approximate the effect of using the binomial
distribution.*

The number of photoelectrons arriving at the first
dynodes of each PMTube is dependent on the collection
efficiency and the probability of collection is applied
to each photoelectron. The numbers of secondary
electrons from the first dynodes resulting from the
incident primary photoelectrons is determined by a
Monte Carlo decision based on a Polya distribution.[44]

*   Refer to section 3.3.

96

This procedure is repeated for the second dynodes and the resulting numbers of electrons from each is taken to represent the pulse heights of PMT1 and PMT2. These pulses are then analysed and stored by whichever method the programmer has selected.

3.2.3   The Model Logic Design

The logical processes inherent in the model are best described by means of a flowchart.   A simplified flowchart is presented in Fig. F3.6.

3.2.4   Model Implementation

The program is written in VAXPASCAL version V3.0 under a VAX VMS version V4.0 operating system. The program is approximately 1200 lines long and occupies 76 blocks of memory on a VAX 785. Run times vary greatly with isotope and quench. Typical CPU times are 6 hours for the accumulation of 1000 counts for an unquenched ^{14}C sample and around one tenth of this for a ^{3}H sample. Output consists of header information, set-up data and pulse height spectra. Status reports on the batch runs are logged in separate files. Analysis and formatting of the model generated data is performed by ancillary programs which are not detailed here.

The program is listed in appendix B. It is acknowledged that from a computer programming point of view the program is not optimised in terms of storage or runtime. This is largely because the program is still very much a research tool and is liable to modification for a variety of reasons. Originally the output was limited to six types of pulse height spectra (sum, difference, ratio with coincidence or noncoicidence). Modifications have since been made to produce product and other pulse height spectra. A better procedure would be to simply store the whole sequence of pulse pairs from PMT1 and PMT2 for each quenched sample so that an extensive hunt for optimal quench parameters could be made by repeated post-analysis using the data pairs. Batch running of the program

prohibited interactive initialization of program variables and so the initialization part of the program was spilt into separate compilation modules. This also reduced compilation times. The external mathematics functions which have been used are those belonging to the DEC FORTRAN maths reference library as maintained by the Computer Services Department at Trent Polytechnic.

3.2.5   Numerical and Logical Testing of the Model

A vitally important part of the implementation of the model is program validation. To this end each modular procedure was tested and correct functioning proven. All absorption spectra, fluorescence spectra, ß-spectra, Polya distributions, poisson ditributions and other sources of input data error have been manually compared with separately obtained results or data. Over twenty 3D vectors which cover most <u>types</u> of photon behaviour (e.g. total internal reflection in glass wall, and reflection and refraction at curved or plane surfaces at several 3D incident angles) have been manually calculated and fully manually traced. This extremely tedious and time consuming execise resulted in agreement with the models' calculation in all cases. (N.B. a real physical paper mock up of the vial and counting chamber greatly assisted 3D visualization of the photon paths).

This left the problems associated with accumulation and calculation errors. Under certain conditions, due to the random nature of the selected input data and cumulative computational errors, incorrect ray tracing conditions were discovered. These were corrected by the use of computational tolerances put around the geometrical surface intersections. Vectors calculated as being just outside the system were slightly rescaled to lie on the edge of the system. Even so, one error which resulted in underflow occurred approximately once or twice in a series of ten

1000 count ^{14}C runs (i.e. 10,000,000 photons). This rare but catastrophic programming event was treated as a photon loss and was the only case of avoiding rather than correcting program errors.

3.3   Model Input-Data Sources

3.3.1   Introduction

A wide range of input data is required to operate the
model.   Fig. F3.7 shows a list which summarises the data
actually used in the model.   A significant proportion of
the data has been self ascertained and how this was
achieved is detailed overleaf.

3.3.2   Materials and Methods

(a)   Fluorescence Spectra

Equipment :   Perkin   Elmer   model   3000   Fluorescence
Spectrometer.

Perkin Elmer model 561 chart recorder.

Apple   IIe Microcomputer + disc drives +
printer.

XAD2 A to D Card.

TDI psystem Apple Pascal Software.

Gould model 4040 Storage oscilloscope.

Rockwell Aim 65 micro.

Quartz   sample   and   reference cells +

10 g l^{-1} b-PBD in p-Xylene +

either n-hexadecane

or   Orange 7

or   CCl$_4$

Method : Equipment was set up in accordance with
Fig. F3.8 so that depression of the PE3000 scan button
synchronised the commencement of the spectra capture
program on the Apple IIe.   The spectra were obtained
by passing the PE3000 chart recorder   output through
the XAD2 A to D card to   the   Apple   IIe using self
written assembly language subroutines to handle the
binary coded data.   Storage of the data on floppy disk
facilitated the latter incorporation of the data in
the model on the VAX network.

Four separate samples were measured. One was unquenched, one was quenched with CCl_4 and two were quenched with O7 dye. The samples were counted using a Packard 300C LSC to determine the relative quenching present in each prior to fluorescence spectra capture. The unquenched sample was counted twice – once with little O_2 present and once after opening to the atmosphere and allowing the sample to become air saturated.

Spectrometer machine settings were 60 nm/min scan speed, 10 mm excitation slit width, 5 mm emission slit width, 300 nm start wavelength, 600 nm stop wavelength and auto PMT correction was used.

(b) Absorption Spectra

Equipment : As for fluorescence spectra + $CHCl_3$ non fluorescing solvent.

Method : The method employed is largely the same as that for the fluorescence spectra capture. In this experiment the sample was disperse O7 using chloroform as the common solvent. A full scan on the solvent and solvent reference cell allowed background subtraction to be performed. The experiment was performed twice with settings of transmission mode selected, excitation and emission slit widths on 1 mm, a 600 nm to 300 nm scan range and scan speeds of 60 nm/min and 15 nm/min respectively for the two runs.

(c) Optical Dispersion

Equipment : Bellingham and Stanley model 60 Abbe
refractometer.

LKB Multitemp Circulator model 2209.

Sodium lamp.

Mercury lamp.

Optical filters: Evans Electroselenium
Ltd. types 601 and 603, and a Helium-Neon
laser filter (λ = 632.8 nm).

Method :   The temperature of the refractometer was
maintained at 16°C to match the (overnight) measured
temperature of the Packard LSC refrigerated sample
chamber.   In an optical dark room refractive index
readings were taken for the four filtered wavelengths
435.8 nm (λ_V), 491.4 nm (λ_B), 589.2 nm (λ_Y), 632.8 nm
(λ_R).   Materials measured, in sequence, were p-Xylene,
10 g l^{-1} b-PBD in p-Xylene, CCl_4 and n-hexadecane,
with thorough cleaning and drying between each
measurement.

(d) PMTube Photoelectron Distribution

Equipment : Apple IIe computer + disks + printer.

TDI pSystem Apple Pascal software.

Method :   A program was created to compare the
binomial and multipoisson approximation distribution
for small and moderately sized batches of photons with
wavelengths chosen at random and weighted according to
the fluorescence spectrum of 10 g l^{-1} b-PBD/p-Xylene.

106

Quantum efficiencies of the photons were calculated from a quadratic equation which was fitted to the manufacturers quantum efficiency curve for a RCA model 4501/V3 PMTube.

(e) Vials

Vial dimensions shown in Fig. F3.5 are the average of ten measurements on randomly selected low potassium borosilicate glass vials. Vial heights were taken from base to the glass shoulder. It may be noted that the vial (and counting chamber) dimensions may be treated as variables in the model.

(f) PMTube Dynode Shape Factor

Owing to the uncertainty in the appropriate value for the dynode shape factor, the Polya distribution was calculated for a dynode of gain 3.94 for a range of shape factors.

3.3.3   Results and Discussion

(a)   The spectral distribution of light from a LS cocktail
when excited by a soft ß source will include both
fluorescence and phosphorescence in the absence of
oxygen.   The phosphorescence of the O_2-degassed
samples in a LSC is not counted because of the fast
response of the LSC ($\approx$ 100 ns for Packard 300C).
Fluorescence occurs in $<10^{-6}$ s whereas phosphorescence
occurs in $>10^{-3}$ s and a typical count rate of 60,000
cpm, if uniformly spread in time and corresponding to
1 event per millisecond, indicates that counting or
'doubling up' of phosphorescent events is unlikely
within the LSC resolving time.   The LSC is thus a
fluorescence-only monitor.   The PE3000 is not
necessarily a fluorescence-only monitor however.   With
the unquenched sample, the storage scope and Aim micro
were used to capture PMT pulses from the PE3000.
These pulses were shown to be comprised of a fast and
a slow component and the integration of these
components suggested a method of determining the
phosphorescent and fluorescent parts of a composite
emission spectrum, but how much the pulses were a
function of the PE3000 PMTube switching was not
further investigated.   .

Oxygen is a very strong quencher of phosphorescent
states in a LS cocktail.   The spectrum obtained with
O_2 present was used to provide the fluorescence

108

spectrum for the model. The further samples were measured to illustrate the effects of colour and chemical quenchers on the fluorescence spectrum. The spectra are plotted in Fig. F3.9. N.B.: different scaling factors were used for each spectrum to maximise usage of the A to D resolution. The choice of CCl_4 as a chemical-only quencher appears to be a good one since the relative distributions are identical within experimental error. The distortion to the fluorescence spectrum is illustrated by the heavy and light colour quenched samples.

A further point to note is that the fluorescence spectrum as used in the model incorporates the effects of any absorbers present in the O_2 quenched sample. This includes self absorption by the solute. The solute concentration is the same for all the samples used in this study and hence a separate experiment to assess the absorption spectrum (as carried out by Stanley) was not performed.

(b) With the absorption spectrum of O7, the 10 nm step spectra were thought to be of sufficient resolution for the broadband spectra obtained. The 10 nm step spectrum is shown in Fig. F3.10.

(c)   The Cauchy dispersion equation $n(\lambda) = A + B/\lambda^2 + C/\lambda^4$ was used with the four refractive indices ,used for each substance. The red and yellow refractive indices were chosen for two of the three simultaneous equations required to compute A, B and C since these were more accurate. The third value was decided by comparing the results for the blue and violet indices (Table T3.1).

The Cauchy equation was also applied to the estimation of dispersion in the vial glass. For borosilicate glass $N_F(H_\beta)$blue/green=1.5158, $N_d(H_a)$yellow=1.50970 and $N_c(H_a)$red=1.50627 corresponding to wavelengths of 486.1 nm, 587.6 nm and 656.3 nm.

The constants then become A=1.49788933, B=4061.10397 and C=5804367.75.

The variation of refractive index is small over the range of wavelengths examined. The range doesn't extend to the 300 nm higher limit of the stored fluorescence and absorption spectra, but this is relatively unimportant because (a) the fluorescence spectrum high wavelength cut off is around 350 nm and (b) the refractive index is a slowly varying function with wavelength for regions not near an absorption band.

Dispersion of the PMTube glass is not incorporated in the model as yet (a fixed value of n= 1.52 is used), nor are changes in the cocktail composition due to the addition of samples and quenchers. The modelled solution is based on the results for 10 g l^{-1} b-PBD in p-Xylene.

(d) Figs. F3.11 to F3.21 show the distributions for the binomial and multipoisson approximation modelled photocathode. Ten randomly chosen poisson distributions were constructed and averaged from the same input batch in each case. The cumulative effects of using the poisson approximation with batches of photons typified by the 10 g l^{-1} b-PBD in p-Xylene fluorescence spectrum are seen to be almost identical to those using the lengthy full combinatorial binomial distribution for small numbers of incident photons. (For large numbers of incident photons the poisson distribution approximates the binomial distribution as may be shown in many statistics texts).

A further check was made by comparing ten randomly chosen poisson distributions based on different input batches of photons. See Figs. F3.20, F3.21. The cases for m=4 and m=9 are plotted. The great similarity between the distributions is evident.

(e) Vial dimensions have been given in section 3.1.1. The outer radius of the standard glass vial has been extended to 14.7 mm in the model to cover the tolerance gap encountered between the vial and the counter chamber. Although the increased photon losses in the vial top and base in the area of the vial wall annulus will not be identical to losses by refraction and escape through the tolerance gap, the treatment is believed to be adequate for the relatively small % of photons affected. Increased rigour here would demand increased rigour in dealing with other more complex problems - the rounded shoulders of the glass vials and the screw threads for example.

(f) The effects of varying the dynode statistical shape factor on the secondary electron distribution for a dynode with an expected gain of 3.94 is shown in Table T 3.2. The gain of 3.94 is derived from the total gain of 1.4×10^7 (at 2kV applied voltage) for a 12 stage BeO PMTube of type 4501V3 (RCA Corporation). The distributions were obtained using program POLYA.PAS which is listed in appendix B. According to the manufacturers BeO dynodes do not exhibit pure poissonian behaviour due to irregularities in the dynode surface. In the absence of specific information a shape factor of 0.2 is arbitrarily selected in the first instance. The effects of varying the shape factor on the model output is examined in the next chapter.

112

(g) For completeness, the data obtained from the literature is include below:

(i) Aluminium reflection data is linearly inter-polated from Table T3.3. The normal incidence reflection underestimates the true multi-angled incidence of the model. The increased losses may in part be offset be neglect of such sources of absorption as surface dirt and dust and imperfect vial and chamber surface.

(ii) Quantum efficiencies were calculated by use of a quadratic equation fitted to the curve shown in Fig. F1.10. Coordinates chosen for the fit were (260,4), (380,25) and (580,3) and resulted in the quadratic

$$Q(\lambda) = -0.0008906\lambda^2 + 0.745\lambda - 129.49375$$

It is known that the quantum efficiency is not constant over the surface of the PMTube and may vary by as much as 20%. The quoted curve with a maximum of $\approx$ 26% efficiency is used in the model and may therefore be a slight overestimate.

(iii) The scintillation efficiency of the solution in the model is chosen to follow the same curve that Horrocks established for a PPO/POPOP/ Toluene cocktail. The curve is shown in Fig. F3.22 normalized to give a value of 5.2% at 50 keV. The effects of varying this curve on model output is investigated in the next chapter.

113

(iv)   The ß-spectra for ^{3}H and ^{14}C were obtained from
        Fano (National Bureau of standards).[107]   The
        data is included in the listing of the model
        program.   It may be noticed that the spectra
        include correction for screening.

        Other forms of data input,   such as the colour
        or   chemical   quenching   coefficients   or
        electronic   threshold levels are treated as
        variables   and are stated with the output
        results   which are described   in the next
        chapter.

3.4   Model Validation and Performance

3.4.1   Introduction

The ultimate criterion for success of the model is to
produce - without arbitrary adjustment of model variables -
simulated pulse height spectra which are the same as those
obtained with real LSCs over a wide range of quenching
conditions.   This model has been given the properties of a
Packard 300C LSC and hence the criteria relates to spectra
obtained on such a machine.   The comparison of sequences of
spectra is aided by selection of some spectral parameter
such as the mean pulse height of the pulse height spectrum.
This choice of parameter has the additional advantage of
allowing direct comparison with the SIE and SIS of the 300C
and as these QIPs are derived from the mean pulse height.
However, because increased flexibility in analysis of the
spectra was deemed necessary, provision was made to
accumulate the spectra on equipment external to the 300C.

3.4.2   Experimental

A schematic diagram of the equipment used for pulse height spectra capture is shown in Fig. F3.23. LSC signals (pulses) were taken prior to the A/D because (a) the complex digital circuit logic was protected by Packard Instruments Ltd. and (b) access to the raw coincidence gated analogue signal allowed flexibility in further pulse processing.

The line driver was constructed after tests showed the effects of coaxial cable loading of the 300C – see Table T3.4. The performance of the line driver was tested by comparing its input and output pulses. Input pulses were provided by means of a Bradley Model 233 Pulse Generator. T-piece coaxial cable connections to a Gould Digital Oscilloscope 4040 and a MEI millivolt calibrator were used for pulse waveform observation and for pulse amplitude calibration. The pulses used were of 1 to 10 μsec duration and up to 6V amplitude, (corresponding to the maximum amplitude pulses of the 300C), and were shaped to resemble the LSC pulses as displayed on the scope.

Timed accumulation of the spectra were controlled by the NE4625 clock NIM unit. These spectra were then rapidly transferred via a 3D GPIB to a PET 4000 series microcomputer. This was accomplished using a 6502 machine code program which optimized storage by packing the numerical contents of each MCA channel in 2½ 8-bit words.

116

Interleaving of these channel contents allowed a full 1023 channel spectrum to be stored in just 2.5K memory and for numbers exceeding the six digits of the MCA. A suite of ancillary programs allowed (i) dumping of the spectra onto disk or reloading them back into memory, (ii) VDU display with cursor control of screen displayed upper and lower discriminators and (iii) integration over the region of interest together with computation of the mean pulse height (i.e. MCA channel "height"). These programs are listed in appendix B.

The storage scope was used with all spectrum gathering experiments and was particularly useful when the initial pulse handling circuit was changed from the summed configuration. The scope was used to monitor the pulses taken from the LSC. At certain combinations of amplification and time constant settings on the NE4658 Amplifier a sharp spike was produced in the MCA spectrum which corresponded to either regular low level noise or overamplified 'ringing' associated with the valid LSC pulses. A careful (and tedious) watch during spectrum capture ensured correct spectra were accumulated for each sample.

The pulse handling unit labelled SUM/DIFF* in Fig. F3.23 consisted of the standard 300C arrangement for the SUMmed configuration, Fig. F3.24a.

* Refer to chapter 4 for more information concerning difference pulse height analysis.

With the DIFFerence configuration use was made of the good
A.C. and transient properties of isolation transformers. A
16-pin RS Data Bus Isolator (stock No. 208-355) was fitted
with coaxial cable connectors and housed in a shielded box.
Two of the four isolators were set to produce non-inverted
output, one was set to produce inverted output and one was
unused. Pulses of 10-20 nsec duration and up to 0.3 V
amplitude and which were shaped to resemble the LSC pulses
were used to test the isolators. These test pulses were
passed through the isolators in single, summed and
difference configurations. Little or no distortion was
produced by the isolators. When in the summed
configuration the output was observed to be the arithmetic
sum of the inputs and when difference mode the output was
observed to be the arithmetic difference of the inputs
together with a little ringing caused by mismatching the
experimantal test circuit. The difference configuation
using the isolation transformers in the LSC is shown in
Fig. F3.24b.

The second non-inverting transformer was used in place of
the inverter to reproduce the summed configuration in the
LSC but this time with the extra components present.
Investigation of any effects of the additional components
resulted in little or no detection of changes in the output
see Figs. F3.25 and F3.26. Propagation delays on these
isolators is less than 5 ns and is well within the delay
loop (of approx 150 ns) incorporated in the 300C. No
attempt was made to adjust the delay loop.

Other pulse handling configurations such as ratios (P_1/P_2)
or products (P_1P_2) were not implemented experimentally.
They could be readily installed by means of logarithmic
amplification of each PMT pulse separately prior to summing
or differencing.

Being satisfied with the experimental technique used for
the experimental pulse height spectra capture, a variety of
colour and chemically quenched ^{3}H and ^{14}C-labelled samples
were counted. These samples were those used previously for
triple-label dpm determination in chapter 2. The resultant
spectra were then used to obtain calibration curves and
hence assess model performance.

In assessing this performance the model variables used to generate the simulated data were as follows:

NUCLIDE	= H or C	for ^{3}H and ^{14}C respectively
CNTMODE	= C	to select accumulation of No. of counts and No. of disintegrations.
NDISNTGS	= 1000	and is the No. of accumulated counts or No. of disintegrations.
BSF[1] and [2]	= 0.2, 0.2	shape factor 'B' for the two dynodes
DYM[1] and [2]	= 3.94, 3.94	dynode mean gain for the two dynodes
VHT	= 0.047	vial height
VRAD	= 0.0147	vial radius
LHT	= 0.02	liquid height
LRAD	= 0.0125	liquid radius
CHT	= 0.04374	chamber height
CRAD	= 0.02286	chamber radius
THRESHOLD	= 0	electronic (pulse height) threshold

and the quantum efficiencies, fluorescence spectra, absorption spectra, scintillation efficiencies, collection efficiencies, ß-spectra, refractive indices and dispersion are all as defined in section 3.3. The chemical and colour quench factors QCHEM and QCOL are stated with the results. The above model settings are henceforth called the standard model settings and apply to all results unless otherwise stated.

3.4.3 Results and Discussion

Tables T3.5 to T3.8 and Figs. F3.27 and F3.28 show the results obtained experimentally for ^{3}H- and ^{14}C- labelled colour and/or chemically quenched samples. The experimentally obtained calibration curves demonstrate the differences between coloured and chemically quenched samples using the mean summed RPH as a QIP. The results agree with numerous other workers mentioned previously.

The associated results for the model are shown in Tables T3.9 and T3.10 and Figs. F3.29 and F3.30.

The modelled curves show the same trends as found practically, with the model correctly changing its output spectra and resultant calibration curves with changes in both type of quench and isotope energy.

Closer inspection reveals some differences between the experimental and modelled results. The tritium modelled efficiencies reach 67% approximately for an unquenched sample whereas the most unquenched experimental efficiency was approximately 52%. One reason for this is the presence of quenching materials in even the least quenched of the experimental samples. When originally prepared, for triple label work, the samples reached efficiencies approaching 60% as can be seen in Fig. F3.31 although in this case SIE(AEC) was used as the QIP. Results of further runs with the model using a greater number (5000) of counts and with

121

mixtures of colour and chemical quenchers are shown in Tables T3.11 and T3.12 and Figs. F3.32 and F3.33.

The 5000 count samples give similar calibration curves to the 1000 count samples but with more precision. The modelled colour and chemical quench calibration curves separation is observed to be slightly smaller than that observed experimentally. The absence of electronic thresholds or the choice of BSF[1]=0.2, BSF[2]=0.2 may be responsible for this. With the mixed colour/chemical quenched samples, the modelled addition of colour quench to chemically quenched samples shifts the calibration point towards the colour quench curve as expected. Quantification of this shift for ^{3}H does not appear to be feasible for spectra based on 5000 counts or less using the summed pulse height spectra although the results indicate a discernable separation at high quench levels.

With limits of 1000 or 5000 counts being set by time constraints a check on the repeatability of the results was made using modelled ^{14}C: Tables T3.13 (a) and (b).

Overall, the results are encouraging and the effects of other variables of the model were briefly explored in the limited time available.

The effect of imposing a threshold on the PMTube outputs prior to spectral storage is shown in Tables T3.14 (a) and (b) and Figs. F3.34 and F3.35. The results indicate that a

threshold of 1 should perhaps be used in the model. However, in the absence of experimentally determined electronic thresholds the use of the standard model settings was continued and the matching of threshold levels is left as a future development of the model. Known amplitude pulses from a pulse generator could be fed into the LSC in place of the PMTube pulses and the coincidence pulses. Variations in pulse amplitude and observations of the resulting LSC output would lead to estimation of the threshold. Careful matching of impedances of the equipment to resemble the PMTube output impedence would, of course, be necessary.

Since the model is capable of utilizing purely colour quenched samples, the effects of a series of hypothetical quenchers were compared. One of the colour quenchers has a uniform absorption spectrum over the range 300 nm to 400 nm and the other three had step response absorption spectra from 300 nm to 600 nm, from 400 nm to 500 nm and from 500 nm to 600 nm respectively. These are shown along with the O7 absorption spectrum colour quenching results in Table T3.15 and Fig. F3.36. It is observed that although different amounts of the colour quencher are needed to reduce the counting efficiency by comparable degrees, (as expected from the differences in spectral matching to the solute fluorescence spectrum), the resultant calibration curves follow the same trend. A single general colour quenching curve could be used for all the different colour quenchers measured. Of course, practical colour quenchers

also have an associated chemical quench when added to a LS cocktail and it is the colour to chemical quench ratio that requires determination.

Also briefly examined was the effect of varying the PMTube quantum efficiency and PMTube dynode shape factor, (Tables T3.16 and T3.17 and Figs. F3.37 and F3.38), and the scintillation efficiency (Table T3.18 and Fig. F3.39). The choice of an exponential shape factor is seen to degrade the PMTube resolution so much that the effects of colour and chemical quenching are indistinguishable. This doesn't present a method of quench correction independent of the colour/chemical ratio however because of the larger scatter associated with the poorer resolution. A move to a more poissonian shape factor than 0.2 would not appear to lead to much greater colour or chemical quench curve separation. The reduced quantum efficiency was chosen to be 21.5% on the basis of Persyk's comments on the quantum efficiency variation over the surface of a PMTube. The results more closely resemble the experimental curves. The PMTube face is an area which requires further modifications including the variation of quantum efficiency of the surface and the curvature of the face glass. Changing the scintillation efficiency from Horrocks data to a constant 4.5% caused an increase in efficiency and in mean pulse heights but in such a way as to make the calibration curve more bowed in the direction seen for isotopes of increasing energy. This implies that selection of a constant 4.5% scintillation efficiency for all ^{3}H ß-particle energies is incorrect and

124

too high. Future runs with the model may shed further light on the effects of scintillation efficiency as a function of ß-particle energy.

One last study shows the effects of varying the solution volume. Results are shown in Table T3.19 and Fig. F3.40 and agree with results obtained experimentally.

It is evident that the model opens several avenues of research, but the main reason for its developement was to provide a tool for the investigation of new quench correction techniques. This subject is dealt with in the next chapter.

Chapter 4

QUENCH CORRECTION INDEPENDENT OF THE TYPE OF QUENCH

This chapter summarises the results of the application of
the LSC Model to the colour-chemical quench correction
problem. A practical method of quench correction which is
independent of the type of quench for homogeneous systems
is presented and experimentally confirmed.

4.1 Application of the LSC Model to the Colour-Chemical Quench Correction Problem

4.1.1 Introduction

Recalling the comments made in section 3.1 there are two approaches to solve the colour-chemical quench correction problem. Simultaneous summed-pulse-height analysis – differenced-pulse-height analysis and simultaneous summed and ratioed pulse-height analysis are representative of the approach to quantify the colour/chemical ratio, whereas product pulse height analysis, singly-applied upper-discriminator pulse-height analysis and modified-product pulse height analysis are representative of the approach to produce a single calibration curve which is applicable to both colour and chemically quenched samples. The difference, ratio and product pulse height spectra have been defined previously.

The singly-applied upper-discriminator approach simply involves the use of an ordinary summed pulse height spectrum, but for pulses where both are less than an upper discriminator which is applied to each pulse prior to summation. Events which produce pulses exceeding the discriminators are used only to provide the total count and not as part of the spectrum upon which the QIP is based. The discriminators are decreased with increasing quench. The basic idea behind the method can be regarded as an inverted case of Laneys' crosstalk eliminator

127

discriminators. The modified-product spectrum is a development of the product spectrum. It consists of a product spectrum which is linearly stored for events corresponding to approximately $\frac{1}{3}$ mean ß-particle energy with the rest of the spectrum linearly compressed into a few channels. (See Fig. F4.1).

All counts are used for the efficiency determination provided coincidence is achieved and the mean channel is taken over the whole modified spectrum to give the QIP.

The results of the application of all these methods using the model are described below.

4.1.2   Results and Discussion

Tables T4.1, T4.2 and T4.3 present model generated results
for simultaneous coincidence sum, difference and ratio
pulse height spectra for ^{14}C and ^{3}H respectively. (Plots
of counting efficiency vs mean summed pulse height have
been presented in section 3.4).

For difference pulse height spectra and ratio pulse height
spectra to be useful as second parameters for colour/
chemical ratio quantification the variation in these pulse
height spectra must be different from that of the sum pulse
height spectra under conditions of varying colour or
chemical quench.   That this is, in fact, the case, as first
supposed in section 3.1, is shown in Figs. F4.2 to F4.8.
With ^{14}C the mean difference pulse height vs mean summed
pulse height curves for colour and chemical quench are
widely different, thus indicating that these parameters may
be used for colour-chemical ratio quantification.   The form
of the divergence between the curves may be explained by
considering typical pulses (P_1 and P_2) produced with colour
and with chemical quenched samples.   With coloured samples
P_1 and P_2 are more often dissimilar (and by larger margins)
than with chemical quenched samples.   The difference
between the two pulses will thus, on average, be greater
for coloured samples than for chemical quenched samples.
Without the distortions caused to the relative pulse
heights P_1 and P_2 by colour · quenching the relationship
between the mean of the summed pulse heights to the mean of

the differenced pulse heights is approximately linear.
With ^{3}H the same general trend is observed but is smaller
owing to the smaller energy range (and hence pulse heights)
involved.

The use of ratio pulse height spectra as a route to
quantification of the colour-chemical ratio met with only
limited success. The colour quenched samples result in a
curve which is greater than that for chemical quenched
samples because the ratios of the more dissimilar colour
quenched pulses deviate more from the mean. The ratio
pulse height spectra as modelled ranges from 0 to 1 with
the mean value being 0.5 for all samples and colour
quenching be characterised by greater spread. The standard
deviation, σ, was used as a measure of the spread and it is
because of the reliance on the 2nd moment of a distribution
that the ratio σ approach suffers more from scatter than
does the difference-mean. Whether the ratio σ method would
be good enough experimentally depends on the relative
benefits of using full pulse heights and not differences in
the prescence of machine noise, thresholds and background.
A simpler technique relying on the 1st and 2nd moments of a
distribution is measurement of the mean and standard
deviation of the ordinary summed pulse height spectra and
use of efficiency vs sum pulse height and sum σ vs mean sum
as calibration curves. However, Fig. F4.6 shows no
calibration curve separation is achieved for ^{3}H. This is
not so surprising since the sum pulse height spectra does
not exaggerate colour and chemical quenching effects, as

explained previously.

The efficiency vs product pulse height spectra quench indicating parameter calibration curves for ^{3}H and ^{14}C are shown in Figs. F4.9 and F4.10. (Tables T4.4 and T4.5). As explained in chapter 3, colour quenched product pulses are weakly dependent on the β-event position in the vial. By analogy to the summed pulse height case this results in the colour quenched product pulse height spectra being broader (and thus having a greater mean) than the chemically quenched product pulse height spectra for samples of equivalent efficiency. As quenching increases, this effect becomes more pronounced until quenching is so great that the statistical variation in the (small) numbers of photons destined for each PMTube begins to contribute significantly to the pulse height spectra and thus mask the effect. Also, the product spectrum reduces the differences between the two types of quench because of the logarithmic transformation of the individual pulse heights <u>before</u> summation. Small pulses are little affected, in contrast to larger pulses, and because of the relative sizes of the ^{3}H and ^{14}C pulses the effect of the logarithmic transformation is more pronounced with ^{14}C. It is suggested that within the limitations imposed by the amount of data obtained, the combination of the above effects accounts for the efficiency vs mean product pulse-height calibration curves. The modified pulse height spectrum for ^{3}H gives the desired single calibration curve for colour and chemically quenched samples. (Fig. F4.11 and Table T4.6). ^{14}C results are not

131

available.

Although more data on the product-based pulse height spectra is needed before any firm conclusions can be drawn, it would be interesting to further check the model predictions and perhaps put the product-based techniques into practice. The methods would have the advantages over the sum + difference method in (i) not relying on small _difference_ pulse heights and (ii) using just one calibration curve for each isotope.

The singly-applied upper discriminator approach failed to produce a uniform quench calibration curve for colour and chemically quenched samples, (see Fig. F4.12 and Table T4.7), and was thus not studied further.

From the above model-based studies the sum + difference, the sum + ratio and product and modified product methods all seem capable of quench correction independent of the colour-chemical quench ratio and are all worthy of experimental investigation. However, the sum + difference method was selected as the most promising to put theory into practice. The experimental performance of this quench correction technique is described in the next section (4.2).

4.2   Quench Correction Independent of the Type of Quench

4.2.1   Introduction

The technique of quench correction independent of the colour-chemical quench ratio using the summed pulse height spectra and differenced pulse height spectra, (the SD technique) involves the following stages:

(a) accumulate the summed pulse height spectra simultaneously or sequentially

(b) accumulate the differenced pulse height spectra simultaneously or sequentially

(c) use the mean difference pulse height and mean sum pulse height to determine the F_2 ratio

(d) use the F_2 ratio and the $F_1 F_2$ calibration curve to derive F_1 and hence the corrected efficiency.

The ratios F_1 and F_2 are defined in Fig. F4.13 and are the fractional distances between the chemically quenched and colour quenched calibration curves of efficiency vs mean sum pulse height and mean difference pulse height vs mean sum pulse height respectively.

So far, only results based on the spectra obtained with isotopes which are internally dissolved in the LS solution have been modelled and experimentally verified. However, a common disadvantage of all internal-isotope quench correction techniques is their poor performance with low activity and/or low energy isotopes.

133

For the sum + difference quench correction technique (or SD technique) to be universally accepted it must be practicable with a high activity, high energy external standard. Extension of the SD technique to cover the use of external standards, although earmarked as a future development, presents problems which lie outside of the scope of the first generation of the LSC simulation.

It was believed however that the same distance dependency with colour quenched samples should be observed with the external standard as a source unless the distribution of events was randomly spread throughout the vial solution. If there existed a non-symetrical distribution of external standard fluorescence-events in the solution the difference pulse height spectra, which is specifically designed to exaggerate colour quenching effects, should vary in a manner similar to that obtained with internally dissolved ß-emitters.

The ^{226}Ra external standard of the Packard 300C is pneumatically driven to a point close to the outside of the vial which is nearer to one PMTube than the other and hence gives a fluorescent event distribution which is non-symmetrical in relation to the two PMTubes. This feature was exploited to investigate the plausability of the SD technique.

4.2.2   Experimental

^{3}H and ^{14}C colour and chemically quenched samples were those previously used in section 2.3 and 2.2. A series of ten of each isotope and type of quench were reserved for efficiency vs mean sum pulse height calibration curves and mean sum pulse height vs mean difference pulse height calibration curves. To the remaining samples random amounts of disperse orange dye O7 and carbon tetrachloride colour and chemical quenchers were added such that the total volume was within 10% of 10 ml and within the efficiency range >90% to <1% for ^{14}C, and 50% to 1% for ^{3}H. All the samples were counted using the equipment and methods described in section 3.3. Although simultaneous counting of the sum and difference pulse height spectra was performed during simulation and is desirable commercially, the spectra were obtained sequentially in these experiments.

When using external standards short counting times were used in keeping with currently accepted practices. The samples used were those containing ^{14}C and ^{3}H described above. All pulse height spectra were stripped of the ^{14}C or ^{3}H contribution by successive equal timed counting with and without the external standard present.

135

4.2.3 Results and Discussion

Tables T4.8 and T4.9 and Figs. F4.14 and F4.15 give results obtained for the $^{14}C-$ and ^{3}H-labelled colour and chemically quenched samples.   With the ^{14}C samples the form of the variation of the mean of the difference pulse height spectra with the mean of the sum pulse height spectra for colour and chemically quenched samples is in accord with the   model predictions.   This promotes   even greater confidence in the model which now correctly accounts for sum and difference pulse height behaviour with colour or chemical quench and ^{3}H or ^{14}C isotopes.   With ^{3}H the general trend of greater mean difference pulse heights for colour quenched samples is demonstrated but is almost obscured by the large scatter` associated with taking differences of small pulses in the presence of noise.   The noise factor was not incorporated into the model and seems the most likely explanation of the results obtained.   An interesting feature of the ^{14}C results is the fact the the difference between the two calibration curves is larger than that predicted.   This occurred to some extent with the efficiency vs mean sum pulse height calibration curves and may be a feature of the chosen variables in the model. Another possible cause, and one not present in the model, may be mismatching in the response of the two PMTubes plus the counting circuit.   This would be equivalent to having uneven electronic thresholds in the model.   The possibility of mismatching was investigated by means of a vial (containing an unquenched cocktail of 10 g l^{-1} b-PBD in

p-Xylene) which was half coated with red tape such that the full length and half circumference of the curved surface was covered. This vial was counted in the presence of the external standard for various rotational orientations with each PMTube individually. Results are shown in Table T4.10 and Fig. F4.16. The different levels of recorded external standard activity for each PMTube indicate that some mismatching was present. The actual form of these curves shows the effect that a non symmetrical colour quench distribution has on the recorded external standard activity using single pulse height spectra and encouraged the investigation of the external standard SD technique (ESSD technique).

The insensitivity of the mean sum pulse height of the external standard to type of quench has been reported by many authors and is confirmed here - the colour and chemical quenched samples following an identical curve (Fig. F4.17 and Table T4.11). (N.B. The external standard counting efficiencies are quoted as relative to that obtained with the least quenched sample).

The variation of the mean differenced pulse height with mean summed pulse height is observed to follow the general pattern predicted by the model for internal isotopes of increased energy and confirms the expected colour-chemical dependence for a non symmetrically positioned external standard. The colour chemical dependence can even be shown with just the coincidence single PMTube pulse height

137

spectra (see Table T4.12 and Fig. F4.18). The very positive results of Tables T4.11 and T4.13 which are shown in Fig. F4.19 validates the use of the SD technique over the same wide range of homogenous samples currently counted using external standards.

Results of the implementation of the ESSD technique are given in Tables T4.14 to T4.18. The ^{14}C efficiency vs External Standard mean sum pulse height spectra and the efficiency vs ES mean sum pulse height spectra calibration curves for colour, chemical and mixed colour and chemical quenched samples are shown in Figs. F4.20 and F4.21. From these curves suitable candidates (part way between the pairs of curves) were chosen to determine the relationship between position relative to the colour and chemical curves of Figs. F4.20 and F4.21 for ^{3}H and ^{14}C respectively and position relative to the colour and chemical curves of Fig. F4.19. To do this natural cubic splines were fitted to the curves of Figs. F4.20 and F4.21 in accordance with the conlusions of section 2.3 and least squares cubic polynomials were fitted to the curves of Figs. F4.19. The F_1 and F_2 ratios were then plotted for the selected mixed colour and chemical quenched standards (see Figs. F4.22 and F4.23 and Tables T4.16 (a) and (b)).

Owing to the large scatter of the F_1F_2 plots a simpler least squares quadratic was fitted to the data. It is noted that the relative variation in the F_1F_2 ratios is similar and appears largely independent of the isotope.

An approach using distance below the chemical quench curve (and not limited to the mean sum pulse height range of the colour quench curve) gave a series of colour-chemical calibration curves dependent on the combined total amount of quench and was therefore rejected.

The efficiencies predicted by the ESSD technique are presented in Table T4.17 for ^{14}C and Table T4.18 for ^{3}H and are compared with the efficiences calculated from the known dispensed activity of each sample. For the ^{14}C samples which do not require extrapolation of the colour quenched efficiencies vs mean sum pulse height calibration curve, efficiencies are determined to within 2.5% down to counting efficiencies of 60%. Also, even with extrapolation, results are still within 3.5% down to counting efficiencies of only 30%. For ^{3}H sample efficiencies are determined to within 1.5% over the range of cocktail, colour quencher and chemical quencher composition used.

In view of the use of non-optimal external standard position and samples with up to 10% volume variation and only 20s external standard counting times these results are excellent. They prove that a significant improvement in LSC can be achieved by adoption of the ESSD (and SD) method. The success of the method also completely vindicates the use of simulation in LSC and increases confidence in the likely success of the other methods proposed in this chapter.

4.3 Future Work and Recent Developments

Future work which promises to be of practical benefit includes experimental investigation of product based pulse height spectra, and extension of the model to include the effects of noise and background and alternative vial-counter geometries. More challenging extensions would be to include the external standard option and to include non-homogeneous micellar solutions. A second generation model should attempt to incorporate the time dimension. This would greatly enhance the usefulness of the model, allowing such techniques as pulse shape discrimination to be studied in detail and hopefully lead to the development of new α, β and γ counting and quench correction techniques.

The importance of attempts to attain a widely applicable quench correction method is not lost on the LSC industry. Recently, LKB-Wallac OY of Finland have introduced a new LSC (the LKB Spectral) which is claimed to be capable of quench correction independent of the colour-chemical quench ratio. No data has yet been published describing the actual techniques used in the Scientific Literature, although a source from within the industry has indicated that two pulse height spectra are jointly used.

Addendum

Since the completion of this thesis a Product News Bulletin
from LKB-Wallac has been obtained.[*] In it there is a
description of the quench correction technique used by the
model "1219 Spectral". The essential point is that use is
made of a simultaneously gathered summed-coincidence pulse
height spectrum (p.h.s.) and a pulse height spectrum
dependent on the ratio of the individual PMTube pulses
(from a two PMTube system). Unfortunately, the exact form
of this p.h.s is not stated nor whether the external
standard is used for the determination of the colour quench
parameter.

However, the basis of the technique is apparently similar
to one of the methods proposed in this thesis. This adds
yet further support for the (anticipated) utility of those
methods and for the use of simulation in Liquid
Scintillation Counting.

[*] LKB-Wallac "Product News", August 1985, K Rundt, T
Oikari and H Kouru

140a

COLLECTED FIGURES
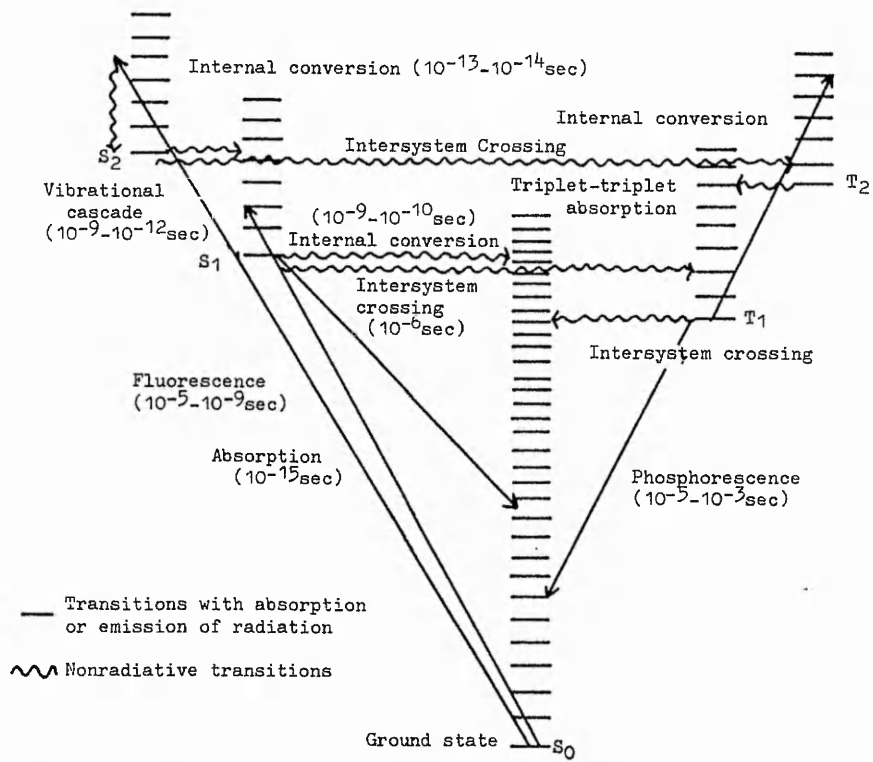
Fig. F1.1   Modified Jablonski diagram showing the various processes that can occur upon excitation of an organic molecule

Fig. F1.2   Excimer photophysical processes

Lines with // through them are not implemented in my model

Fig. F1.3 Photon pathways from Scintillation Liquid to PMT

143

Figure panels (left column, ^{14}C in toluene):

- ^{14}C in toluene 80% eff. — Chemical quench, Colour quench; CPMx10^3/channel vs Relative pulse height or channel number
- ^{14}C in toluene 70% eff. — Chemical quench, Colour quench; CPMx10^3/channel vs Relative pulse height or channel number
- ^{14}C in toluene 60% eff. — Chemical quench, Colour quench; CPMx10^3/channel vs Realtive pulse height or channel number

Figure panels (right column, ^{3}H in toluene):

- ^{3}H in toluene -40% eff. — Colour quench, Colour quench, Chemical quench; CPMx10^3/channel vs Relative pulse height or channel number
- ^{3}H in toluene -25% eff. — Colour quench, Colour quench, Chemical quench; CPMx10^3/channel vs Realtive pulse height or channel number
- ^{3}H in toluene -15% eff. — Colour quench, Colour quench, Chemical quench; CPMx10^3/channel vs Realtive pulse height or channel number

Colour versus chemical quenching of ^{14}C; differences between spectra at same levels of efficiency.

Colour versus chemical quenching of ^{3}H; differences between spectra at same levels of efficiency.

Fig. F1.4
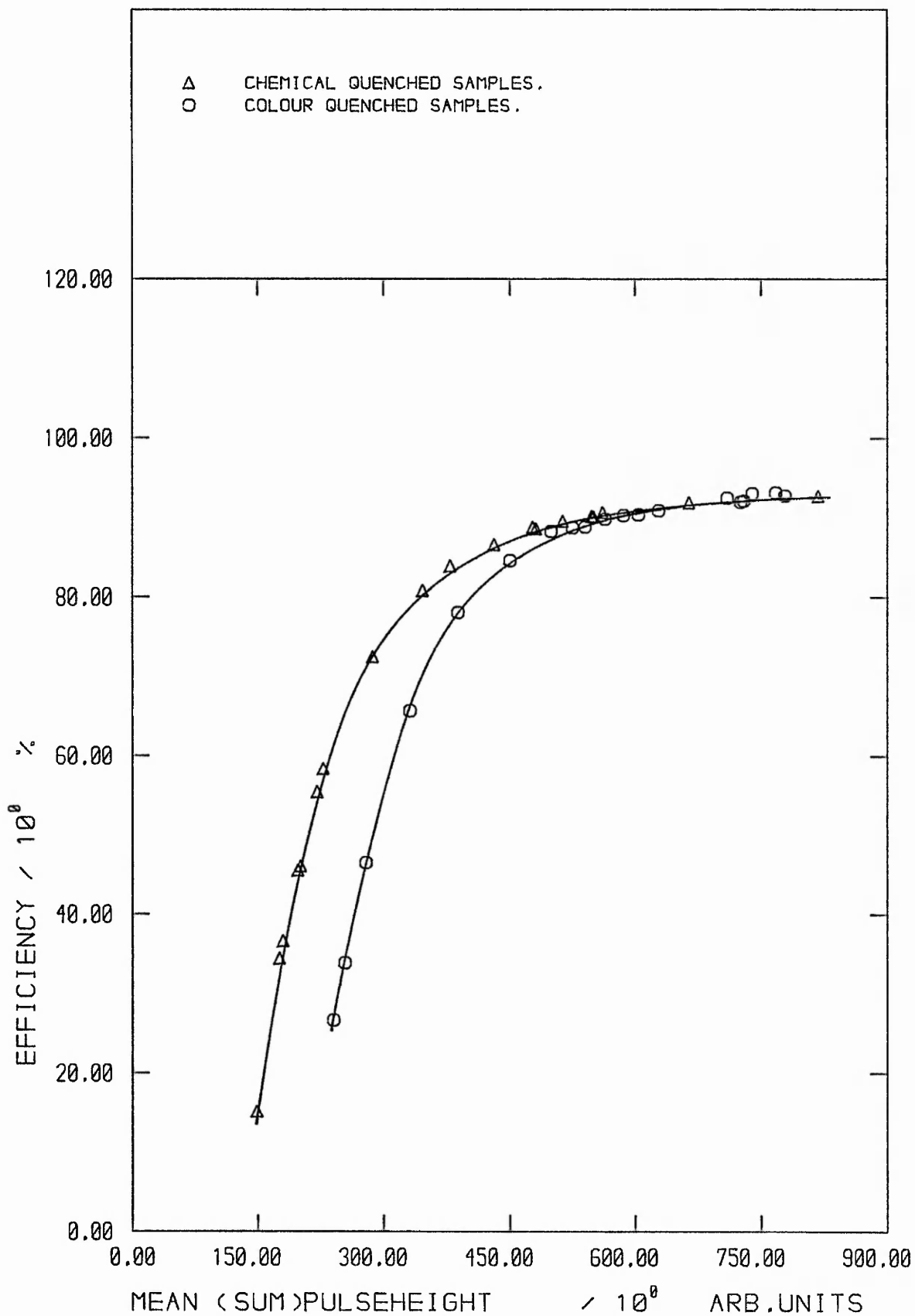
FIG F1.5 : TYPICAL EFFICIENCY v SIE(AEC)
COLOUR/CHEMICAL QUENCH CALIBRATION CURVES

Two-parameter spectrum of ^{36}Cl

Two-parameter spectrum of ^{3}H

Two-parameter spectrum of ^{14}C

Background 2-parameter spectrum

^{14}C chemically quenched to 70% efficiency

^{14}C colour quenched to 70% efficiency
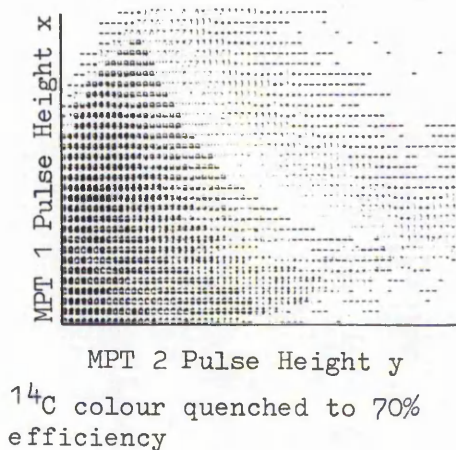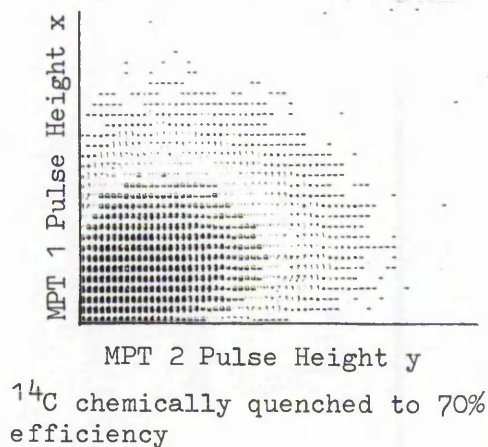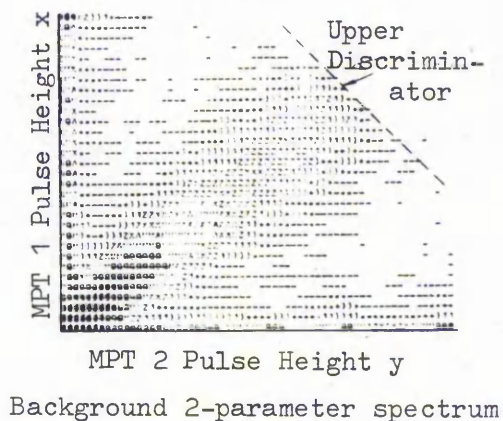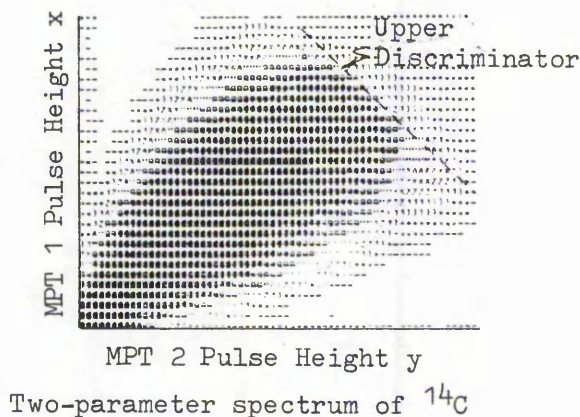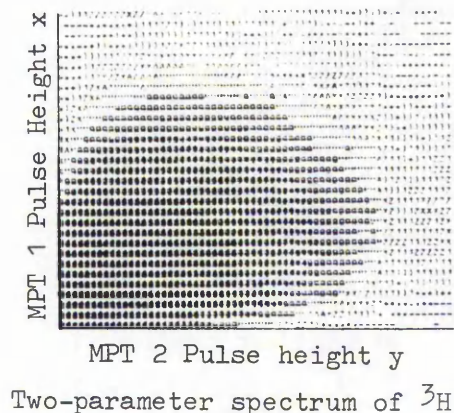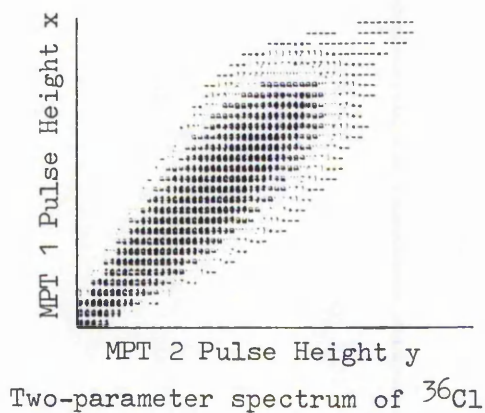
Fig. F1.6 Two parameter pulse height spectra

Perfect
absorber

Threads

Glass wall

Solution

H

Irregular
base

Perfect
absorber

EXPERIMENTAL
VIAL

SIMULATED
VIAL

Perfect
absorber

Glass wall
and
Solution
are assumed to be
optically continous

Perfect
absorber
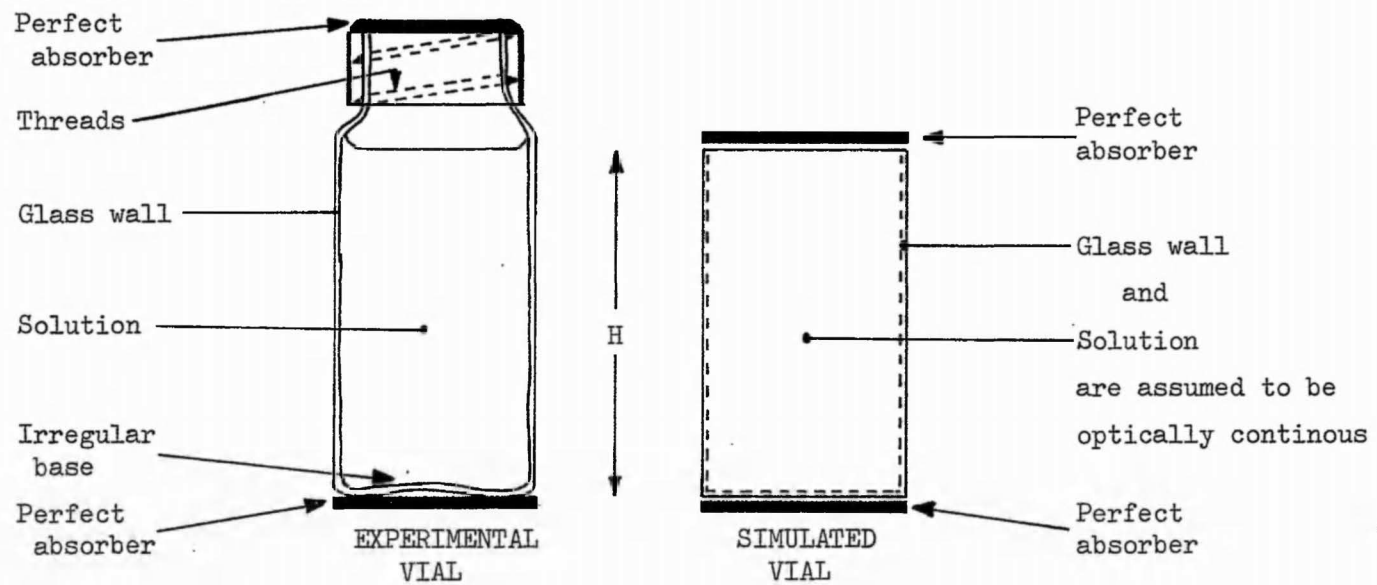
Fig. F1.7   Diagram comparing experimental and simulated vials in Stanley's Model

```
┌─────────────────────────────────────────┐
│   Nuclear energy available/released      │
│          e.g. 19keV for 3H               │
└─────────────────────────────────────────┘
                    │
┌─────────────────────────────────────────┐
│       'Nuclear quenching' due to         │
│     antineutrino taking some energy      │
└─────────────────────────────────────────┘
                    │
┌─────────────────────────────────────────┐
│      Ionization quenching due to         │
│    <100% scintillation efficiency        │
│           of LSC cocktail                │
└─────────────────────────────────────────┘
                    │
┌─────────────────────────────────────────┐
│       Chemical quenching due to          │
│   extra energy scavenging material       │
│           added to cocktail              │
└─────────────────────────────────────────┘
                    │
┌─────────────────────────────────────────┐
│        Colour quenching due to           │
│   photon absorbtion in the cocktail      │
└─────────────────────────────────────────┘
                    │
┌─────────────────────────────────────────┐
│       Optical quenching due to           │
│   photon absorbtion in vial glass,       │
│        in counter chamber, etc.          │
└─────────────────────────────────────────┘
                    │
┌─────────────────────────────────────────┐
│      'Quantum quenching' due to          │
│    <100% efficiency of photocathode      │
│      of each photomultiplier tube        │
└─────────────────────────────────────────┘
                    │
┌─────────────────────────────────────────┐
│         'PMT quenching' due to           │
│   <100% efficiency of photomultiplier    │
│               dynodes                     │
└─────────────────────────────────────────┘
                    │
┌─────────────────────────────────────────┐
│     'Electronic quenching' due to        │
│    detection threshold of counting       │
│               system                     │
└─────────────────────────────────────────┘
                    │
┌─────────────────────────────────────────┐
│    Pulse output to counter/storage       │
└─────────────────────────────────────────┘
```

Fig. F1.8   Quenching and the LSC Process

Relative pulse distributions for single-labeled ^3H and single-labeled ^{14}C containing sample (a) compared with sample labeled with both ^3H and ^{14}C (b).
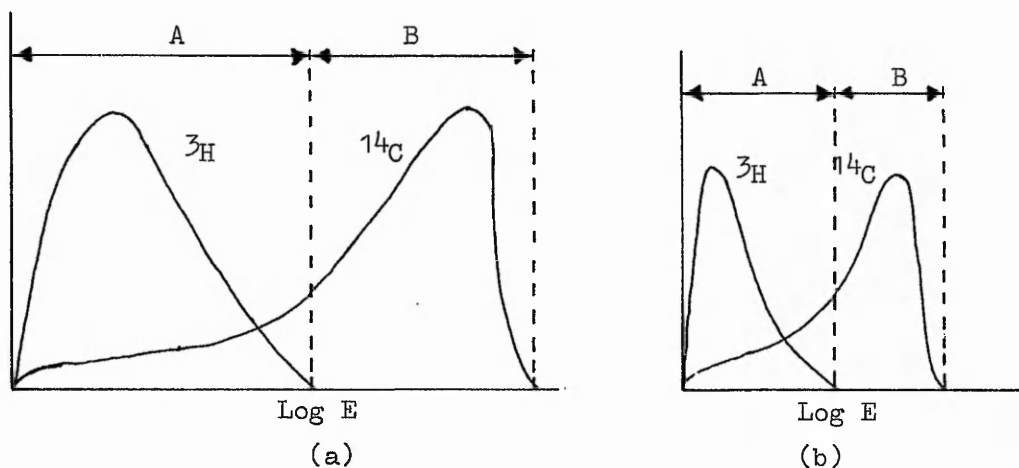
Window settings for counting ^3H- and ^{14}C-containing samples with optimization of separation of ^{14}C- and ^3H-produced pulses, showing settings for (a) unquenched sample and (b) quenched sample.

Fig. F1.9 Dual label windows for ^{14}C and ^3H
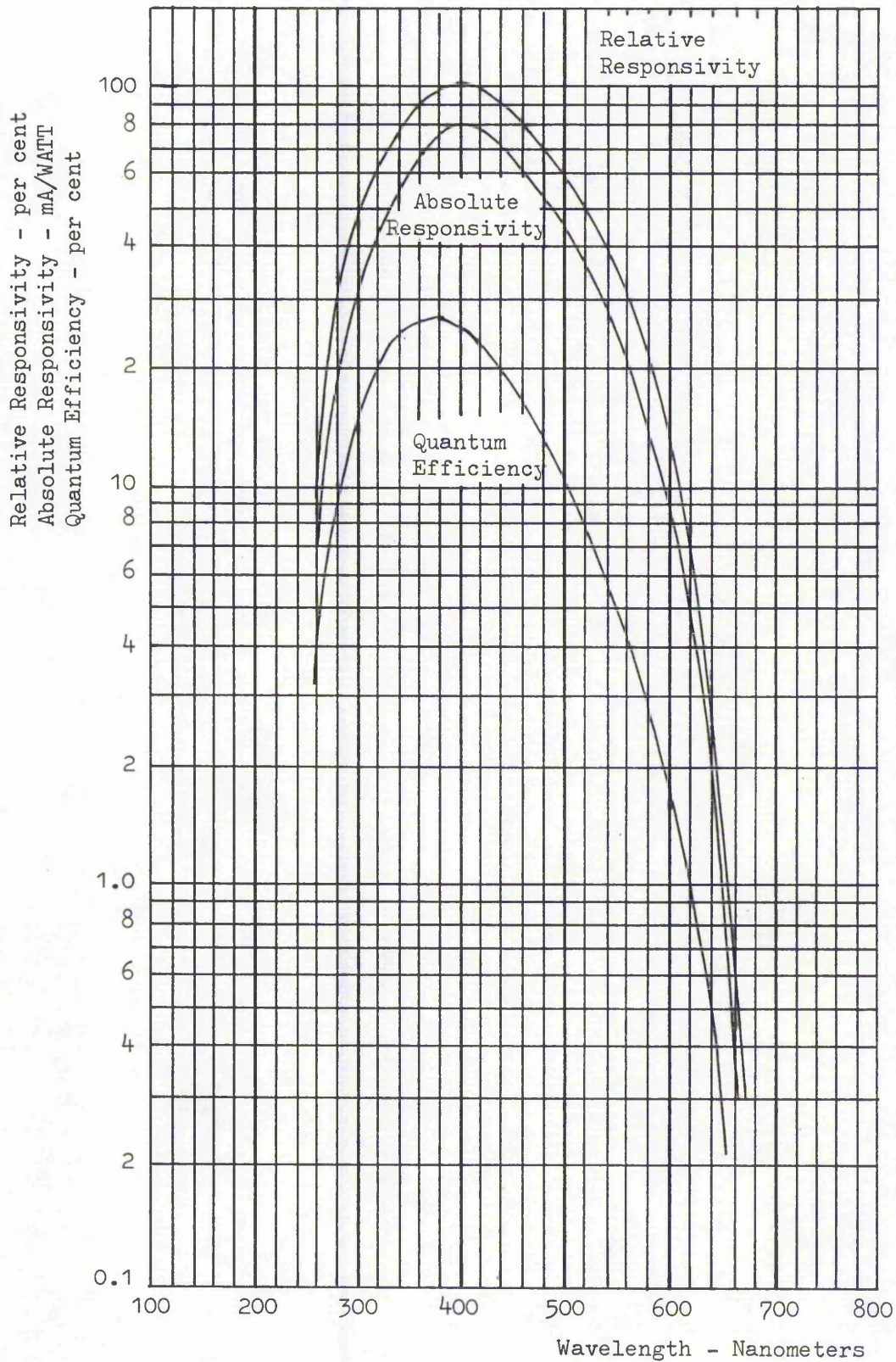
Fig. F1.10 Typical Photocathode Responsivity Characteristics
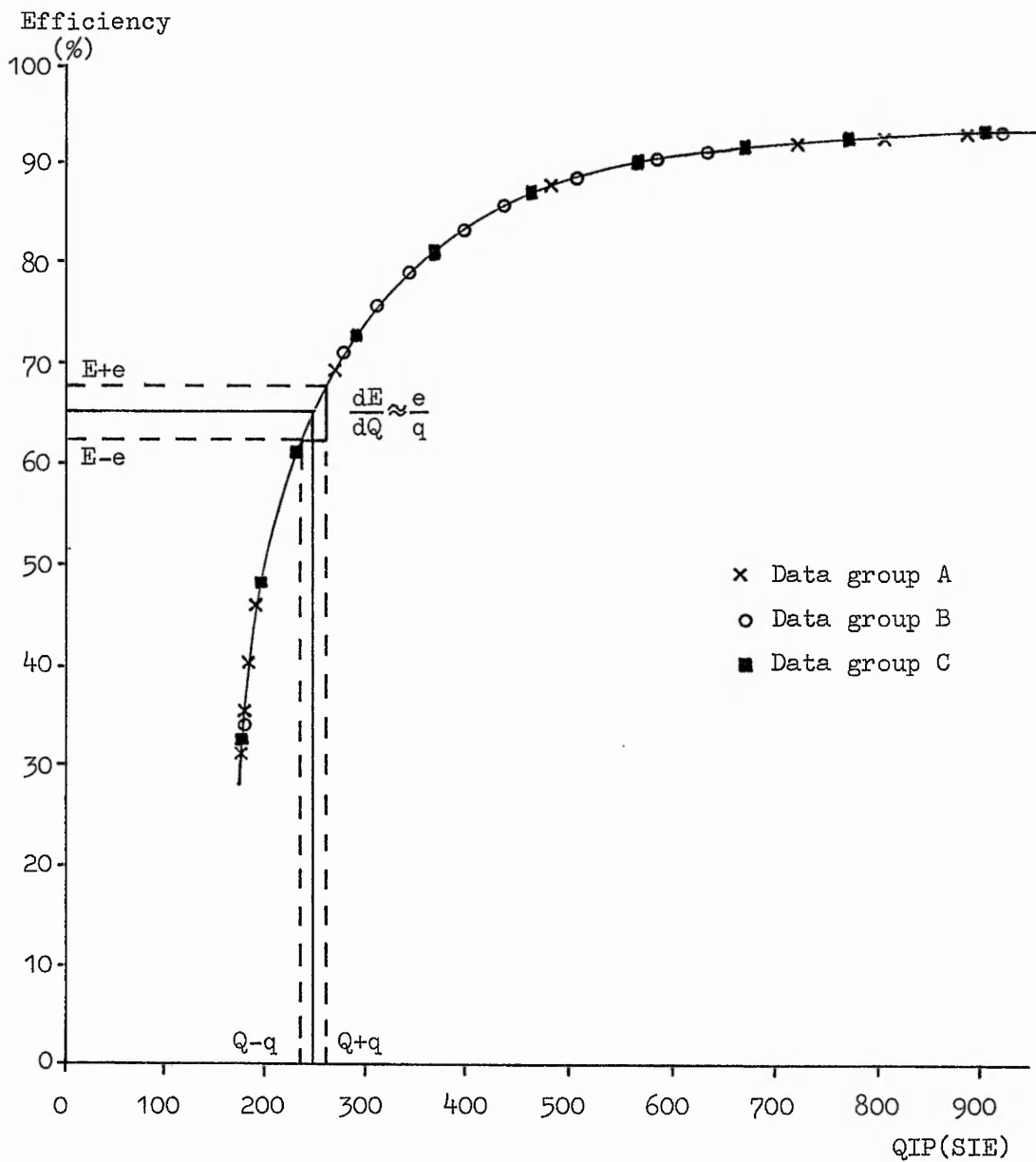
Fig. F2.1 Typical ^{14}C Efficiency v QIP curve showing data group types

151
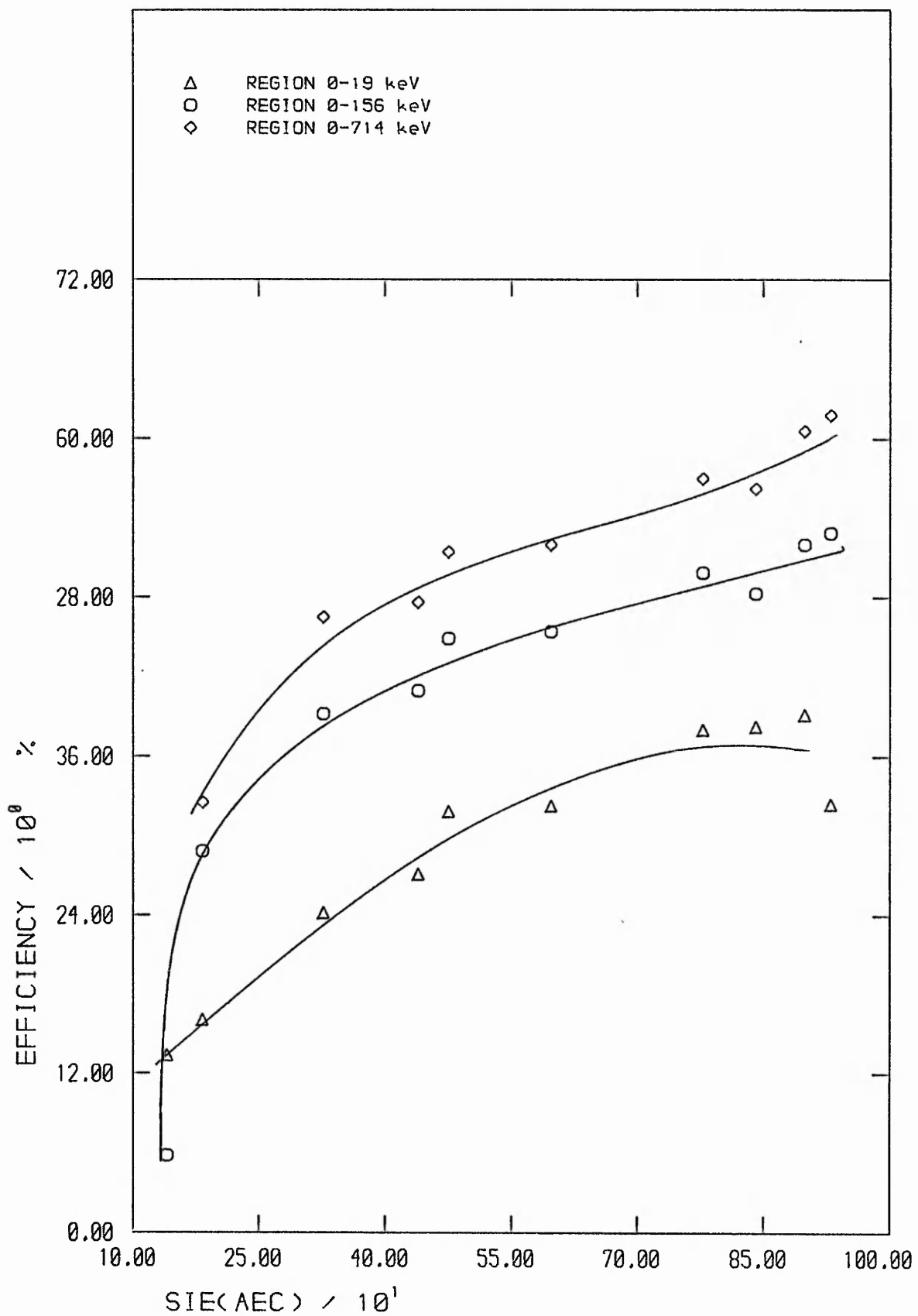
FIGF2.2 : BACKGROUND COUNTRATE vs SIE(AEC)
        - SINGLE LABEL REGIONS

152
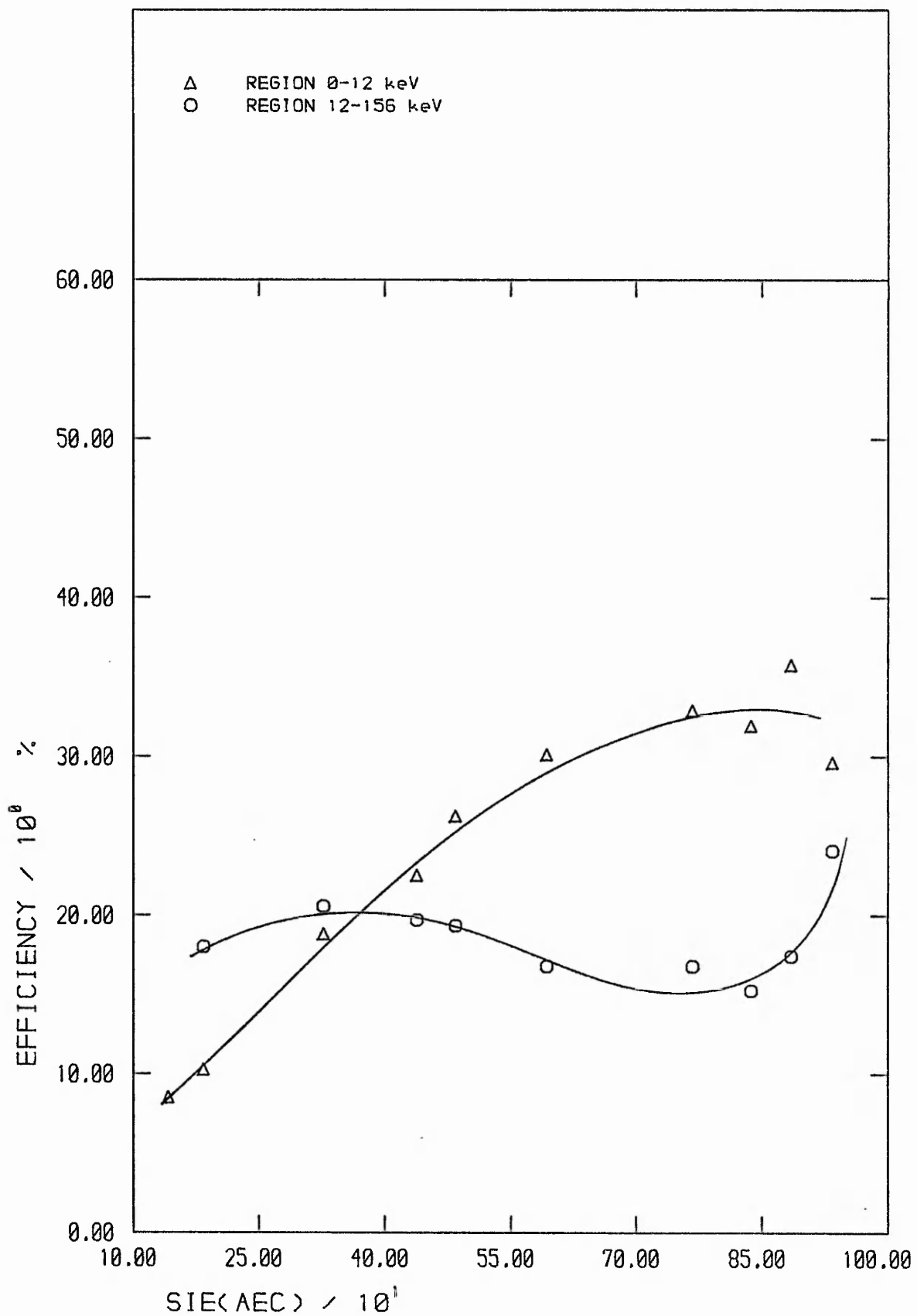
FIGF2.3 : BACKGROUND COUNTRATE vs SIE(AEC)
         - DUAL LABEL REGIONS

153
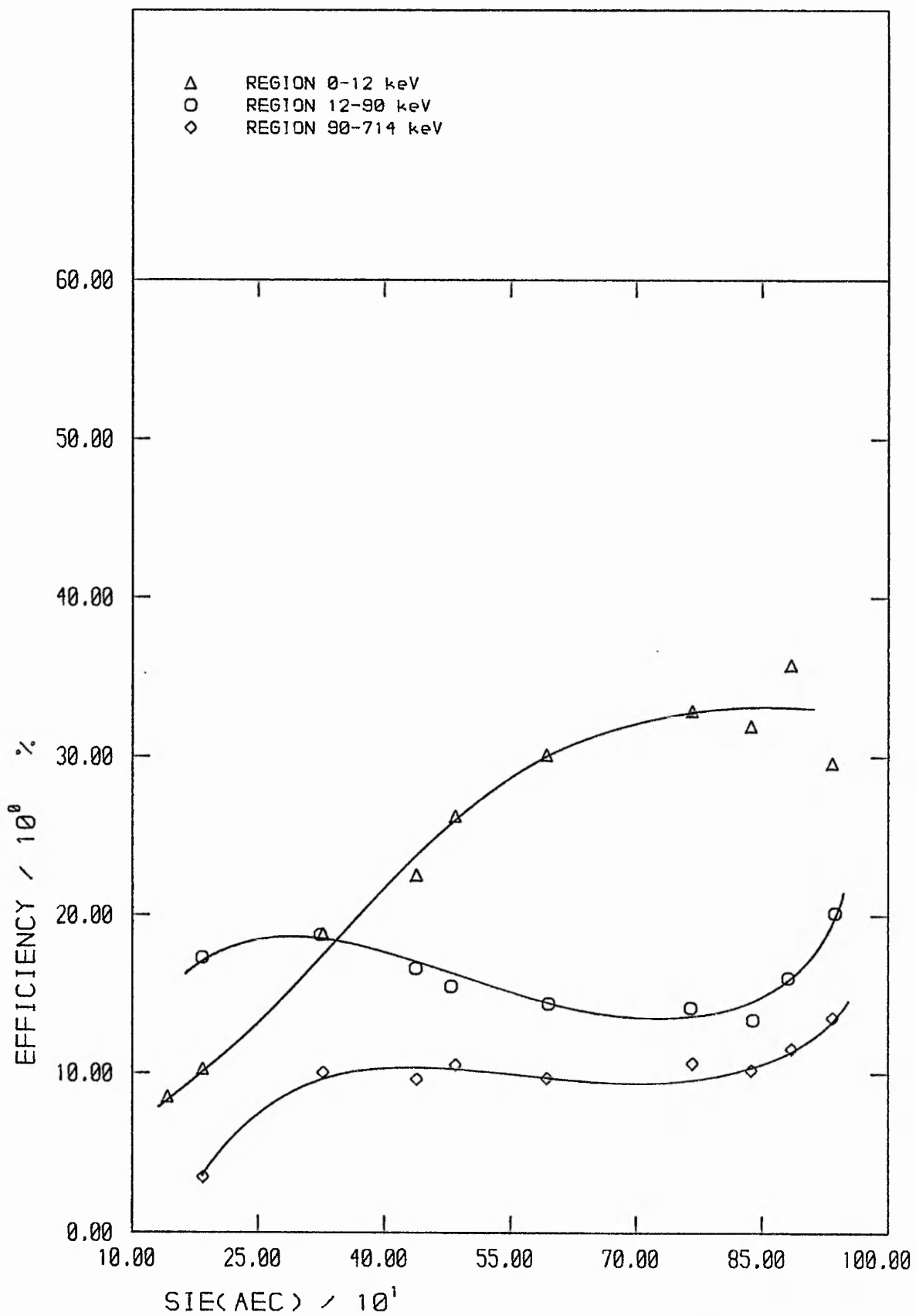
FIGF2.4 : BACKGROUND COUNTRATE vs SIE(AEC)
     - TRIPLE LABEL REGIONS

154
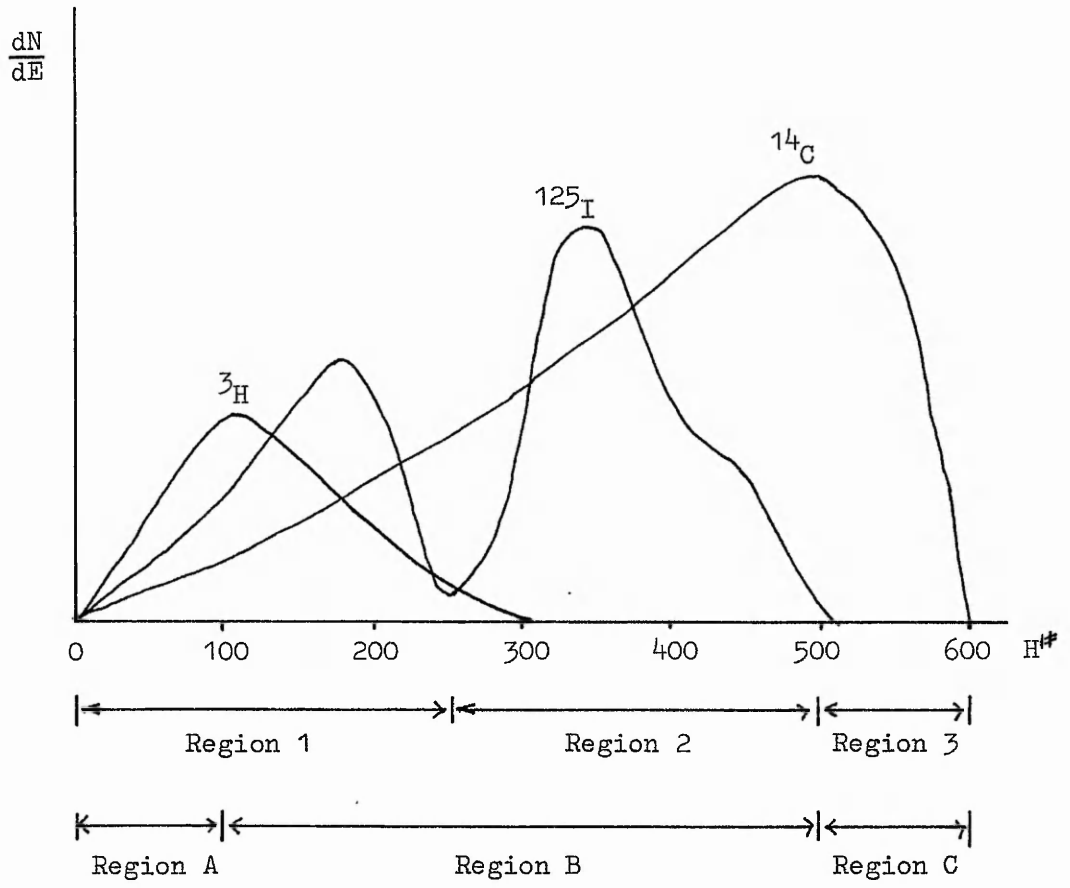
Fig. F 2.5   Triple Label Counting Regions

$$
\begin{bmatrix}
e_{11} & e_{12} & e_{13} \\
e_{21} & e_{22} & e_{23} \\
e_{31} & e_{32} & e_{33}
\end{bmatrix}
$$

where $e_{ij} = e_{region,nuclide}$

Fig. F2.6   Triple Label Efficiency Matrix

155
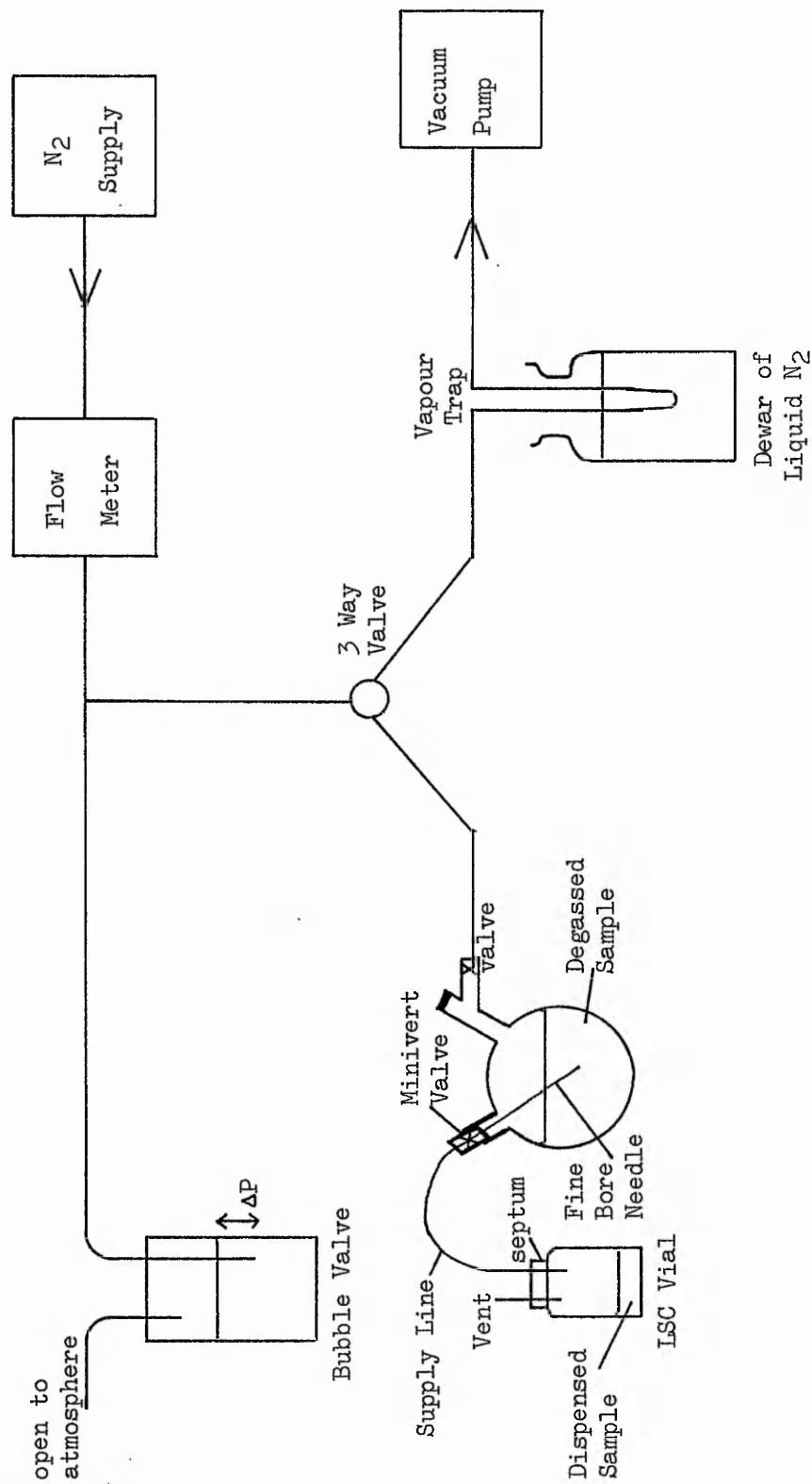
Fig. F2.7 Oxygen Purging Apparatus
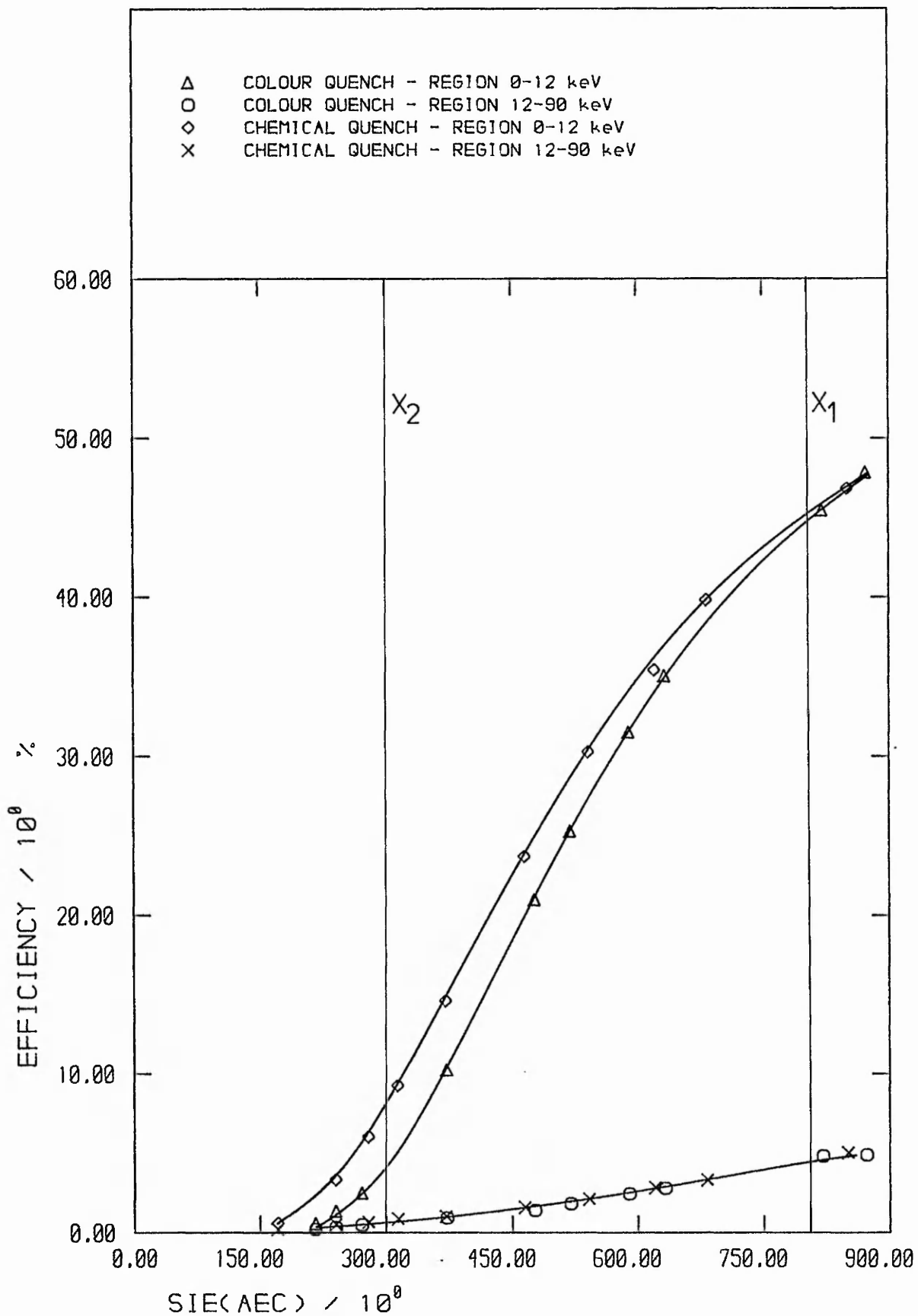
FIG F2.8 : 3H QUENCH CALIBRATION CURVES
-TRIPLE LABEL REGIONS.

158
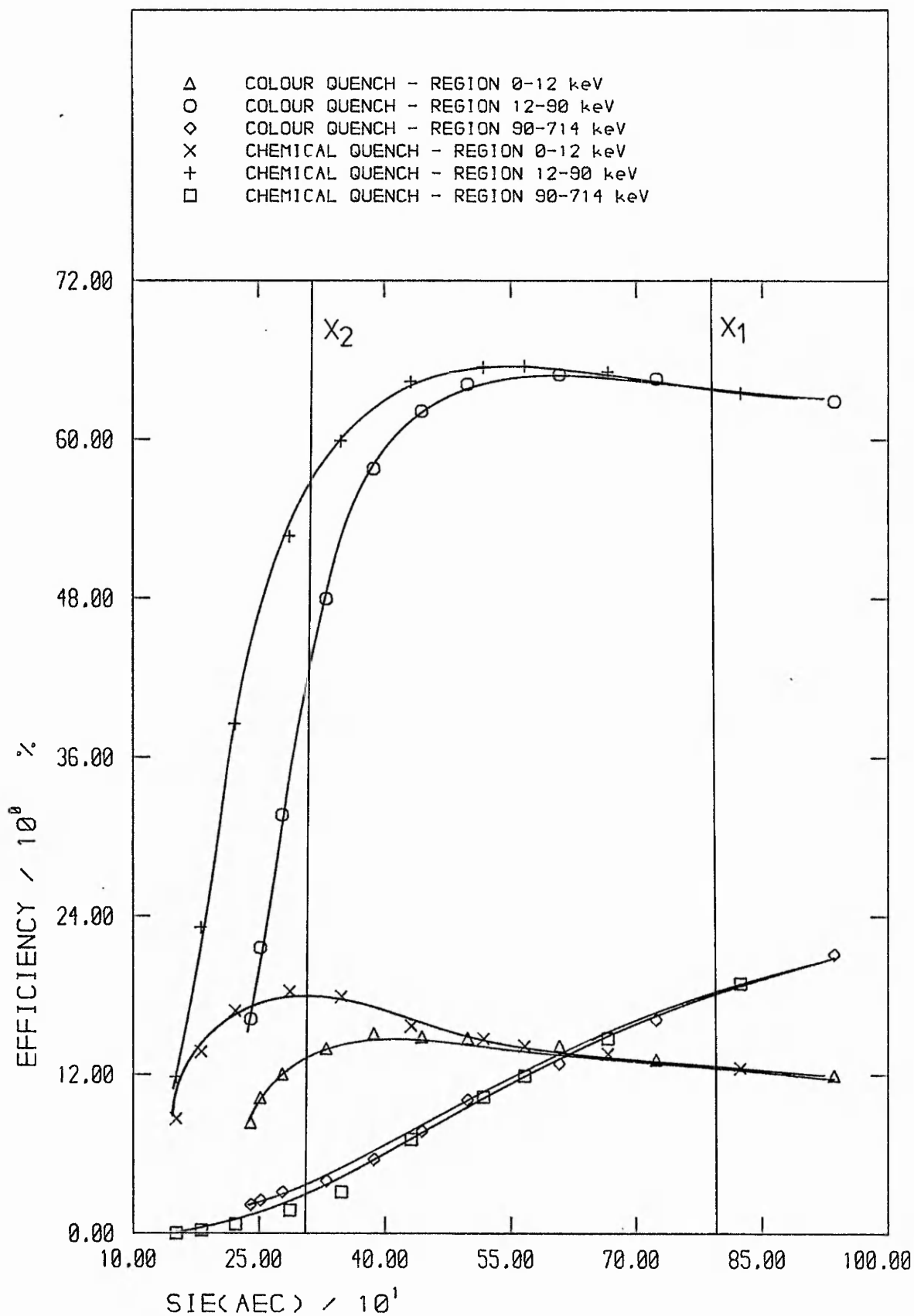
FIG F2.9 : 14C QUENCH CALIBRATION CURVES
        - TRIPLE LABEL REGIONS

159
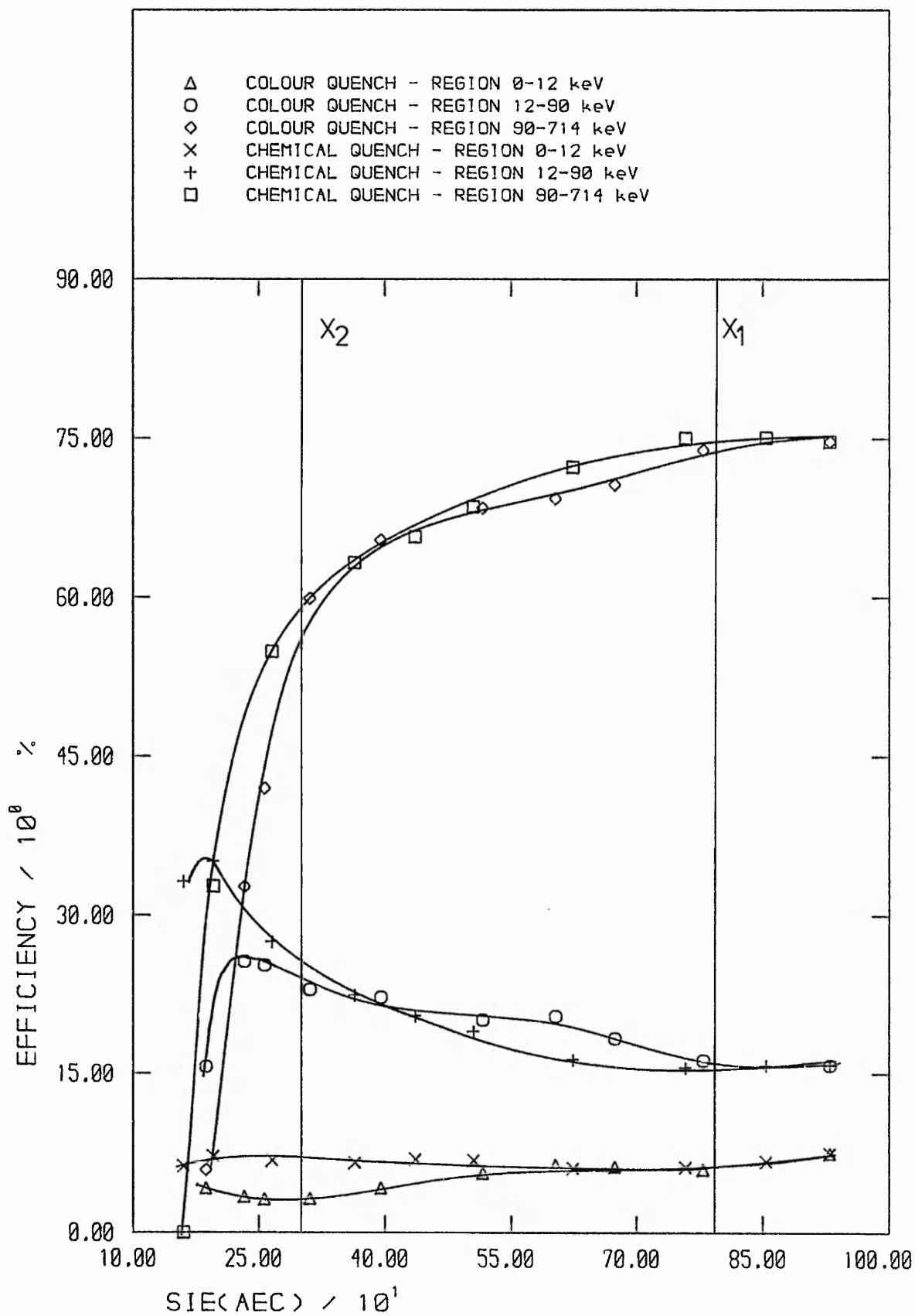
FIG F2.10 : 36CL QUENCH CALIBRATION CURVES
- TRIPLE LABEL REGIONS
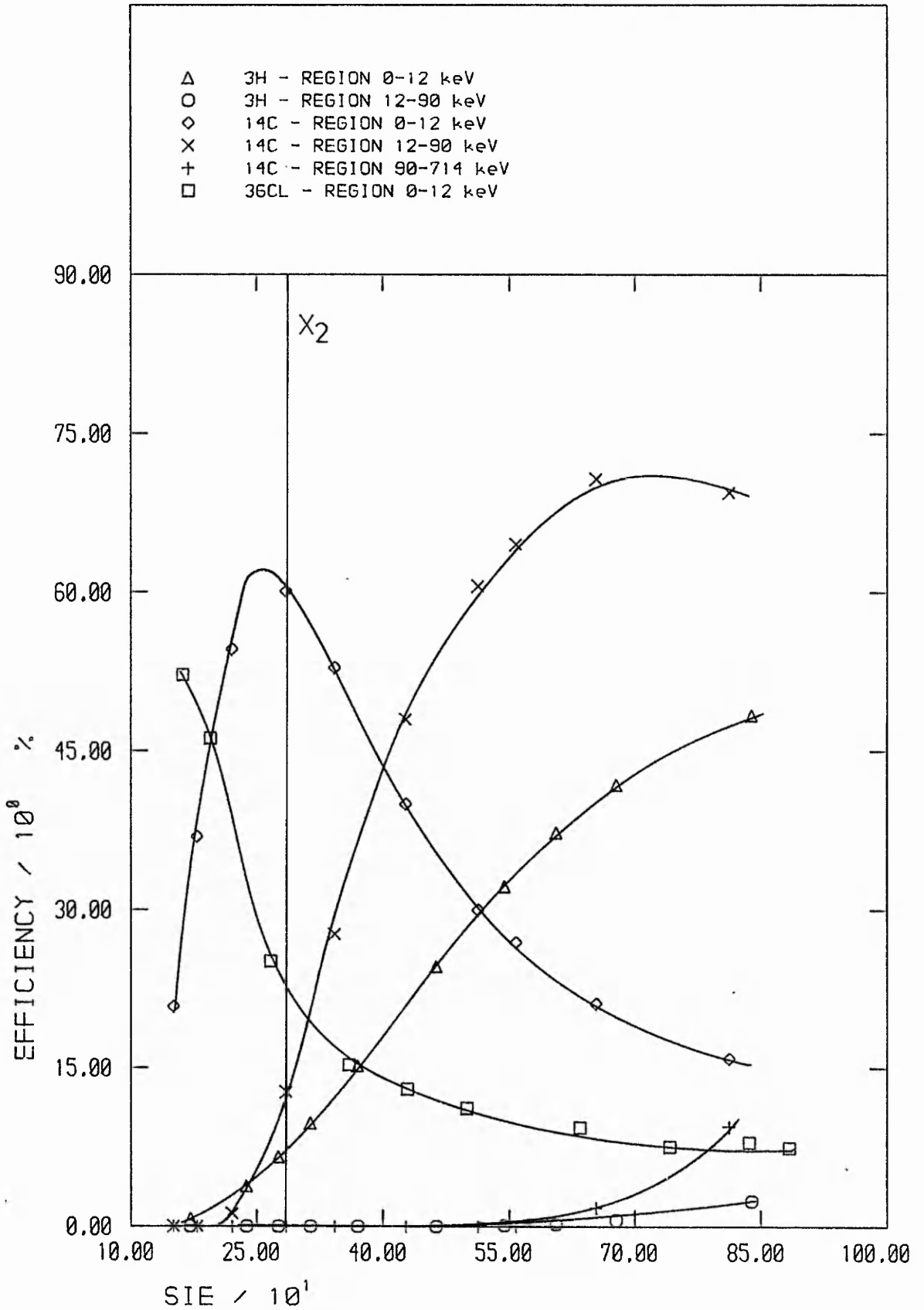
FIG F2.11 : 3H,14C,36CL CALIBRATION CURVES
-TRIPLE LABEL REGIONS (NO AEC)

VIAL

PM TUBE 1

PM TUBE 2

* event

$$\xrightarrow{x}$$

PMT 1 axis _ _ _ _ _ 0 _____ 1

$$\xleftarrow{1 - x}$$

1 _____ 0 _ _ _ _ PMT 2 axis
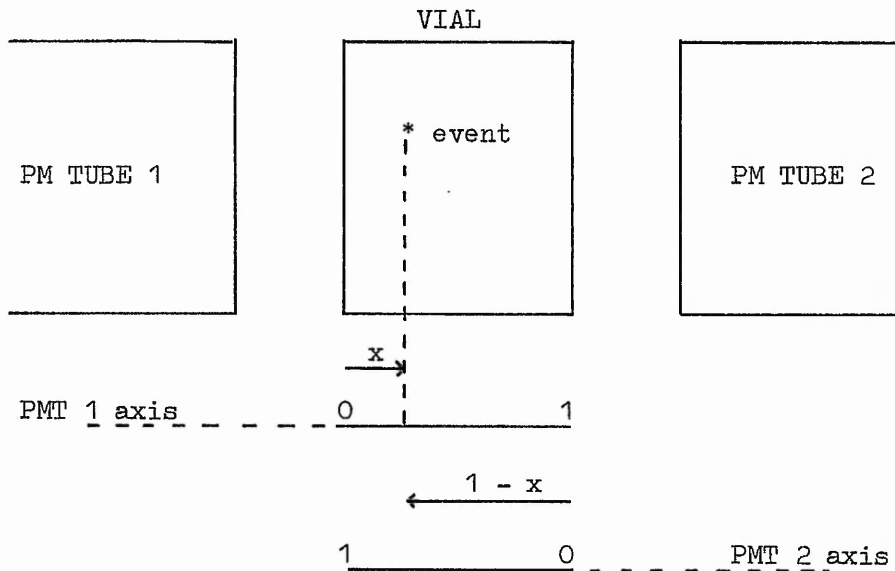
Fig. F3.1 The Two P.M.Tube LSC System

Y_1 = plot of pulse heights from PMT 1 against position in vial (colour quench present)
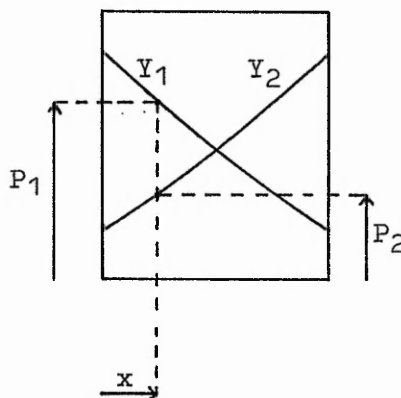
Y_2 = polt of pulse heights from PMT 2 against position in vial (colour quench present)

P_1

Y_1 Y_2

P_2

x

Fig. F3.2 The Two P.M.Tube LSC System
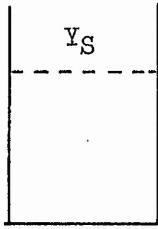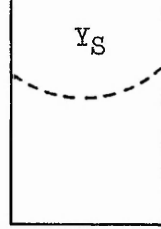
162

SUMMED   DIFFERENCED

Y_S Y_S Y_D Y_D

$Y_3=P_1+P_2$ $Y_4=P_1+P_2$ $Y_5=P_1-P_2$ $Y_6=P_1+P_2$
Chemical   Colour   Colour   Chemical
Quench   Quench   Quench   Quench
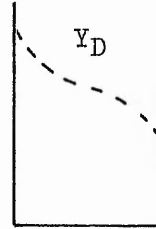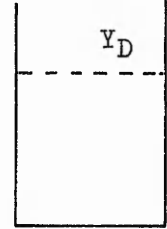
LESSER   RATIO
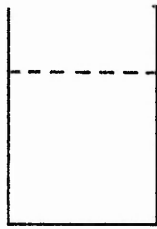
$Y_7=$ P_1,P_1 P_2 $Y_8=$ P_1,P_1 P_2 $Y_9=$ P_1or P_1 $Y_{10}=P_1$or P_1
      P_2,P_2 P_1 P_2,P_2 P_1 $\overline{P_2}$ $\overline{P_1+P_2}$ $\overline{P_2}$ $\overline{P_1+P_2}$
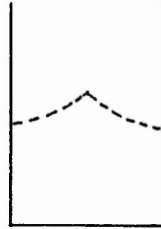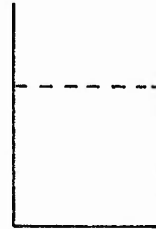
Chemical   Colour   Chemical   Colour
Quench   Quench   Quench   Quench

PRODUCT

$Y_{11}=P_1P_2$ $Y_{12}=P_1P_2$
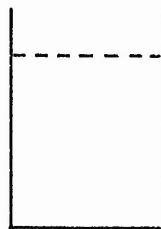
Chemical   Colour
Quench   Quench

Fig. F3.3   The two P.M.Tube LSC System

163

Fig. F3.4

164

SECTION

Black surface

Cylindrical mirror

PMT face

Vial outer wall

Vial inner wall

Cocktail/Air interface

Plane mirror

4.6 cm 4.7 cm

2.0 cm

z
x —→ y

PLAN

Plane mirror

Vial

Counter chamber

PMT face

z ⊙ —→ y
x

2.5 cm 2.9 cm 4.6 cm
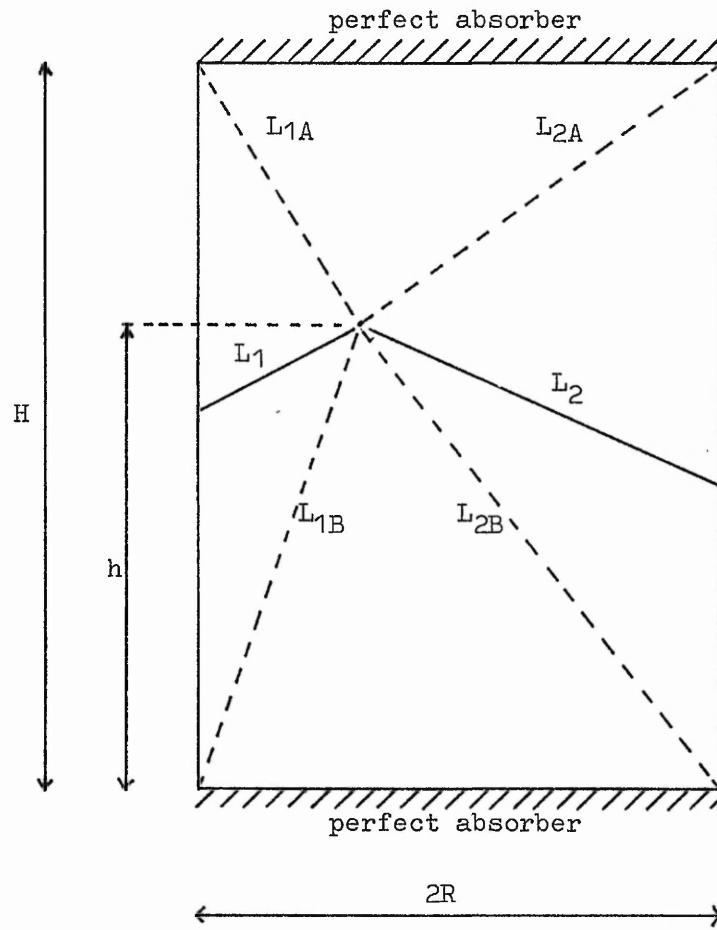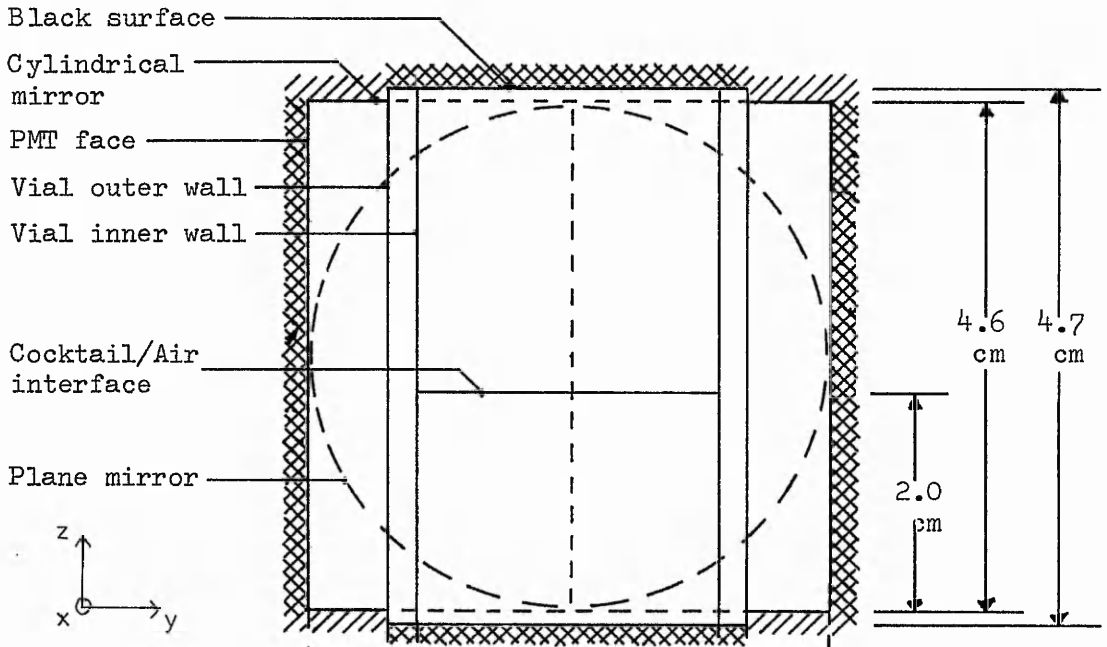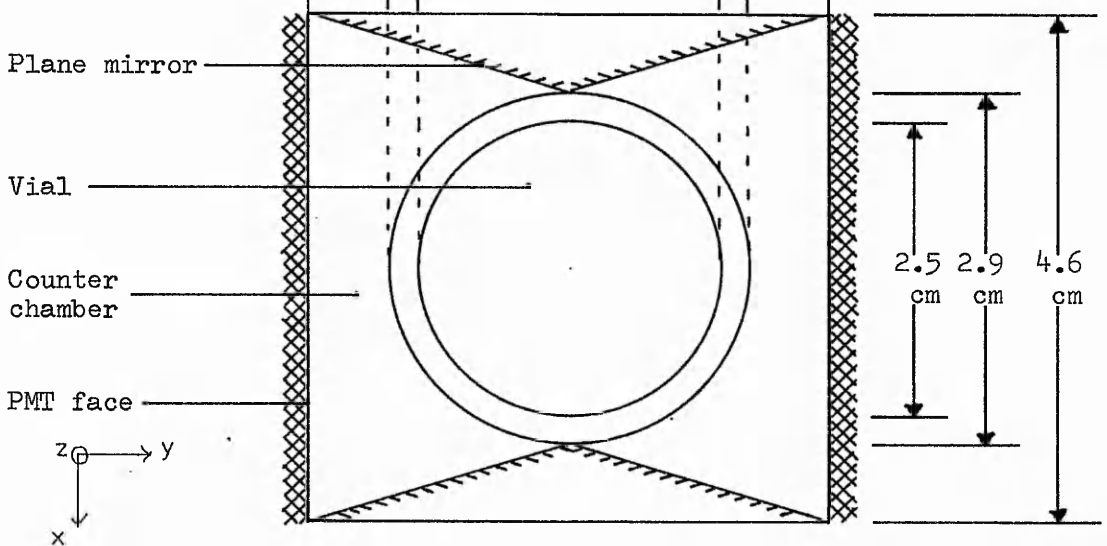
Fig. F3.5 Model Geometry

165
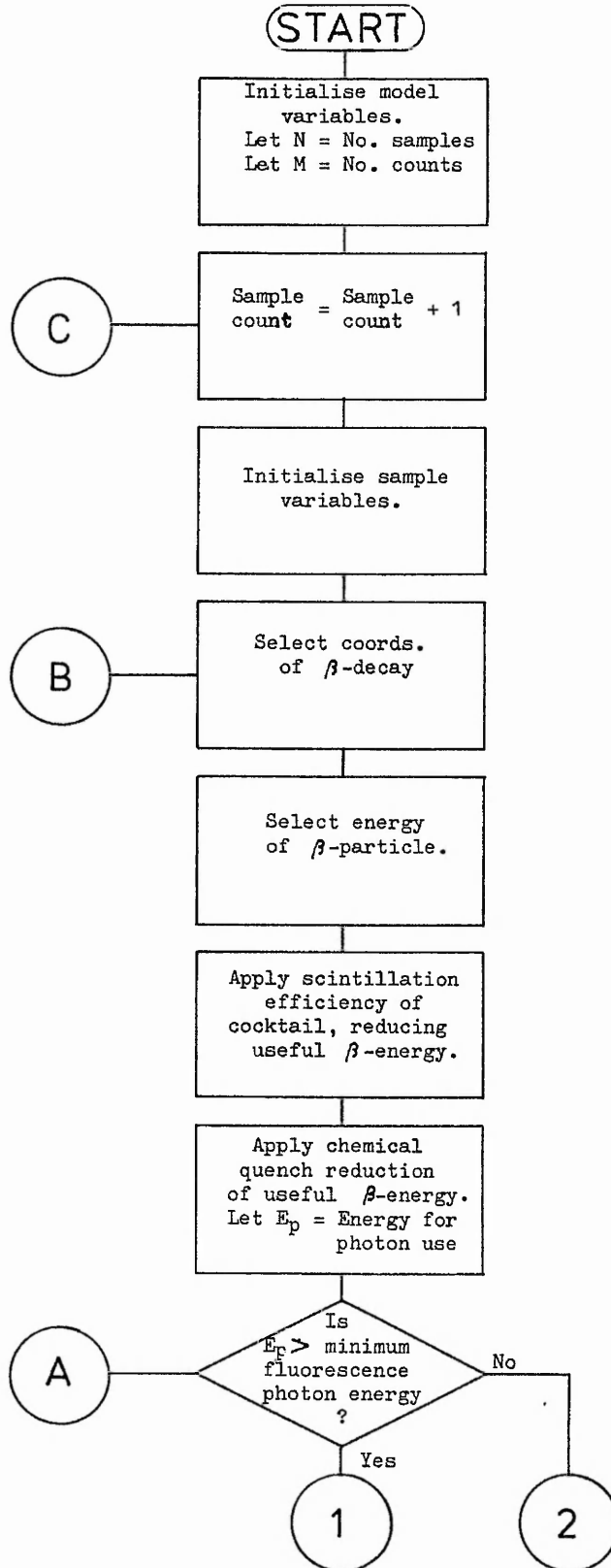
Fig. F3.6   Flowchart of LSC Model

A

1

Select photon
energy = P

Let
$E_p = E_p - P$

Select photon
direction

Trace the
photon to
extinction

The
photon got
to one of the
PMT's
?

No

Did
it hit the
PMT
?

Yes

No

Update left PMT
quantum efficiency
array.
Update left PMT
photon count.

Update right PMT
quantum efficiency
array.
Update right PMT
photon count.

C   B   2

Generate left
PMT pulse using
left photon No.
and quantum
efficiency array

Generate right
PMT pulse using
right photon No.
and quantum
efficiency array

Was
the β-event
lost ?

No

Yes

Update number
of lost counts

Update storage
of pulse height
spectra

Let
No.events = No.events
+ 1

Does
M(No. counts)=
No.events-lost
counts
?

No

Yes

Store final pulse
height spectra.
Store lost counts,
efficiency etc.
Perform spectral
analysis & store.

Does
Sample count = N
?

No

Yes

STOP

DATA	SOURCE	VALUE
Pi	Casio Calculator (Japan industrial stds) (JIS Z.8202-1978)	3.141592654
Plancks Constant	" "	6.6262E-34
Charge on electron	" "	1.60219E-19
Speed of light	" "	2.997925E8
β particle E_{max} for ^3H		18.6 keV
β particle E_{max} for ^{14}C		156 keV
Fermi β spectrum for ^3H		-
Fermi β spectrum for ^{14}C		-
Scintillation Efficiency Curve	D. L. Horrocks[88]	-
Colour quencher Absorbtion spectrum - 07 dye	Self measured	-
RCA 4501/v3 PMTube dynode (BeO) shape factor	RCA Handbook (book B17)	0.2
RCA 4501/v3 PMTube dynode (BeO) gain	D. E. Persyck[145]	3.94
PMTube collection efficiency	RCA Handbook (book B17)	0.85
Aluminium Absorbtion spectrum	CRC Handbook (book B20)	-
b-PBD Fluorescence spectrum	Self measured	-
Dispersion of b-PBD + pXylene	Self measured	-
Dispersion of vial glass (borosilicate)	Tables of Physical and Chemical Constants (book B19)	-
Dispersion of PMT glass (pyrex)	Tables of Physical and Chemical Constants (book B19)	-
Vial height	Self measured	0.047 m
Vial radius	Self measured	0.0147 m

Fig. F3.7 Data used in the LSC Model

DATA	SOURCE	VALUE
Liquid height	-	0.02 m
Liquid radius	Self measured	0.0125 m
Chamber height	Packard Instruments Inc.	0.04374 m
Chamber radius	Packard Instruments Inc.	0.02286 m
Low wavelength cut-off for spectra	Self measured	600 nm
High wavelength cut-off for spectra	Self measured	300 nm
PMTube Quantum efficiency	Packard Instruments Inc.	-

Fig. F3.7 (contd.) Data used in the LSC Model
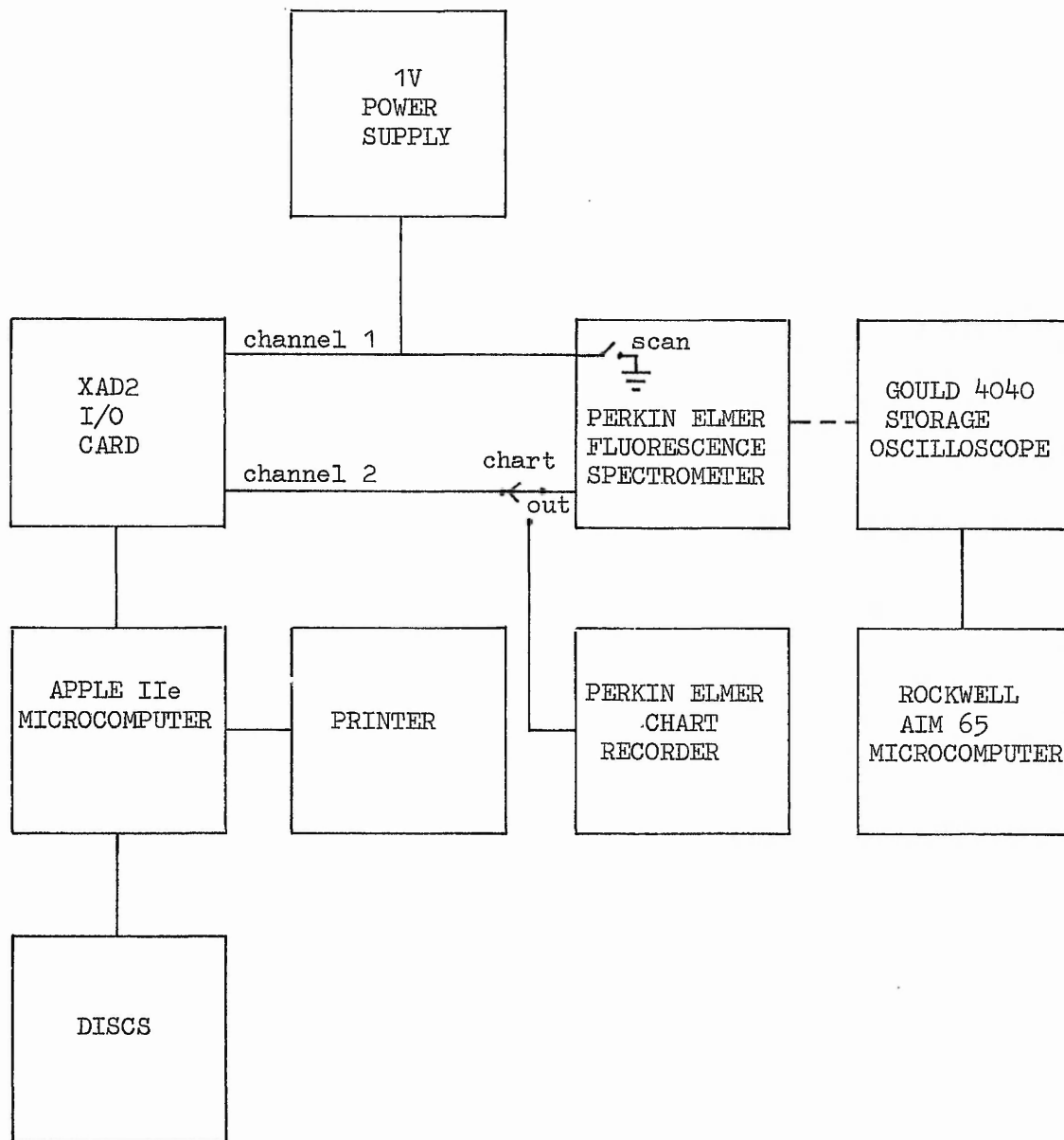
Fig. F3.8 Block diagram of equipment used for Fluorescence and
Absorption spectra capture.
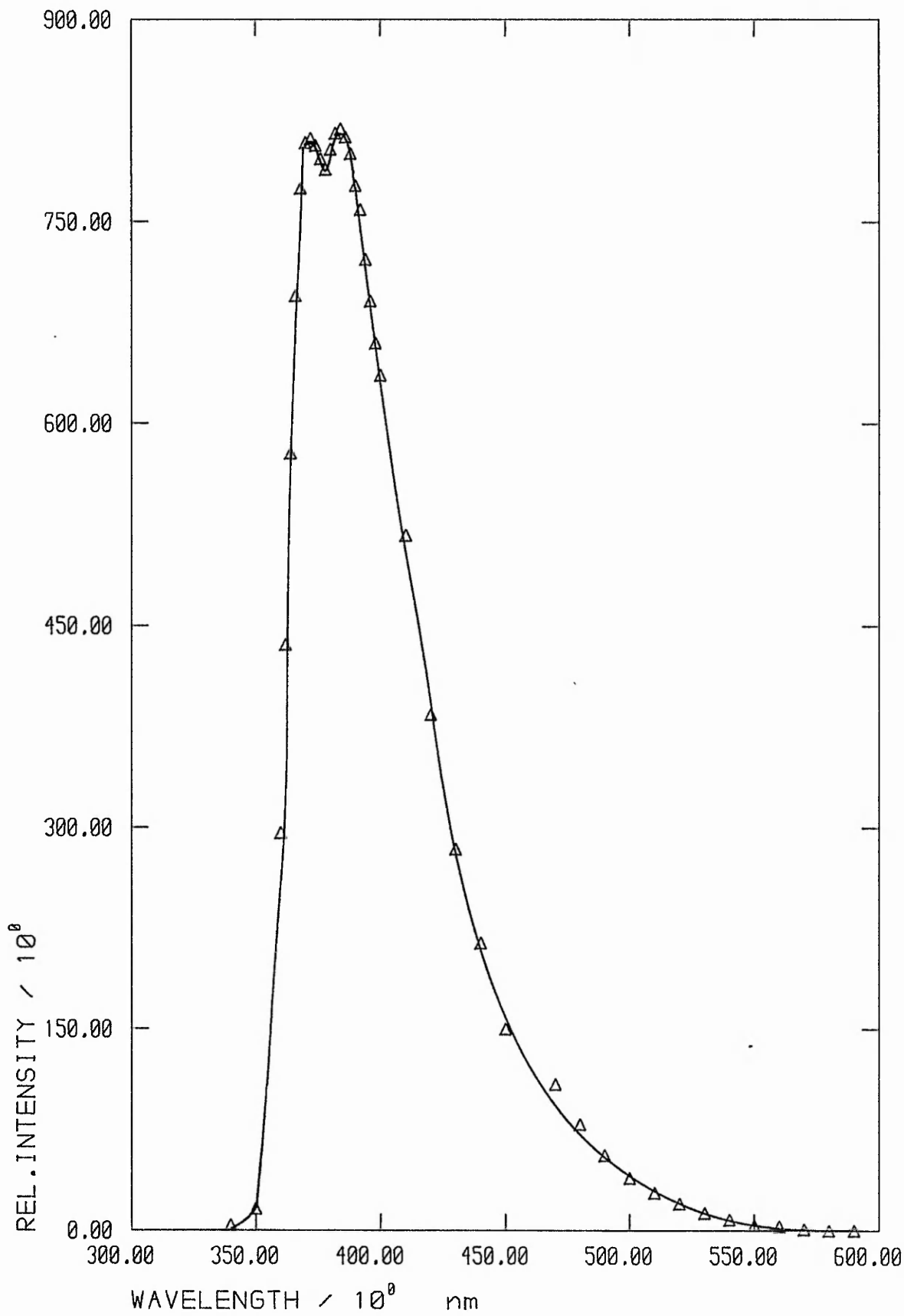
FIG F3.9 : FLUORESCENCE SPECTRUM USED
IN MODEL

172
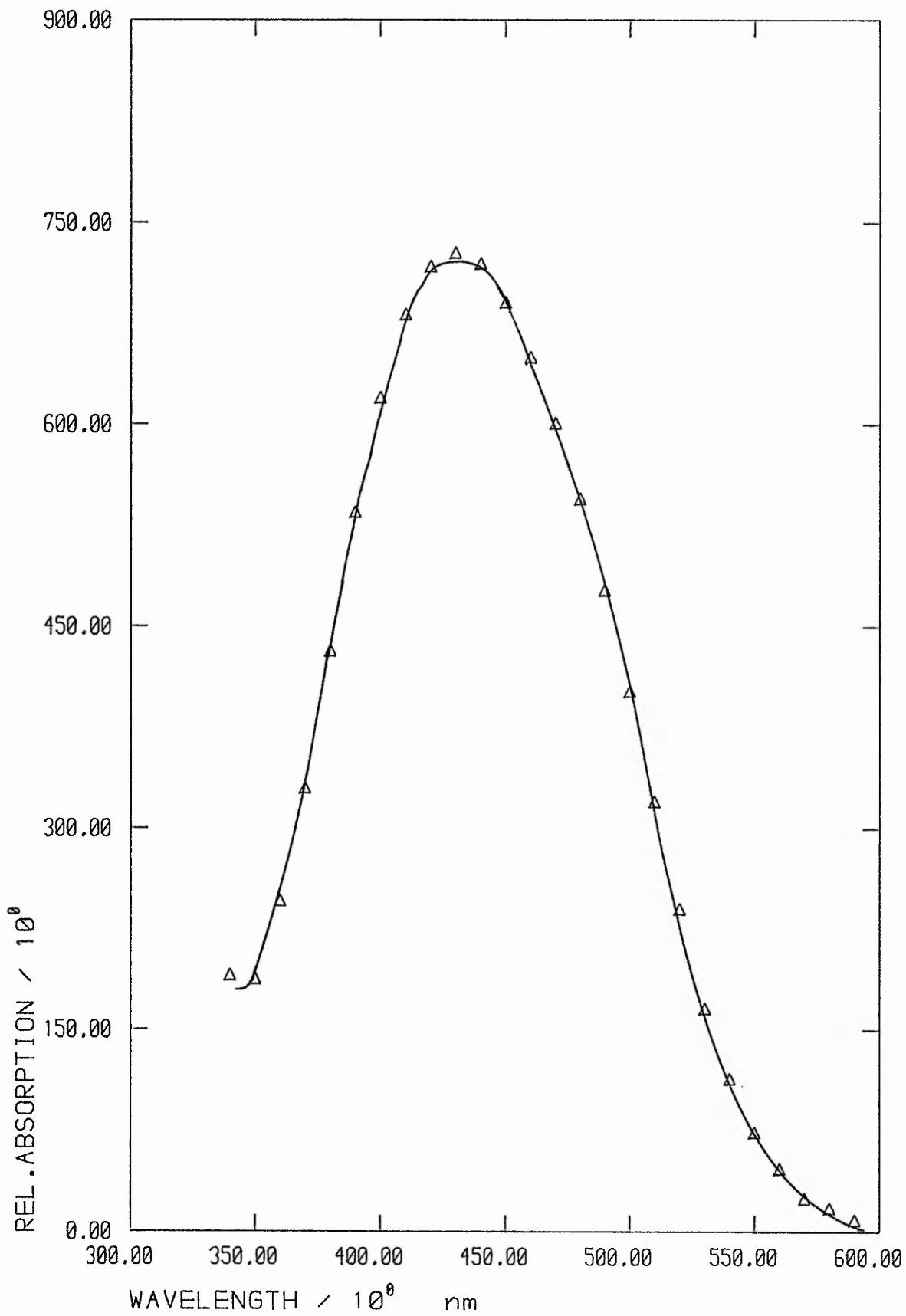
FIG F3.10 : ABSORPTION SPECTRA USED IN
MODEL
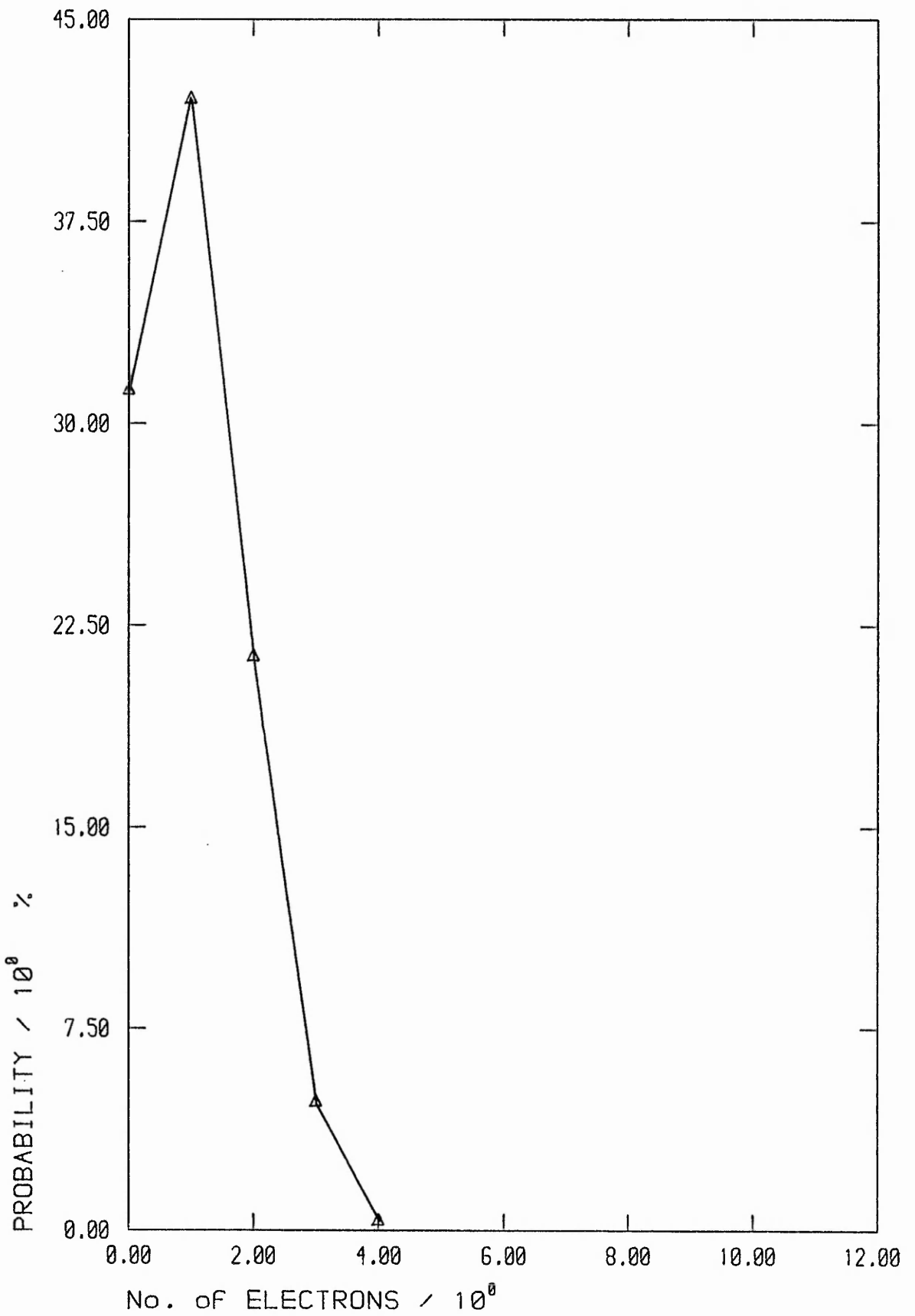
FIG F3.11 : PMTube STATISTICS
for 4 photons

174
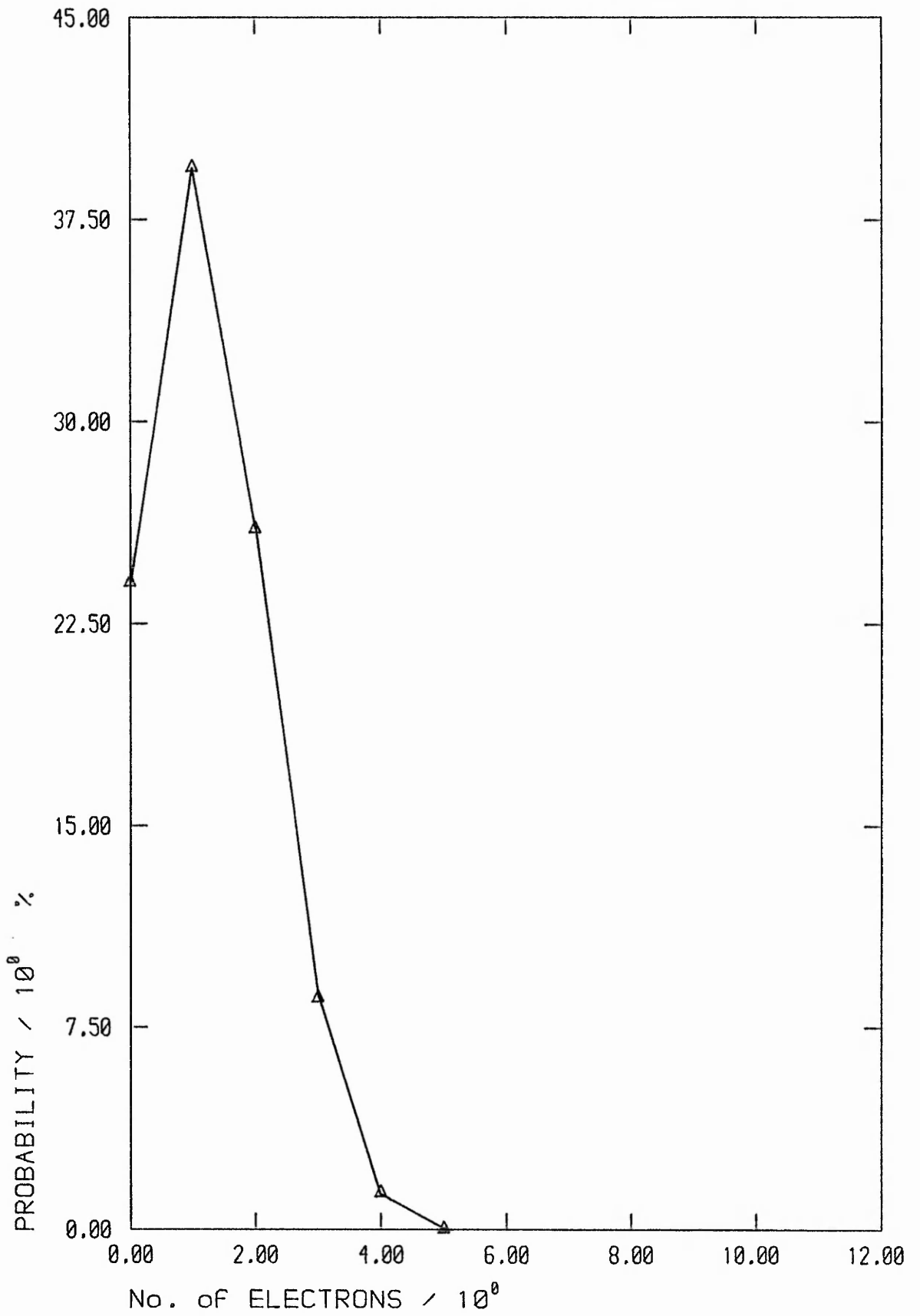
FIG F3.12 : PMTube STATISTICS
for 5 photons

175
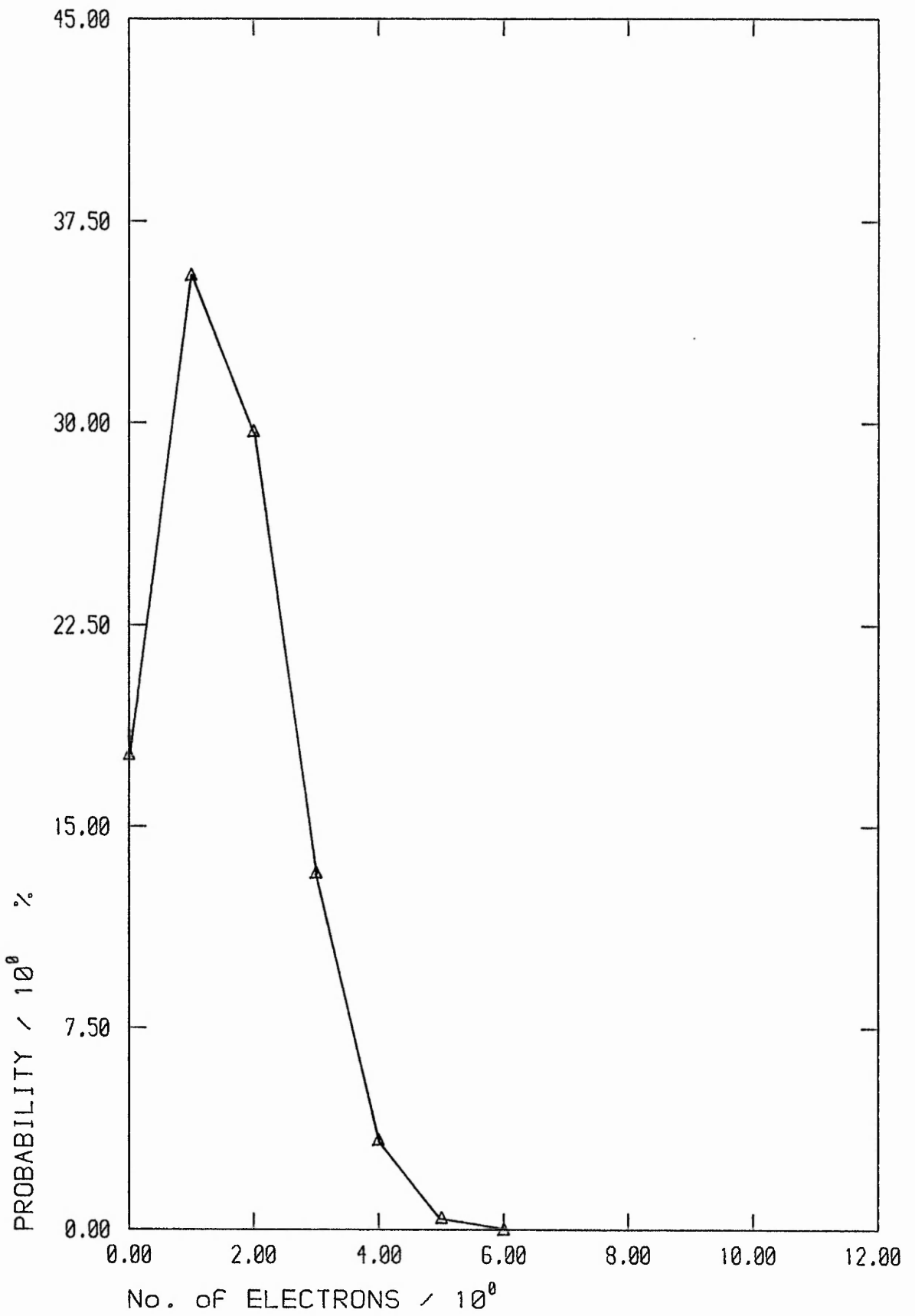
FIG F3.13 : PMTube STATISTICS
for 6 photons

176
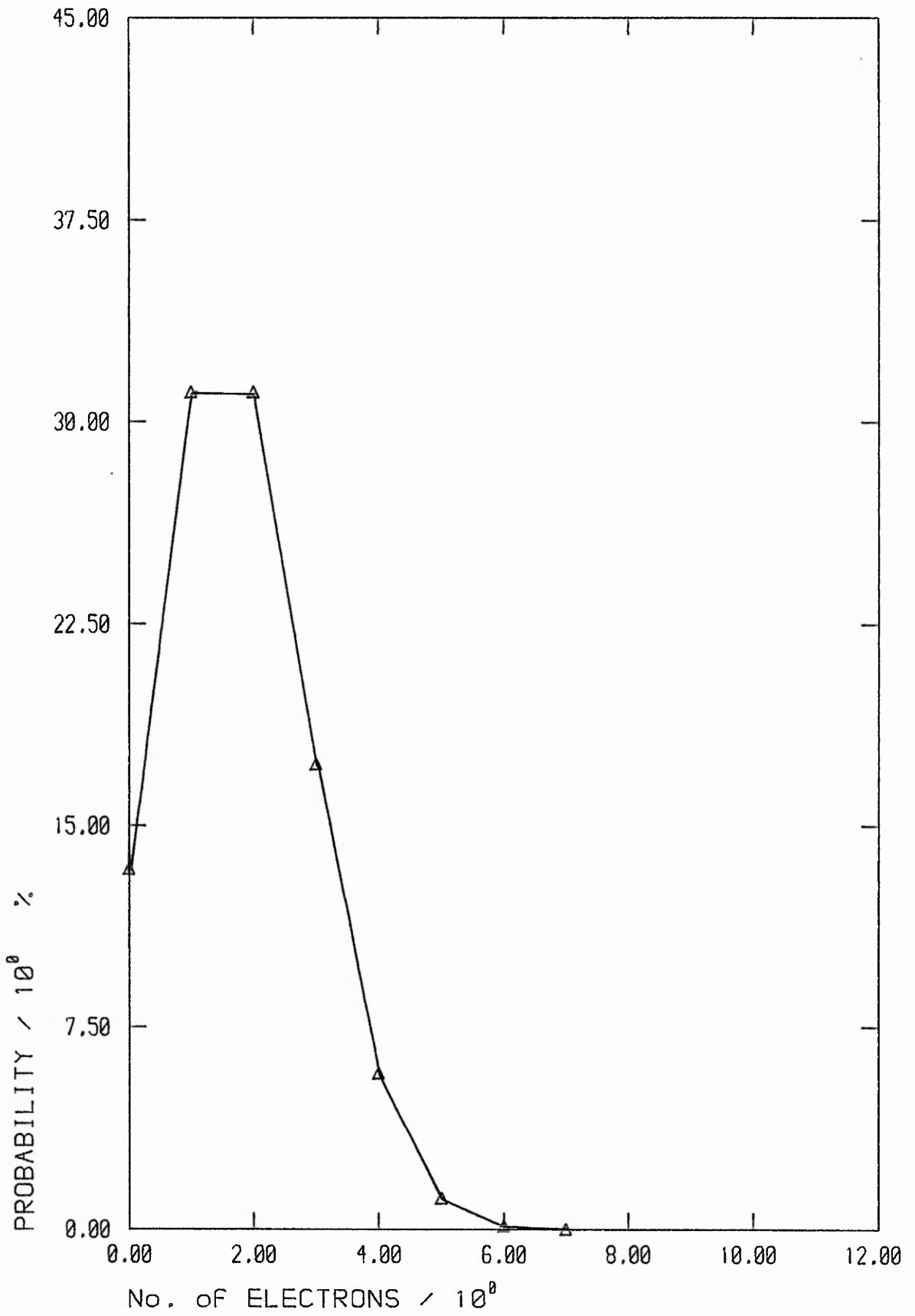
FIG F3.14 : PMTube STATISTICS
for 7 photons

177
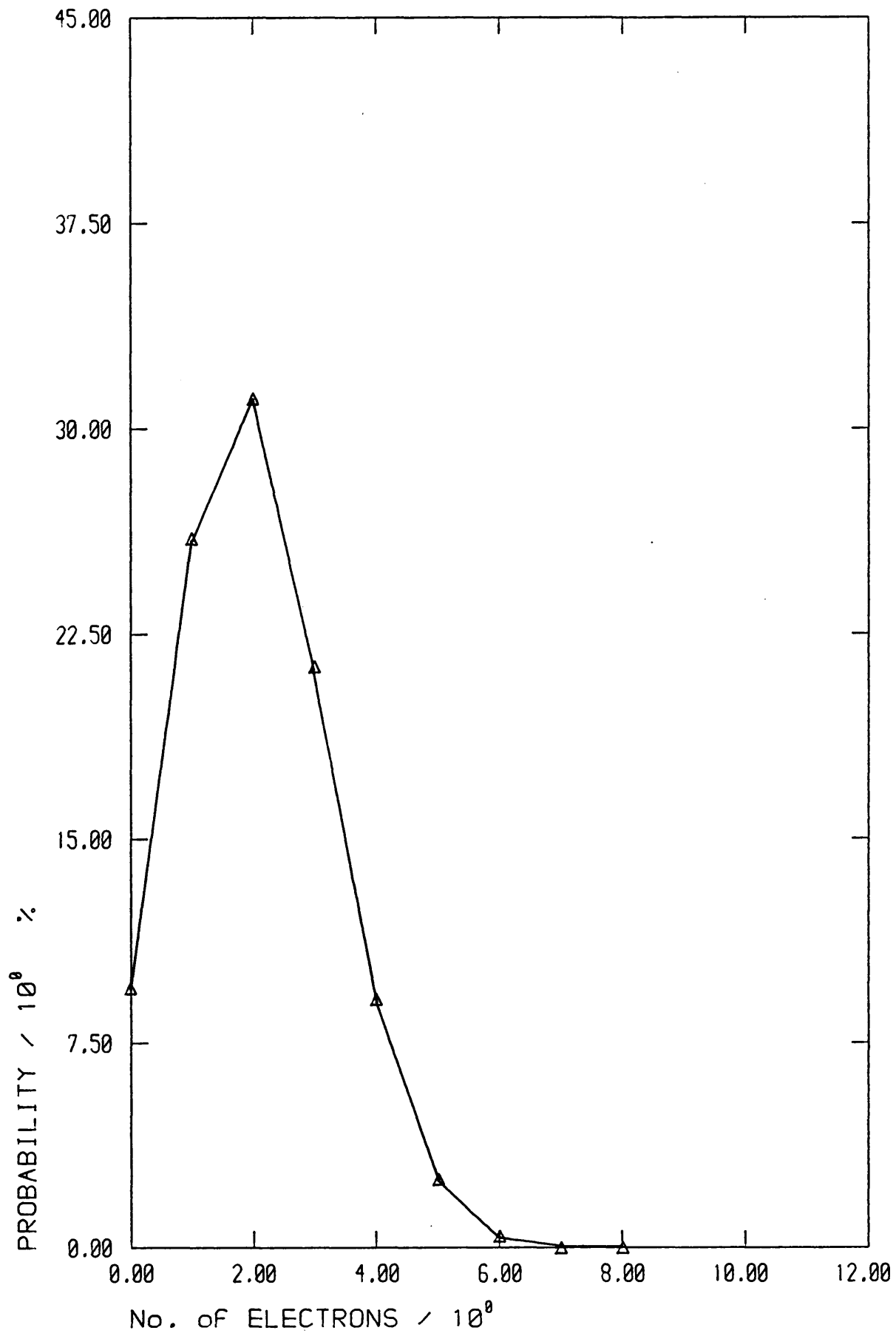
FIG F3.15 : PMTube STATISTICS
for 8 photons

178
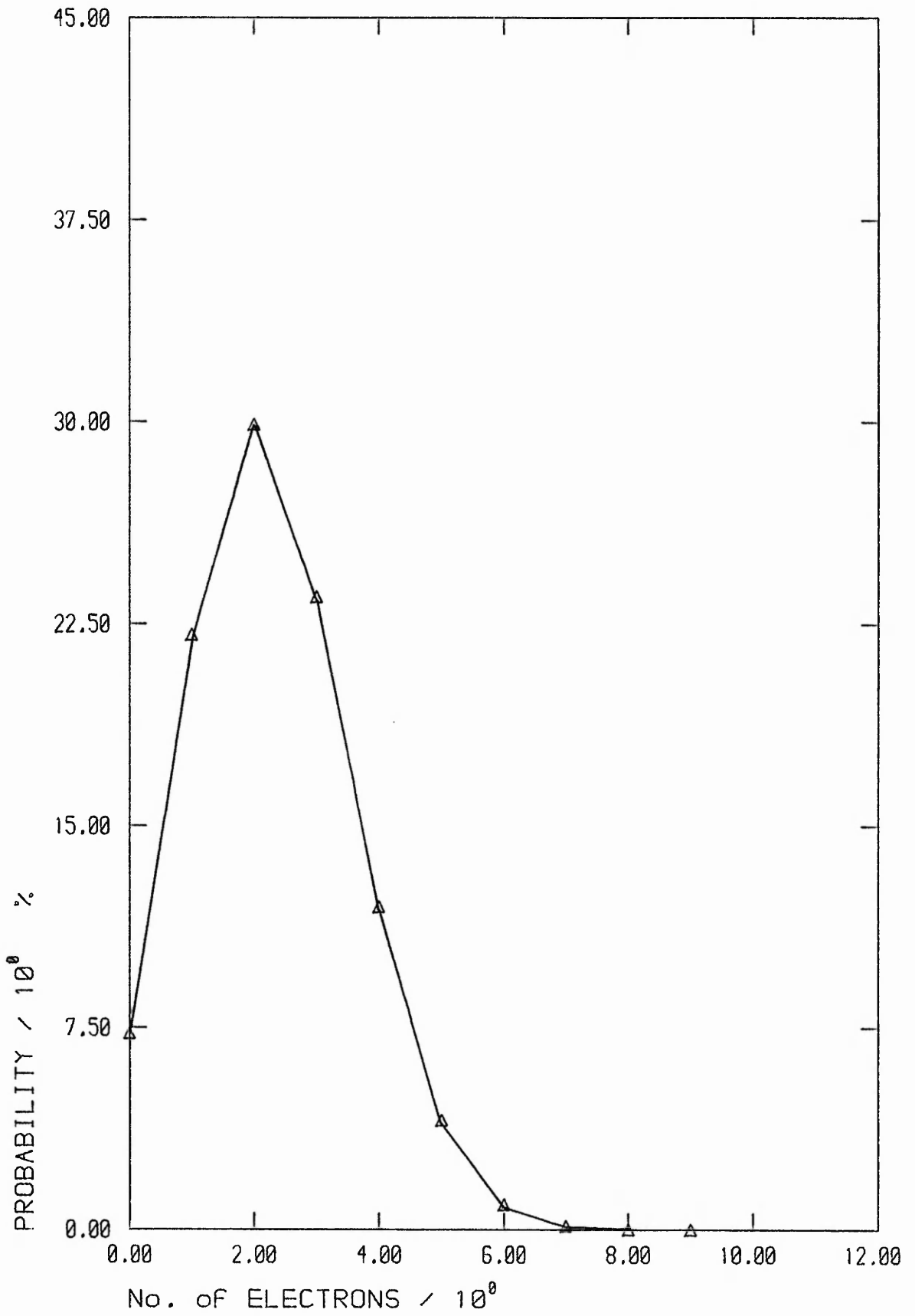
FIG F3.16 : PMTube STATISTICS
for 9 photons

179
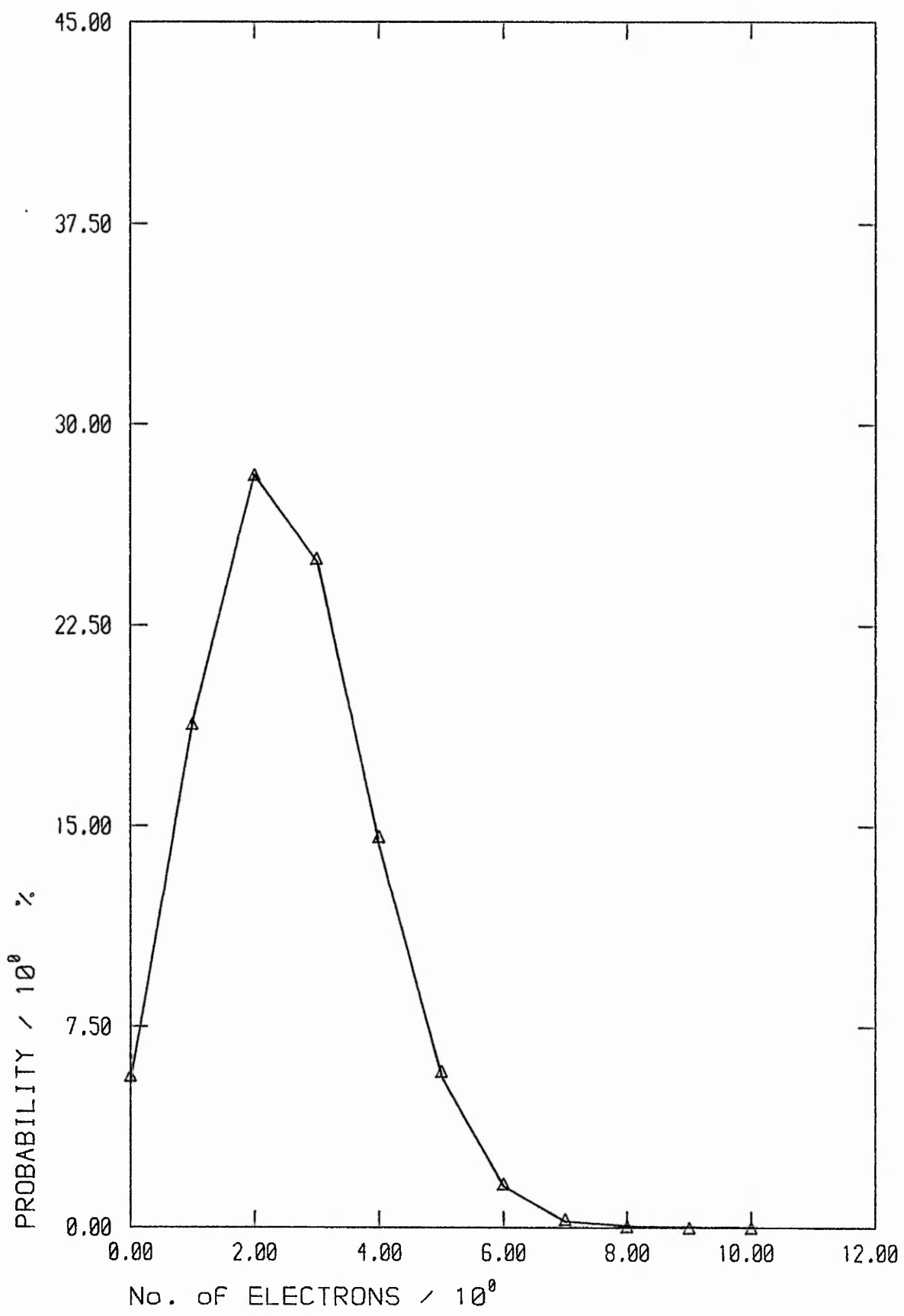
FIG F3.17 : PMTube STATISTICS
for 10 photons

180
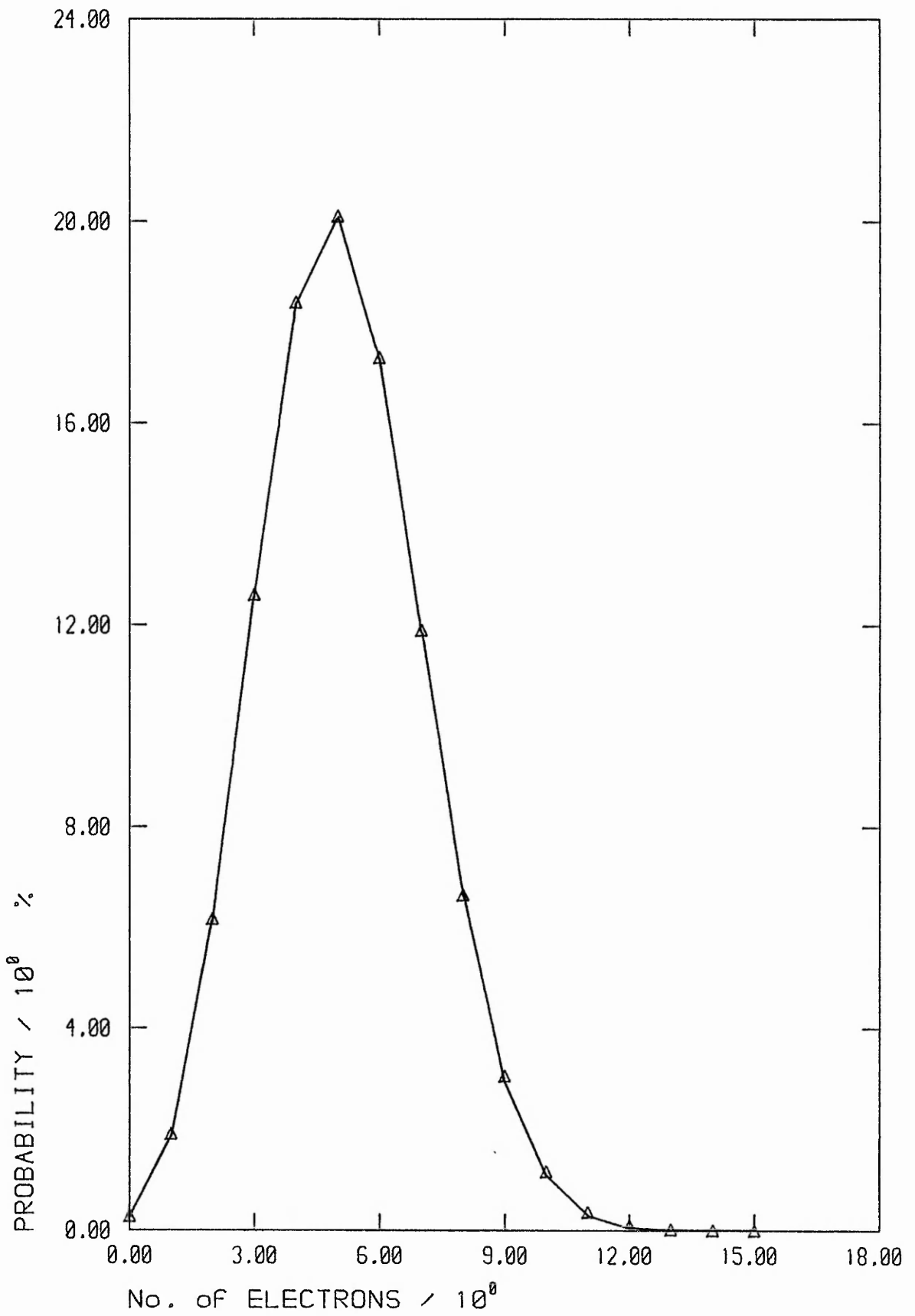
FIG F3.18 : PMTube STATISTICS
For 20 photons

181
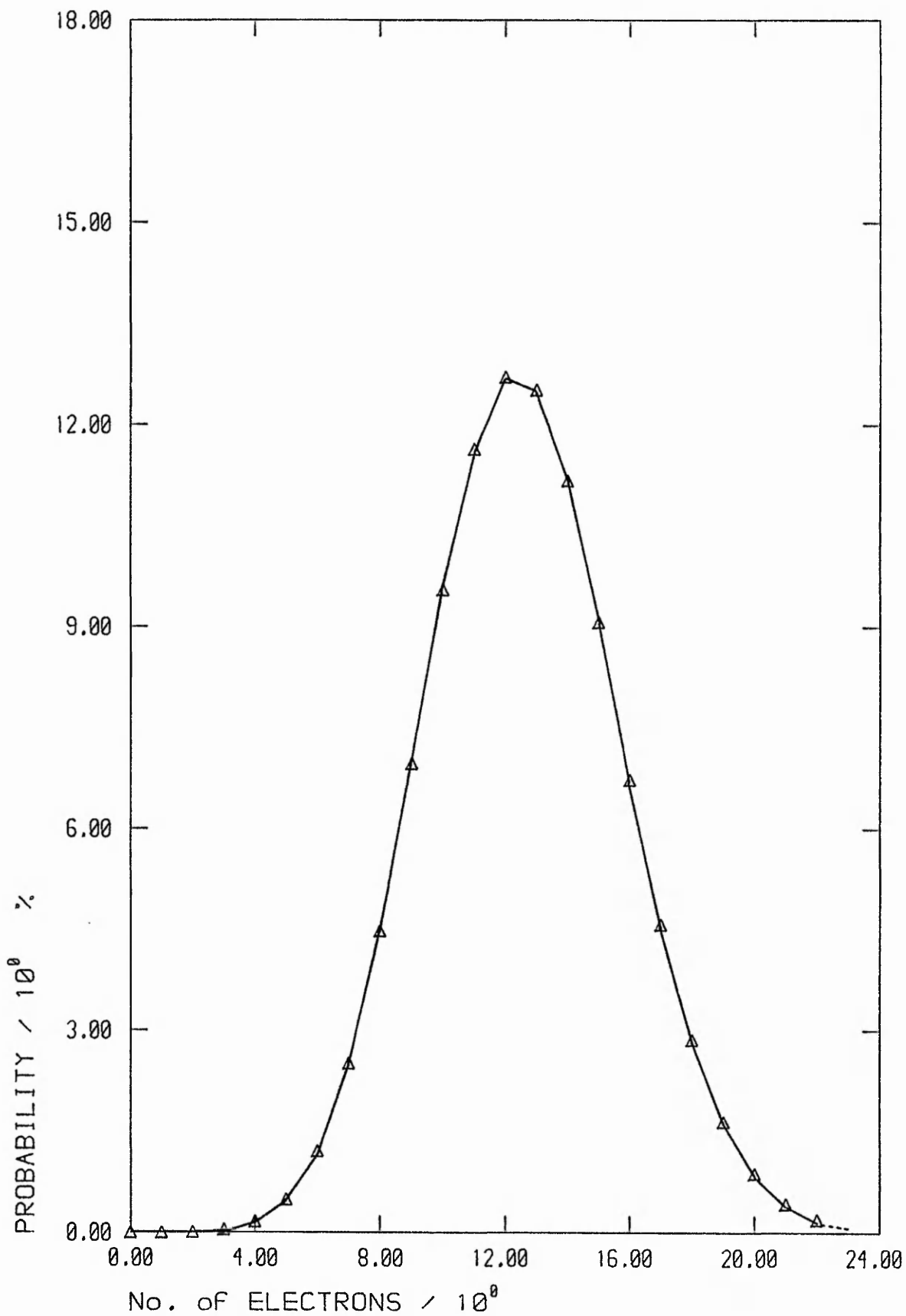
FIG F3.19 : PMTube STATISTICS
for 50 photons

182
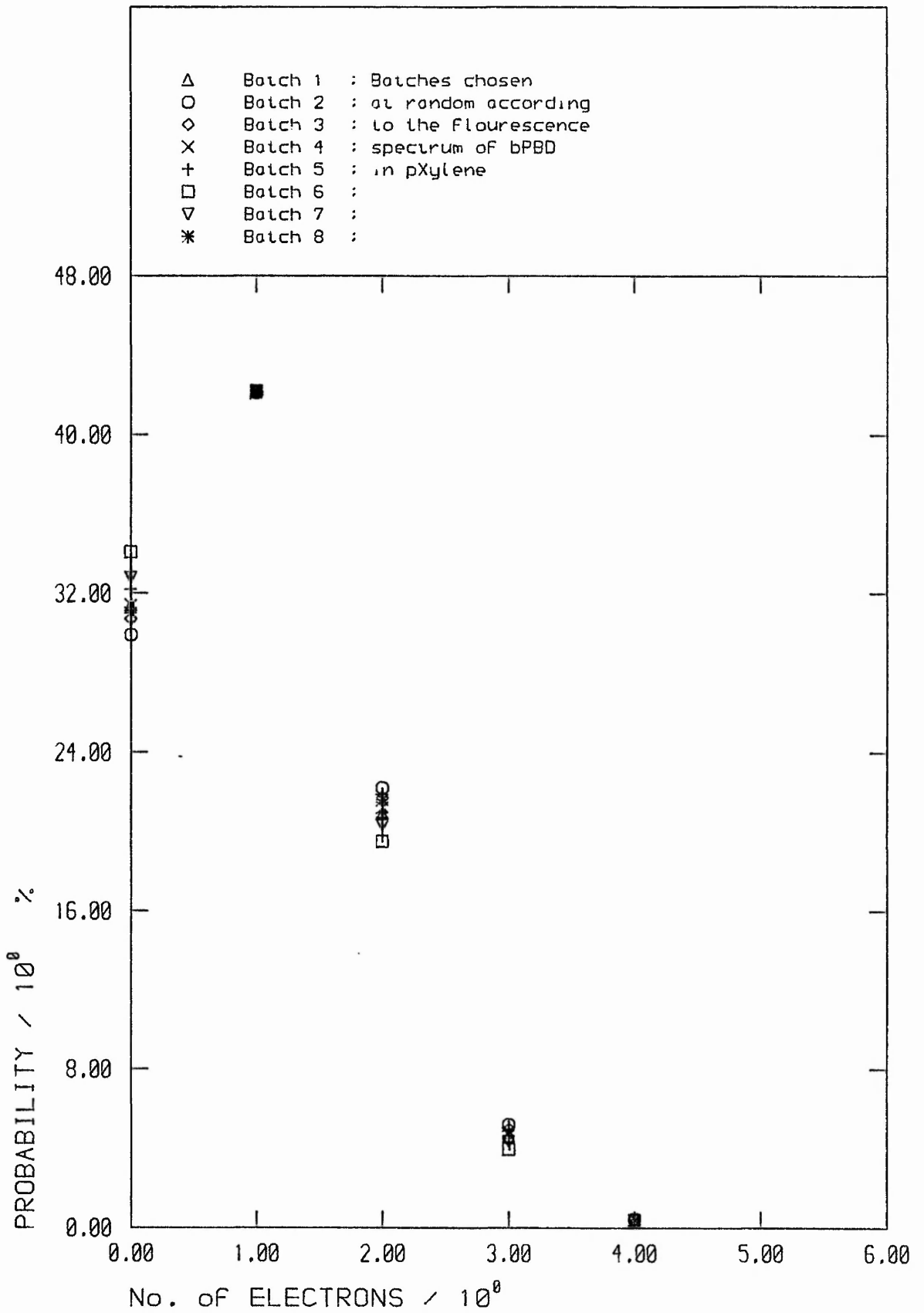
FIG F3.20 : PMTube Poisson distribution
batch to batch variation for 4 photons

183
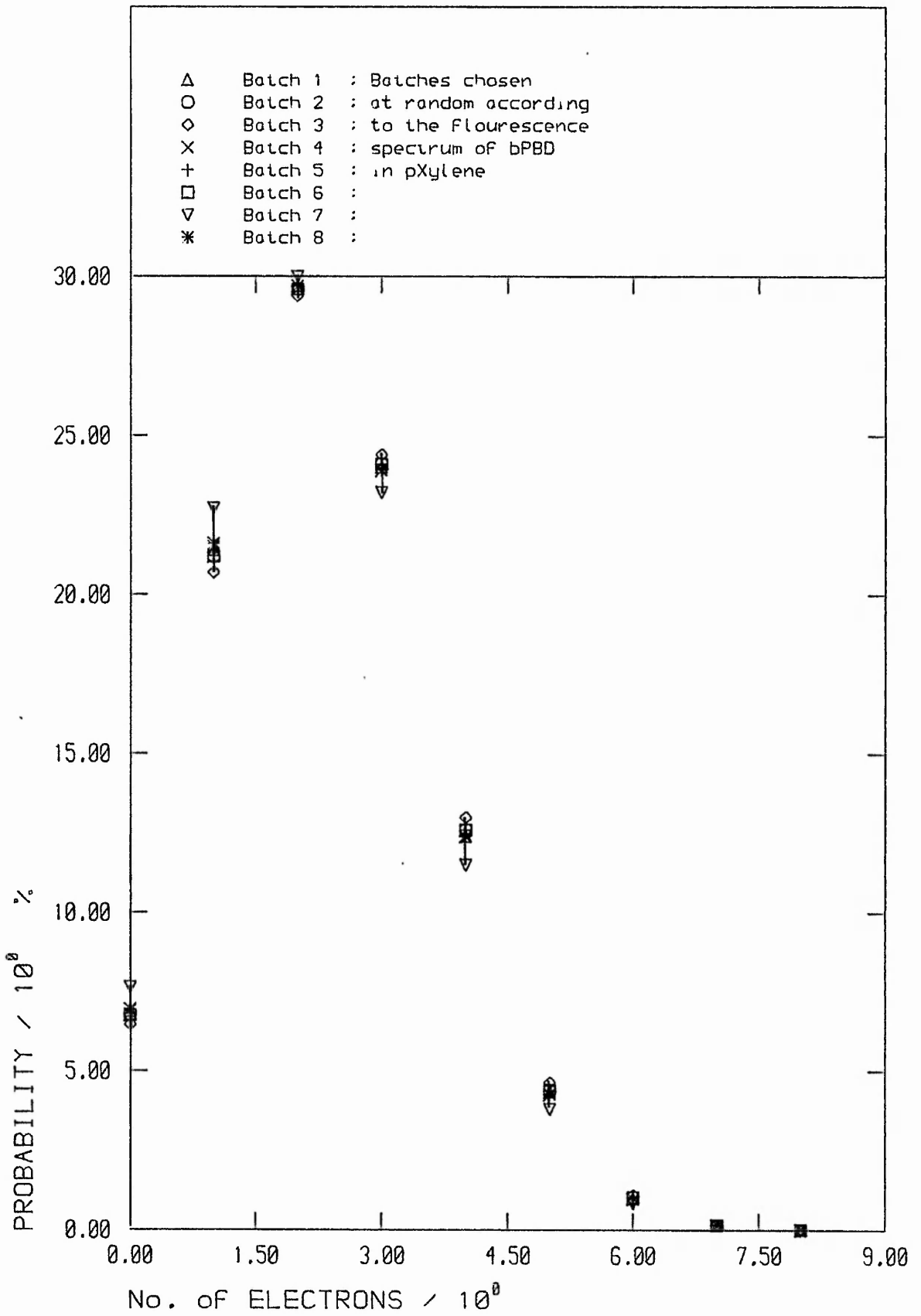
FIG F3.21 : PMTube Poisson distribution
batch to batch variation for 9 photons

184
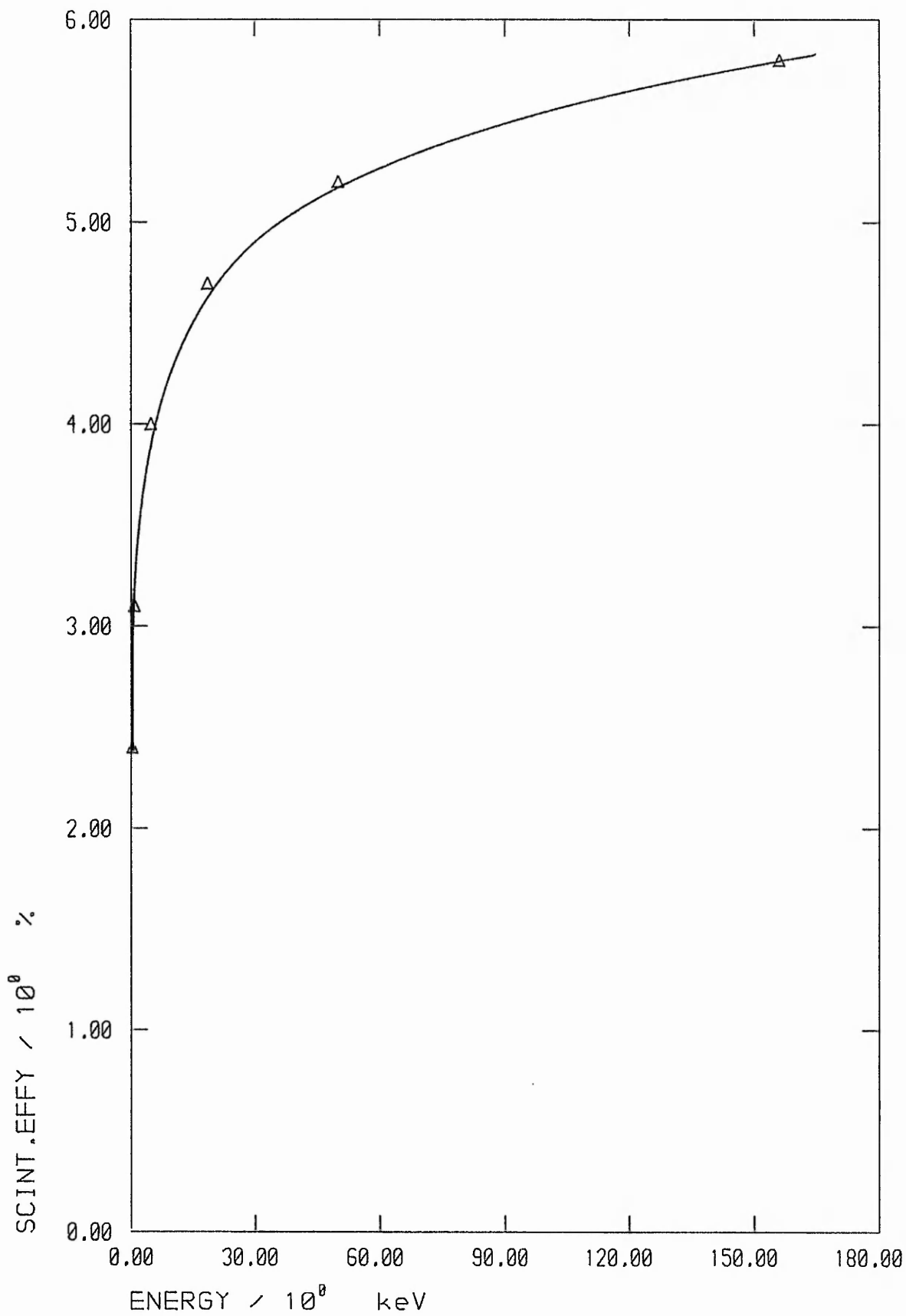
FIG F3.22 : SCINTILLATION EFFICIENCY vs BETA
PARTICLE ENERGY (HORROCKS' DATA)

185
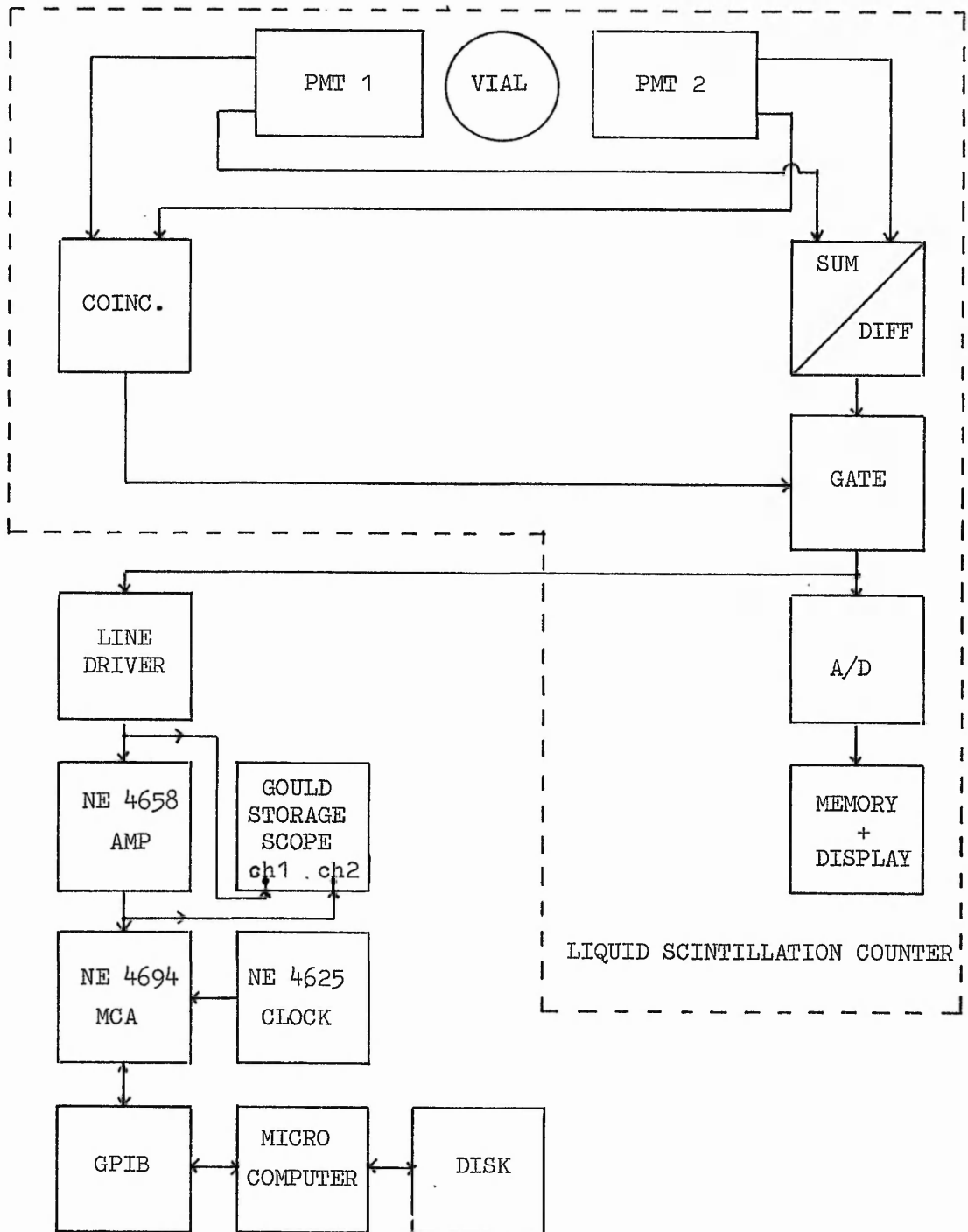
Fig. F3.23   Block Diagram of Equipment used for Pulse Height Spectra
Capture and Analysis
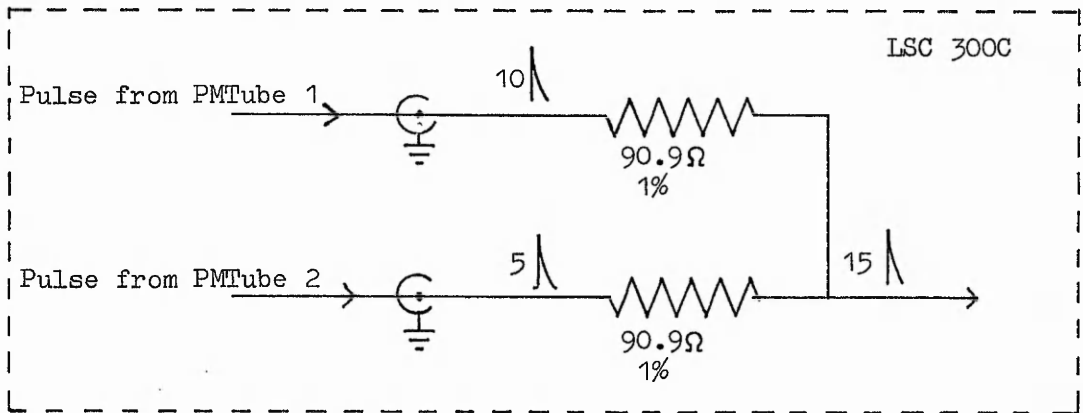
(a)   Summed pulse handling circuit
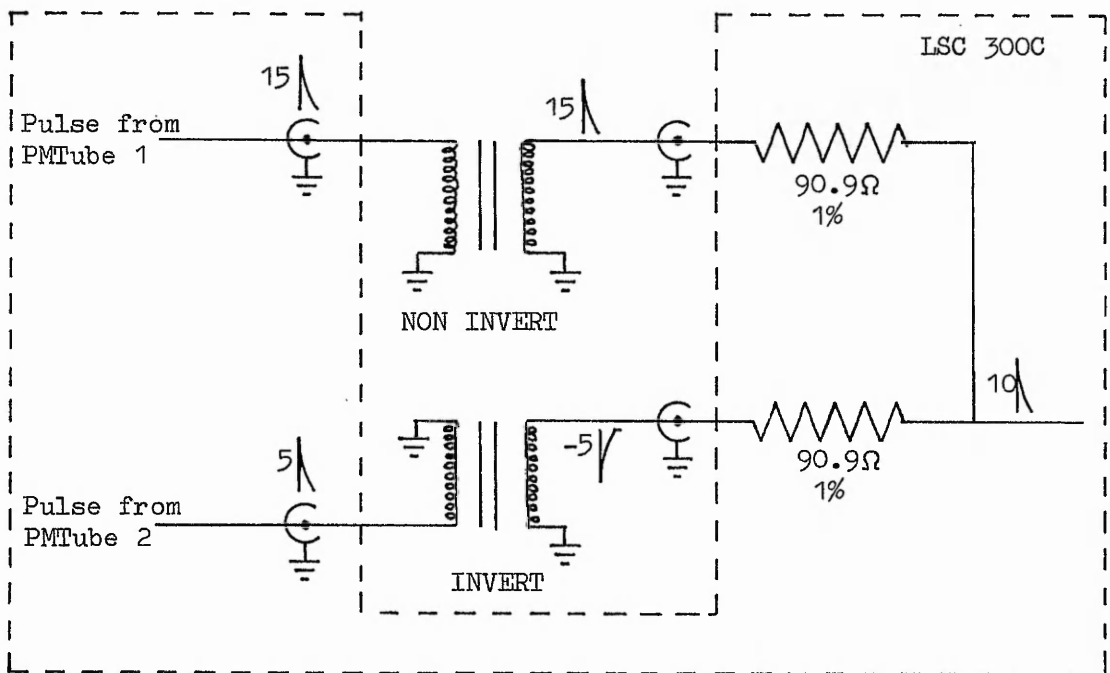
(b)   Differenced pulse handling circuit

Fig. F3.24   Summed and Differenced pulse handling circuits

187

CIRCUIT NOT INSTALLED
CIRCUIT INSTALLED
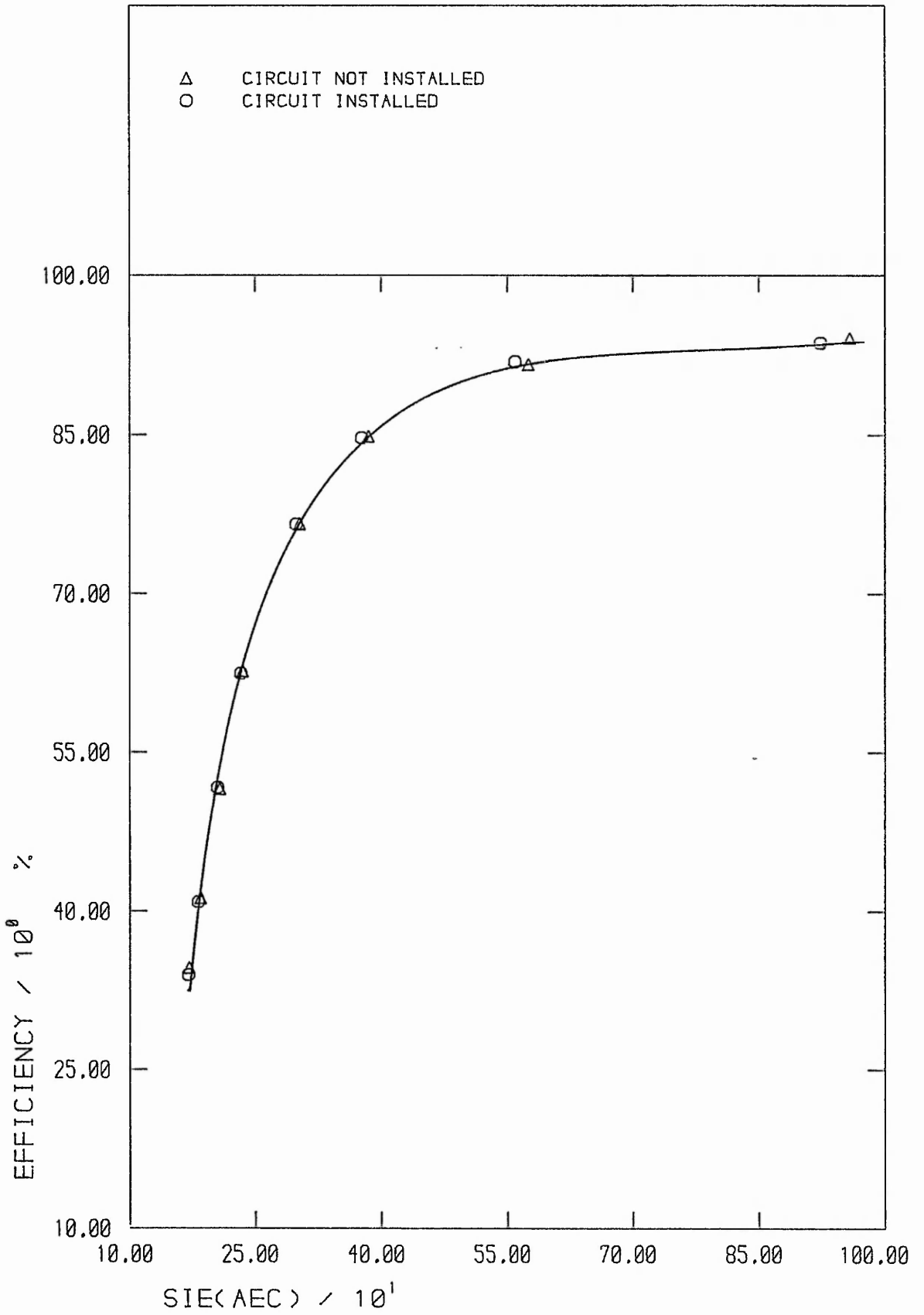
FIG F3.25: EFFICIENCY vs SIE(AEC) CURVE
-EFFECT OF INSTALLED DIFFERENCE CIRCUIT

188
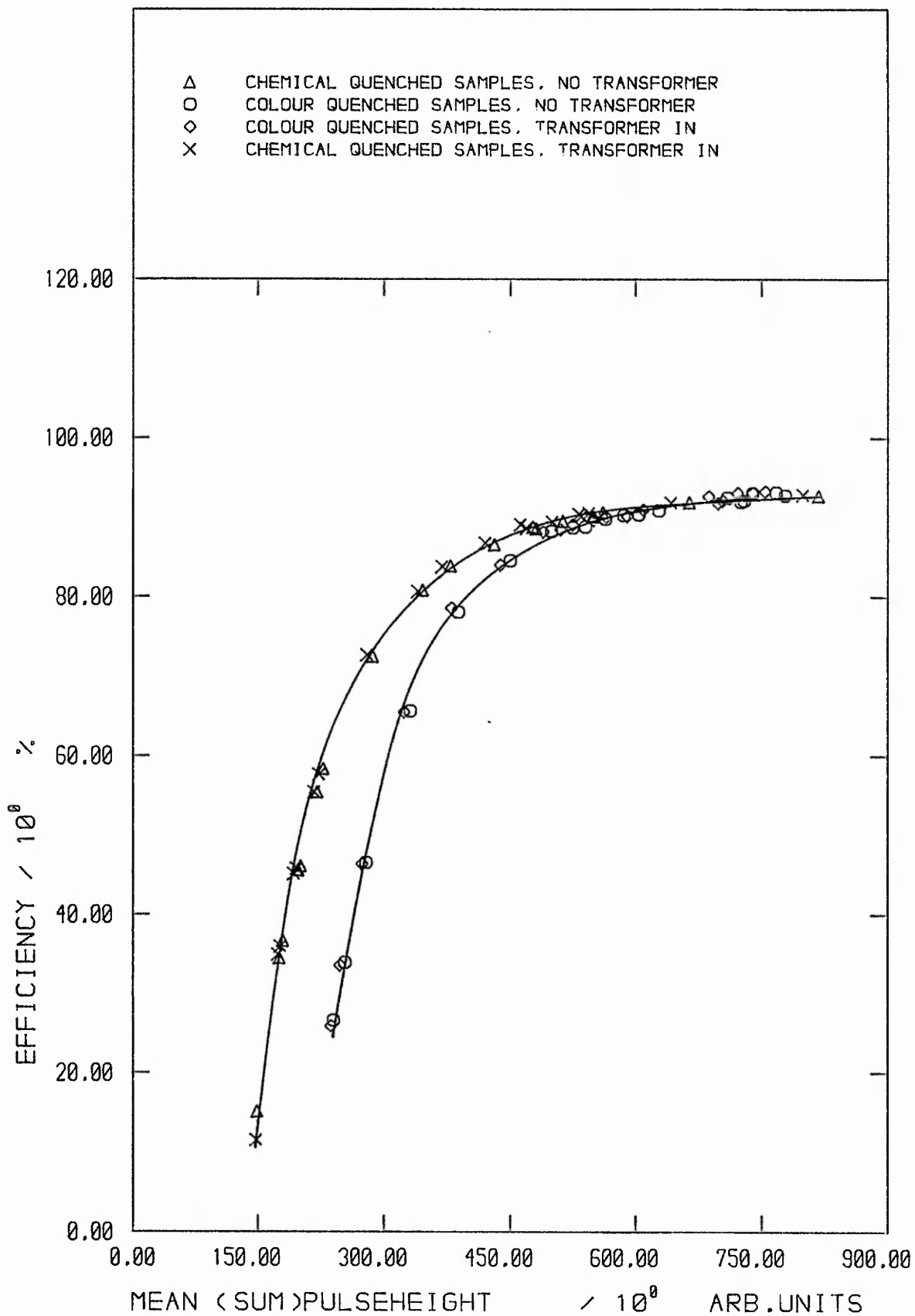
FIG F3.26: 14C EFFICIENCY v SIE(AEC) CURVES WITH
COLOUR/CHEMICAL QUENCH & TRANSFORMER IN/OUT

189
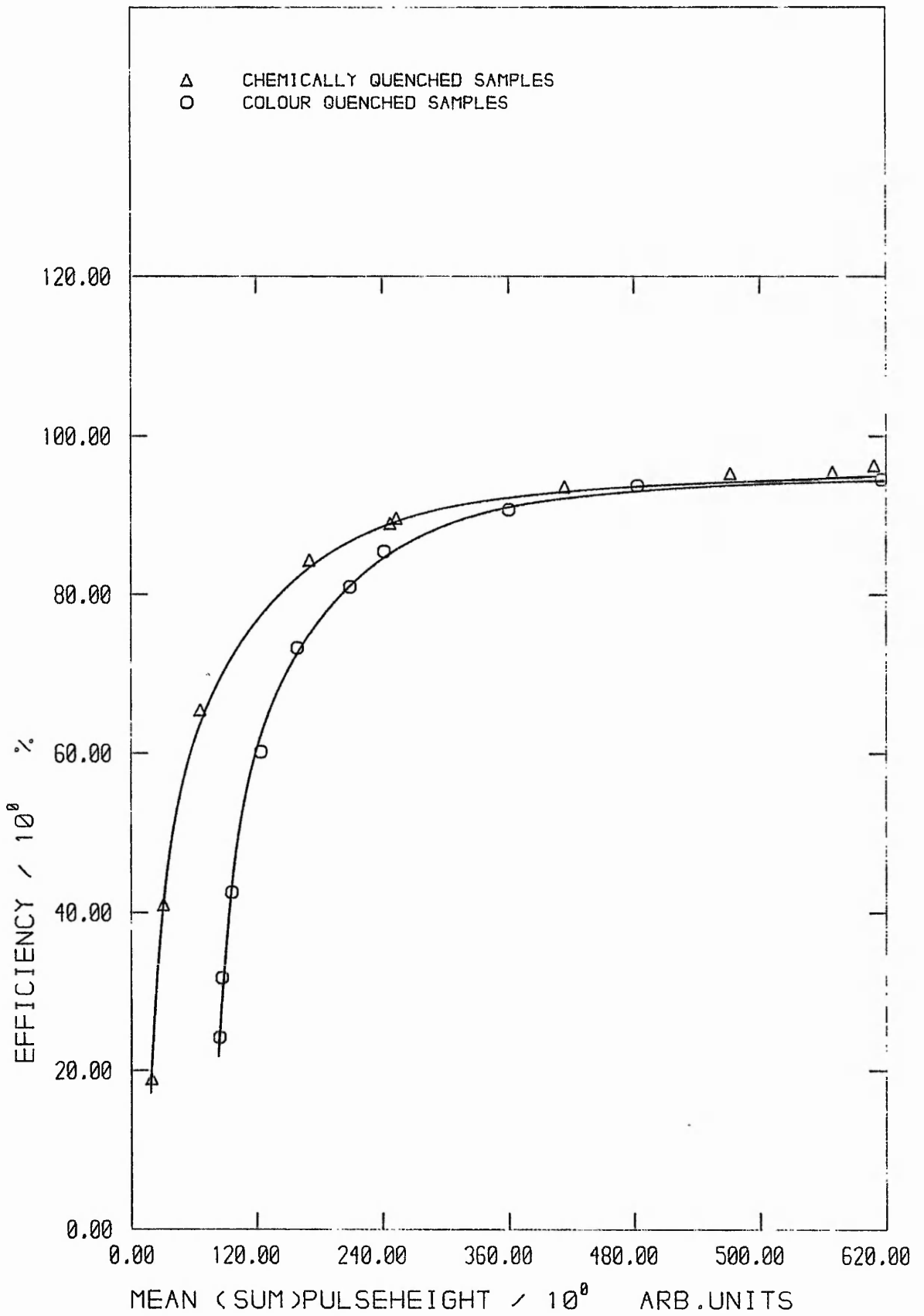
FIG F3.27 : 14C QUENCH CALIBRATION CURVES
- EXPERIMENTAL DATA

190
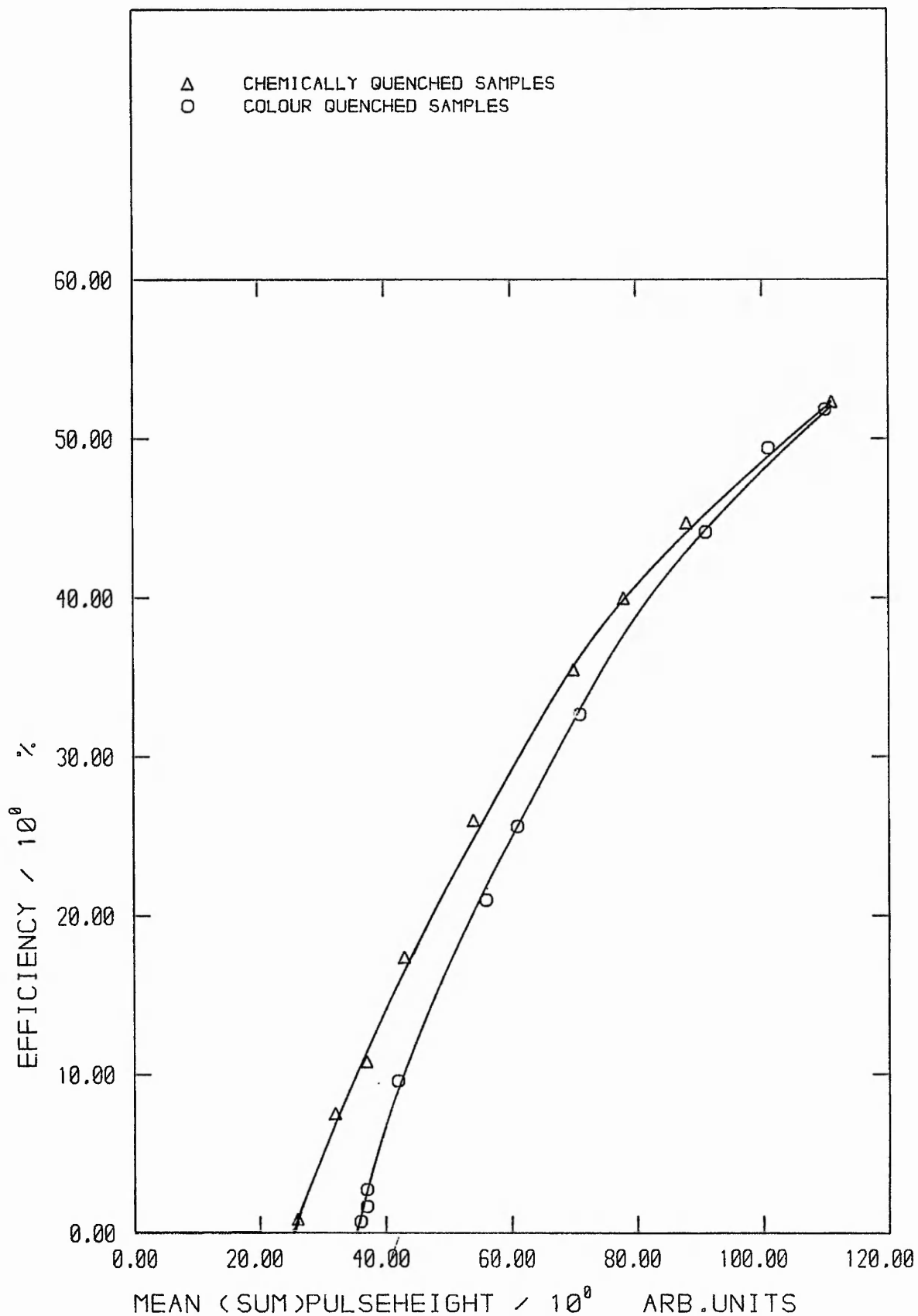
FIG F3.28 : H3 QUENCH CALIBRATION CURVES
        - EXPERIMENTAL DATA
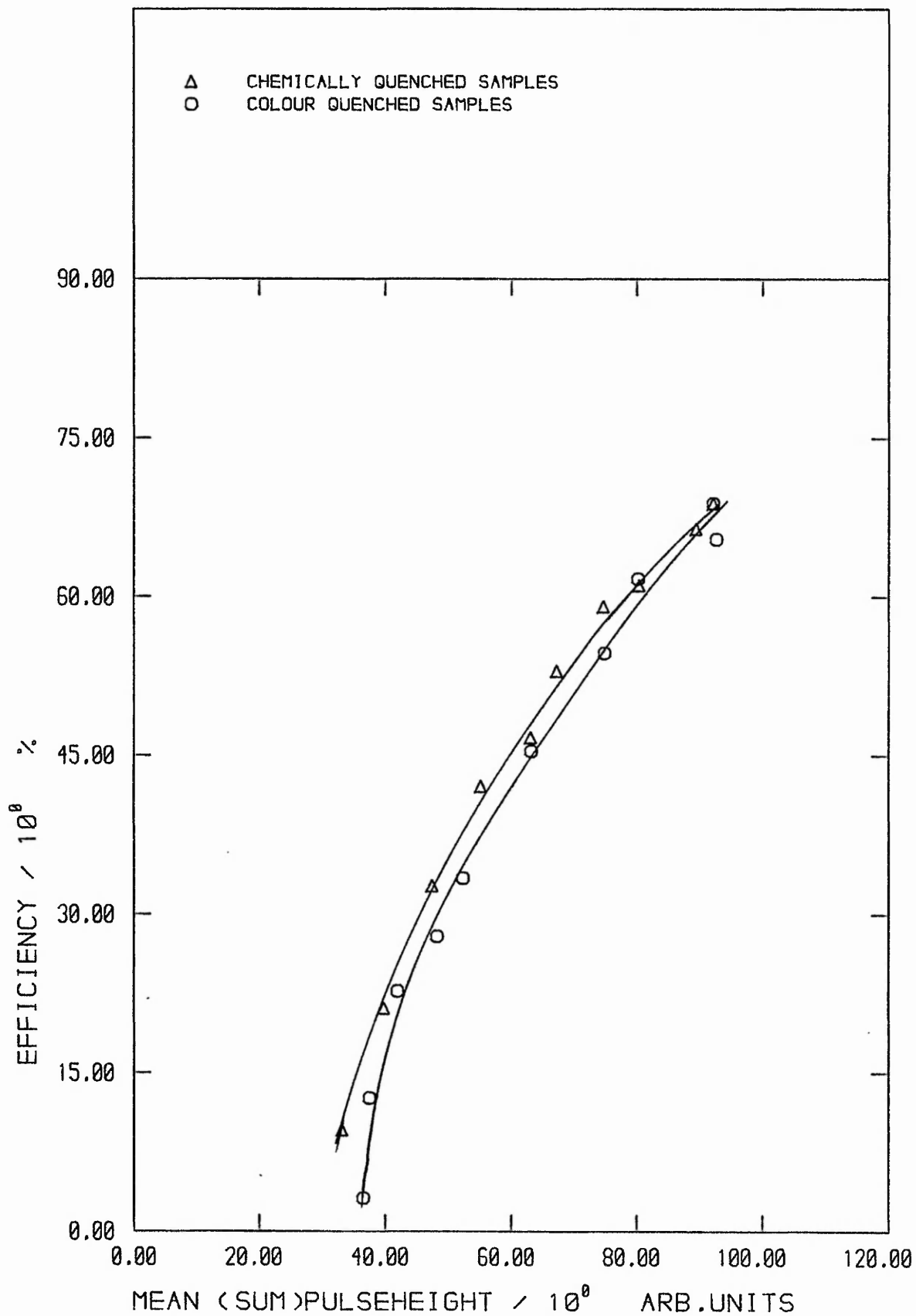
FIG F3.29 : H3 QUENCH CALIBRATION CURVES
— MODEL GENERATED DATA
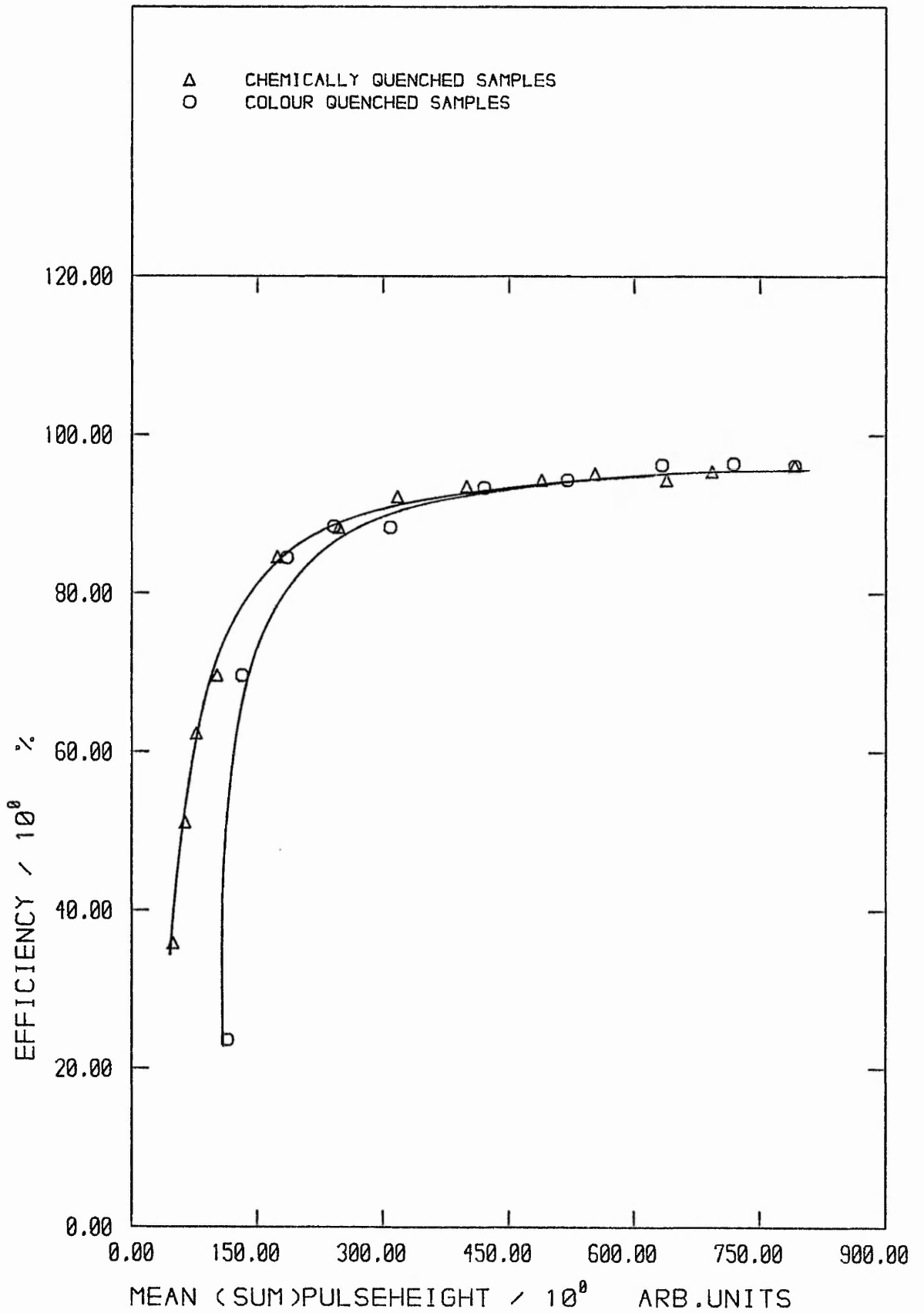
FIG F3.30 : C14 QUENCH CALIBRATION CURVES
— MODEL GENERATED DATA
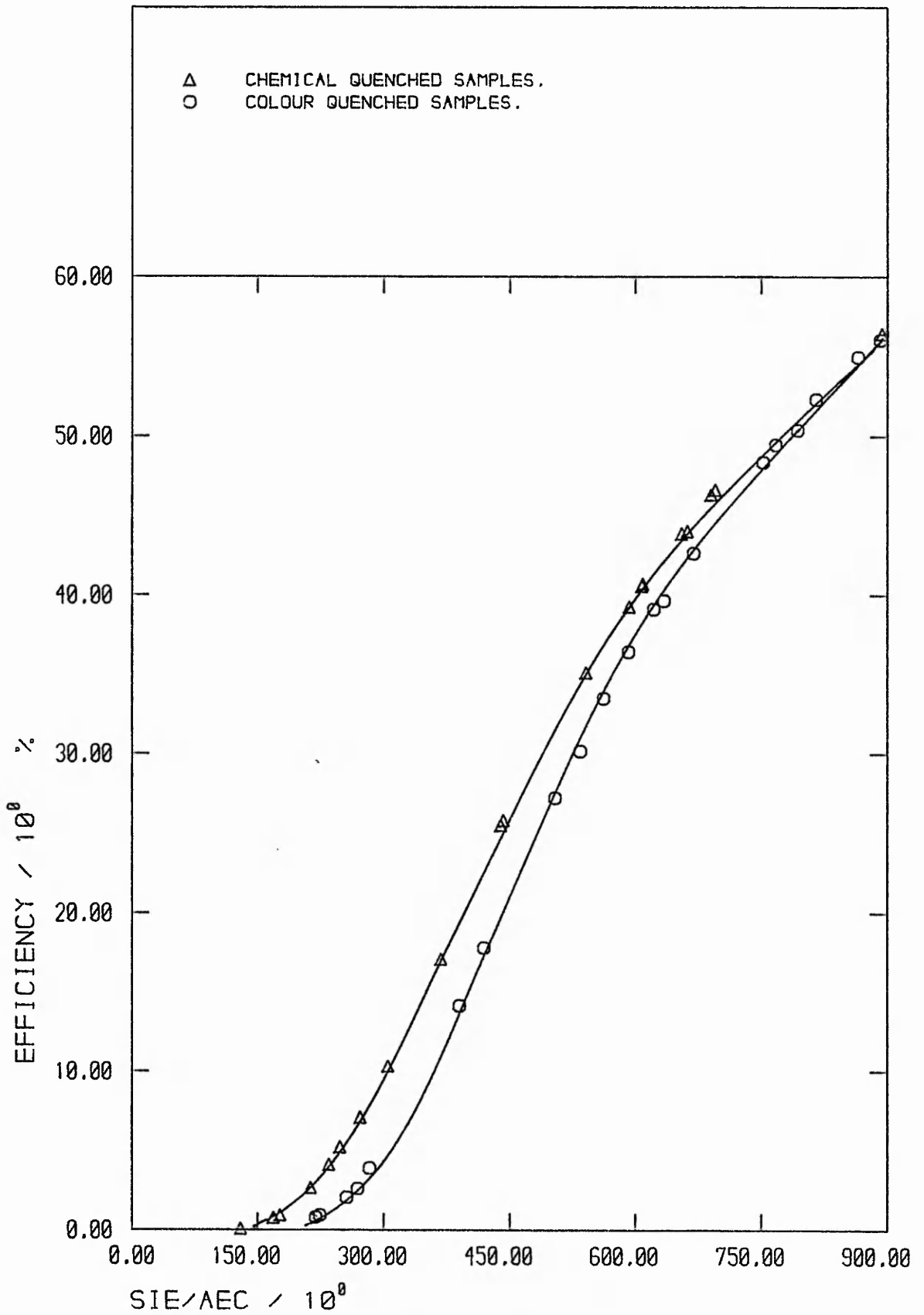
FIG F3.31: ORIGINAL EFFICIENCY v SIE(AEC)
CURVES FOR TRITIUM

194
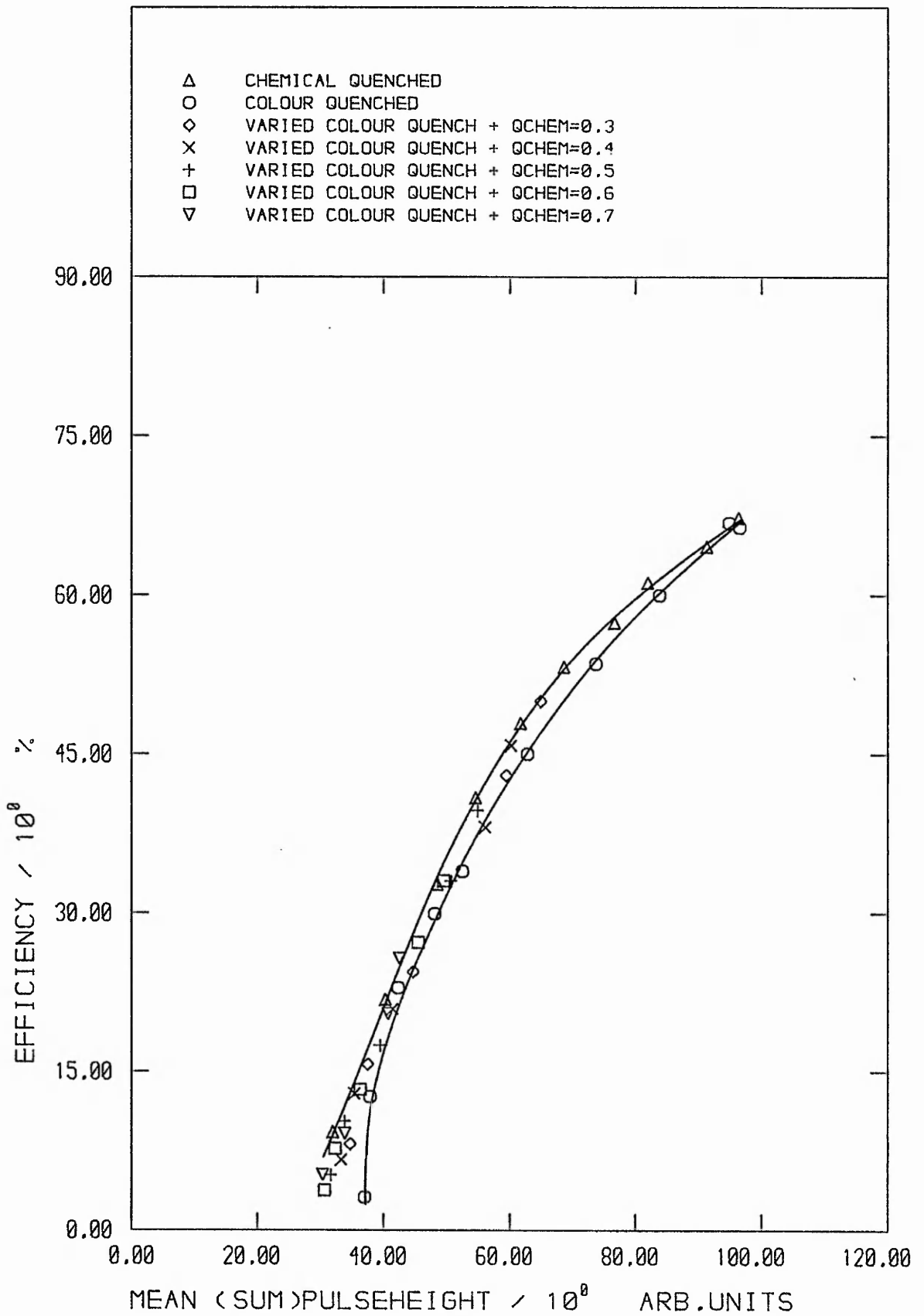
FIG F3.32: MODEL GENERATED H3 CALIBRATION
CURVES WITH MIXED COL/CHEM QUENCH (5000 pts)
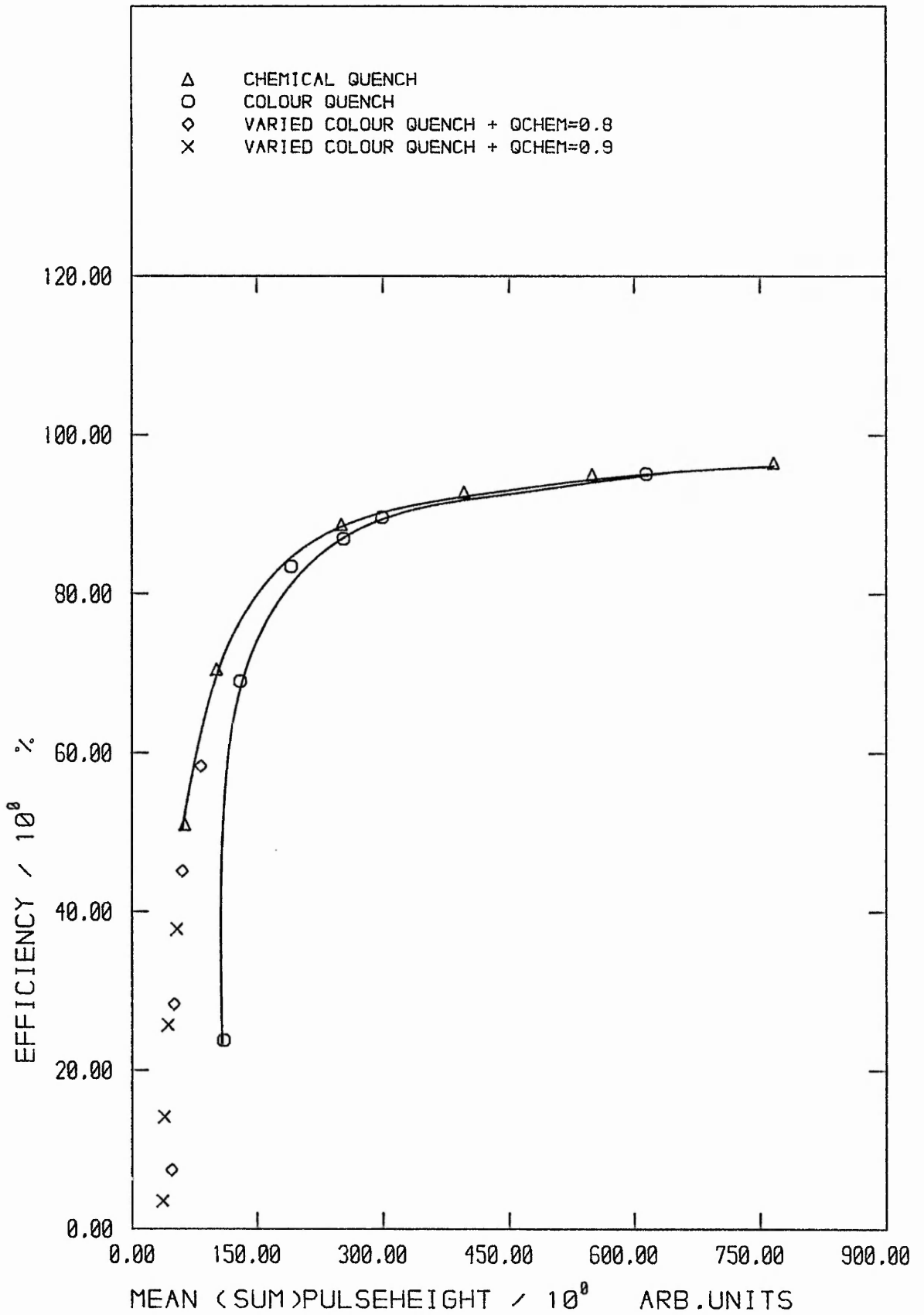
FIG F3.33: MODEL GENERATED C14 CALIBRATION
CURVES + MIXED COL/CHEM QUENCH (5000 pts)

196
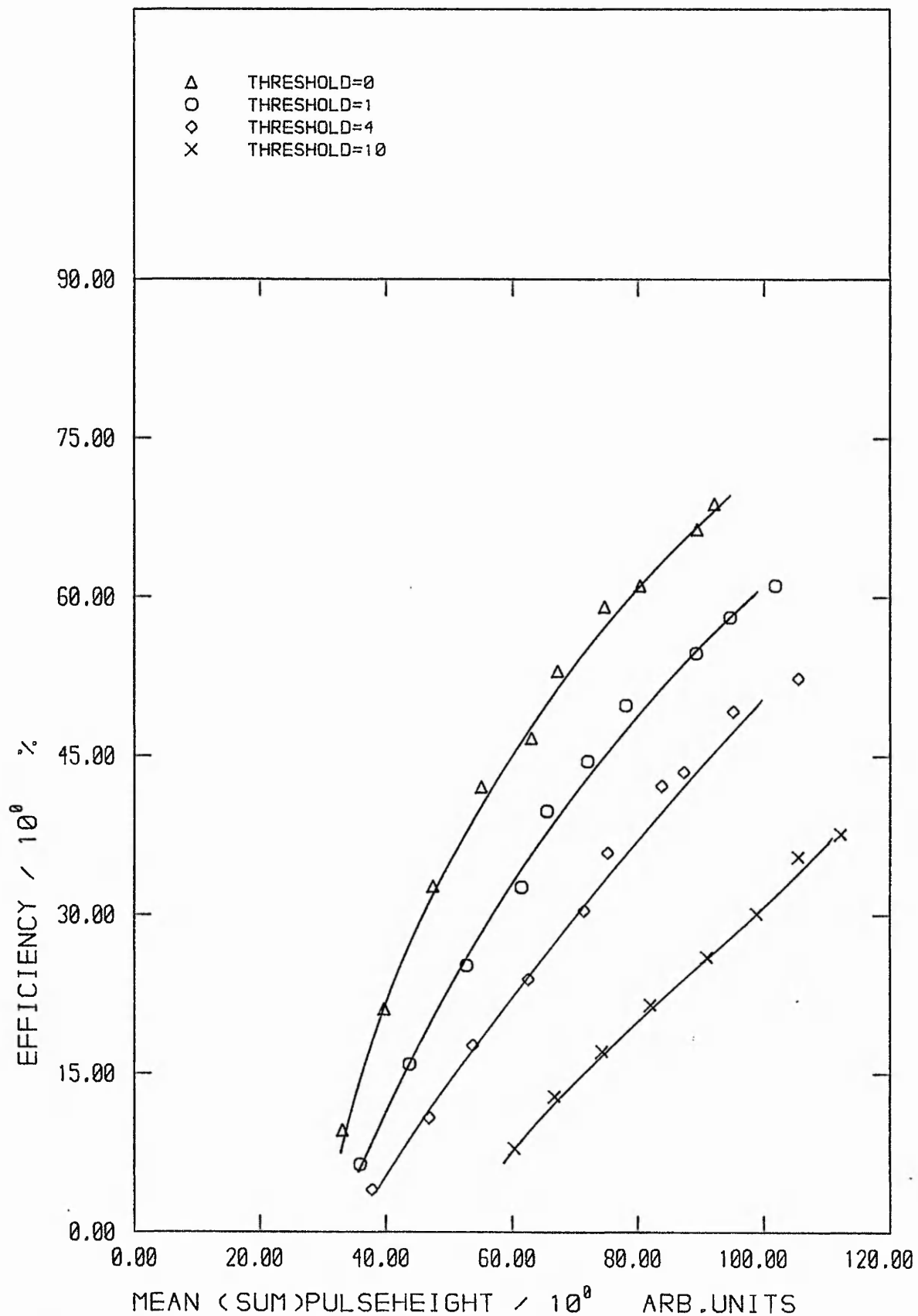
FIG F3.34: MODEL GENERATED 3H CALIBRATION
CURVES - THRESHOLD EFFECT
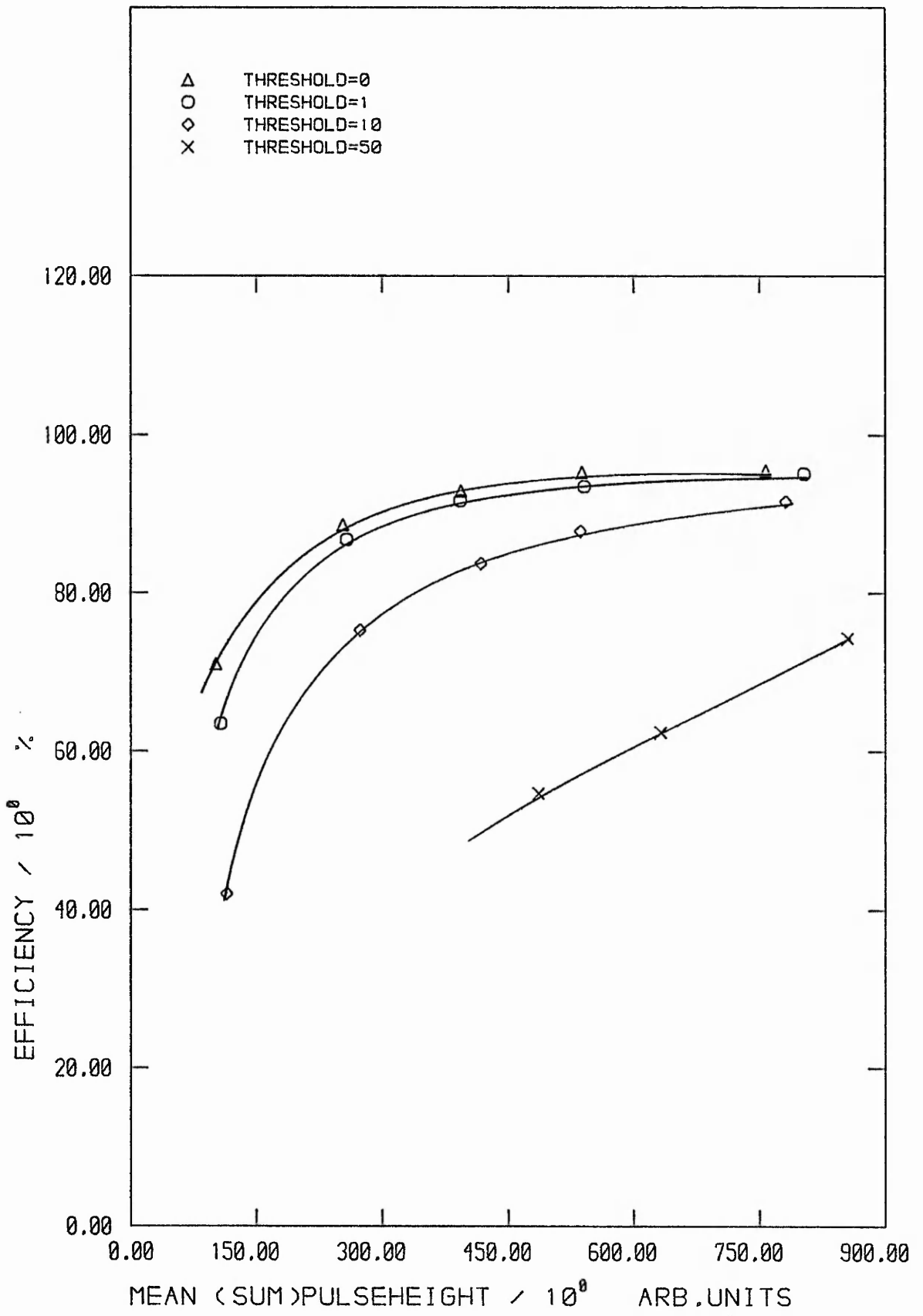
FIG F3.35: MODEL GENERATED 14C CALIBRATION
CURVES - THRESHOLD EFFECT

198
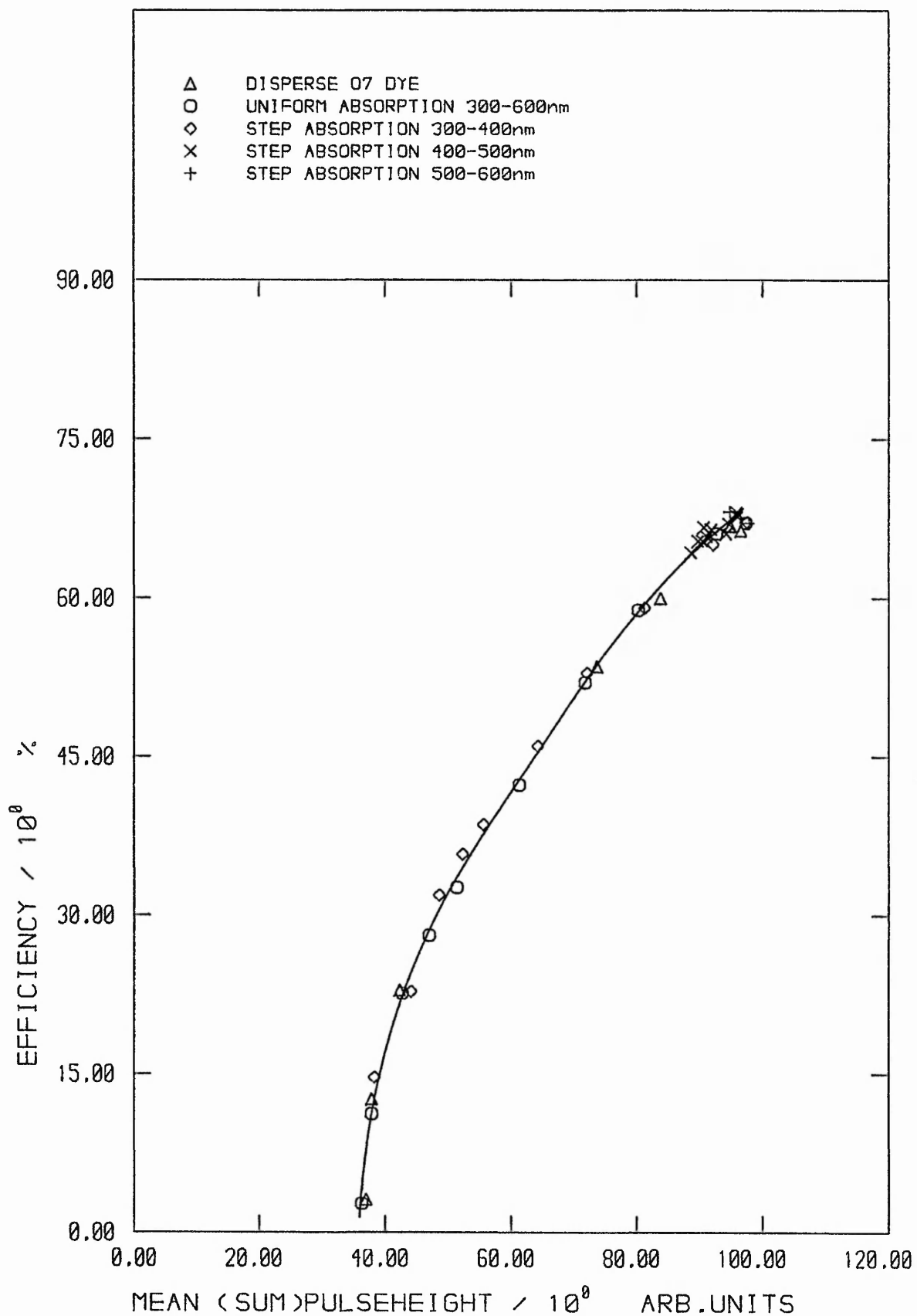
FIG F3.36: MODEL GENERATED 3H CALIBRATION
CURVES- VARIOUS COLOUR QUENCHERS(5000pts)
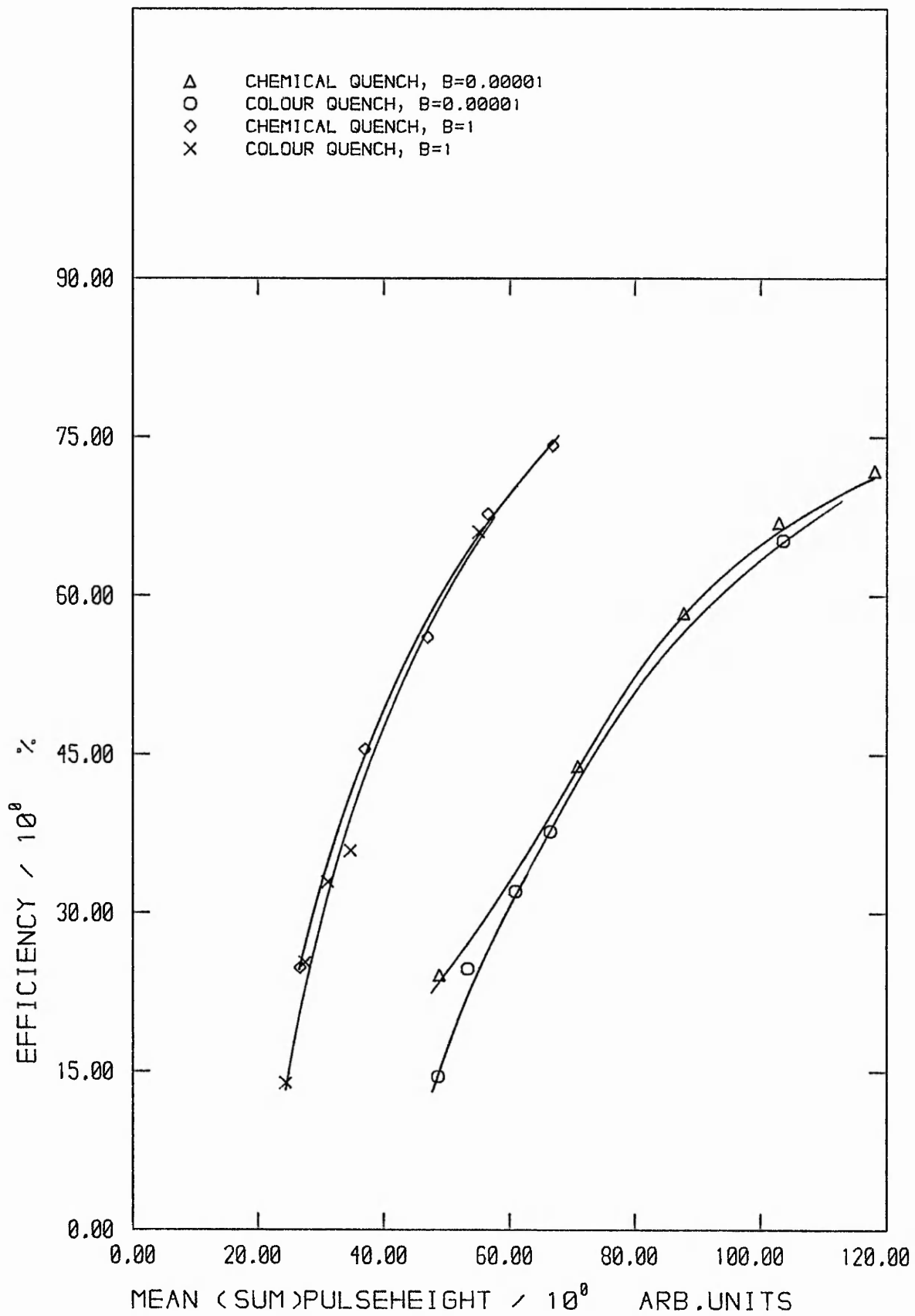
FIG F3.37: EFFECT OF SHAPE FACTOR B
ON 3H MODEL OUTPUT
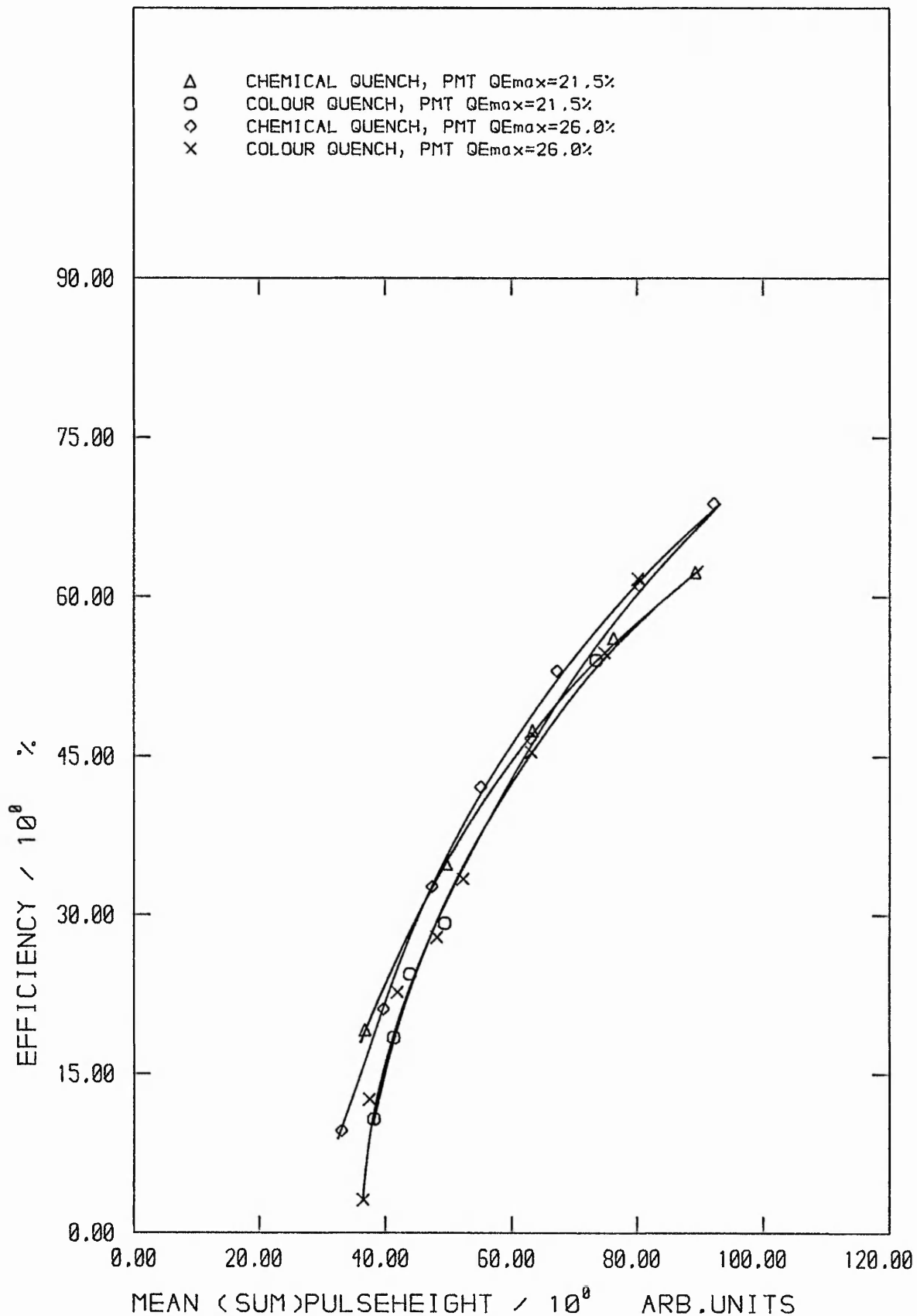
FIG F3.38: EFFECT OF PMT QUANTUM
EFFICIENCY ON 3H MODEL OUTPUT
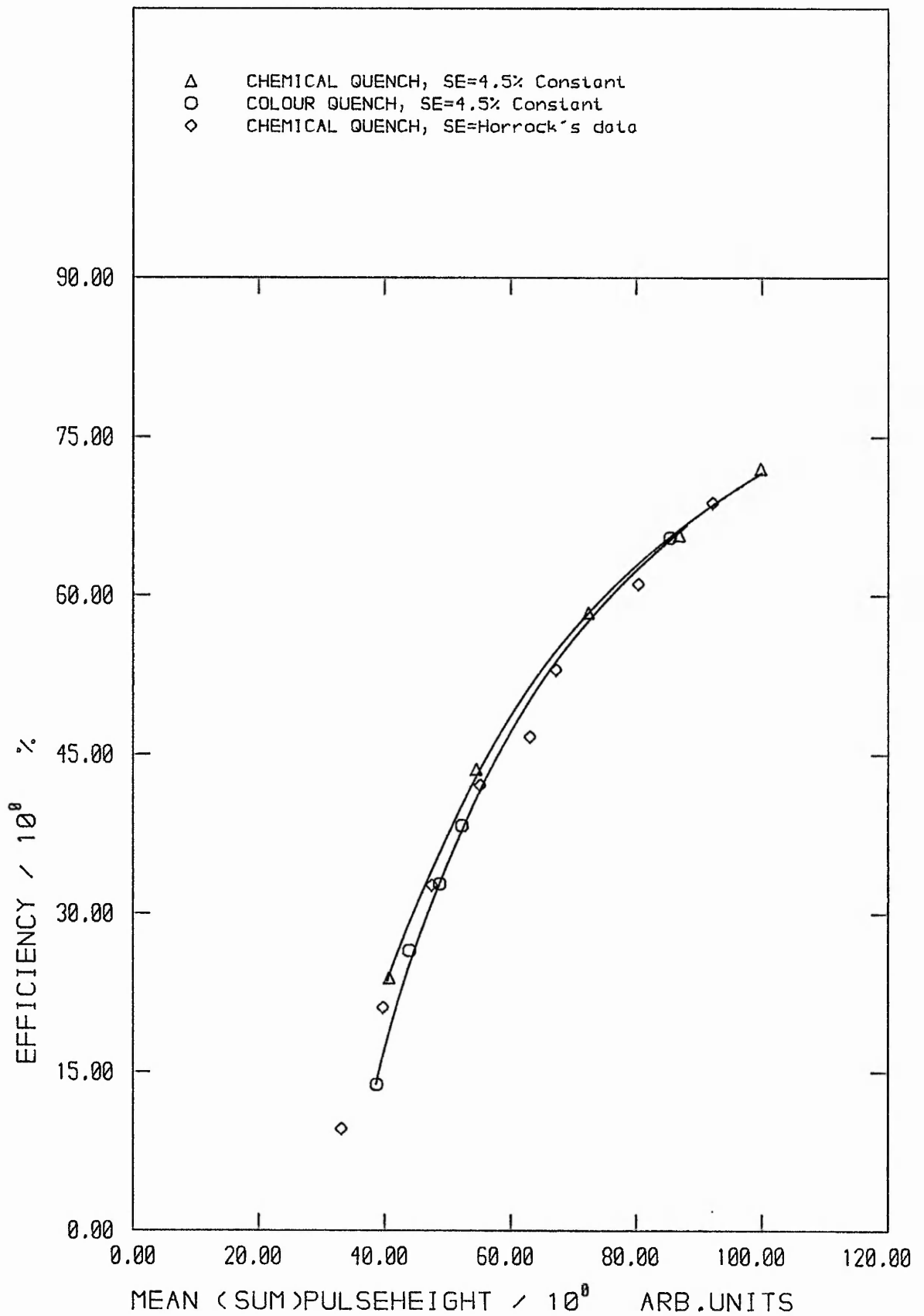
FIG F3.39: EFFECT OF CONSTANT SCINTILLATION
EFFICIENCY ON 3H MODEL OUTPUT
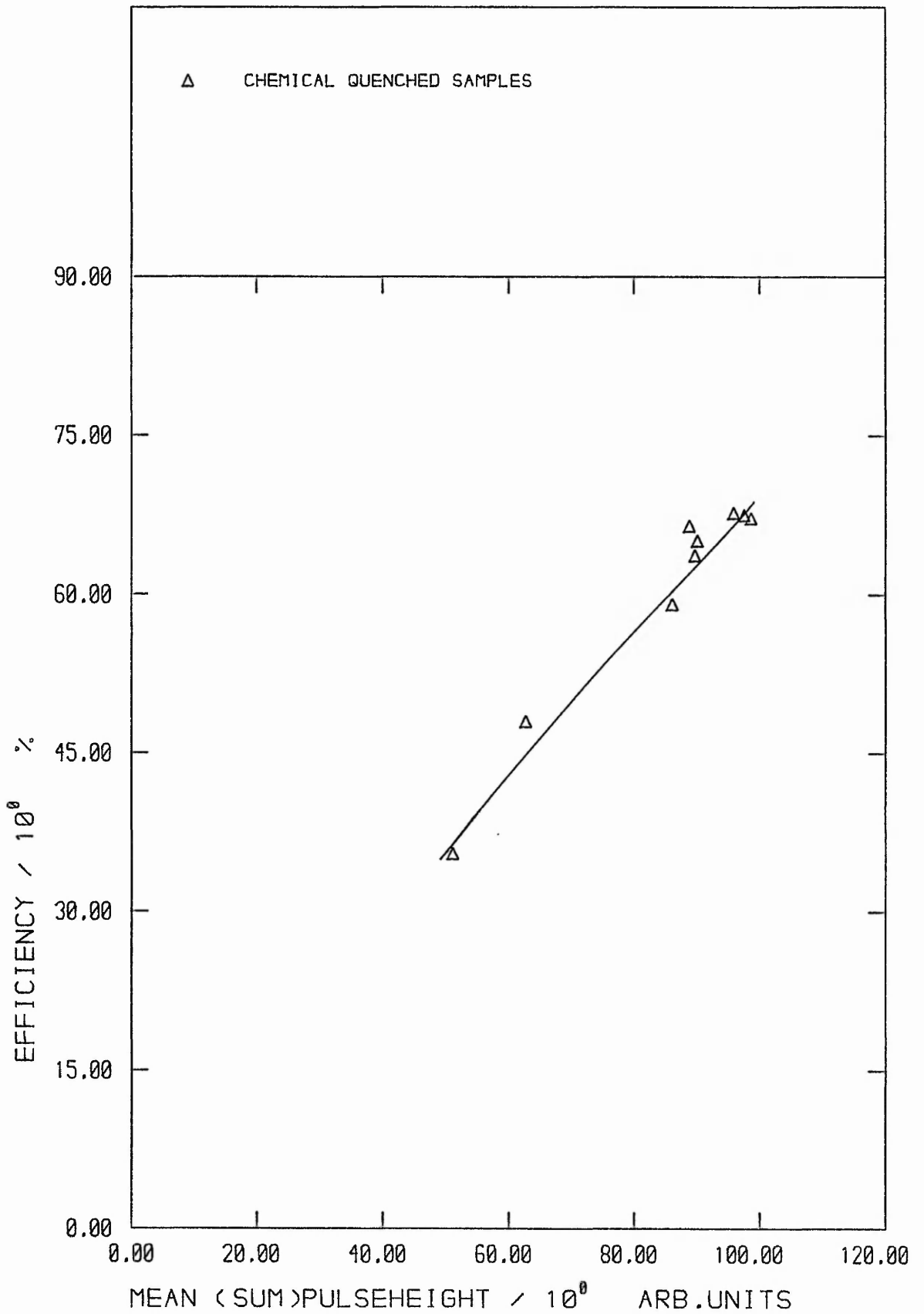
FIG F3.40a: VOLUME EFFECT ON 3H MODEL OUTPUT
 - 'GEOMETRY QUENCHING'
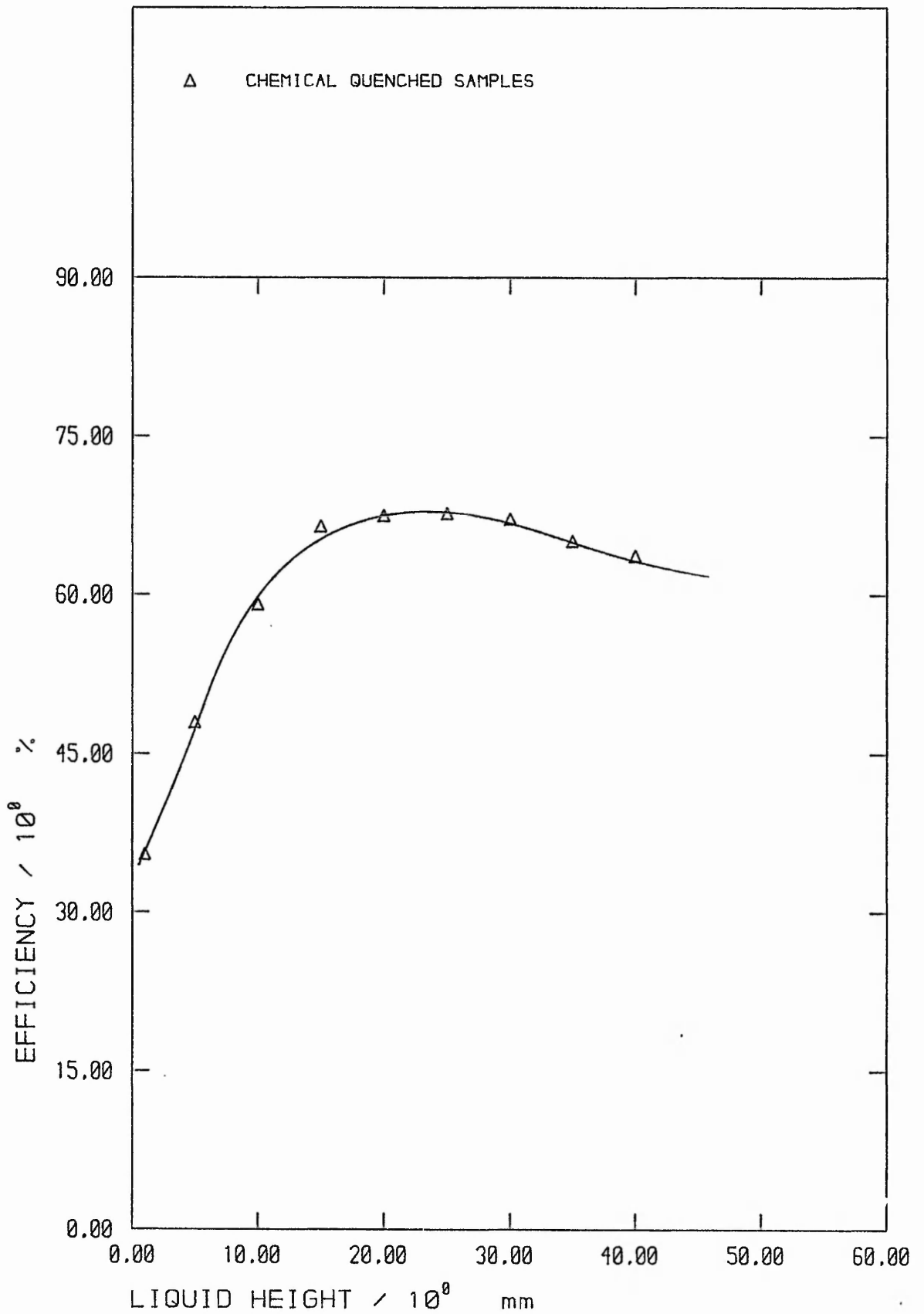
FIG F3.40b: VOLUME EFFECT ON 3H MODEL OUTPUT

204

Total No. MCA channels = 8000 ; Width of first 4000 = 1 unit
Width of last 4000 = 4000 units

$\frac{dN}{dE}$

reduced verical scale for 2nd half

0   100   200   300   400   (400)2
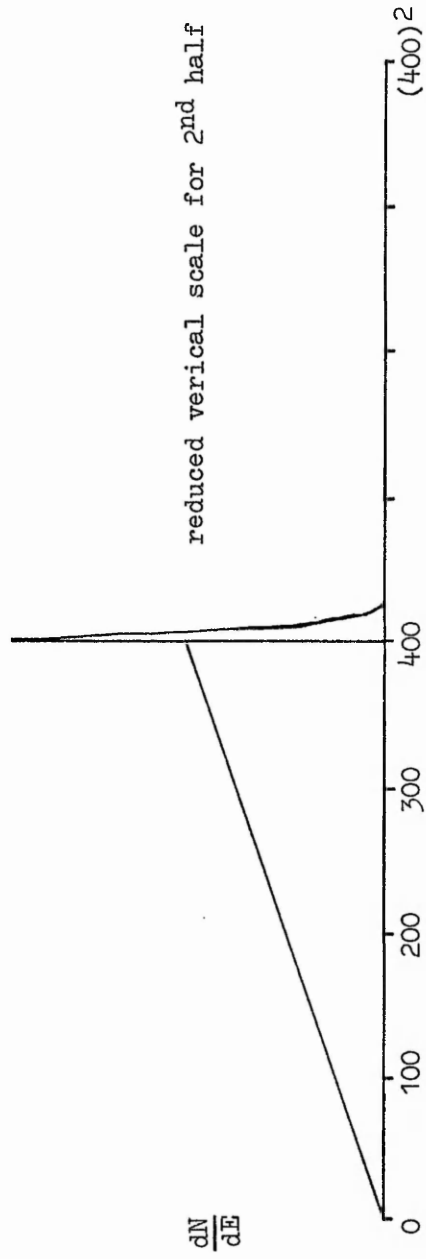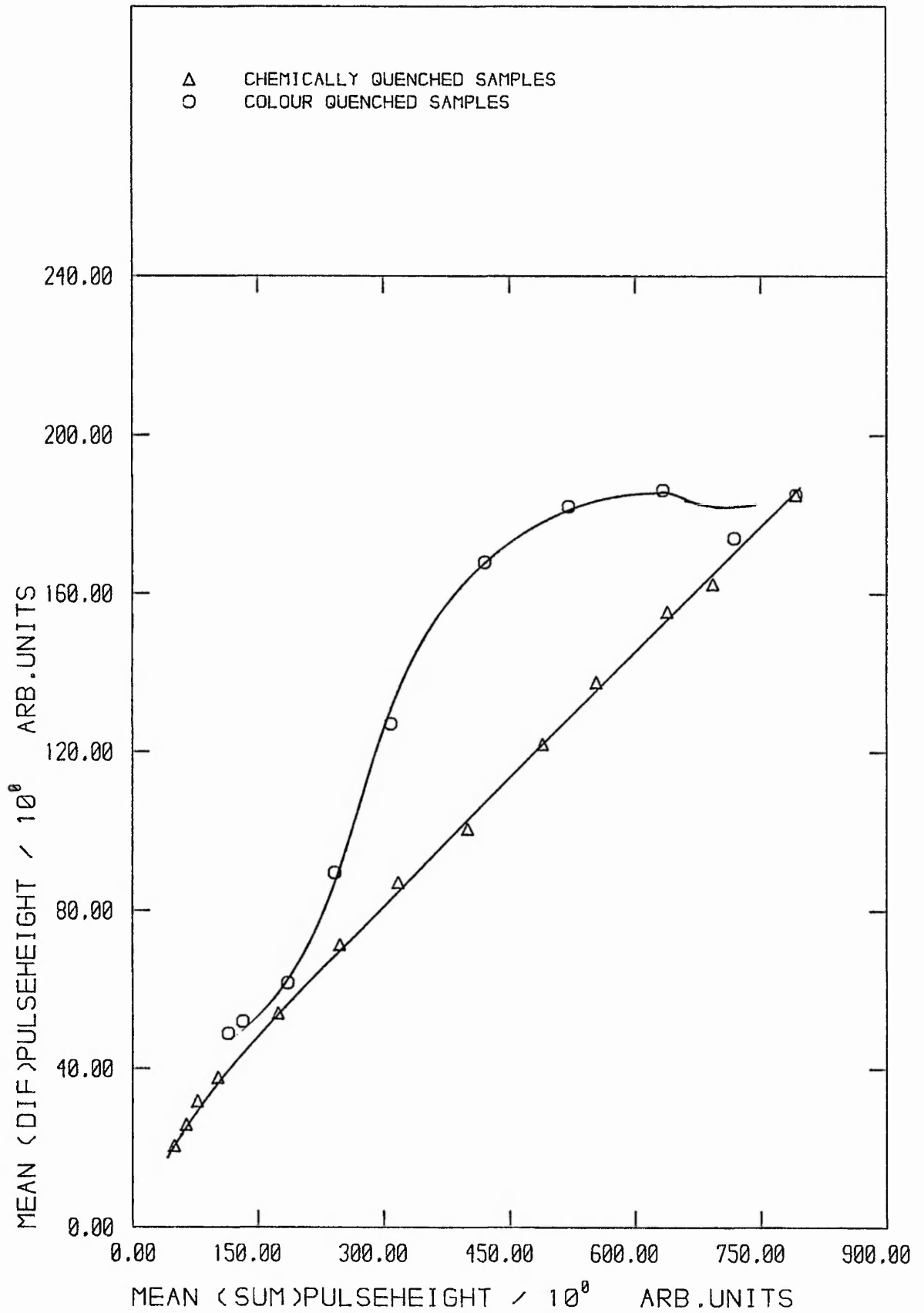
Fig. F4.1

FIG F4.2: MODEL GENERATED MEAN SUM PULSE-HEIGHT
vs MEAN DIFFERENCE PULSE-HEIGHT FOR 14C
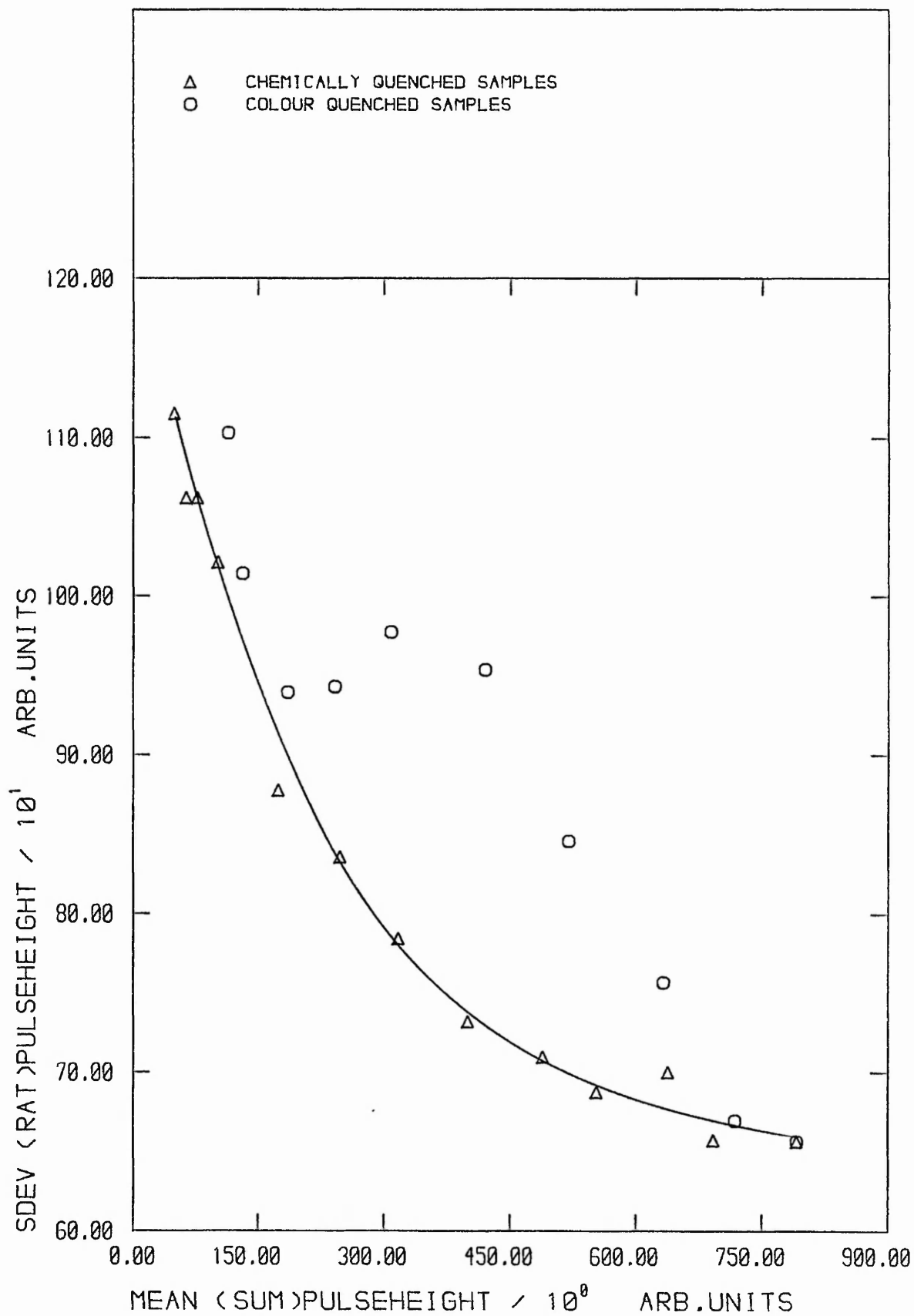
FIG F4.3: MODEL GENERATED MEAN SUM PULSE-HEIGHT
vs STD.DEV OF RATIO PULSE-HEIGHT SPECTRUM (14C)

207
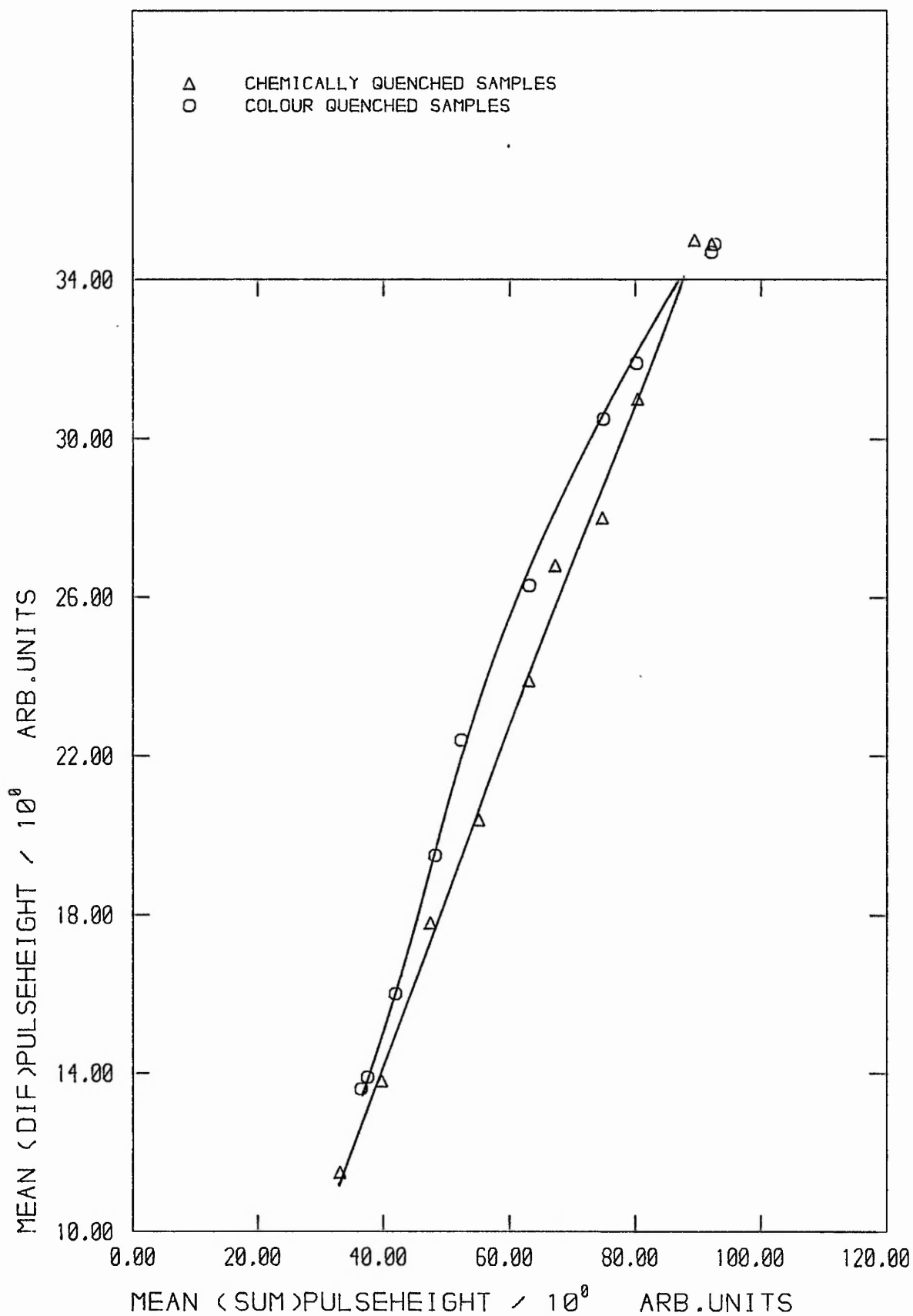
FIG F4.4: MODEL GENERATED MEAN SUM PULSEHEIGHT
vs MEAN DIFFERENCE PULSEHEIGHT FOR 3H

208
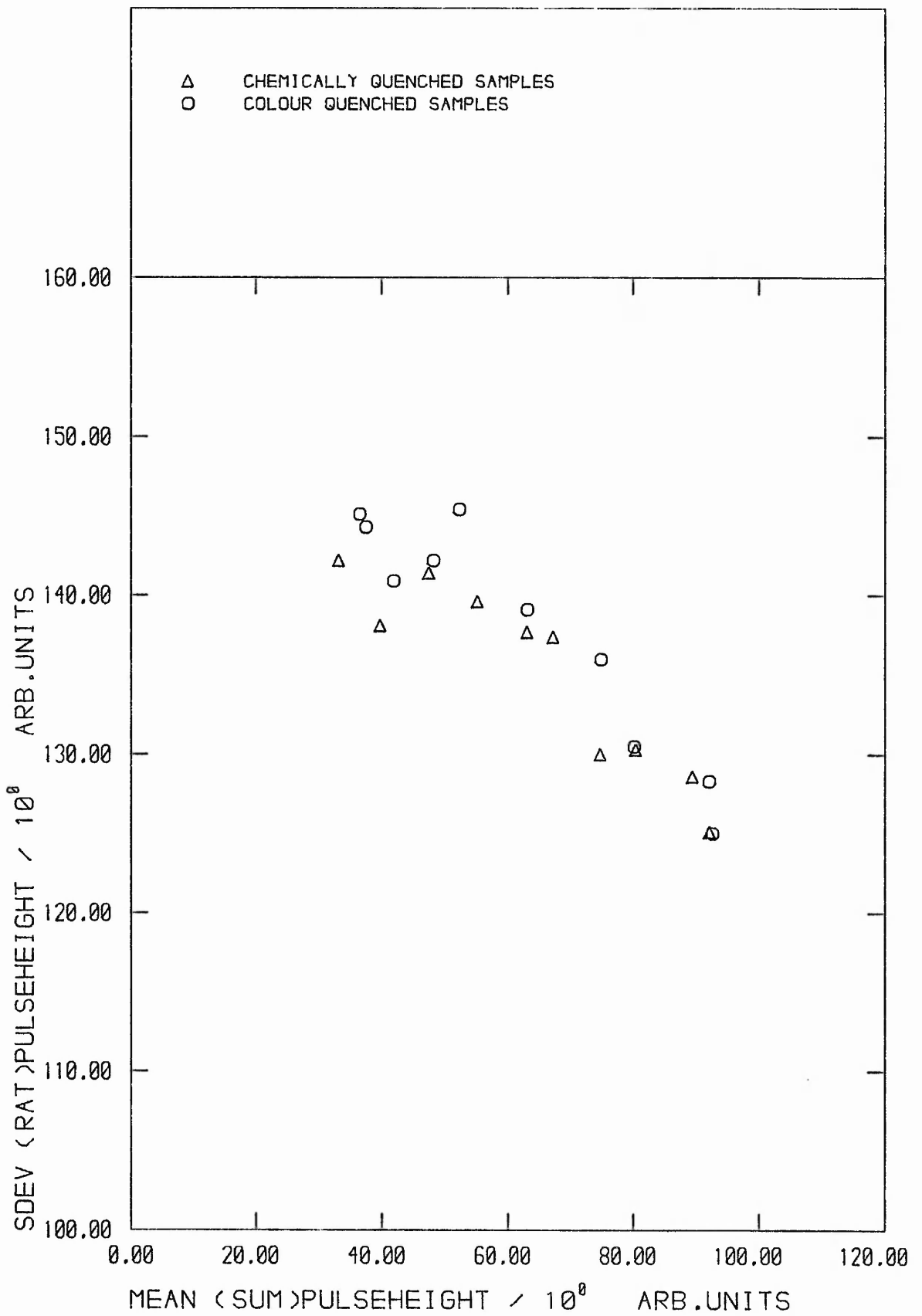
FIG F4.5 : MODEL GENERATED MEAN SUM PULSEHEIGHT
vs STD.DEV OF RATIO PULSEHEIGHT SPECTRUM FOR 3H
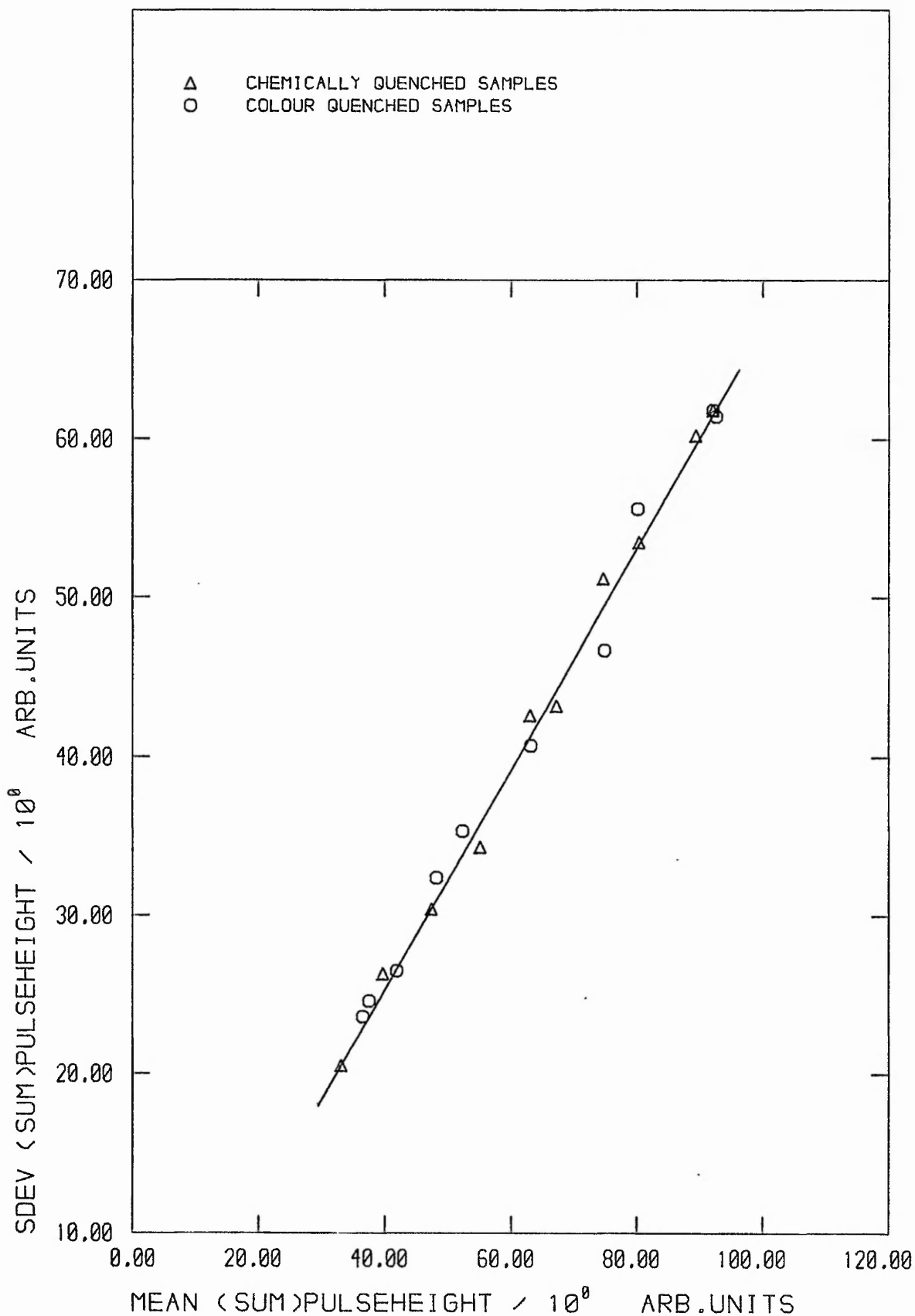
FIG F4.6 : MODEL GENERATED MEAN SUM PULSEHEIGHT
vs STD.DEV OF SUM PULSEHEIGHT SPECTRUM FOR 14C

210
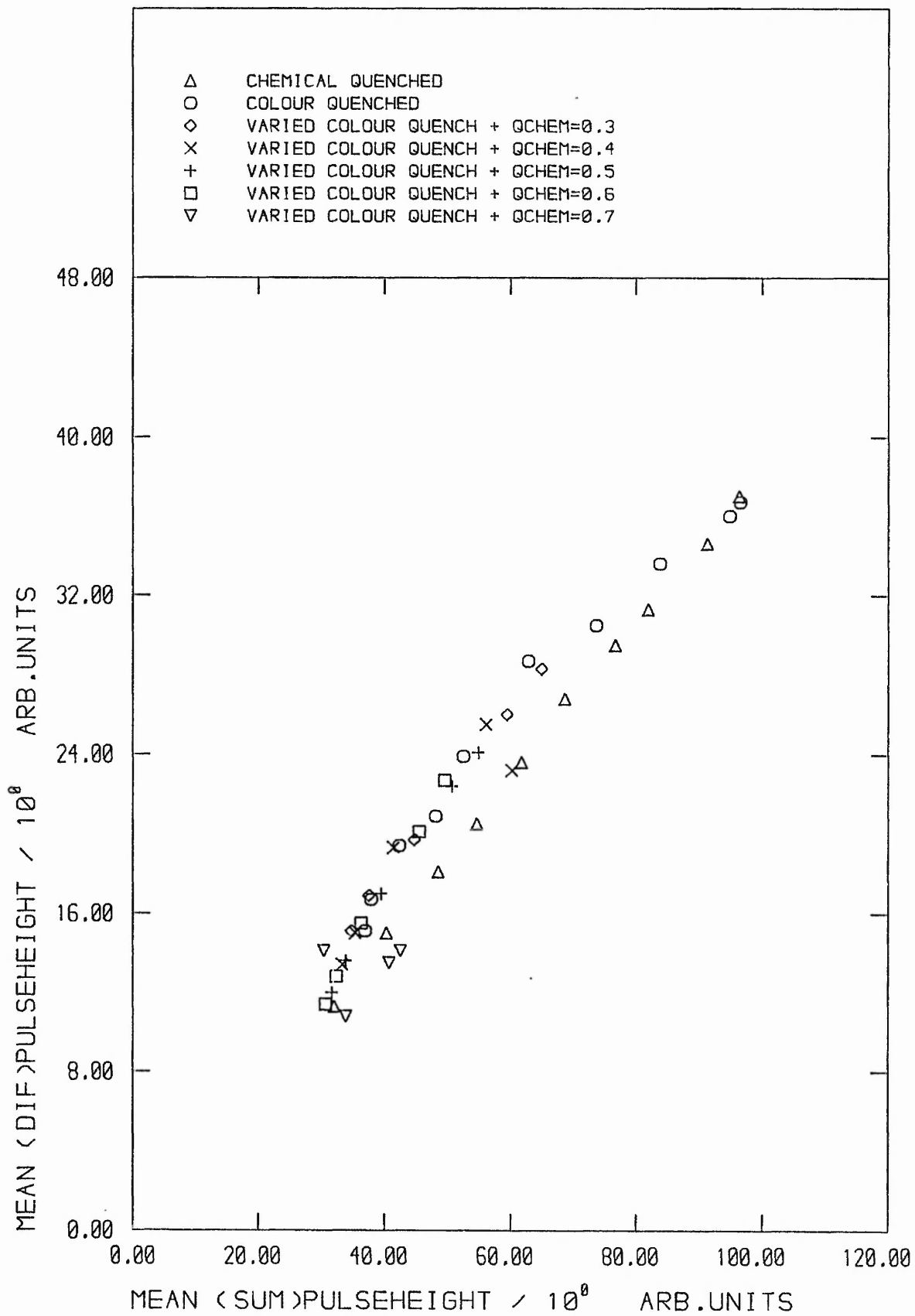
FIG F4.7 : MODEL GENERATED MEAN SUM PULSEHEIGHT
vs MEAN DIFFERENCE PULSEHEIGHT FOR 3H (5000 pts)

211
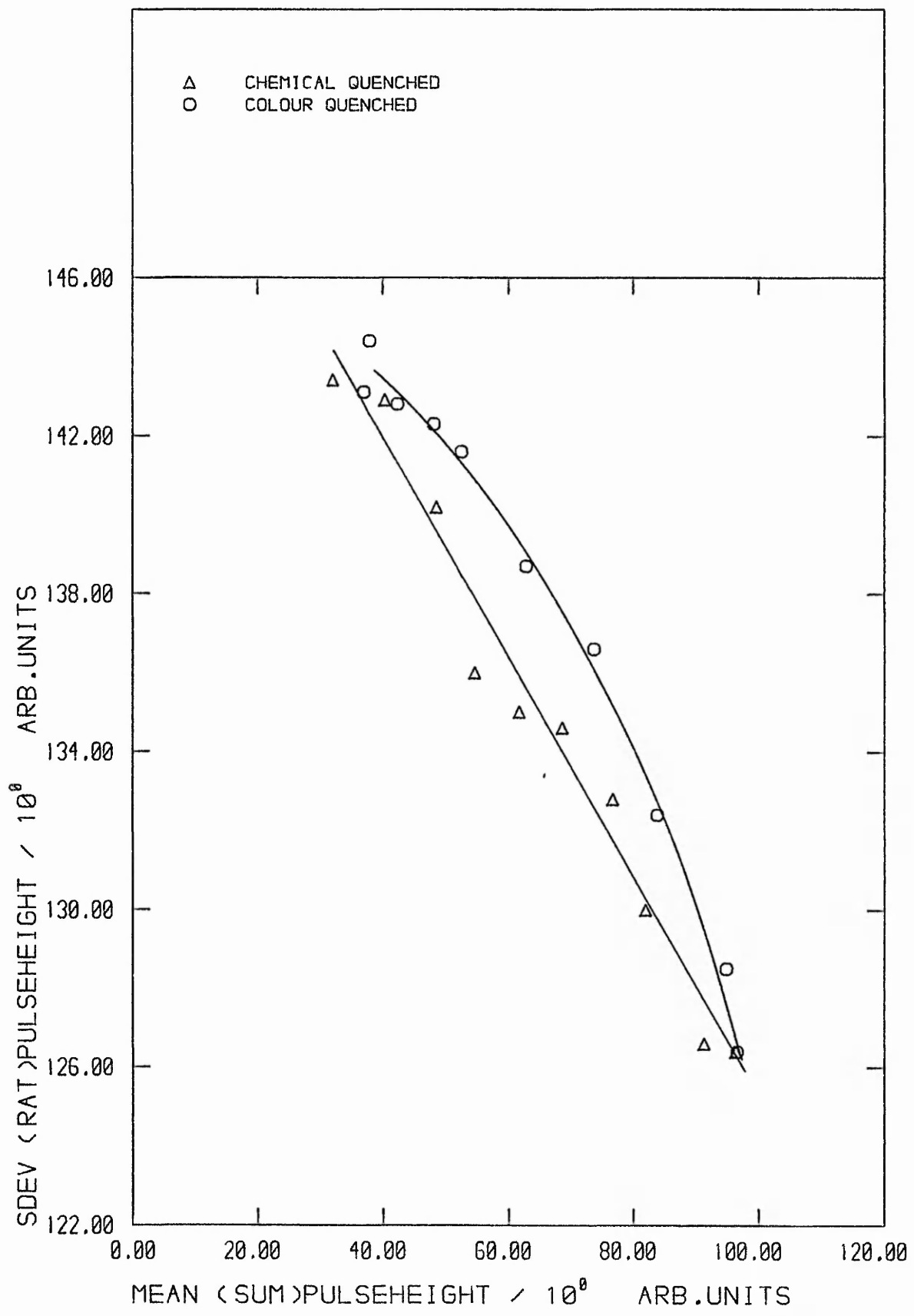
FIG F4.8 : MODEL GENERATED MEAN SUM PULSEHEIGHT
vs STD.DEV OF RATIO PH-SPECTRUM FOR 3H (5000 pts)
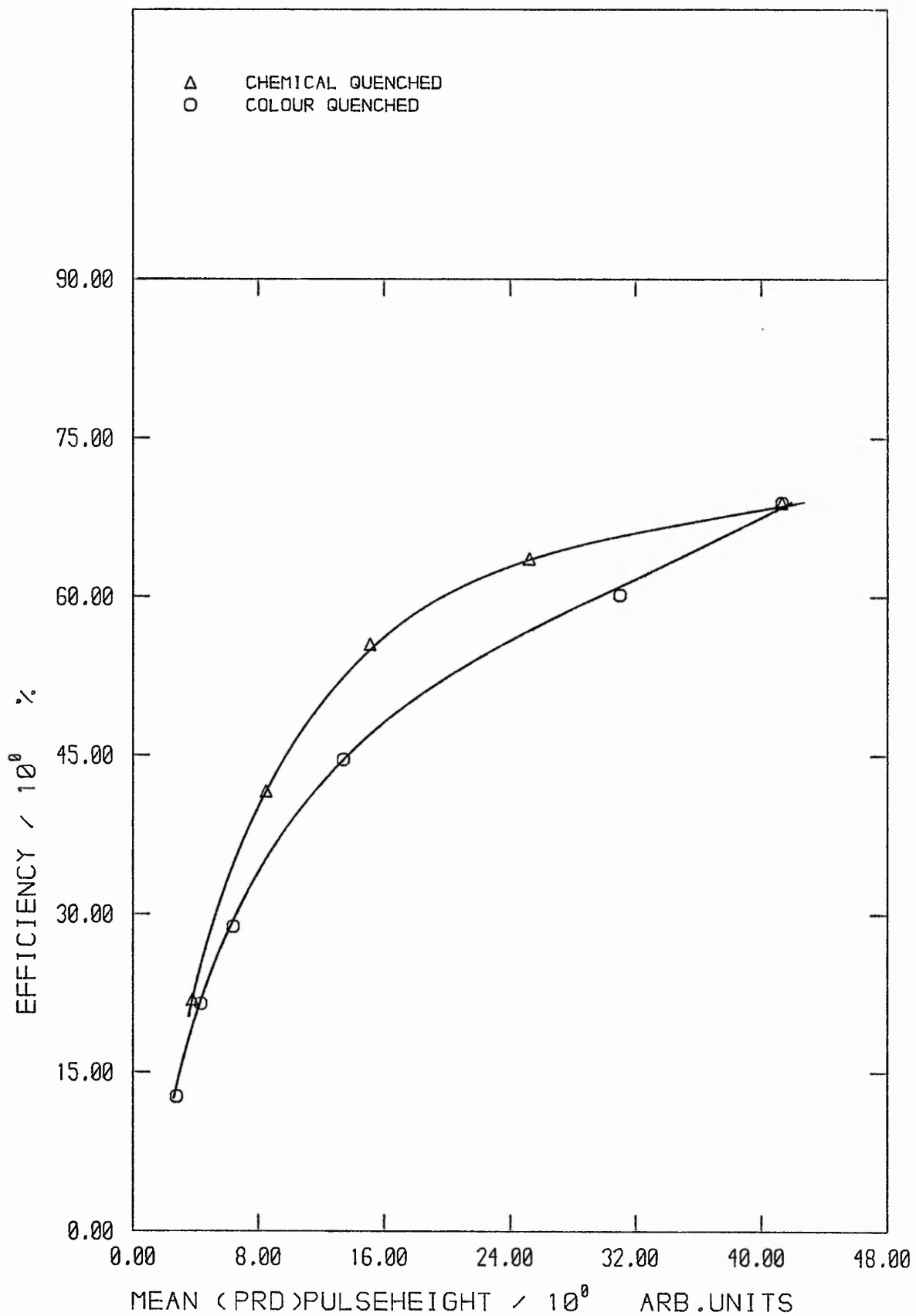
FIG F4.9 : MODEL GENERATED EFFICIENCY vs
MEAN PRODUCT PULSEHEIGHT FOR 3H
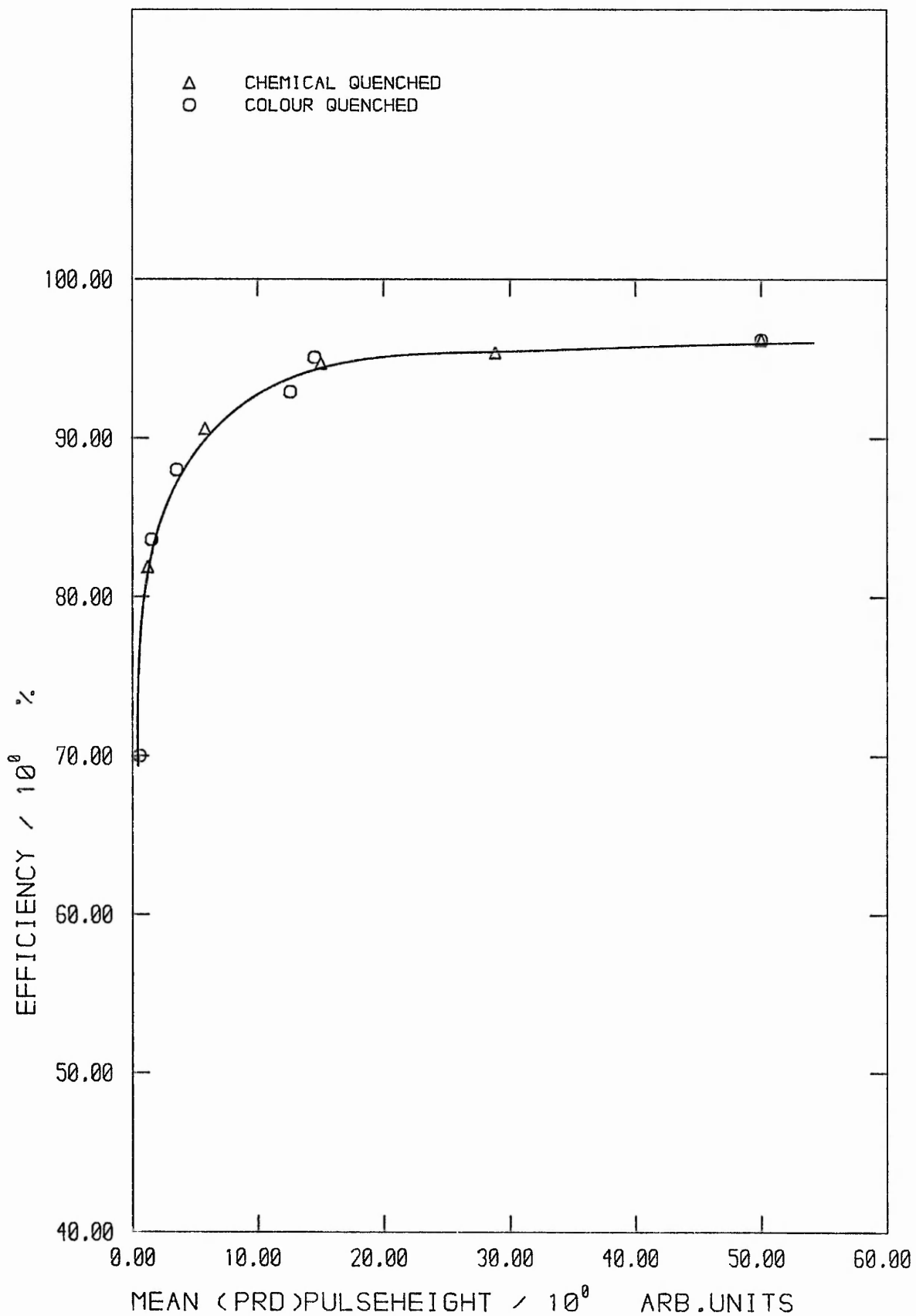
FIG F4.10 : MODEL GENERATED EFFICIENCY vs
MEAN PRODUCT PULSEHEIGHT FOR 14C

214
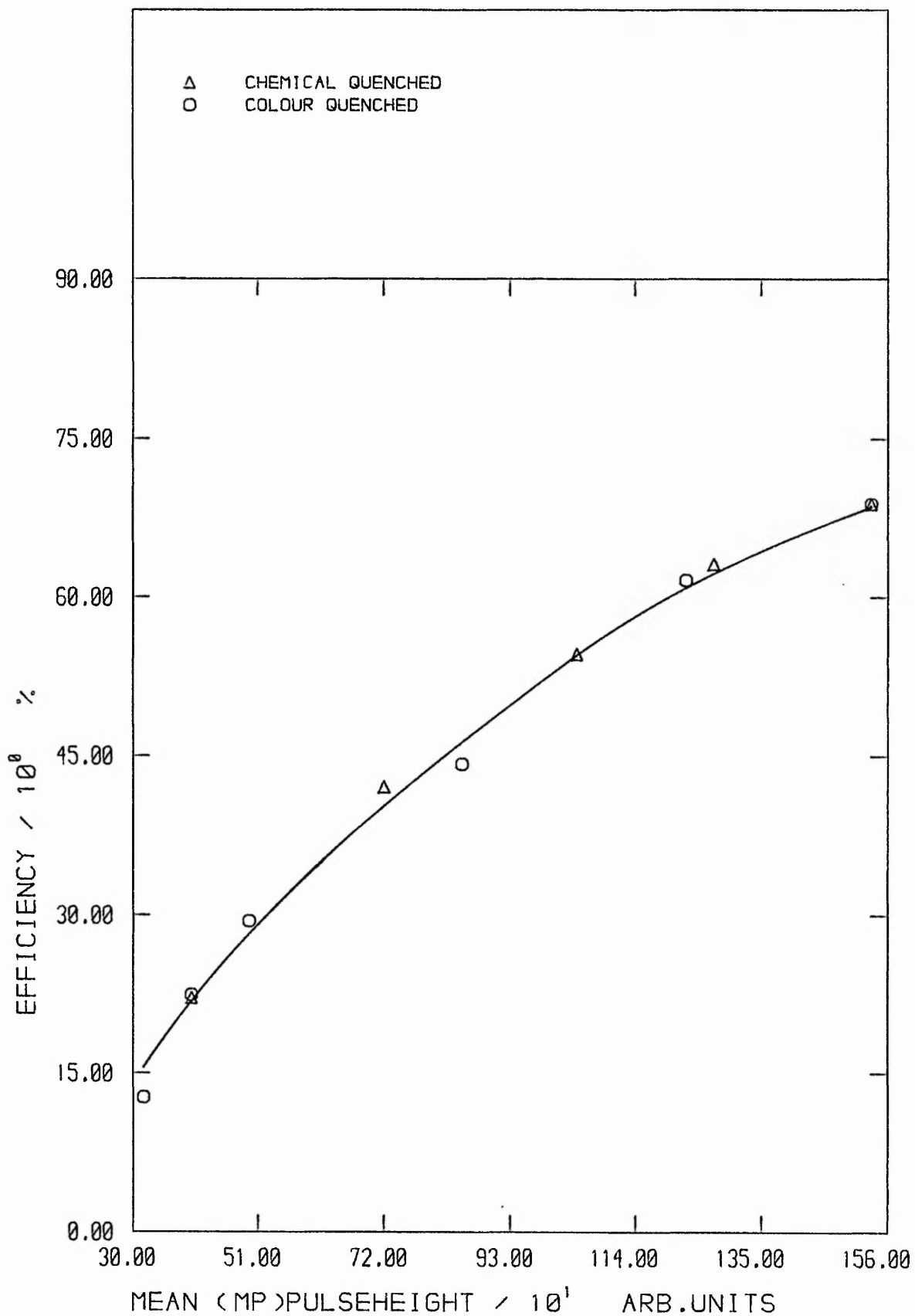
FIG F4.11 : MODEL GENERATED EFFICIENCY vs
MEAN MODIFIED-PRODUCT PULSEHEIGHT FOR 3H

215
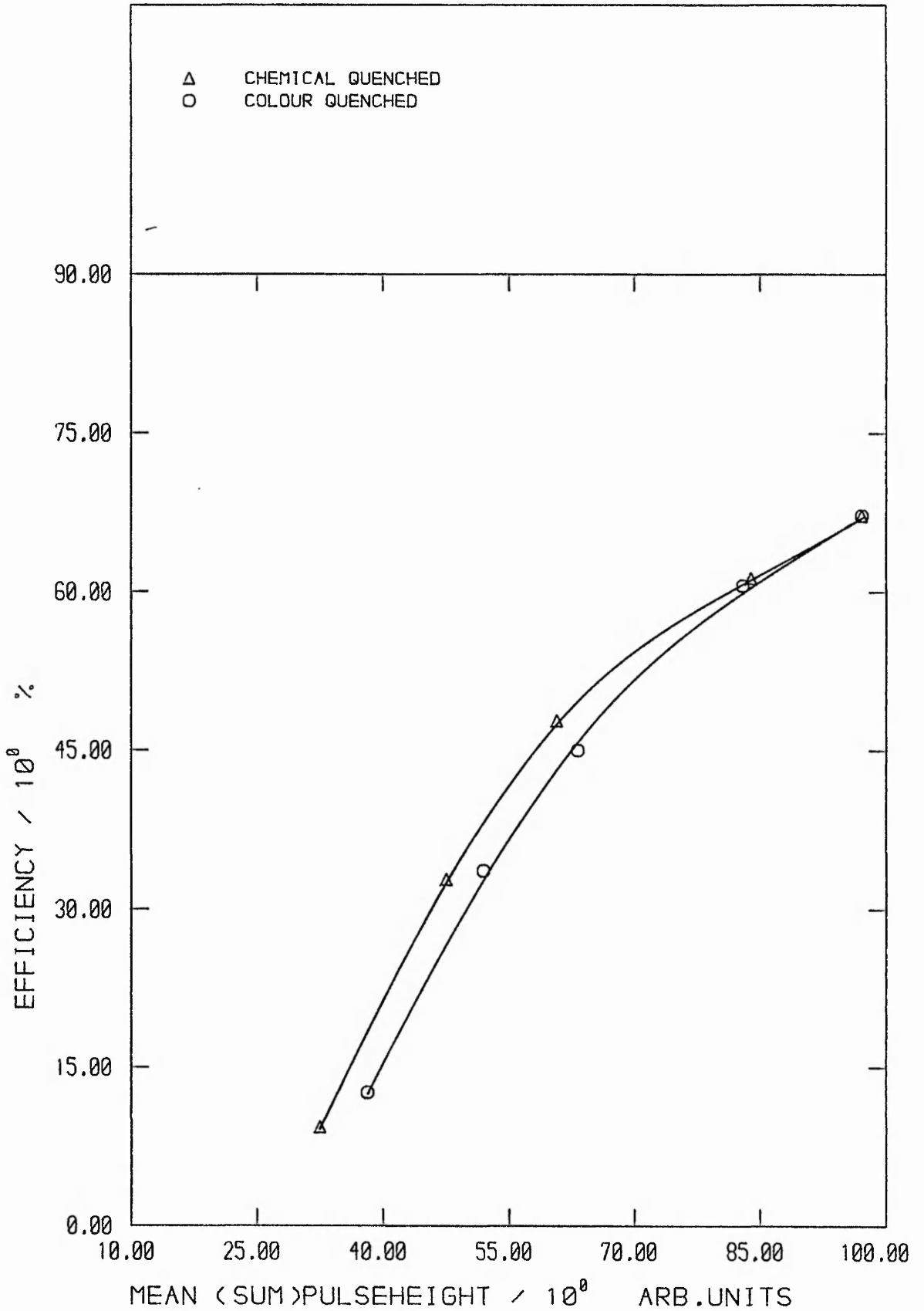
FIG F4.12 : MODEL GENERATED EFFICIENCY vs MEAN
SUM PULSEHEIGHT FOR 3H WITH SAU DISCRIMINATORS

216
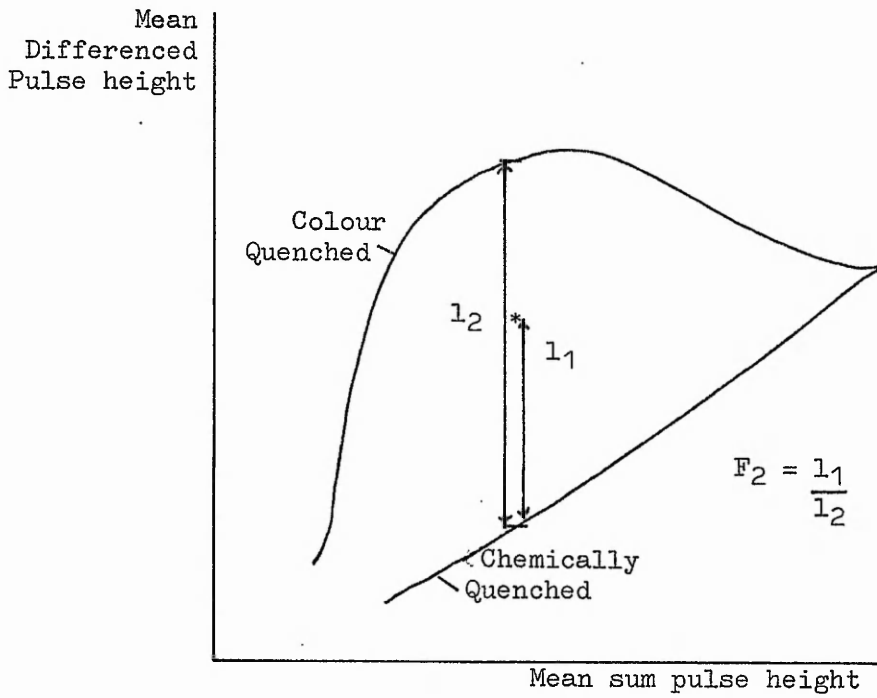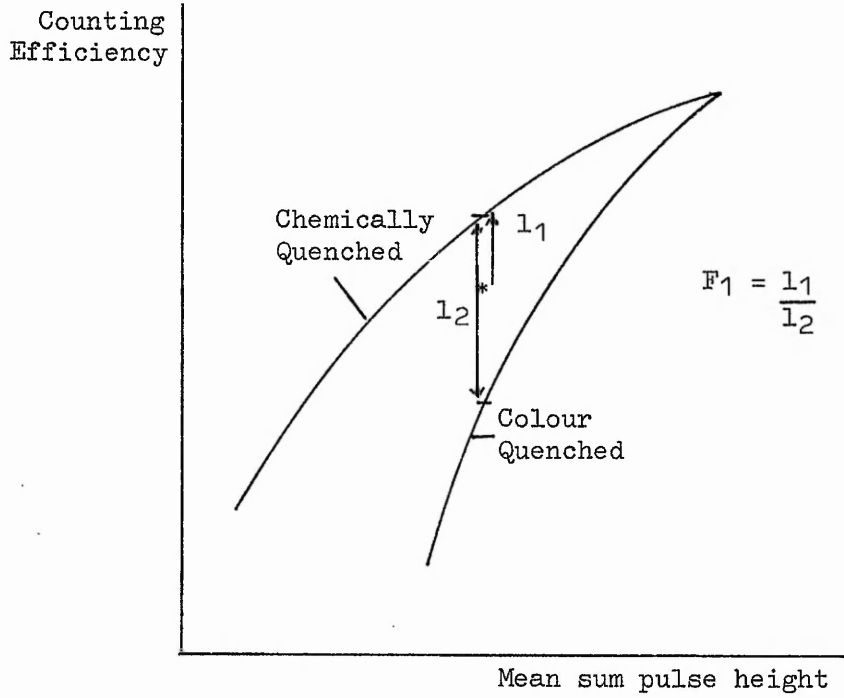
Fig. F4.13 Definition of F_1 and F_2 ratios
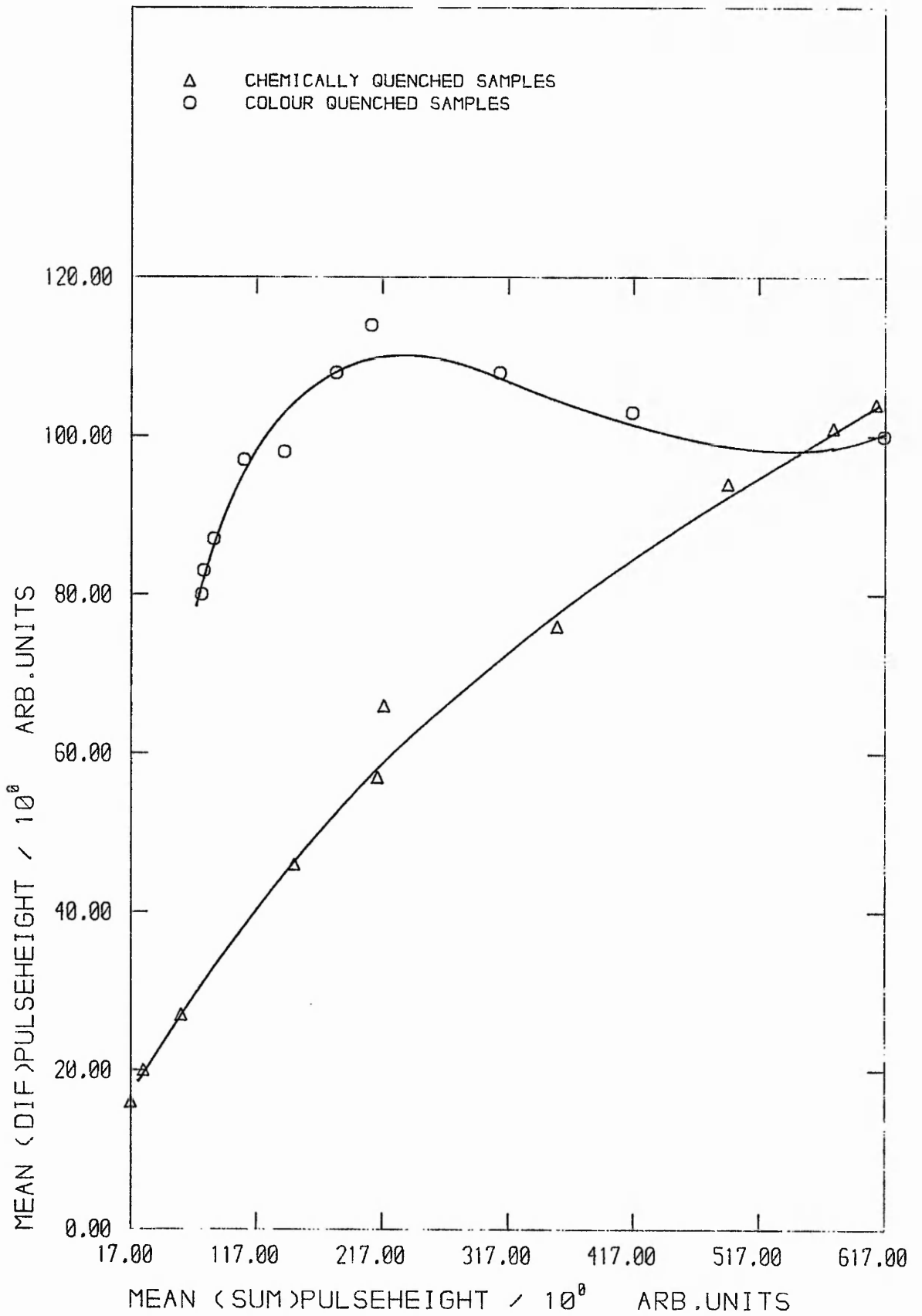
FIG F4.14:EXPERIMENTAL MEAN SUM PULSE-HEIGHT
vs MEAN DIFFERENCE PULSE-HEIGHT FOR 14C

218
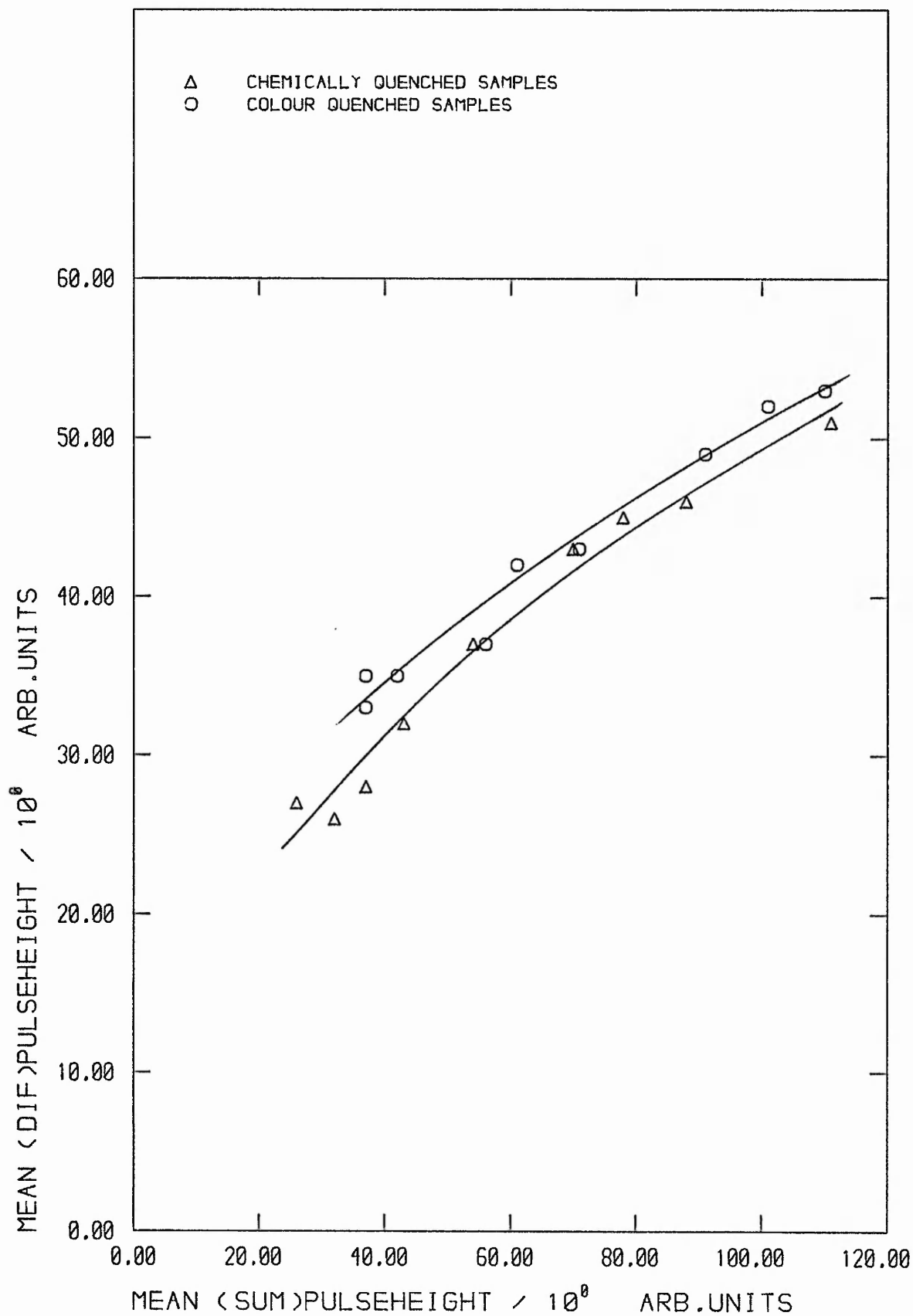
FIG F4.15:EXPERIMENTAL MEAN SUM PULSE-HEIGHT
vs MEAN DIFFERENCE PULSE-HEIGHT FOR 3H

219
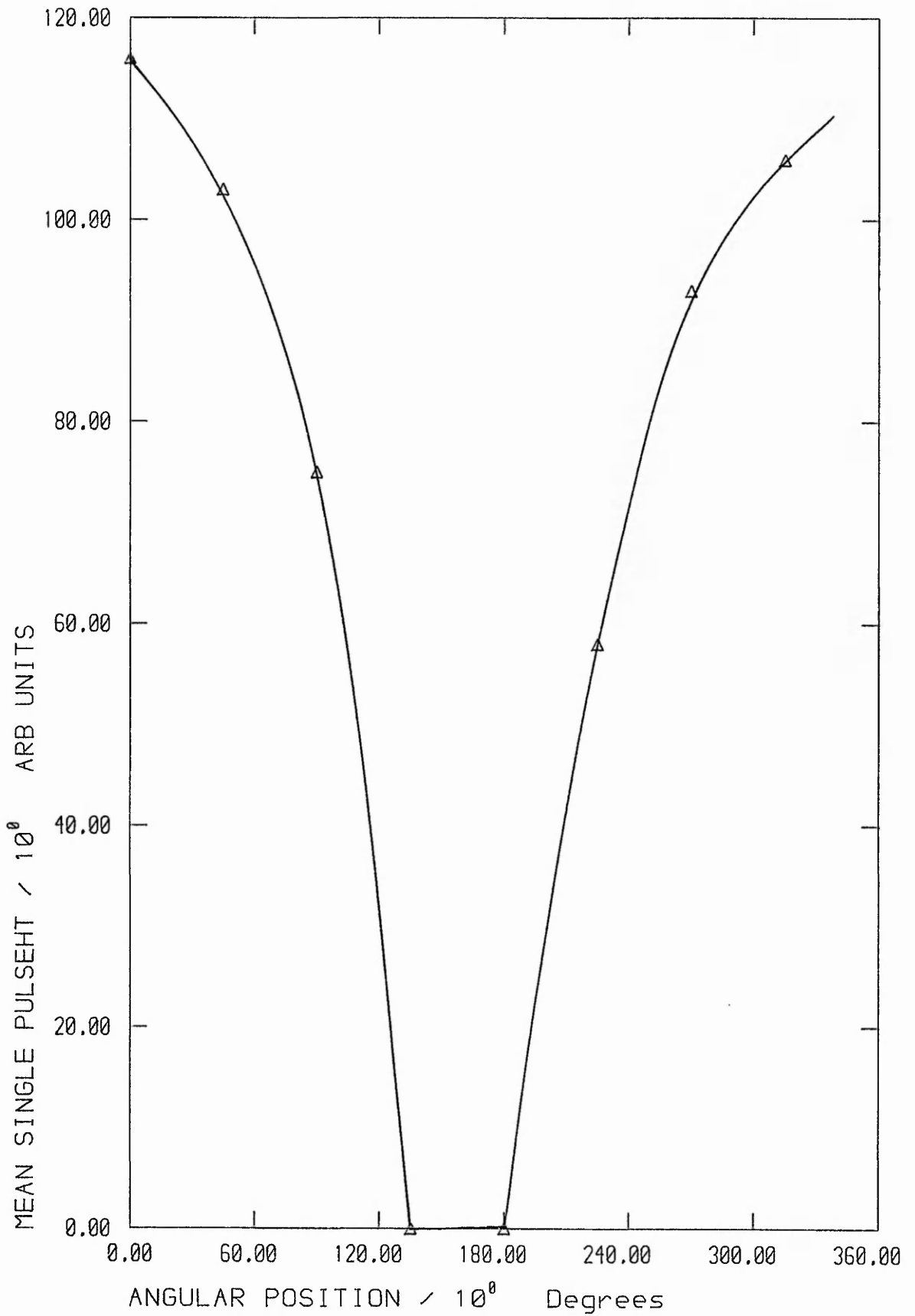
FIG F4.16 : ExtStd MEAN SINGLE PULSE
HEIGHT USING HALF COLOURED VIAL

220
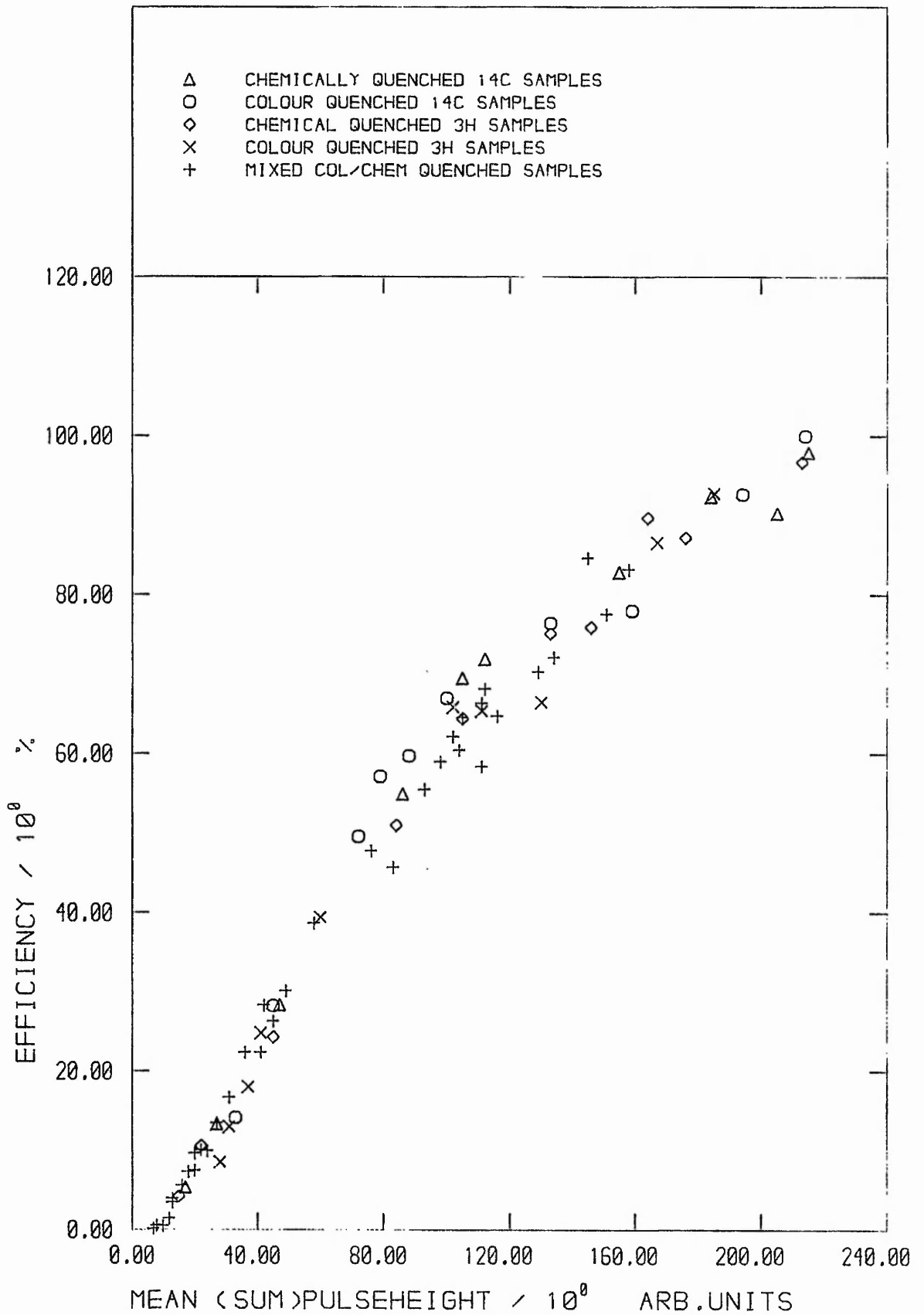
FIG F4.17 : EXT.STD. NORMALISED
EFFICIENCY vs MEAN SUMMED PULSEHEIGHT
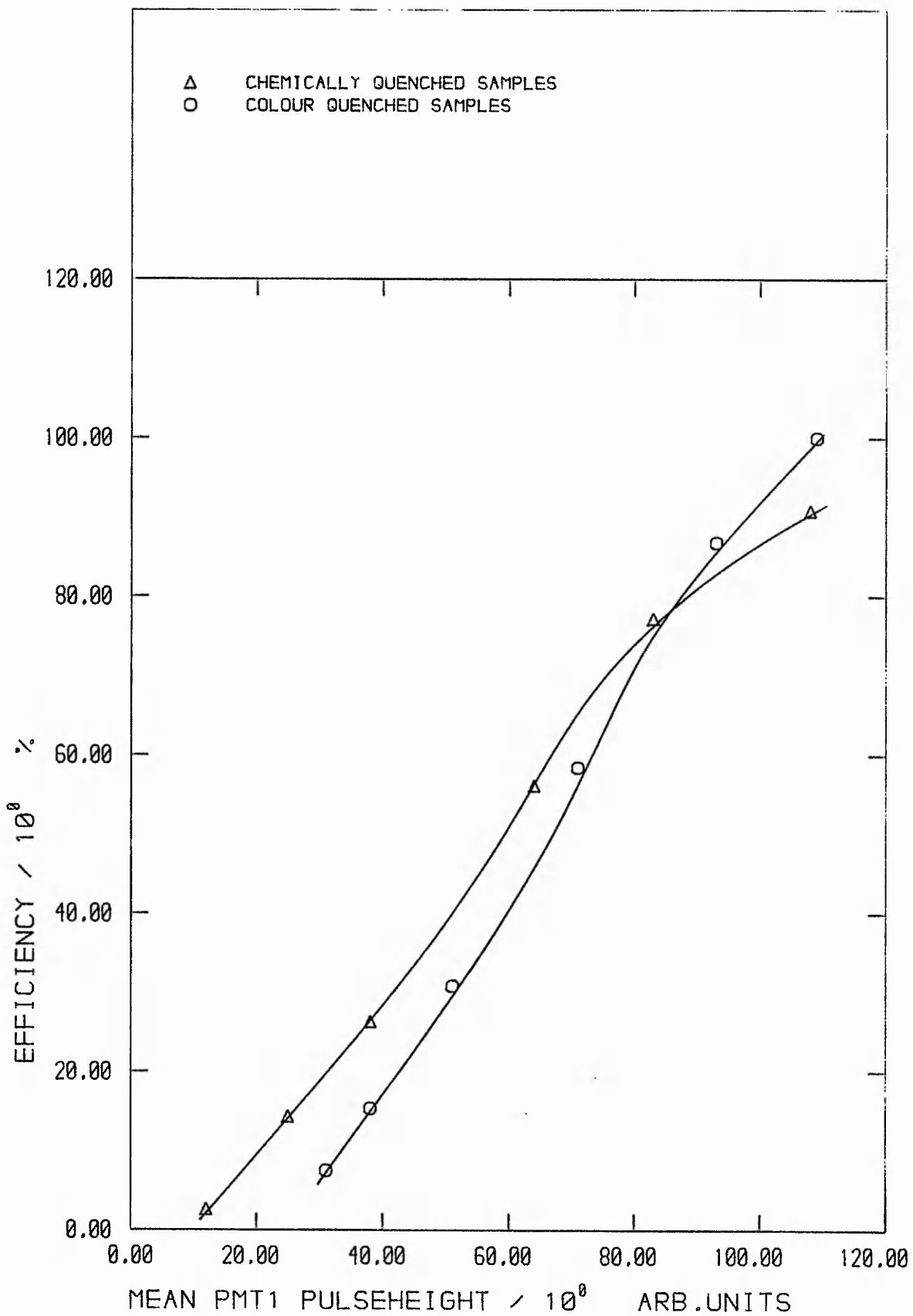
FIG F4.18 : EXT.STD. NORMALISED
EFFICIENCY vs MEAN SINGLE PULSEHEIGHT

222
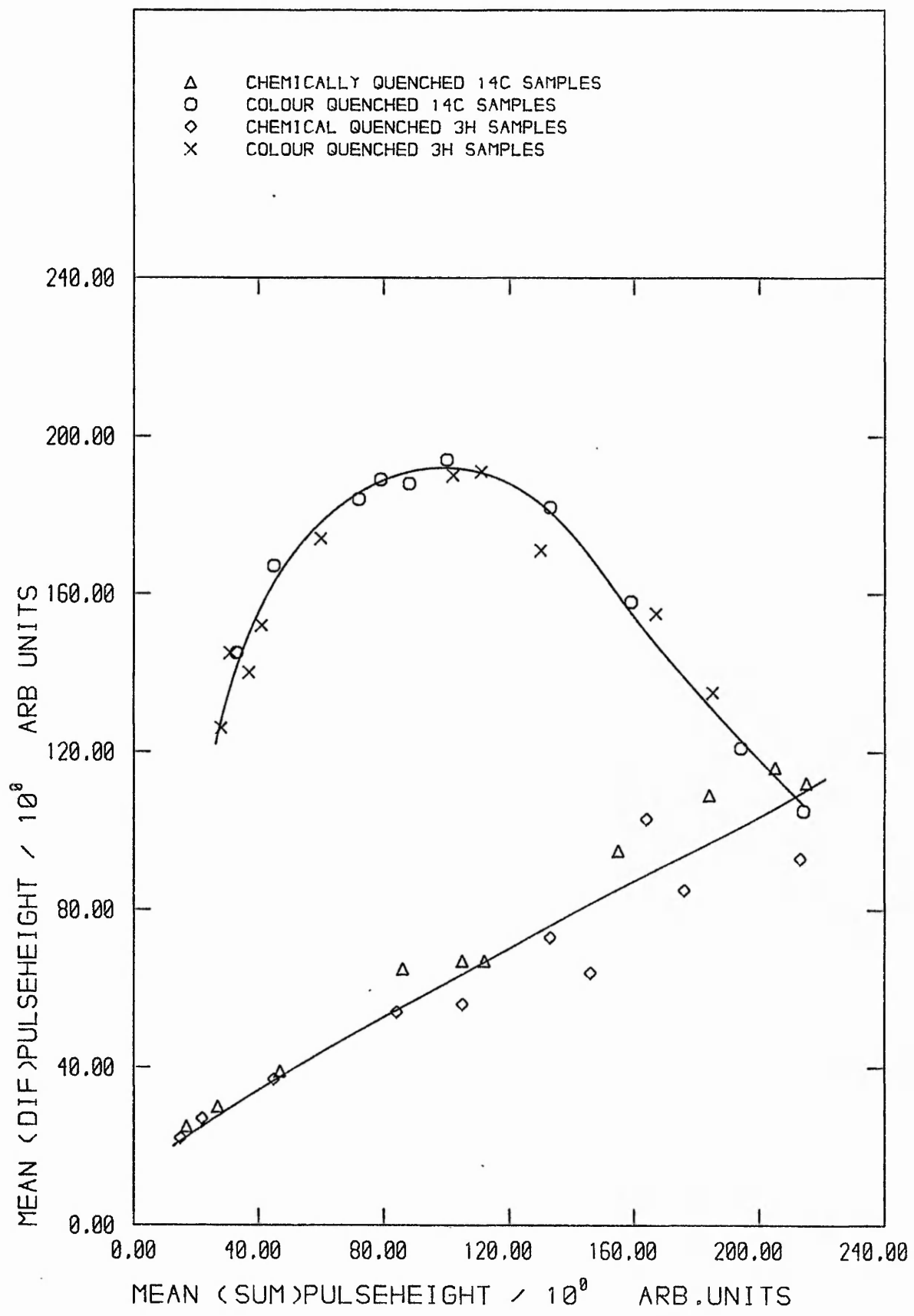
FIG F4.19 : EXT.STD MEAN SUMMED PULSEHT
vs EXT.STD MEAN DIFFERENCED PULSEHEIGHT

223
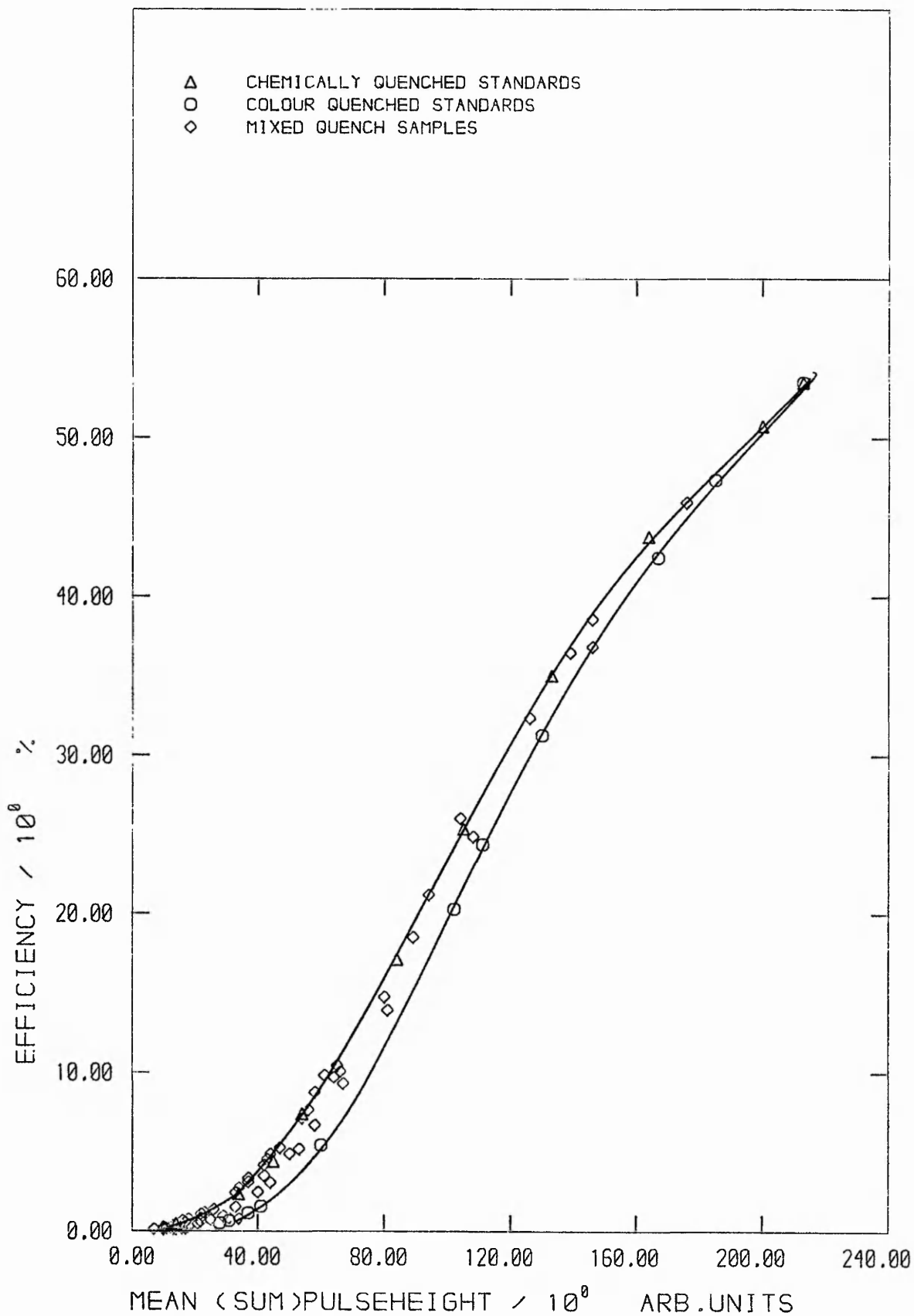
FIG F4.20 : EXPERIMENTALLY OBTAINED
EFFICIENCY vs MEAN SUM PULSEHEIGHT FOR 3H
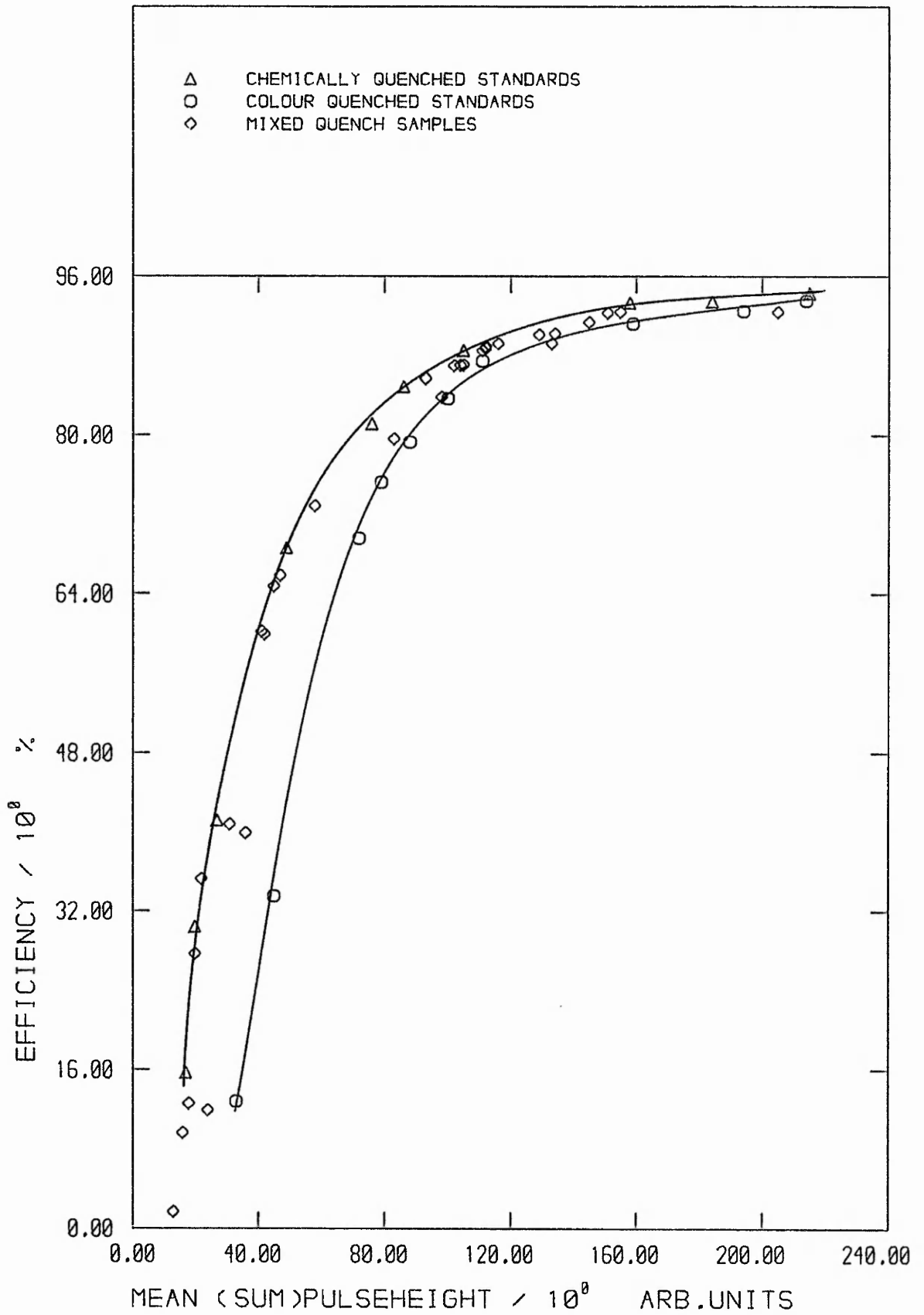
FIG F4.21 : EXPERIMENTALLY OBTAINED
EFFICIENCY vs MEAN SUM PULSEHEIGHT FOR 14C

225
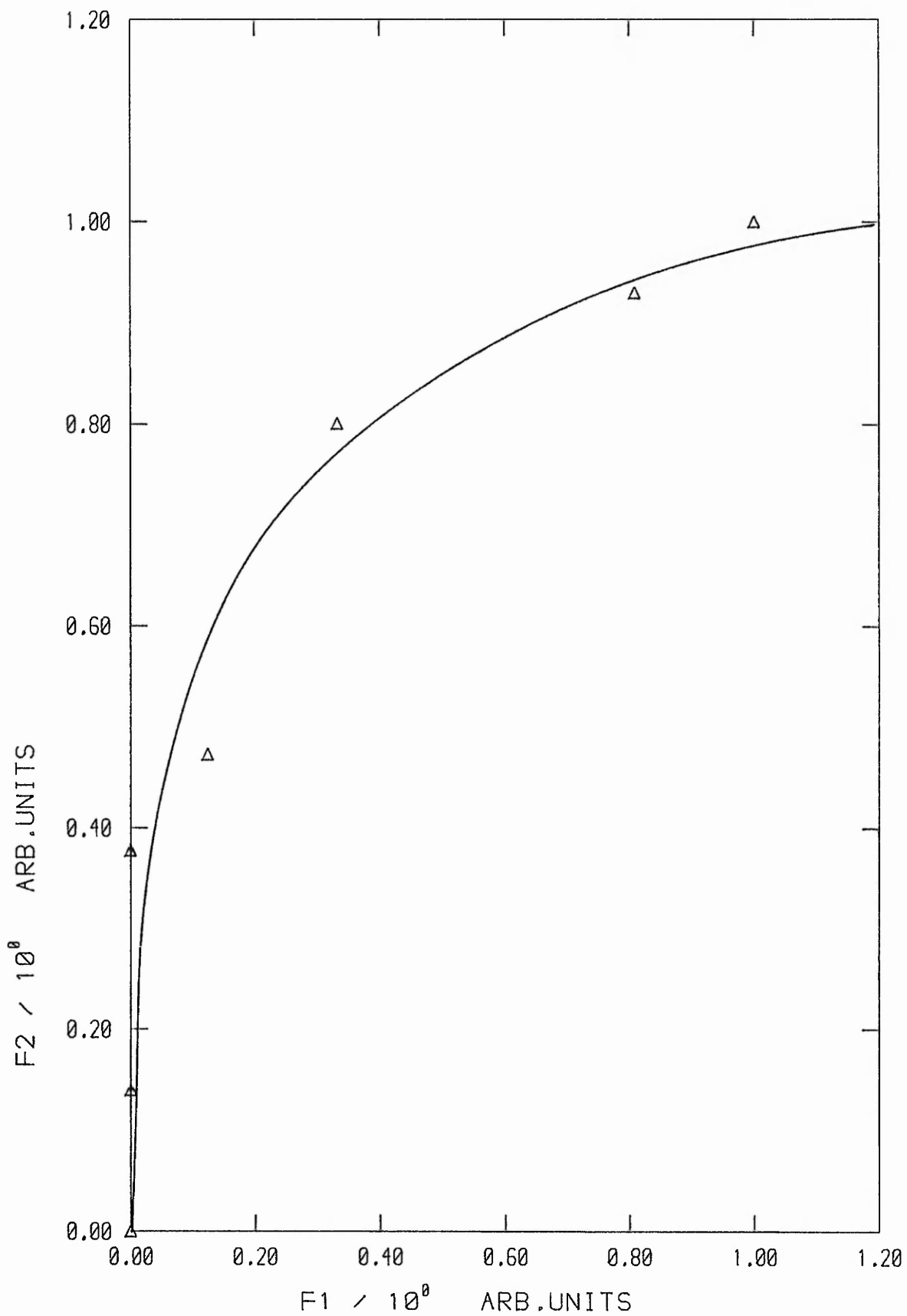
FIG F4.22 : MIXED COLOUR/CHEMICAL
QUENCHED C14 STANDARDS F1-F2 PLOT

226
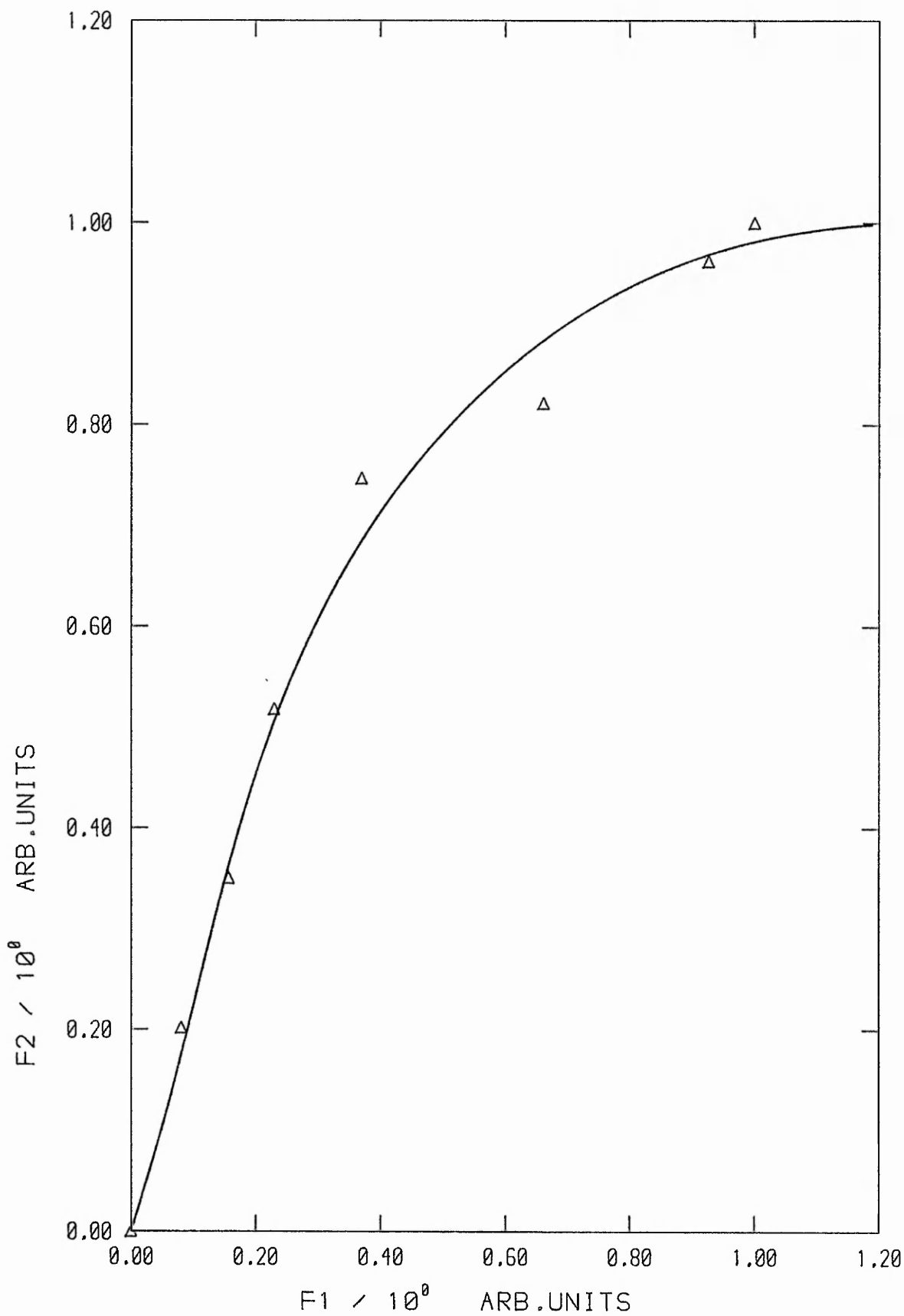
FIG F4.23 : MIXED COLOUR/CHEMICAL
QUENCHED 3H STANDARDS F1-F2 PLOT

COLLECTED TABLES

Table T2.1

Function type: ^{3}H
Number of standards: 10
Data group: A
Number of comparison points: 65

FIT TYPE	LOW QIP EXTRAPOLATED		INTERPOLATED		HIGH QIP EXTRAPOLATED	
	$\Sigma ABS(Y-Y_i)$	$\Sigma(Y-Y_i)^2$	$\Sigma ABS(Y-Y_i)$	$\Sigma(Y-Y_i)^2$	$\Sigma ABS(Y-Y_i)$	$\Sigma(Y-Y_i)^2$
Piecewise linear	2.07 E-1	6.12 E-3	9.46 E-2	4.44 E-4	8.06 E-3	1.95 E-3
Least squares 4° polynomial	1.98 E-1	4.82 E-3	7.40 E-3	1.52 E-6	6.64 E-3	1.15 E-5
Least squares 3° polynomial	5.13 E-1	2.92 E-2	4.44 E-2	5.66 E-5	7.98 E-2	7.75 E-5
Quadratic spline S"=L" end conditions	1.71 E-1	4.43 E-3	1.52 E-3	4.52 E-8	6.21 E-4	1.34 E-7
Quadratic spline S'=L' end conditions	1.71 E-1	4.43 E-3	1.52 E-3	4.52 E-8	6.21 E-4	1.34 E-7
Quadratic spline Linear end conditions	4.46 E-2	2.56 E-4	6.67 E-3	1.46 E-6	8.06 E-3	8.95 E-5
Stineman	2.07 E-1	6.12 E-3	4.62 E-3	1.36 E-6	8.63 E-3	2.20 E-5
Cubic spline Forsythe's L"=S'''	7.69 E-2	9.21 E-4	1.44 E-3	9.34 E-3	9.86 E-2	1.56 E-4
Cubic spline L"=S" end conditions	5.31 E-1	4.02 E-2	1.57 E-3	9.04 E-3	9.36 E-6	1.95 E-11
Cubic spline Swartz L'=S'	2.50 E-2	1.12 E-4	1.57 E-3	8.75 E-8	1.00 E-2	3.68 E-3
Cubic spline Parabolic end conds.	1.89 E-1	5.26 E-3	1.43 E-3	9.85 E-8	1.97 E-2	3.41 E-4
Cubic spline Natural	2.88 E-1	1.20 E-2	1.43 E-3	9.26 E-8	1.97 E-2	3.41 E-4
Lagrangian polynomial	1.51 E-5	4.70 E-9	3.16 E-7	5.12 E-12	6.02 E-7	1.55 E-13

229

Table T2.2

Function type: ^{3}H
Number of standards: 10
Data group: B
Number of comparison points: 65

FIT TYPE	LOW QIP EXTRAPOLATED		INTERPOLATED		HIGH QIP EXTRAPOLATED	
	$\Sigma ABS(Y-Y_i)$	$\Sigma(Y-Y_i)^2$	$\Sigma ABS(Y-Y_i)$	$\Sigma(Y-Y_i)^2$	$\Sigma ABS(Y-Y_i)$	$\Sigma(Y-Y_i)^2$
Piecewise linear	1.67 E-1	4.49 E-3	5.26 E-2	1.04 E-4	2.60 E-2	1.74 E-4
Least squares 4° polynomial	2.06 E-1	5.26 E-3	8.44 E-3	2.51 E-6	5.87 E-3	9.51 E-6
Least squares 3° polynomial	5.18 E-1	3.00 E-2	4.84 E-2	7.62 E-5	1.73 E-2	7.42 E-5
Quadratic spline S"=L" end conditions	3.82 E-1	1.79 E-2	8.58 E-3	3.62 E-6	5.09 E-3	6.16 E-6
Quadratic spline S'=L' end conditions	3.82 E-1	1.79 E-2	8.58 E-3	3.62 E-6	5.09 E-3	6.16 E-6
Quadratic spline Linear end conditions	7.59 E-2	7.24 E-4	7.11 E-2	1.66 E-4	2.60 E-2	1.75 E-4
Stineman	4.44 E-1	2.34 E-2	3.38 E-2	7.34 E-5	3.50 E-2	3.30 E-4
Cubic spline Forsythe's L"=S"'	2.35 E-1	7.11 E-3	1.28 E-2	1.30 E-5	2.29 E-2	1.43 E-4
Cubic spline L"=S" end conditions	4.67 E-2	4.12 E-4	4.61 E-3	1.59 E-6	1.52 E-3	6.54 E-7
Cubic spline Swartz L'=S'	2.70 E-1	9.18 E-3	9.03 E-3	4.32 E-6	1.26 E-2	4.38 E-5
Cubic spline Parabolic end conds.	4.02 E-1	1.95 E-2	1.54 E-2	1.28 E-5	1.84 E-2	9.30 E-5
Cubic spline Natural	1.55 E-1	3.35 E-3	9.74 E-3	8.32 E-6	1.84 E-2	9.30 E-5
Lagrangian polynomial	4.33 E-4	3.18 E-8	7.28 E-7	4.33 E-14	3.66 E-6	4.33 E-12

Table T2.3

Function type: ^3H
Number of standards: 10
Data group: C
Number of comparison points: 65

FIT TYPE	LOW QIP EXTRAPOLATED		INTERPOLATED		HIGH QIP EXTRAPOLATED	
	$\Sigma ABS(Y-Y_i)$	$\Sigma(Y-Y_i)^2$	$\Sigma ABS(Y-Y_i)$	$\Sigma(Y-Y_i)^2$	$\Sigma ABS(Y-Y_i)$	$\Sigma(Y-Y_i)^2$
Piecewise linear	2.02 E-1	5.93 E-3	2.47 E-2	1.97 E-5	1.56 E-2	6.61 E-5
Least squares 4° polynomial	2.00 E-1	4.96 E-3	7.48 E-3	1.57 E-6	6.39 E-3	1.08 E-5
Least squares 3° polynomial	5.27 E-1	3.05 E-2	4.00 E-2	4.53 E-5	2.03 E-2	9.68 E-5
Quadratic spline S"=L" end conditions	2.61 E-1	9.11 E-3	1.69 E-3	9.10 E-8	2.26 E-3	1.47 E-6
Quadratic spline S'=L' end conditions	2.61 E-1	9.11 E-3	1.69 E-3	9.10 E-8	2.26 E-3	1.47 E-6
Quadratic spline Linear end conditions	5.97 E-2	4.57 E-4	2.31 E-3	1.54 E-5	1.57 E-2	6.61 E-5
Stineman	3.19 E-1	1.30 E-2	4.05 E-3	1.97 E-6	1.99 E-2	1.04 E-4
Cubic spline Forsythe's L"'=S"'	1.49 E-1	3.09 E-3	1.64 E-3	3.04 E-7	1.60 E-2	7.63 E-5
Cubic spline L"=S" end conditions	1.56 E-1	3.35 E-3	3.50 E-4	1.46 E-8	4.29 E-4	5.50 E-8
Cubic spline Swartz L'=S'	1.56 E-1	3.35 E-3	1.01 E-3	9.17 E-8	8.24 E-3	2.02 E-5
Cubic spline Parabolic end conds.	2.90 E-1	1.10 E-2	1.97 E-3	3.18 E-7	1.39 E-2	5.81 E-5
Cubic spline Natural	1.56 E-1	3.36 E-3	1.49 E-3	2.36 E-7	1.39 E-2	5.81 E-5
Lagrangian polynomial	2.66 E-6	1.36 E-8	9.35 E-8	7.81 E-16	1.90 E-6	1.31 E-12
Cubic Spline Cantilever end conds.	7.65 E-2	5.87 E-4	1.71 E-3	2.66 E-7	1.39 E-2	5.81 E-5
Least squares 5° polynomial	5.41 E-2	4.02 E-4	8.20 E-4	1.95 E-8	1.27 E-3	4.71 E-7

Table T2.3a   Effect of bias of points selected for comparison coinciding with interpolatory nodes

Function type: ^{3}H
Number of standards: 10
Data group: C
Number of comparison points: 650

FIT TYPE	LOW QIP EXTRAPOLATED		INTERPOLATED		HIGH QIP EXTRAPOLATED	
	$\Sigma ABS(Y-Y_i)$	$\Sigma(Y-Y_i)^2$	$\Sigma ABS(Y-Y_i)$	$\Sigma(Y-Y_i)^2$	$\Sigma ABS(Y-Y_i)$	$\Sigma(Y-Y_i)^2$
Least squares 3° polynomial	4.82 E 0	2.62 E-1	4.00 E-1	4.51 E-4	1.77 E-1	7.59 E-4
Stineman	2.88 E 0	1.09 E-1	4.22 E-2	1.97 E-5	1.65 E-1	7.74 E-4

Table T2.4

Function type: ^3H
Number of standards: 6
Data group: C
Number of comparison points: 65

FIT TYPE	LOW QIP EXTRAPOLATED		INTERPOLATED		HIGH QIP EXTRAPOLATED	
	$\Sigma ABS(Y-Y_i)$	$\Sigma(Y-Y_i)^2$	$\Sigma ABS(Y-Y_i)$	$\Sigma(Y-Y_i)^2$	$\Sigma ABS(Y-Y_i)$	$\Sigma(Y-Y_i)^2$
Piecewise linear	1.76 E-1	4.85 E-3	8.25 E-2	2.05 E-4	2.38 E-2	1.48 E-4
Least squares 4° polynomial	1.99 E-1	4.96 E-3	8.19 E-3	2.03 E-6	5.59 E-3	8.65 E-6
Least squares 3° polynomial	5.02 E-1	2.85 E-2	4.70 E-2	6.29 E-5	1.64 E-2	6.69 E-5
Quadratic spline S"=L" end conditions	3.56 E-1	1.57 E-2	9.74 E-3	2.99 E-6	4.89 E-3	6.57 E-6
Quadratic spline S'=L' end conditions	3.56 E-1	1.57 E-2	9.74 E-3	2.99 E-6	4.89 E-3	6.57 E-6
Quadratic spline Linear end conditions	7.15 E-2	6.14 E-4	8.10 E-2	1.80 E-4	2.38 E-2	1.48 E-4
Stineman	4.41 E-1	2.31 E-2	2.67 E-2	4.51 E-5	3.30 E-2	2.76 E-4
Cubic spline Forsythe's L"=S"'	2.77 E-1	9.59 E-3	1.17 E-2	7.11 E-6	2.03 E-2	1.15 E-4
Cubic spline L"=S" end conditions	2.51 E-2	9.12 E-5	3.03 E-3	5.54 E-7	2.04 E-3	1.16 E-6
Cubic spline Swartz L'=S'	2.89 E-1	1.04 E-2	9.51 E-3	3.77 E-6	1.23 E-2	4.10 E-5
Cubic spline Parabolic end conds.	3.95 E-1	1.89 E-2	1.29 E-2	7.79 E-6	1.70 E-2	8.10 E-5
Cubic spline Natural	1.54 E-1	3.21 E-3	7.92 E-3	4.77 E-6	1.70 E-2	8.11 E-5
Lagrangian polynomial	1.60 E-1	3.41 E-3	2.89 E-3	3.34 E-7	1.67 E-1	3.41 E-3
Cubic spline Cantilever end conds.	2.84 E-1	7.22 E-3	1.58 E-2	1.09 E-5	1.71 E-1	8.14 E-3

233

Table T2.5

Function type: ^{14}C
Number of standards: 10
Data group: A
Number of comparison points: 65

FIT TYPE	LOW QIP EXTRAPOLATED		INTERPOLATED		HIGH QIP EXTRAPOLATED	
	$\Sigma ABS(Y-Y_i)$	$\Sigma(Y-Y_i)^2$	$\Sigma ABS(Y-Y_i)$	$\Sigma(Y-Y_i)^2$	$\Sigma ABS(Y-Y_i)$	$\Sigma(Y-Y_i)^2$
Piecewise linear	6.86 E-3	1.90 E-5	3.52 E-1	6.11 E-3	4.40 E-3	1.87 E-6
Least squares 4° polynomial	2.33 E-1	1.41 E-2	1.56 E-1	6.90 E-4	1.16 E 0	1.44 E-1
Least squares 3° polynomial	2.35 E-1	1.43 E-2	1.55 E-1	6.82 E-4	1.14 E 0	1.38 E-1
Quadratic spline S"=L" end conditions	1.09 E-1	3.41 E-3	7.96 E-2	9.32 E-4	8.08 E-3	8.04 E-6
Quadratic spline S'=L' end conditions	1.09 E-1	3.41 E-3	7.96 E-2	9.32 E-4	8.08 E-3	8.04 E-6
Quadratic spline Linear end conditions	1.10 E-1	3.45 E-3	7.99 E-2	3.35 E-4	4.40 E-3	1.87 E-6
Stineman	4.17 E-2	6.10 E-4	6.46 E-2	2.44 E-4	4.54 E-3	1.99 E-6
Cubic spline Forsythe's L"'=S"'	1.46 E-2	7.58 E-5	2.85 E-2	3.70 E-5	8.18 E-2	9.49 E-4
Cubic spline L"=S" end conditions	9.13 E-2	3.05 E-3	2.68 E-2	3.27 E-5	1.94 E-2	5.44 E-5
Cubic spline Swartz L'=S'	5.70 E-3	1.17 E-5	2.83 E-2	3.67 E-5	8.56 E-3	9.60 E-6
Cubic spline Parabolic end conds.	3.53 E-2	4.51 E-4	2.88 E-2	3.80 E-5	5.38 E-2	4.12 E-4
Cubic spline Natural	4.05 E-2	6.03 E-4	2.76 E-2	3.47 E-5	5.38 E-2	4.12 E-4
Lagrangian polynomial	7.08 E-4	2.04 E-7	1.02 E-3	5.47 E-8	6.26 E-1	8.10 E-2

Table T2.6

Function type: ^{14}C
Number of standards: 10
Data group: B
Number of comparison points: 65

FIT TYPE	LOW QIP EXTRAPOLATED		INTERPOLATED		HIGH QIP EXTRAPOLATED	
	$\Sigma ABS(Y-Y_i)$	$\Sigma(Y-Y_i)^2$	$\Sigma ABS(Y-Y_i)$	$\Sigma(Y-Y_i)^2$	$\Sigma ABS(Y-Y_i)$	$\Sigma(Y-Y_i)^2$
Piecewise linear	1.18 E-1	3.28 E-3	2.45 E-1	4.78 E-3	2.46 E-2	5.33 E-5
Least squares 4° polynomial	2.44 E-1	1.67 E-2	1.67 E-1	1.17 E-3	7.84 E-1	6.56 E-2
Least squares 3° polynomial	2.09 E-1	1.24 E-2	1.80 E-1	1.09 E-3	1.26 E 0	1.69 E-1
Quadratic spline S"=L" end conditions	1.63 E-1	7.56 E-3	7.00 E-2	3.19 E-4	1.42 E-1	2.06 E-3
Quadratic spline S'=L' end conditions	1.63 E-1	7.56 E-3	7.00 E-2	3.19 E-4	1.42 E-1	2.06 E-3
Quadratic spline Linear end conditions	1.48 E-1	6.37 E-3	4.55 E-2	1.84 E-4	2.46 E-2	5.33 E-5
Stineman	2.20 E-1	1.35 E-2	1.20 E-1	1.17 E-3	7.01 E-2	4.14 E-4
Cubic spline Forsythe's L"=S"'	1.75 E-1	8.75 E-3	6.20 E-2	2.99 E-4	5.66 E-1	3.60 E-2
Cubic spline L"=S" end conditions	2.99 E-1	2.41 E-2	1.78 E-1	3.05 E-3	3.50 E-1	1.39 E-2
Cubic spline Swartz L'=S'	1.75 E-1	8.80 E-3	5.42 E-2	2.81 E-4	2.25 E-1	5.78 E-3
Cubic spline Parabolic end conds.	1.42 E-1	5.88 E-3	3.56 E-2	1.40 E-4	2.89 E-2	1.17 E-4
Cubic spline Natural	5.24 E-2	6.65 E-4	5.84 E-2	3.23 E-4	2.89 E-2	1.17 E-4
Lagrangian polynomial	1.36 E-2	6.09 E-5	2.50 E-3	5.38 E-7	2.35 E 0	9.79 E-1

Table T2.7

Function type: ^{14}C
Number of standards: 10
Data group: C
Number of comparison points: 65

FIT TYPE	LOW QIP EXTRAPOLATED		INTERPOLATED		HIGH QIP EXTRAPOLATED	
	$\Sigma ABS(Y-Y_i)$	$\Sigma(Y-Y_i)^2$	$\Sigma ABS(Y-Y_i)$	$\Sigma(Y-Y_i)^2$	$\Sigma ABS(Y-Y_i)$	$\Sigma(Y-Y_i)^2$
Piecewise linear	3.64 E-2	2.95 E-4	1.06 E-1	5.53 E-4	9.74 E-3	8.59 E-6
Least squares 4° polynomial	2.35 E-1	1.47 E-2	1.52 E-1	6.87 E-4	1.03 E 0	1.13 E-1
Least squares 3° polynomial	2.21 E-1	1.32 E-2	1.57 E-1	7.08 E-4	1.19 E 0	1.50 E-1
Quadratic spline S"=L" end conditions	6.98 E-2	1.56 E-3	4.83 E-3	1.25 E-6	3.60 E-2	1.41 E-4
Quadratic spline S'=L' end conditions	6.98 E-2	1.56 E-3	4.83 E-3	1.25 E-6	3.60 E-2	1.41 E-4
Quadratic spline Linear end conditions	6.66 E-2	1.43 E-3	4.50 E-3	1.10 E-6	9.74 E-3	8.59 E-6
Stineman	1.32 E-1	5.16 E-3	2.12 E-2	3.93 E-5	1.59 E-2	2.21 E-5
Cubic spline Forsythe's L'''=S'''	7.11 E-2	1.56 E-3	5.79 E-3	4.07 E-6	1.62 E-1	3.28 E-3
Cubic spline L"=S" end conditions	1.26 E-1	4.69 E-3	1.20 E-2	2.19 E-5	9.39 E-2	1.11 E-3
Cubic spline Swartz L'=S'	7.56 E-2	1.77 E-3	5.87 E-3	4.71 E-6	5.78 E-2	4.26 E-4
Cubic spline Parabolic end conds.	9.48 E-2	2.75 E-3	7.37 E-3	7.86 E-6	2.62 E-2	9.13 E-5
Cubic spline Natural	2.36 E-2	1.53 E-4	3.07 E-3	1.48 E-6	2.62 E-2	9.11 E-5
Lagrangian polynomial	5.47 E-3	1.05 E-5	4.22 E-4	1.80 E-8	1.48 E 0	4.12 E-1

Table T2.8

Effect of near-coincident points

Function type: ^{14}C
Number of standards: 6
Number of comparison points: 20
$\partial = 0.0000001$

	$\Sigma ABS(X_i - Y_i)$ and comments	
QIP Values FIT TYPE	150,150+ ,200,250,300,350	150,200,250,250+ ,300,350
Piecewise linear	2.15 E-1	2.15 E-1 visibly satis.
Quadratic spline, L"=S"	4.74 E-2	2.62 E-1 oscillatory
Stineman	7.79 E-2 All	1.14 E-1 visibly satis.
Cubic spline, Forsythe	4.28 E-2 visibly	
Cubic spline, Parabolic	2.11 E-2 satisfactory	
Cubic spline, Natural	4.29 E-2	2.64 E-1 oscillatory
Lagrange	3.79 E-2	7.67 E-1 v. oscillatory
Tension spline, Z=1		1.69 E-1)
Tension spline, Z=2		8.77 E-2) visibly
Tension spline, Z=3		1.79 E-1) satisfactory

Table T2.9

Comparison of calculated and dispensed DPM for ³H single label.

Sample No	QIP	Dispensed DPM	Piecewise Linear DPM ± ΔDPM	Lst Squares *3 Polynomial	Lst squares *4 Polynomial	Quadratic Spline Natural EC	Quadratic Spline L-=S'	Cubic Spline Natural	Cubic Spline Parabolic	Cubic Spline Swartz S'-L'	Cubic Spline Forsythe S'=L''	Stineman
A1	177	69691	58429 ± 2161	49439 ± 11394	71956 ± 12395	54789 ± 1891	59526 ± 2054	65104 ± 2321	64343 ± 2304	64383 ± 2305	64448 ± 2306	63940 ± 2395
A2	235	86294	83320 ± 1327	69691 ± 4694	85248 ± 3625	90245 ± 1340	87628 ± 1301	84744 ± 1326	84775 ± 1326	84774 ± 1326	84771 ± 1326	84470 ± 1348
A3	272	87006	83646 ± 1006	76781 ± 3727	84816 ± 2441	79973 ± 905	82118 ± 929	84798 ± 1013	84775 ± 1013	84777 ± 1013	84779 ± 1013	85099 ± 1026
A4	593	96780	97470 ± 446	96304 ± 1150	95558 ± 713	95382 ± 713	96575 ± 437	96764 ± 443	96764 ± 443	96859 ± 444	96759 ± 443	96551 ± 442
A5	609	86128	87213 ± 423	85609 ± 1107	85598 ± 710	85237 ± 410	86365 ± 415	86509 ± 420	86509 ± 420	86611 ± 421	86504 ± 420	86329 ± 419
B1	130	78102	x	x	x	x	x	x	x	x	x	x
B2	235	86294	83320 ± 1327	73463 ± 6117	85164 ± 2952	86401 ± 1283	86630 ± 1316	84888 ± 1325	84720 ± 1326	84687 ± 1127	84661 ± 1127	86401 ± 1283
B3	272	87006	83646 ± 1006	76513 ± 4353	85029 ± 2061	83211 ± 942	81267 ± 920	84692 ± 1013	84816 ± 1013	84841 ± 1013	84860 ± 1013	83211 ± 941
B4	591	96780	96512 ± 442	96746 ± 1326	95809 ± 645	96628 ± 438	96246 ± 436	96350 ± 442	96350 ± 442	96348 ± 442	96352 ± 442	96628 ± 438
B5	655	82244	82249 ± 398	80882 ± 1093	81883 ± 589	81519 ± 392	82027 ± 395	81945 ± 397	81945 ± 397	81959 ± 397	81934 ± 397	81519 ± 392
C1	269	89800	83197 ± 1644	81376 ± 1583	67638 ± 6378	77712 ± 1429	79379 ± 1459	85168 ± 1646	84976 ± 1648	84978 ± 1647	84946 ± 1648	84758 ± 1679
C2	534	99801	99127 ± 518	98534 ± 505	101374 ± 1402	97193 ± 495	97785 ± 495	98814 ± 517	98812 ± 518	98816 ± 517	98813 ± 517	98842 ± 516
C3	562	80162	80645 ± 453	80244 ± 462	82363 ± 1201	79208 ± 437	79648 ± 439	80262 ± 451	80261 ± 451	80266 ± 451	80262 ± 451	80329 ± 451
C4	622	102579	103317 ± 473	102627 ± 520	104015 ± 1421	103631 ± 469	103168 ± 467	102836 ± 473	102836 ± 473	102827 ± 473	102835 ± 473	102974 ± 472
C5	815	90629	91341 ± 376	91616 ± 429	89479 ± 979	91341 ± 375	90854 ± 373	90945 ± 375	90945 ± 375	90664 ± 374	90902 ± 375	91310 ± 376
D1	219	93827	100601 ± 3675	118035 ± 7356	x	83028 ± 2677	86956 ± 2804	96188 ± 3359	90386 ± 3031	86769 ± 2856	89257 ± 2974	102119 ± 3743
D2	256	85400	81874 ± 1805	82286 ± 2623	70185 ± 10648	93330 ± 1980	90070 ± 1910	86294 ± 1884	87616 ± 1889	88554 ± 1896	87899 ± 1891	82644 ± 1823
D3	534	99801	98789 ± 517	98465 ± 505	100766 ± 1696	99420 ± 506	99071 ± 505	98671 ± 516	98672 ± 516	98672 ± 516	98673 ± 516	98685 ± 516
D4	669	89202	89535 ± 409	88377 ± 401	88652 ± 1176	89844 ± 407	89378 ± 405	89007 ± 407	89007 ± 407	88961 ± 407	88996 ± 407	88938 ± 406
D5	865	82009	82304 ± 350	82445 ± 356	82257 ± 923	82304 ± 349	82116 ± 349	82177 ± 350	82177 ± 350	82018 ± 349	82139 ± 350	82314 ± 350

A and B groups are two chemically quenched calibration curves with different standards

C and D groups are two colour quenched calibration curves with different standards

Table T2.10

Comparison of calculated and dispensed DPM for ^{14}C single label

Sample Number	QIP	Dispensed DPM	Piecewise Linear	Least Squares 3° Polynomial	Least Squares 4° Polynomial	Quadratic Spline Natural	Quadratic Spline L'=S'	Cubic Spline Natural	Cubic Spline Parabolic	Cubic Spline Swartz	Cubic Spline Forsythe	Stineman
1	175	120543	121240 + 786	129332 + 10168	131056 + 7801	120771 + 513	120791 + 513	119705 + 916	119454 + 893	120026 + 887	120080 + 882	120477 + 779
2	329	96384	97406 + 321	93724 + 3410	93999 + 2500	95843 + 312	95797 + 312	96294 + 321	96236 + 322	96219 + 322	96206 + 322	46228 + 317
3	426	75431	75747 + 268	75147 + 2772	71638 + 1911	75549 + 267	25585 + 267	75342 + 268	75356 + 268	75360 + 268	75362 + 268	75449 + 267

Table T2.11

	Piecewise Linear	Least Squares 3° Polynomial	Quadratic Spline	Quadratic Spline	Cubic Spline	Cubic Spline	Cubic Spline	Cubic Spline	Stineman
End conditions			Natural	$L' = S'$	Natural	Parabolic	Swartz	Forsythe	
^3H mean error (%)	2.95	8.10	4.37	3.21	1.48	1.70	1.96	1.77	2.11
^{14}C mean error (%)	0.69	5.41	0.30	0.34	0.30	0.25	0.23	0.22	0.08
Mean of ^3H and ^{14}C	1.82	6.76	2.34	1.78	0.89	0.97	1.10	1.00	1.10

Table T2.12

0-19 keV Count rate	% Dev	0-156 keV Count rate	% Dev	0-714 keV Count rate	% Dev	SIE	0-12 keV Count rate	% Dev	12-156 keV Count rate	% Dev	90-714 keV Count rate	% Dev	SIE	12-90 keV Count rate	% Dev	SIE
32.39	6.90	52.90	5.40	61.78	5.00	930	29.63	4.52	24.07	5.01	13.55	6.68	934	20.15	6.00	937
39.16	6.22	52.02	5.39	60.58	5.00	899	35.78	5.00	17.41	7.16	11.58	8.78	885	16.04	7.31	881
38.26	6.26	48.31	5.39	56.22	5.00	841	31.94	5.00	15.26	7.23	10.22	8.84	837	13.41	7.92	839
38.04	6.12	49.89	5.34	56.98	5.00	778	32.90	4.98	16.78	6.98	10.65	8.76	767	14.17	7.64	765
32.27	6.38	45.42	5.38	52.58	5.00	597	30.13	4.99	16.79	6.69	9.71	8.80	593	14.42	7.09	595
27.10	6.63	40.96	5.39	47.62	5.00	439	22.51	4.95	19.70	5.30	9.64	7.57	438	16.62	5.85	437
31.83	6.36	44.89	5.35	51.45	5.00	475	26.24	4.95	19.32	5.76	10.53	7.81	484	15.49	6.32	479
24.19	6.93	39.19	5.45	46.51	5.00	327	18.80	5.39	20.55	5.16	10.04	7.38	327	18.72	5.52	324
16.07	7.10	28.81	5.30	32.49	5.00	183	10.27	6.62	17.99	5.00	3.47	11.40	184	17.29	4.99	183
13.37	5.47	5.78	8.32	-	-	141	8.53	6.85	-	-	-	-	142	-	-	-

Table T2.13

<u>Coefficients of the °3 Least Squares Polynomials used to
fit the background data.</u>

Region	a_0	a_1	a_2	a_3
0-19	8.22222	33.21226	59.42225	-68.58234
0-156	-27.12587	353.96925	-568.79719	303.35668
0-714	3.30382	215.47564	-326.65731	174.95804
0-12	3.10007	31.92439	65.81563	-72.81374
12-156	0.24714	149.80508	-333.73327	213.78200
90-714	-13.05051	128.68608	-228.08991	129.22932
12-90	7.03592	92.48893	-226.14439	151.19346

Equation : $y = a_0 + a_1 x + a_2 x^2 + a_3 x^3$

and y = Background in CPM

x = SIE(AEC) ÷ 1000

Table T2.14

SIE/AEC	%DPM Recovery			^{3}H:^{14}C:^{36}Cl Ratio (1≡20,000 cpm)
	^{3}H	^{14}C	^{36}Cl	
913	96.2	94.9	106.1	1 : 1 : 2
868	97.3	97.6	106.8	1 : 1 : 2
830	98.6	96.4	105.3	2 : 1 : 2
765	99.7	96.8	105.7	2 : 1 : 2
567	98.6	103.6	104.4	1½ : 1 : 2
451	97.3	102.3	105.4	1½ : 1 : 2
395	94.7	106.6	102.5	1½ : 1 : 2
266	52.0	107.6	107.7	1 : 1 : 2
238	89.4	109.0	104.8	2 : 1 : 3

Table T2.15

SIE/AEC	%DPM Recovery			^{3}H:^{14}C:^{36}Cl Ratio (1≡20,000 cpm)
	^{3}H	^{14}C	^{36}Cl	
945	98.3	97.8	103.5	1 : 1 : 1
920	97.8	98.2	104.1	1 : 1 : 1
851	97.8	97.7	105.6	1 : 1 : 1
807	100.6	99.3	102.4	1 : 1 : 1
731	99.8	99.9	101.1	1 : 1 : 1
575	99.1	103.4	96.3	2 : 1 : 1
435	103.0	104.5	97.4	1 : 1 : 1
391	109.6	114.1	78.7	1 : 1 : 1
321	119.9	114.9	74.8	1 : 1 : 1
236	185.2	103.4	95.3	1 : 1 : 1

Table T2.16

SIE/AEC	%DPM Recovery			^{3}H:^{14}C:^{36}Cl Ratio (1≡12,000 cpm)
	^{3}H	^{14}C	^{36}Cl	
944	98.4	97.9	101.2	3 : 1 : 1
887	99.6	97.4	107.9	3 : 2 : 1
845	100.5	97.7	103.0	3 : 1 : 1
791	100.5	98.1	107.1	3 : 2 : 1
708	100.1	99.6	104.1	3 : 2 : 1
568	100.5	102.3	97.1	3 : 1 : 1
430	100.5	98.7	100.8	3 : 1 : 1
389	100.5	101.1	87.5	3 : 1 : 1
358	99.2	106.1	85.6	3 : 2 : 1
235	134.7	105.6	93.1	3 : 1 : 1

Table T2.17

SIE/AEC	%DPM Recovery			^{3}H:^{14}C:^{36}Cl Ratio (1≡6,000 cpm)
	^{3}H	^{14}C	^{36}Cl	
942	99.3	98.3	109.7	6 : 4 : 1
904	100.3	98.3	104.4	6 : 2 : 1
881	100.1	96.7	114.2	8 : 3 : 1
837	100.5	98.1	111.2	7 : 3 : 1
548	102.7	99.1	98.2	5 : 2 : 1
422	100.4	99.2	88.6	6 : 3 : 1
375	97.5	97.7	104.2	6 : 4 : 1
302	96.0	99.4	99.4	8 : 3 : 1
241	139.3	104.3	94.5	4 : 2 : 1

Table T2.18

Results for Colour Quenched Samples using Chemical
Standards Calibration Curves

SIE/AEC	%DPM Recovery			$^{3}H:^{14}C:^{36}Cl$ Ratio (1≡20,000 cpm)
	^{3}H	^{14}C	^{36}Cl	
679	89.2	104.5	98.3	1 : 1 : 1½
553	80.0	105.2	100.1	1 : 1 : 1½
462	58.2	98.2	105.0	1 : 1½ : 1½
432	47.3	96.5	106.6	1 : 1½ : 1½
333	–	84.9	102.1	1 : 1 : 1½
331	–	88.3	101.7	1 : 1 : 1½
243	–	–	–	1 : 1 : 1½

Table T2.19

Results for Colour Quenched Samples using Colour Quenched
Standards Calibration Curves

SIE/AEC	%DPM Recovery			$^{3}H:^{14}C:^{36}Cl$ Ratio (1≡20,000 cpm)
	^{3}H	^{14}C	^{36}Cl	
679	97.0	100.8	100.5	1 : 1 : 1½
553	90.1	93.9	103.5	1 : 1 : 1½
462	99.5	97.5	102.5	1 : 1½ : 1½
432	106.0	98.5	102.6	1 : 1½ : 1½
333	96.8	98.4	94.3	1 : 1 : 1½
331	102.0	103.7	94.1	1 : 1 : 1½
243	–	–	–	1 : 1 : 1½

Table T3.1

		Substance			
		p-Xylene	10 g l^{-1} bPBD in p-Xylene	CCl$_4$	n-Hexadecane
Measured	$N_{\lambda R}$	1.4987	1.5006	1.4650	1.4403
"	$N_{\lambda Y}$	1.4974	1.4992	1.4622	1.4373
"	$N_{\lambda B}$	1.4925	1.4964	1.4582	1.4365
"	$N_{\lambda V}$	1.4850	1.4868	1.4412	1.4140
Calculated using $\lambda_R \lambda_Y \lambda_B$	A	1.50608488	1.51286338	1.4923113	1.47214743
"	B	-2580.27797	-6001.20807	-14083.989	-17022.8845
"	C	-150921742	436679096	1.26042472E9	1.70987482E9
"	$N_{\lambda V}$	1.4882	1.4933	1.4531	1.4562
Calculated using $\lambda_R \lambda_Y \lambda_V$	A	1.50368545	1.50675199	1.48042353	1.45616846
"	B	-786.478293	-1432.37733	-5196.90174	1.45616846
"	C	-484476726	-412889718	-392118921	-511424519
"	$N_{\lambda B}$	1.4921	1.4937	1.4522	1.4264

Table T3.2

Probability of 'n' electrons when expected gain = 3.94 and variation with Shape factor (b)

n	b = 0	b = 0.01	b = 0.05	b = 0.1	b = 0.2	b = 0.3	b = 0.5	b = 1
0	1.94482E-02	2.09763E-02	2.74231E-02	3.60888E-02	5.47220E-02	7.42137E-02	1.13367E-01	2.02429E-01
1	7.66260E-02	7.95139E-02	9.02649E-02	1.02001E-01	1.20584E-01	1.34006E-01	1.50393E-01	1.61452E-01
2	1.50953E-01	1.52212E-01	1.55984E-01	1.58563E-01	1.59430E-01	1.57282E-01	1.49633E-01	1.28768E-01
3	1.98252E-01	1.96174E-01	1.88258E-01	1.79265E-01	1.63948E-01	1.51468E-01	1.32336E-01	1.02702E-01
4	1.95278E-01	1.91483E-01	1.78153E-01	1.64669E-01	1.44509E-01	1.29914E-01	1.09723E-01	8.19125E-02
5	1.53879E-01	1.50976E-01	1.40737E-01	1.30318E-01	1.14637E-01	1.03217E-01	8.73348E-02	6.53310E-02
6	1.01047E-01	1.00152E-01	9.65091E-02	9.20825E-02	7.76570E-02	6.76570E-02	6.75840E-02	5.21061E-02
7	5.68752E-02	5.74885E-02	5.89950E-02	5.94884E-02	5.83159E-02	5.60895E-02	5.12325E-02	4.15583E-02
8	2.80110E-02	2.91466E-02	3.27688E-02	3.57293E-02	3.85511E-02	3.92459E-02	3.82303E-02	3.31457E-02
9	1.22626E-02	1.32581E-02	1.67783E-02	2.01970E-02	2.45412E-02	2.67715E-02	2.81757E-02	2.64360E-02
10	4.83147e-03	5.47801E-03	8.00790E-03	1.08461E-02	1.51420E-02	1.78861E-02	2.05578E-02	2.10846E-02
11	1.73054E-03	2.07652E-03	3.59434E-03	5.57372E-03	9.09997E-03	1.17442E-02	1.48756E-02	1.68165E-02
12	5.68195E-04	7.28101E-04	1.52817E-03	2.75688E-03	5.34734E-03	7.59893E-03	1.06892E-02	1.34123E-02
13			6.19084E-04	1.31865E-03	3.08178E-03	4.85521E-03	7.63556E-03	1.06973E-02
14				6.12298E-04	1.74624E-03	3.06844E-03	5.42644E-03	8.53184E-03
15					9.74822E-04	1.92075E-03	3.83931E-03	6.8047E-03
16						1.19222E-03	2.70578E-03	5.42726E-03
17						7.34475E-04	1.90032E-03	4.32864E-03

247

Table T3.2 cont.

n	b = 0	b = 0.01	b = 0.05	b = 0.1	b = 0.2	b = 0.3	b = 0.5	b = 1
18							1.33050E-03	3.45239E-03
19							9.28968E-04	2.75353E-03
20								2.19613E-03
21								1.75157E-03
22								1.39700E-03
23								1.11421E-03
24								8.88661E-04
SUM =	9.99763E-01	9.99663E-01	9.99621E-01	9.99510E-01	9.98836E-01	9.98865E-01	9.97898E-01	9.96499E-01

248

Table T3.3

<u>Aluminium Reflection Data</u>

Wavelength of incident radiation, nm	Normal Incidence Reflection
620	0.9148
564	0.9200
517	0.9228
477	0.9238
443	0.9242
414	0.9241
388	0.9243
365	0.9245
345	0.9246
327	0.9247
310	0.9248
295	0.9248

Table T3.4

Effect of Loading on Packard 300C

Unaltered LSC (and + line driver, results ≃ same)			6" Coax. cable + Scope + MCA (no line driver)			4m Coax. cable + Scope + MCA (no line driver)		
SIE	CPM	% Dev	SIE	CPM	% Dev	SIE	CPM	% Dev
913	187130	1.46	913	187779	1.46	932	181130	1.49
558	180909	1.49	557	180730	1.49	570	178230	1.50
371	168240	1.54	372	170320	1.53	378	167810	1.54
295	149220	1.64	298	151449	1.63	302	150170	1.63
229	125230	1.79	229	124550	1.79	240	124160	1.79
203	103160	1.97	203	103210	1.97	214	1.4450	1.96
180	81680	2.21	180	81690	2.21	192	84560	2.17
164	68400	2.42	167	68280	2.42	180	69930	2.39

Table T3.5

Coincidence Summed Spectra Results for ^{14}C Colour Quenched Samples

MCA settings Coarse	Fine	TC	MCA Count	MCA time s	MCA CPM	MCA/PET Integration limits LL	UL	MCA/PET Mean p.h. *	MCA Effy %	Packard CPM **	Packard SIS Effy	Dispensed DPM
8	0	3.2	844132	600	84413	22	740	616	79.2	101205	94.5	106537
8	0	3.2	702743	600	70274	22	550	416	72.8	90450	93.7	96522
16	0	3.2	697478	600	69748	22	800	310	75.5	83472	90.7	92072
16	0	3.2	528938	600	52894	22	600	208	56.1	80517	85.4	94278
32	0	3.2	694831	600	69483	22	1000	180	73.5	76580	81.0	94575
32	0	3.2	759592	600	75959	22	960	139	64.9	85679	73.3	117016
32	0	3.2	508053	600	50805	22	880	107	52.6	58129	60.2	96575
32	0	3.2	319704	600	31970	22	808	83	34.7	39234	42.5	92232
32	0	3.2	216894	600	21689	22	720	75	24.9	27956	31.7	87110
32	0	3.2	189912	600	18991	22	688	73	18.1	25368	24.2	104789

* (i) Spectra rescaled by amplification factor 32 = x1, 16 = x2, 8 = x4

  (ii) LL offset removed

** SIS CPM based on 11 min count

251

Table T3.6

Coincidence Summed Spectra Results for ^{14}C Chemically Quenched Samples

MCA settings Coarse	Fine	TC	MCA Count	MCA time s	MCA CPM	MCA/PET Integration limits LL	UL	MCA/PET Mean p.h. *	MCA Effy %	Packard CPM **	Packard SIS Effy	Dispensed DPM
8	0	3.2	237076	600	23708	22	740	610	82.0	27857	96.3	28931
8	0	3.2	243727	600	24373	22	680	576	80.2	28997	95.4	30385
8	0	3.2	236135	600	23624	22	600	492	77.9	28880	95.3	30314
16	0	3.2	239865	600	23987	22	832	356	81.1	27678	93.6	29583
16	0	3.2	219566	600	21957	22	600	218	72.7	27069	89.6	30220
32	0	3.2	250979	600	25098	22	1000	213	82.2	27149	88.9	30526
32	0	3.2	233049	600	23305	22	760	147	76.5	25685	84.3	30456
32	0	3.2	176002	600	17600	22	400	57	53.7	21432	65.4	32672
32	0	3.2	137383	1000	8243	22	232	27	26.4	12743	40.8	31249
32	0	3.2	86511	2000	2595	22	232	17	8.4	5861	18.9	30951

* (i) Spectra rescaled by amplification factor 32 = x1, 16 = x2, 8 = x4

  (ii) LL offset removed

** SIS CPM based on 11 min counts

Table T3.7

Coincidence Summed Spectra Results for ^{3}H Colour Quenched Samples

MCA settings Coarse	Fine	TC s	MCA Count	MCA time s	MCA CPM	MCA/PET Integration limits LL	UL	MCA/PET Mean Pulse Height	MCA Effy %	Packard CPM	Packard Effy %	Dispensed DPM
64	0	3.2	398160	600	39816	22	700	110	44.83	41537	51.83	88822
64	0	3.2	382587	600	38259	22	660	101	42.12	40481	49.40	90829
64	0	3.2	327498	600	32750	22	600	91	37.99	34320	44.12	86211
64	0	3.2	236464	600	23646	22	500	71	23.05	30219	32.65	102579
64	0	3.2	172532	600	17253	22	410	61	21.52	18522	25.61	80162
64	0	3.2	151907	600	15191	22	400	56	17.52	16396	20.96	86703
64	0	3.2	107855	1000	6471	22	380	42	7.71	7257	9.59	83894
64	0	3.2	30394	1000	1824	22	260	37	2.10	2145	2.74	86726
64	0	3.2	35288	2000	1057	22	240	37	1.24	1278	1.66	85400
64	0	3.2	24281	3000	486	22	200	36	0.52	597	0.71	93827

Table T3.8

Coincidence Summed Spectra Results for ^{3}H Chemical Quenched Samples

MCA settings Coarse	Fine	TC s	MCA Count	MCA time s	MCA CPM	MCA/PET Integration limits LL	UL	MCA/PET Mean Pulse Height	MCA Effy %	Packard CPM	Packard Effy %	Dispensed DPM
64	0	3.2	386513	600	38651	22	700	111	44.89	40637	52.30	86105
64	0	3.2	328257	600	32826	22	600	88	38.10	34750	44.70	86158
64	0	3.2	293839	600	29384	22	500	78	34.12	31060	39.97	86128
64	0	3.2	286578	600	28658	22	480	70	30.06	30503	35.46	95342
64	0	3.2	135819	600	13582	22	400	54	21.72	14797	26.22	62536
64	0	3.2	102973	600	10297	22	320	43	14.56	11086	17.38	70706
64	0	3.2	71455	1000	4287	22	240	37	8.24	5077	10.82	52020
64	0	3.2	78816	1000	4729	22	240	32	5.44	5902	7.51	87006
64	0	3.2	22494	3000	450	22	200	26	0.58	609	0.86	78140

Table T3.9

Model Generated Coincidence-Summed Colour and Chemically Quenched ³H Samples

QCOL	QCHEM	Coincidence Mean Pulse ht	Coincidence Efficiency
0	0	92.1	68.8
0	0.1	89.4	66.4
0	0.2	80.4	61.1
0	0.3	74.7	59.1
0	0.4	67.2	53.0
0	0.5	63.0	46.7
0	0.6	55.1	42.1
0	0.7	47.4	32.7
0	0.8	39.7	21.1
0	0.9	33.1	9.61
0	0	92.1	68.8
0.01	0	92.6	65.4
0.05	0	80.2	61.7
0.10	0	74.9	54.7
0.20	0	63.1	45.4
0.50	0	52.3	33.4
1	0	48.2	27.9
10	0	41.9	22.7
100	0	37.5	12.6
500	0	36.5	3.13

Table T3.10

Model Generated Coincidence Summed Colour and Chemically
Quenched ^{14}C Samples

QCOL	QCHEM	Coincidence Mean pulse ht	Coincidence Efficiency
0	0	791.4	96.1
0	0.1	692.5	95.4
0	0.2	638.5	94.3
0	0.3	553.0	95.1
0	0.4	488.9	94.3
0	0.5	399.4	93.5
0	0.6	317.0	92.2
0	0.7	247.6	88.3
0	0.8	174.3	84.6
0	0.9	102.5	69.6
0	0.93	77.8	62.3
0	0.95	64.4	51.1
0	0.97	49.9	35.8
0.01	0	718.1	96.4
0.05	0	633.1	96.2
0.1	0	519.9	94.3
0.2	0	420.1	93.3
0.5	0	308.6	88.3
1	0	241.6	88.4
10	0	185.6	84.5
100	0	132.0	69.6
500	0	114.5	23.6

256

Table T3.11

Model Generated Coincidence Summed Colour and Chemically
Quenched ^{3}H Samples using 5000 counts Spectra

QCOL	QCHEM	Mean	Efficiency
0	0	96.3	67.3
0	0.1	91.3	64.6
0	0.2	82.0	61.2
0	0.3	76.6	57.4
0	0.4	68.6	53.2
0	0.5	61.7	47.9
0	0.6	54.6	40.9
0	0.7	48.5	32.7
0	0.8	40.3	21.8
0	0.9	32.0	9.28
0	0	96.5	66.4
0.01	0	94.8	66.8
0.05	0	83.8	60.0
0.1	0	73.7	53.5
0.2	0	62.8	45.0
0.5	0	52.5	33.9
1	0	48.1	29.9
10	0	42.3	22.9
100	0	37.9	12.6
500	0	37.0	3.11
0.05	0.3	64.9	50.0
0.1	0.3	59.4	43.0

Table T3.11 Continued

QCOL	QCHEM	Mean	Efficiency
0.5	0.3	44.7	24.4
10	0.3	37.5	15.7
100	0.3	34.7	8.14
0.05	0.4	60.2	45.8
0.1	0.4	56.1	38.1
0.5	0.4	41.4	20.9
10	0.4	35.4	12.9
100	0.4	33.3	6.66
0.05	0.5	54.9	39.7
0.1	0.5	50.7	33.0
0.5	0.5	39.5	17.5
10	0.5	33.9	10.3
100	0.5	31.7	5.24
0.05	0.6	49.5	33.0
0.1	0.6	45.5	27.2
0.5	0.6	36.3	13.3
10	0.6	32.4	7.74
100	0.6	30.7	3.75
0.05	0.7	42.5	25.7
0.1	0.7	40.7	20.5
0.5	0.7	33.9	9.17
10	0.7	30.4	5.24

Table T3.12

Model Generated Coincidence Summed Colour and Chemically
Quenched ^{14}C Samples using 5000 counts

QCOL	QCHEM	Mean	Efficiency
0	0	766.3	96.5
0	0.3	549.6	95.0
0	0.5	396.4	92.8
0	0.7	250.8	88.7
0	0.9	102.1	70.5
0	0.95	64.2	51.0
0.05	0	614.1	95.1
0.5	0	298.8	89.6
1	0	253.2	86.9
10	0	191.0	83.4
100	0	130.3	69.0
500	0	110.4	23.8
0.5	0.8	83.1	58.3
10	0.8	61.3	45.1
100	0.8	51.1	28.3
500	0.8	48.2	7.46
0.5	0.9	54.7	37.8
10	0.9	43.8	25.7
100	0.9	39.5	14.1
500	0.9	37.5	3.54

Table T3.13(a)

Model Generated Coincidence Summed ^{14}C samples – Repeatability

QCOL	QCHEM	Mean ph	Efficiency
O	O	744.6	96.8
O	O	773.0	96.9
O	O	773.3	96.5
O	O	791.4	96.5
O	O	781.8	97.0
O	O	779.1	95.4
O	O	776.1	94.9
O	O	755.8	97.0
O	O	752.6	96.9
O	O	749.5	96.1

$$\Sigma = 7677.2 \qquad \Sigma = 964.0$$
$$\overline{x} = 767.7 \qquad \overline{x} = 96.4$$
$$\sigma = 15.8 \qquad \sigma = 0.73$$

Table T3.13(b)

QCOL	QCHEM	Mean ph	Efficiency
0	0	791.4	96.1
0	0.3	553.0	95.1
0	0.5	399.4	93.5
0	0.7	247.6	88.3
0	0.9	102.5	69.6
0	0	757.3	95.5
0	0.3	538.2	95.3
0	0.5	393.5	92.9
0	0.7	253.6	88.6
0	0.9	101.9	71.0

Table T3.14

Threshold effect on Model calibration curves

(a) Tritium

QCHEM	Threshold=0		Threshold=1		Threshold=4		Threshold=10	
	mean p.h.	eff. %	mean p.h.	eff. %	mean p.h.	eff. %	mean p.h.	eff. %
0	92.1	68.8	101.8	61.1	105.5	52.3	112.2	37.7
0.1	89.4	66.4	94.6	58.1	95.1	49.2	105.5	35.5
0.2	80.4	61.1	89.2	54.7	87.3	43.5	98.8	30.1
0.3	74.7	59.1	78.1	49.8	83.8	42.2	90.9	26.0
0.4	67.2	53.0	72.0	44.5	75.2	35.9	82.0	21.5
0.5	63.0	46.7	65.5	39.8	71.4	30.4	74.3	17.1
0.6	55.1	42.1	61.4	32.6	62.5	23.9	66.7	12.8
0.7	47.4	32.7	52.7	25.2	53.7	17.7	60.3	7.91
0.8	39.7	21.1	43.7	15.9	46.8	10.8		
0.9	33.1	9.61	35.9	6.41	37.8	4.03		

(b) Carbon-14

QCHEM	Threshold=0		Threshold=1		Threshold=10		Threshold=50	
	mean p.h.	eff. %	mean p.h.	eff. %	mean p.h.	eff. %	mean p.h.	eff. %
0	757.3	95.5	803.2	95.1	781.2	91.6	855.5	74.3
0.3	538.2	95.3	541.0	93.5	536.4	87.8	632.6	62.4
.0.5	393.5	92.9	392.7	91.7	417.4	83.7	486.1	54.7
0.7	253.6	88.6	257.9	86.7	273.7	75.3		
0.9	101.9	71.0	107.4	63.5	114.7	42.0		

Table T3.15

Model Generated Coincidence Summed Purely Colour Quenched ^{3}H Samples Data using 5000 count Samples

QCOL	07 DVE		Uniform		Step 300 - 400 nm		Step 400 - 500 nm		Step 500 - 600 nm	
	Mean p.h.	Effy	Mean p.h.	Effy	Mean p.h.	Effy	Mean p.h.	Effy	Mean p.h.	Effy
0	96.5	66.4	97.3	67.1	97.4	67.2	95.9	67.7	97.8	67.1
0.01	94.8	66.8	92.6	66.1	92.1	65.1	95.8	68.1		
0.05	83.8	60.0	80.3	58.9	81.3	59.1	94.6	67.0		
0.1	73.7	53.5	71.8	52.0	72.1	52.9	94.1	66.1		
0.2			61.3	42.3	64.2	46.0	90.6	66.7		
0.5			51.4	32.6	55.6	38.6	91.1	65.8		
1			47.0	28.1	52.3	35.8	90.4	65.4		
10	42.3	22.9	42.7	22.6	48.6	31.9	91.8	66.5		
100	37.9	12.6	37.9	11.2	44.1	22.8	89.7	65.4		
500	37.0	3.11	36.3	2.72	38.3	14.7	88.6	64.3	94.7	68.2

263

Table T3.16

Model Generated Coincidence Summed Colour and Chemical Quenched ^{3}H : shape factor B = 0.00001 (almost Poissonian) and B = 1 (exponential)

QCOL	QCHEM	B = 0.00001		B = 1	
		mean p.h.	efficiency	mean p.h.	efficiency
0	0	118.1	71.8	66.9	74.2
0	0.2	102.9	66.9	56.5	67.7
0	0.4	·87.8	58.4	47.0	56.1
0	0.6	70.9	43.9	37.0	45.5
0	0.8	48.8	24.1	26.7	24.8
0.05	0	103.6	65.2	55.1	66.0
0.5	0	66.5	37.7	34.7	35.9
1	0	60.9	32.0	31.1	32.9
10	0	53.3	24.7	27.5	25.3
100	0	48.6	14.5	24.4	13.9

264

Table T3.17

Model Generated Coincidence-Summed Colour and Chemical
Quenched ^{3}H : PMTube Quantum Efficiency scaled down by
0.173% to 21.5% peak efficiency

QCOL	QCHEM	Mean p.h.	Efficiency
0	0	89.2	62.3
0	0.2	76.3	56.1
0	0.4	63.3	47.4
0	0.6	49.7	34.8
0	0.8	36.8	19.1
0.05	0	73.5	54.0
0.5	0	49.4	29.2
1	0	43.9	24.4
10	0	41.3	18.4
100	0	38.2	10.7

Table T3.18

<u>Model Generated Coincidence-Summed Colour and Chemical</u>

<u>Quenched ^{3}H : Scintillation efficiency = 4.5% constant</u>

QCOL	QCHEM	Mean p.h.	Efficiency
0	0	99.8	72.0
0	0.2	86.9	65.7
0	0.4	72.4	58.4
0	0.6	54.5	43.6
0	0.8	40.7	23.9
0.5	0	85.4	65.5
0.5	0	52.2	38.3
1	0	48.7	32.8
10	0	43.9	26.5
100	0	38.7	13.8

Table T3.19

Model Generated Coincidence Summed Unquenched ^{3}H : Effect of Volume variation

Liquid ht.	Mean	Efficiency
0.001	51.1	35.5
0.005	62.7	48.0
0.010	86.1	59.1
0.015	88.8	66.5
0.020	97.5	67.5
0.025	95.8	67.7
0.030	98.6	67.2
0.035	90.1	65.1
0.040	89.7	63.7

Table T4.1

<u>Model generated results for simultaneous coincidence</u>

<u>summed, difference and ratio pulse height spectra – ^{14}C</u>

QCOL	QCHEM	Mean pulse ht.		Std. dev. of ratio p.h.s.	Counting eff.
		Summed	Diff.		
0	0	791.3	184.9	656.6	96.1
0	0.1	692.5	162.5	657.3	95.4
0	0.2	638.5	155.5	700.3	94.3
0	0.3	553.0	137.7	687.6	95.1
0	0.4	488.9	122.0	709.8	94.3
0	0.5	399.4	100.6	731.8	93.4
0	0.6	317.0	87.1	784.4	92.2
0	0.7	247.6	71.3	835.7	88.3
0	0.8	174.3	54.1	877.4	84.6
0	0.9	102.5	37.7	1021.0	69.6
0	0.93	77.7	31.8	1062.0	62.3
0	0.95	64.4	26.0	1062.0	51.1
0	0.97	49.9	20.6	1115.0	35.8
0.01	0	718.6	173.9	669.5	96.4
0.05	0	633.1	186.1	756.7	96.1
0.1	0	519.9	181.9	846.0	94.3
0.2	0	420.1	167.9	953.7	93.2
0.5	0	308.6	127.1	977.5	88.3
1	0	241.6	89.6	942.8	88.4
10	0	185.5	61.6	939.4	84.5
100	0	132.0	52.0	1014.0	69.6
500	0	114.5	48.9	1103.0	23.6

Table T4.2

Model generated results for simultaneous coincidence summed, difference and ratio pulse height spectra - ^{3}H

QCOL	QCHEM	Mean pulse ht. Summed	Diff.	Std. dev. of ratio p.h.s.	Counting eff.
0	0	92.1	34.9	125.1	68.8
0	0.1	89.4	35.0	128.6	66.4
0	0.2	80.4	31.0	130.3	61.1
0	0.3	74.7	28.0	130.0	59.1
0	0.4	67.2	26.8	137.4	53.0
0	0.5	63.0	23.9	137.7	46.7
0	0.6	55.1	20.4	139.6	42.1
0	0.7	47.4	17.8	141.4	32.7
0	0.8	39.7	13.8	138.1	21.1
0	0.9	33.1	11.5	142.2	9.61
0	0	92.1	34.9	125.0	68.8
0.01	0	92.6	34.7	128.3	65.4
0.05	0	80.2	31.9	130.5	61.7
0.1	0	74.9	30.5	136.0	54.7
0.2	0	63.1	26.3	139.1	45.4
0.5	0	52.3	22.4	145.4	33.4
1	0	48.2	19.5	142.2	27.9
10	0	41.9	16.0	140.9	22.7
100	0	37.5	13.9	144.3	12.6
500	0	36.5	13.6	145.1	3.13

Table T4.3

<u>Model generated results for simultaneous coincidence sum</u>

<u>difference and ratio pulse height spectra for ^{3}H using</u>

<u>5000 counts</u>

QCOL	QCHEM	Mean pulse ht. Summed	Diff.	Std. dev. of ratio p.h.s.	Counting eff.
0	0	96.3	37.0	126.4	67.3
0	0.1	91.3	34.6	126.6	64.6
0	0.2	82.0	31.3	130.0	61.2
0	0.3	76.6	29.5	132.8	57.4
0	0.4	68.6	26.8	134.6	53.2
0	0.5	61.7	23.6	135.0	47.9
0	0.6	54.6	20.5	136.0	40.9
0	0.7	48.5	18.1	140.2	32.7
0	0.8	40.3	15.0	142.9	21.8
0	0.9	32.0	11.3	143.4	9.28
0	0	96.5	36.7	126.4	66.3
0.01	0	94.8	36.0	128.5	66.8
0.05	0	83.8	33.6	132.4	60.0
0.1	0	73.7	30.5	136.6	53.5
0.2	0	62.8	28.7	139.7	45.0
0.5	0	52.5	23.9	141.6	33.9
1	0	48.1	20.9	142.3	29.9
10	0	42.3	19.4	142.8	22.9
100	0	37.9	16.7	144.4	12.6
500	0	36.9	15.1	143.1	3.11

Table T4.3 cont

QCOL	QCHEM	Mean pulse ht. Summed	Diff.	Std. dev. of ratio p.h.s.	Counting eff.
0.05	0.3	64.9	28.3	–	50.0
0.1	0.3	59.4	26.0	–	43.0
0.5	0.3	44.7	19.7	–	24.4
10	0.3	37.5	16.9	–	15.7
100	0.3	34.7	15.1	–	8.14
0.05	0.4	60.2	23.2	–	45.8
0.1	0.4	56.1	25.5	–	38.1
0.5	0.4	41.4	19.3	–	20.9
10	0.4	35.4	15.0	–	12.9
100	0.4	33.2	13.4	–	6.66
0.05	0.5	54.9	24.1	–	39.7
0.1	0.5	50.7	22.4	–	33.0
0.5	0.5	39.5	17.0	–	17.5
10	0.5	33.9	13.6	–	10.3
100	0.5	31.7	12.0	–	5.24
0.05	0.6	49.5	22.7	–	33.0
0.1	0.6	45.5	20.1	–	27.2
0.5	0.6	36.3	15.5	–	13.3
10	0.6	32.4	12.8	–	7.74
100	0.6	30.7	11.4	–	3.75
0.05	0.7	42.5	14.1	–	25.7
0.1	0.7	40.7	13.5	–	20.5
0.5	0.7	33.9	10.8	–	9.17
10	0.7	30.4	14.1	–	5.24

Table T4.4

Model generated results for coincidence product pulse
height spectra for ³H

QCOL	QCHEM	Mean product p.h.	Efficiency
0	0	41.3	68.9
0	0.2	25.2	63.6
0	0.4	15.1	55.5
0	0.6	8.5	41.6
0	0.8	3.81	21.9
0.05	0	31.0	60.2
0.2	0	13.4	44.6
1	0	6.42	28.8
10	0	4.34	21.5
100	0	2.79	12.7

Table T4.5

<u>Model generated results for coincidence product pulse
height spectra for ^{14}C</u>

QCOL	QCHEM	Mean product p.h.	Efficiency
0	0	50.0	96.2
0	0.2	28.8	95.4
0	0.4	15.0	94.7
0	0.6	5.81	90.6
0	0.8	1.27	81.9
0.05	0	14.5	95.1
0.2	0	12.6	92.9
1	0	3.54	88.0
10	0	1.55	83.6
100	0	0.598	70.0

Table T4.6

Model generated results for coincidence modified-product pulse height spectra with ³H

QCOL	QCHEM	Mean product p.h.	Efficiency
0	0	1533	68.8
0	0.2	1271	63.1
0	0.4	1042	54.6
0	0.6	720.5	42.1
0	0.8	399.1	22.1
0.05	0	1225	61.6
0.2	0	849.5	44.2
1	0	495.6	29.4
10	0	398.7	22.4
100	0	318.1	12.7

.

.

Table T4.7

Model generated output for coinciddence summed pulse height
spectra with ³H using singly applied upper discriminators
and 5000 counts

QCOL	QCHEM	Mean summed p.h.	Efficiency
0	0	97.1	67.2
0	0.2	83.9	61.3
0	0.5	60.7	47.8
0	0.7	47.5	32.8
0	0.9	32.5	9.34
0.05	0	82.9	60.6
0.2	0	63.2	45.0
0.5	0	51.9	33.6
100	0	38.1	12.6

Table T4.8

Coincidence Difference Spectra results for ^{14}C Samples

MCA settings coarse 64, fine 0, TC 64 μs.

MCA Count	MCA time s	MCA Count rate CPM	Channel limits LL UL		Mean diff. p.h.	Quench type	Mean* summed p.h.
361264	600	36126	22	960	100	Colour	616
329140	600	32914	22	960	103	Colour	416
311282	600	31128	22	960	108	Colour	310
315744	600	31574	22	920	114	Colour	208
286117	600	28612	22	920	108	Colour	180
309120	600	30912	22	880	98	Colour	139
194909	600	19491	22	780	97	Colour	107
121033	600	12103	22	720	87	Colour	83
79629	600	7963	22	720	83	Colour	75
67176	600	6718	22	680	80	Colour	73
107414	600	10741	22	800	104	Chemical	610
185399	1000	11124	22	800	101	Chemical	576
181847	1000	10911	22	760	94	Chemical	492
167407	1000	10044	22	600	76	Chemical	356
146298	1000	8778	22	520	66	Chemical	218
141396	1000	8484	22	500	57	Chemical	213
119275	1000	7157	22	400	46	Chemical	147
82211	1000	4933	22	240	27	Chemical	57
45245	2000	1357	22	200	20	Chemical	27
12638	2000	379	22	160	16	Chemical	17

* - taken from tables T3.5 and T3.6

Table T4.9

Coincidence Difference Spectra results for ^{3}H Samples

MCA settings coarse 128, fine 0, TC 6.4 μs.

MCA Count	MCA time s	MCA count rate CPM	Channel limits LL	UL	Mean diff. p.h.	Quench type	Mean* summed p.h.
282227	1000	16933.6	22	480	53	Colour	110
273099	1000	16385.9	22	480	52	Colour	107
224577	1000	13474.6	22	440	49	Colour	91
186765	1000	11205.9	22	400	43	Colour	71
110111	1000	6606.7	22	360	42	Colour	61
7740	1000	464.4	22	203	37	Colour	56
71892	2000	2156.8	22	280	35	Colour	42
19172	2000	575.2	22	240	33	Colour	37
8551	2000	256.5	22	240	35	Colour	37
242473	1000	14548.4	22	480	51	Chemical	111
243327	1000	14599.6	22	440	46	Chemical	88
185550	1000	11133.0	22	400	45	Chemical	78
189645	1000	11378.7	22	360	43	Chemical	70
80871	1000	4852.3	22	320	37	Chemical	54
55278	1000	3316.7	22	260	32	Chemical	43
49034	2000	1471.0	22	240	28	Chemical	37
47991	2000	1439.7	22	200	26	Chemical	32
7421	2000	222.6	22	240	27	Chemical	26

Table T4.10

<u>External standard single pulse height spectra results using</u>
<u>a half-coloured vial (containing lightly quenched cocktail)</u>
<u>for various orientations</u>

Relative rotational position (°)	Count	Time (s)	Channel limits LL UL		Mean pulse height
0	29532	10	20	520	116
45	25906	10	20	520	103
90	15014	10	20	520	75
135	0	10	20	520	−
180	0	10	20	520	−
225	7282	10	20	520	58
270	23622	10	20	520	93
315	29670	10	20	520	106

Table T4.11

<u>External Standard Coincident Summed Pulse Height Spectra</u>

(MCA Amp set to 2 coarse, 0.0 fine; Time constant set to
3.2 μs; unipolar pulse output)
(Count time = 20 seconds)

Sample I.D.	Total Count	MCA channel limits Lower	Upper	Mean channel	Normalized efficiency*	**
C40	98741	22	880	145	84.6	M
C24	77459	22	720	111	66.4	M
C29	8826	22	200	20	7.6	M
C39	53272	22	520	83	45.7	M
C21	213	22	80	7	0.18	M
C25	19425	22	200	31	16.7	M
C27	26125	22	240	36	22.4	M
C28	8610	22	100	18	7.4	M
C38	591	22	80	10	0.51	M
C22	1690	22	100	12	1.45	M
C4	11766	22	140	22	10.1	M
C20	30694	22	293	45	26.3	M
C9	6588	22	110	16	5.65	M
C5	64773	22	600	93	55.5	M
C12	11678	22	180	24	10.0	M
C18	70619	22	640	104	60.5	M
C19	68779	22	586	98	59.0	M
C17	81957	22	780	129	70.3	M
C1N	114198	22	1023	215	97.9	H
C2N	105274	22	1023	205	90.2	H

Table T4.11 cont.

Sample I.D.	Total Count	MCA channel limits Lower	Upper	Mean channel	Normalized efficiency*	⁕⁕⁕
C3N	107679	22	1023	184	92.3	H
C4N	96537	22	840	155	82.8	H
C5N	83845	22	680	112	71.9	H
C6N	81040	22	680	105	69.5	H
C7N	64080	22	520	86	54.9	H
C8N	32960	22	320	47	28.3	H
C9N	15508	22	200	27	13.3	H
C10N	6239	22	120	17	5.35	H
C11N	116654	22	1023	214	100	O
C12N	90961	22	960	159	78.0	O
C13N	78150	22	600	100	67.0	O
C14N	69643	22	520	88	59.7	O
C15N	57859	22	480	72	49.6	O
C16N	33282	22	320	45	28.5	O
C17N	16466	22	240	33	14.1	O
C18N	66652	22	500	79	57.1	O
C19N	107988	22	1023	194	92.6	O
C20N	89165	22	800	133	76.4	O
C26	26142	22	240	41	22.4	M
C35	35143	22	320	49	30.1	M
C37	97050	22	920	158	83.2	M
C33	72610	22	660	102	62.2	M
C36	11331	22	140	20	9.71	M
C31	75400	22	740	105	64.6	M

Table T4.11 cont.

Sample I.D.	Total Count	MCA channel limits Lower	Upper	Mean channel	Normalized efficiency*	**
C30	4665	22	100	13	4.00	M
C34	45089	22	400	58	38.7	M
C23	671	22	50	8	0.57	M
C32	33052	22	280	42	28.3	M
C8	68068	22	680	111	58.4	M
C13	15770	22	148	27	13.5	M
C3	4087	22	80	13	3.5	M
C16	55777	22	480	76	47.8	M
C10	76731	22	720	116	65.8	M
C14	79555	22	720	112	68.2	M
C15	90568	22	840	151	77.6	M
C11	84089	22	810	134	72.1	M
H25	110621	22	1023	222	94.8	M
H29	108162	22	1023	185	92.7	O
H37	100952	22	1000	167	86.5	O
H23	77583	22	800	130	66.5	O
H30	76321	22	700	111	65.4	O
H35	76878	22	680	102	65.9	O
H32	260	22	50	7	0.223	M
H22	28930	22	300	41	24.8	O
H38	15138	22	280	31	13.0	O
H4	104554	22	900	164	89.6	H
H3	88505	22	880	146	75.9	H
H8	87582	22	800	133	75.1	H

281

Table T4.11 cont.

Sample I.D.	Total Count	MCA channel limits Lower	Upper	Mean channel	Normalized efficiency*	**
H11	75083	22	640	105	64.4	H
H12	59529	22	520	84	51.0	H
H13	43923	22	440	65	37.7	M
H14	38189	22	400	54	32.7	M
H17	28332	22	300	45	24.3	H
H19	12399	22	160	22	10.6	H
H1N	5933	22	120	14	5.09	M
H2N	101629	22	1000	176	87.1	H
H3N	25062	22	220	33	21.5	M
H4N	66303	22	580	89	56.8	M
H5N	5083	22	120	15	4.36	M
H6N	4671	22	100	14	4.0	M
H7N	4937	22	100	15	4.23	H
H8N	112842	22	1023	213	96.7	H
H9N	15396	22	200	26	13.2	M
H10N	48986	22	400	67	42.0	M
H11N	37654	22	320	50	32.3	M
H12N	45994	22	400	60	39.4	O
H13N	21014	22	240	37	18.0	O
H14N	10024	22	200	28	8.59	O
H15N	32396	22	300	42	27.8	M
H16N	68830	22	600	94	59.0	M
H17N	312	22	50	7	0.267	M
H18N	35670	22	320	44	30.6	M

282

Table T4.11 cont.

Sample I.D.	Total Count	MCA channel limits Lower	Upper	Mean channel	Normalized efficiency*	
H19N	50609	22	400	66	43.4	M
H20N	40653	22	360	54	34.8	M
H21N	11601	22	160	22	9.94	M
H2	94666	22	860	139	81.2	M
H5	89465	22	800	124	76.7	M
H6	18077	22	240	31	15.5	M
H7	68179	22	510	81	58.4	M
H9	41195	22	360	53	35.3	M
H10	14492	22	200	25	12.4	M
H15	9750	22	160	18	8.36	M
H16	13076	22	260	23	11.2	M
H18	7162	22	120	17	6.14	M
H21	2285	22	80	11	1.96	M
H24	109035	22	1023	182	93.5	M
H26	41761	22	400	56	35.8	M
H27	62538	22	520	80	53.6	M
H28	34860	22	320	47	29.9	M
H31	42783	22	380	58	36.7	M
H36	35591	22	360	45	30.5	O
H34	17975	22	240	34	15.4	M
H39	19203	22	240	34	16.5	M
H40	47709	22	400	64	40.9	M
H1.1	18654	22	240	29	16.0	M
H1.2	32865	22	320	40	28.2	M

Table T4.11 cont.

Sample I.D.	Total Count	MCA channel limits Lower	Upper	Mean channel	Normalized efficiency[*]	
H1.3	80557	22	720	108	69.1	M
H1.4	2624	22	100	17	2.25	M
H1.5	98374	22	900	146	84.3	M
H2.1	1919	22	120	16	1.65	M
H2.2	33662	22	320	43	28.6	M
H2.3	8275	22	200	22	7.09	M
H2.4	75799	22	700	104	65.0	M
H2.5	31330	22	300	42	26.9	M
H3.1	8075	22	150	21	6.92	M
H3.2	44373	22	400	58	38.0	M
H3.3	23227	22	400	33	19.9	M
H3.4	23301	22	400	33	20.0	M
H3.5	2316	22	120	17	1.99	M
H4.1	14326	22	200	23	12.3	M
H4.2	1364	22	100	13	1.17	M
H4.3	21983	22	240	34	18.8	M
H4.4	4429	22	140	18	3.80	M
H4.5	46665	22	440	61	40.0	M
H5.1	32461	22	320	44	27.8	M
H5.2	3282	22	120	13	2.81	M
H5.4	525	22	100	10	0.45	M
H5.5	22322	22	240	37	19.1	M
H6.2	1264	22	100	14	1.08	M
H6.3	2092	22	80	10	1.79	M

Table T4.11 cont.

Sample I.D.	Total Count	MCA Channel limits Lower	Upper	Mean Channel	Normalized efficiency*	**
H6.4	24477	22	240	37	21.0	M
H6.5	7974	22	120	16	6.84	M

* – Normalized to most active count i.e. 116654

** – H = chemically quenched

    O = colour quenched

    M = mixed colour/chemically quenched

Table T4.12

External Standard Single Pulse Height Spectra

(Count time = 10 seconds)

| Total Count | MCA channel limits | | Mean channel | Normalized efficiency* | ** |
	Lower	Upper			
41889	20	720	109	100.0	O
36343	20	720	93	86.8	O
24484	20	720	71	58.4	O
12895	20	720	51	30.8	O
6407	20	400	38	15.3	O
6279***	20	400	31	7.5	O
38055	20	720	108	90.8	H
32343	20	720	83	77.2	H
23482	20	720	64	56.1	H
11011	20	720	38	26.3	H
5995	20	400	25	14.3	H
2184***	20	400	12	2.6	H

* - Normalized to 41889

** - H = chemical quench; O = colour quench

*** - count time = 20 seconds

Table T4.13

External Standard Coincident Differenced Pulse Height Spectra

(MCA Amp set to 16 coarse, 0.0 fine; time const. = 3.2 µs; unipolar output)

(Count time = 20 seconds)

Sample I.D.	Total Count	MCA channel limits Lower	Upper	Mean channel	Normalized efficiency*	**
C40	47004	23	1023	100	84.1	M
C24	39488	23	1023	113	70.6	M
C29	10686	23	1023	39	19.1	M
C39	38098	23	1023	158	68.2	M
C21	5147	23	1023	32	9.2	M
C25	25058	23	680	97	44.8	M
C27	31013	23	1023	124	55.5	M
C28	19511	23	591	82	34.9	M
C38	8744	23	1023	47	15.6	M
C22	9022	23	1023	61	16.1	M
C4	12514	23	1023	46	22.9	M
C20	17681	23	1023	54	31.6	M
C9	18682	23	1023	74	33.4	M
C5	28126	23	1023	75	50.3	M
C12	19804	23	1023	108	35.4	M
C18	36312	23	1023	109	65.0	M
C19	46144	23	1023	182	82.6	M
C17	37867	23	1023	129	67.7	M
C1N	52038	23	1023	112	93.1	H

Table T4.13 cont.

Sample I.D.	Total Count	MCA channel limits Lower	Upper	Mean channel	Normalized efficiency*	**
C2N	52413	23	1023	116	93.8	H
C3N	55893	23	1023	109	100.0	H
C4N	49560	23	1023	95	88.7	H
C5N	29787	23	1023	67	53.3	H
C6N	31844	23	1023	67	57.0	H
C7N	32643	23	1023	65	58.4	H
C8N	15530	23	1023	39	27.8	H
C9N	9412	23	348	30	16.8	H
C10N	5948	23	198	25	10.6	H
C11N	46517	23	1023	105	83.2	O
C12N	46764	23	1023	158	83.7	O
C13N	51398	23	1023	194	92.0	O
C14N	50502	23	1023	188	90.4	O
C15N	47269	23	1023	184	84.6	O
C16N	34910	23	1023	167	62.5	O
C17N	20737	23	1023	145	37.1	O
C18N	48707	23	1023	189	87.1	O
C19N	49941	23	1023	121	89.4	O
C20N	48352	23	1023	182	86.5	O
C26	15281	23	1023	42	27.3	M
C35	19754	23	1023	47	35.3	M
C37	47831	23	1023	137	85.6	M
C33	34661	23	1023	95	62.0	M
C36	9618	23	1023	33	17.2	M

Table T4.13 cont.

Sample I.D.	Total Count	MCA channel limits Lower	Upper	Mean channel	Normalized efficiency*	**
C31	41553	23	1023	139	74.3	M
C30	8757	23	811	33	15.7	M
C34	35640	23	1023	105	63.8	M
C23	5221	23	1023	29	9.3	M
C32	29809	23	1023	81	53.3	M
C8	40827	23	1023	179	73.0	M
C13	10627	23	1023	34	19.0	M
C3	10789	23	529	45	19.3	M
C16	29615	23	1023	65	53.0	M
C10	34564	23	1023	90	61.8	M
C14	37414	23	1023	88	66.9	M
C15	41099	23	1023	103	73.5	M
C11	37131	23	1023	96	66.4	M
H25	45231	22	1023	118	80.9	M
H29	52389	22	1023	135	93.7	O
H37	50707	22	1023	155	90.7	O
H23	40616	22	1023	171	72.7	O
H30	45745	22	1023	191	81.8	O
H35	48652	22	1023	190	87.0	O
H32	6804	22	1023	37	12.2	M
H22	31987	22	941	152	57.2	O
H38	18518	22	1023	145	33.1	O
H4	44542	22	1023	103	79.7	H
H3	21060	22	1023	64	37.8	H

Table T4.13 cont.

Sample I.D.	Total Count	MCA channel limits Lower Upper		Mean channel	Normalized efficiency*	**
H8	24749	22	1023	73	44.3	H
H11	21202	22	1023	56	37.9	H
H12	22815	22	1023	54	40.8	H
H13	18150	22	1023	47	32.5	M
H14	17213	22	1023	43	30.8	M
H17	13708	22	1023	37	24.5	H
H19	7357	22	1023	27	13.2	H
H1N	15198	22	1023	55	27.2	M
H2N	39117	22	1023	85	70.0	H
H3N	32813	22	1023	122	58.7	M
H4N	31415	22	1023	81	56.2	M
H5N	15995	22	1023	67	28.6	M
H6N	7168	22	1023	33	12.8	M
H7N	3594	22	1023	22	6.4	H
H8N	42807	22	1023	93	76.6	H
H9N	11727	22	.1023	33	21.0	M
H10N	33904	22	1023	111	60.7	M
H11N	36946	22	1023	134	66.1	M
H12N	40574	22	1023	174	72.6	O
H13N	25055	22	830	140	44.8	O
H14N	14632	22	1023	126	26.2	O
H15N	33886	22	1023	117	60.6	M
H16N	30043	22	1023	82	53.8	M
H17N	6318	22	204	32	11.3	M

Table T4.13 cont.

Sample I.D.	Total Count	MCA channel limits Lower Upper		Mean channel	Normalized efficiency**	**
H18N	39021	22	1023	137	69.8	M
H19N	34748	22	1023	104	62.2	M
H20N	25342	22	1023	67	45.3	M
H21N	11997	22	1023	40	21.5	M
H22N	2043	22	1023	27	3.7	M
H2	42535	22	1023	104	76.1	M
H5	44020	22	1023	112	78.8	M
H6	23708	22	1023	134	42.4	M
H7	48492	22	1023	152	86.8	M
H9	39441	22	1023	149	70.6	M
H10	24742	22	1023	104	44.3	M
H15	17240	22	1023	58	30.8	M
H16	11755	22	1023	40	21.0	M
H18	2971	22	1023	25	5.31	M
H21	1396	22	1023	18	2.5	M
H24	52592	22	1023	150	94.1	M
H26	27364	22	1023	75	49.0	M
H27	40635	22	912	123	72.7	M
H28	28739	22	1023	92	51.4	M
H31	38016	22	1023	144	68.0	M
H36	38526	22	1023	163	68.9	O
H34	21849	22	1023	142	39.1	M
H39	7111	22	1023	29	12.7	M
H40	23601	22	1023	76	42.2	M

Table T4.13 cont.

Sample I.D.	Total Count	MCA channel limits Lower	MCA channel limits Upper	Mean channel	Normalized efficiency*	**
H1.1	25484	22	1023	124	45.6	M
H1.2	34131	22	1023	132	61.1	M
H1.3	35639	22	1023	104	63.8	M
H1.4	6817	22	1023	83	12.8	M
H1.5	34263	22	1023	76	61.3	M
H2.1	4643	22	1023	31	8.31	M
H2.2	28660	22	857	93	51.3	M
H2.3	13806	22	1023	90	24.7	M
H2.4	20120	22	1023	55	36.0	M
H2.5	29515	22	1023	98	52.8	M
H3.1	16270	22	1023	87	29.1	M
H3.2	23747	22	1023	66	42.5	M
H3.3	23936	22	1023	71	42.8	M
H3.4	23802	22	856	74	42.6	M
H3.5	6698	22	567	73	12.0	M
H4.1	19148	22	1023	62	34.3	M
H4.2	8606	22	1023	60	15.4	M
H4.3	16526	22	1023	53	29.6	M
H4.4	11332	22	1023	81	20.3	M
H4.5	12503	22	402	37	22.4	M
H5.1	12506	22	1023	35	22.4	M
H5.2	12441	22	1023	52	22.3	M
H5.4	6241	22	1023	49	11.2	M
H5.5	11250	22	1023	42	20.1	M

Table T4.13 cont.

Sample I.D.	Total Count	MCA Channel limits Lower Upper		Mean channel	Normalized efficiency*	**
H6.2	5559	22	414	59	9.95	M
H6.3	9923	22	1023	41	17.8	M
H6.4	9257	22	1023	30	16.6	M
H6.5	11389	22	1023	38	20.1	M

* - Normalized to highest count, i.e. 55893

** - H = chemical quenched, O = colour quenched, M = mixed colour/chemical quench

Table T4.14

Sample I.D.	Count time (min)	CPM	%DEV	Sample QIP/AEC	Efficiency
C40	4.57	97306.1	.30	592	91.34
C24	5.21	85375.4	.30	477	88.45
C29	10.00	25496.8	.40	161	27.69
C39	5.93	75045.3	.30	372	79.60
C25	9.36	47704.0	.30	203	40.76
C27	10.00	38531.3	.32	220	39.9
C28	10.00	11624.2	.59	158	12.6
C1	10.00	135.8	5.43	135	0.11
C4	10.00	38569.8	.32	174	35.26
C20	9.76	45611.6	.30	245	64.75
C9	10.00	9272.7	.66	150	9.62
C5	6.89	64627.2	.30	406	85.68
C12	10.00	11964.1	.58	178	11.91
C18	4.94	90095.9	.30	444	87.02
C19	6.04	73642.2	.30	431	83.79
C17	5.83	76312.0	.30	539	90.06
C1N	10.00	27285.3	.38	857	94.31
C2N	10.00	28076.0	.38	810	92.40
C3N	10.00	28335.8	.38	748	93.47
C4N	10.00	27330.8	.38	639	92.38
C5N	10.00	26803.0	.39	479	88.69
C6N	10.00	27009.4	.38	457	88.48
C7N	10.00	25842.2	.39	382	84.85
C8N	10.00	21506.7	.43	251	65.83

Table T4.14 cont.

Sample I.D.	Count time (min)	CPM	%DEV	Sample QIP/AEC	Efficiency
C9N	10.00	12862.3	.56	189	41.16
C10N	10.00	4862.7	.91	150	15.71
C11N	10.00	28753.0	.37	863	93.54
C12N	10.00	28212.2	.38	646	91.20
C13N	10.00	29031.6	.37	437	83.63
C14N	10.00	24427.3	.40	397	79.25
C15N	10.00	24672.3	.40	341	69.54
C16N	10.00	10587.5	.61	249	33.88
C17N	10.00	4293.5	.97	206	12.78
C18N	10.00	23744.9	.41	367	75.23
C19N	10.00	32618.6	.35	784	92.47
C20N	10.00	37368.9	.33	553	89.27
C26	8.67	51339.5	.30	231	60.23
C35	7.37	60371.2	.30	260	68.59
C37	5.97	74568.8	.30	644	93.32
C33	6.37	69856.0	.30	443	86.97
C36	10.00	25832.8	.39	166	30.41
C31	7.30	60935.4	.30	458	87.06
C30	10.00	1155.3	1.86	138	1.68
C34	9.53	46697.2	.30	295	72.86
C32	10.00	36480.5	.33	236	59.93
C8	7.14	62286.4	.30	478	87.41
C13	10.00	44099.2	.30	187	41.84
C3	10.00	1504.4	1.63	139	1.71

Table T4.14 cont.

Sample I.D.	Count time (min)	CPM	%DEV	Sample QIP/AEC	Efficiency
C16	5.23	85128.6	.30	349	81.12
C10	5.32	83692.8	.30	486	89.16
C14	5.61	79316.5	.30	481	88.89
C15	5.50	80911.6	.30	619	92.29
C11	5.38	82756.7	.30	559	90.17

Table T4.15

Sample I.D.	Count time (min)	CPM	%DEV	Sample QIP/AEC	Efficiency
H25	10.00	40671.0	.31	801	50.75
H29	10.00	38799.6	.32	746	47.35
H37	10.00	33028.9	.35	673	42.46
H23	10.00	28937.9	.37	540	31.27
H30	10.00	17632.6	.48	482	24.38
H35	10.00	15879.5	.50	443	20.30
H32	10.00	1205.5	1.82	238	1.56
H38	10.00	535.2	2.73	204	0.63
H4	10.00	34040.5	.34	678	43.79
H3	10.00	29985.6	.37	602	38.59
H8	10.00	30135.0	.36	656	35.03
H11	10.00	14318.8	.53	454	25.38
H12	10.00	10944.2	.60	377	17.16
H13	10.00	4913.7	.90	315	10.47
H14	10.00	5802.5	.83	279	7.39
H17	10.00	3413.6	1.08	244	4.38
H19	10.00	572.7	2.64	170	0.81
H1N	10.00	117.0	5.85	145	0.44
H2N	10.00	12302.3	.57	713	45.95
H3N	10.00	395.1	3.18	209	1.51
H4N	10.00	4957.7	.90	393	18.55
H5N	10.00	62.2	8.02	143	0.28
H6N	10.00	96.0	6.45	142	0.43
H7N	10.00	75.2	7.29	144	0.28

Table T4.15 cont.

Sample I.D.	Count time (min)	CPM	%DEV	Sample QIP/AEC	Efficiency
H8N	10.00	14390.5	.53	864	53.50
H9N	10.00	366.4	3.30	185	1.36
H10N	10.00	2509.6	1.26	325	9.34
H11N	10.00	1265.6	1.78	268	4.87
H12N	10.00	1495.7	1.64	302	5.41
H13N	10.00	301.3	3.64	223	1.13
H14N	10.00	131.3	5.52	190	0.49
H15N	10.00	850.7	2.17	241	3.48
H16N	10.00	4317.1	.96	416	21.22
H17N	10.00	20.7	13.9	110	0.09
H18N	10.00	655.2	2.47	245	3.06
H19N	10.00	2220.7	1.34	321	10.07
H20N	10.00	1492.3	1.64	275	7.11
H21N	10.00	354.6	3.36	174	1.07
H2	10.00	29120.4	.37	582	36.47
H5	10.00	21843.6	.43	534	32.34
H6	10.00	534.2	2.74	204	0.79
H7	10.00	10342.6	.62	369	13.94
H9	10.00	4517.5	.94	279	5.17
H10	10.00	761.8	2.29	181	0.70
H15	10.00	622.8	2.53	160	0.76
H16	10.00	756.8	2.30	178	1.17
H18	10.00	346.2	3.40	153	0.55
H21	10.00	135.8	5.43	130	0.16

Table T4.15 cont.

Sample I.D.	Count time (min)	CPM	%DEV	Sample QIP/AEC	Efficiency
H24	10.00	34636.8	.34	742	46.06
H26	10.00	6148.2	.81	284	7.64
H27	10.00	11820.5	.58	364	14.79
H28	10.00	4712.4	.92	256	5.24
H31	10.00	5308.4	.87	292	6.69
H36	10.00	1560.0	1.60	251	1.93
H34	10.00	521.7	2.77	213	0.77
H39	10.00	1725.8	1.52	210	2.33
H40	10.00	7401.3	.74	313	9.73
H1.1	10.00	838.1	2.18	201	0.96
H1.2	10.00	2152.1	1.36	235	2.46
H1.3	10.00	21733.5	.43	462	24.88
H1.4	10.00	183.8	4.67	153	0.21
H1.5	10.00	32199.6	.35	596	36.86
H2.1	10.00	136.7	5.41	141	0.15
H2.2	10.00	3945.8	1.01	243	4.51
H2.3	10.00	525.8	2.76	171	0.60
H2.4	10.00	22768.9	.42	449	26.04
H2.5	10.00	3640.9	1.05	240	4.16
H3.1	10.00	400.2	3.16	164	0.46
H3.2	10.00	7668.2	.72	290	8.77
H3.3	10.00	2115.8	1.37	208	2.42
H3.4	10.00	2135.2	1.37	208	2.44
H3.5	10.00	130.3	5.54	144	0.15

Table T4.15 cont.

Sample I.D.	Count time (min)	CPM	%DEV	Sample QIP/AEC	Efficiency
H4.1	10.00	1027.2	1.97	176	1.17
H4.2	10.00	82.5	6.96	135	0.09
H4.3	10.00	2369.0	1.30	209	2.71
H4.4	10.00	212.8	4.34	154	0.24
H4.5	10.00	8611.2	.68	302	9.84
H5.1	10.00	4239.4	.97	245	4.85
H5.2	10.00	305.4	3.62	139	0.35
H5.4	10.00	92.5	6.58	125	0.10
H5.5	10.00	2899.7	1.17	217	3.32
H6.2	10.00	77.5	7.18	133	0.09
H6.3	10.00	198.0	4.49	128	0.22
H6.4	10.00	2702.0	1.22	220	3.09
H6.5	10.00	563.1	2.77	153	0.65

Table T4.16

Mixed Colour and Chemical Standards Data for $F_1 F_2$ Plot
and Least Squares Fit

(a) ^{14}C

Ext Std Mean Sum p.h.	Ext Std Mean Diff. p.h.	Ratio F_1	Ratio F_2	True eff %
36	124	0.332	0.801	39.9
45	54	0.000	0.140	64.75
98	182	0.809	0.930	83.79
58	105	0.124	0.473	72.86
42	81	0.000	0.378	59.93
–	–	0.000	0.000	–
–	–	1.000	1.000	–

(b) ^3H

Ext std mean Sum p.h.	Ext std mean Diff. p.h.	Ratio F_1	Ratio F_2	True eff %
33	122	0.661	0.281	1.51
50	134	0.370	0.747	4.87
54	67	0.0808	0.202	7.11
31	134	0.926	0.962	0.80
126	112	0.157	0.351	32.34
80	123	0.230	0.518	14.79
–	–	0.000	0.000	–
–	–	1.000	1.000	–

Table T4.17

Summary + ^{14}C Sum Diff. Quench Correction Results

Ext. std. mean sum	Ext. std. mean diff.	Sample CPM	True eff.	Predicted eff.	Error %
111	113	85375.4	88.45	89.19	+0.74
20	39	25496.5	27.69	30.41	+2.72
83	158	75045.3	79.60	80.95	+1.35
31	97	47704.0	40.76	37.32	-3.44
22	46	38569.8	35.26	36.22	+0.96
93	75	64627.2	85.68	86.72	+1.04
129	129	76312.0	90.06	91.19	+1.13
41	42	51339.5	60.23	57.82	-2.41
205	116	28076.0	92.40	93.11	0.71
155	95	27330.8	92.38	93.22	+0.84
112	67	26803.0	88.69	89.25	+0.56
105	139	60935.4	87.06	87.95	+0.89
133	182	37368.9	89.27	90.96	+1.69
27	34	44099.2	41.84	40.82	-1.02
47	39	21506.7	65.83	65.25	-0.58
116	90	83692.8	89.16	89.79	+0.63
112	88	79316.5	88.89	89.31	+0.42
151	103	80911.6	92.29	93.03	+0.74
18	82	11624.2	12.60	15.69	+3.09
16	74	9272.7	9.62	8.48	-1.14
24	108	11964.1	11.91	17.61	+5.69

Absolute errors:- $\overline{X}_{total} = 1.51$ $\overline{X}_{non-extrap} = 0.98$

$\overline{X}_{extrap} = 2.58$

302

Table T4.18

³H Sum Diff Quench Correction Results

Sample CPM	Ext. std. mean sum pulse ht.	Ext. std. mean diff. pulse ht.	True eff. %	Predicted eff. %	Error
29985.6	146	64	38.59	38.89	0.30
4913.7	65	47	10.47	10.86	0.39
12302.3	176	85	45.95	46.23	0.28
4957.7	89	81	18.55	18.88	0.33
2509.6	67	111	9.34	10.86	1.52
850.7	42	117	3.48	2.91	0.57
4317.1	94	82	21.22	20.86	0.36
655.2	44	137	3.06	2.76	0.30
2220.7	66	104	10.07	10.72	0.65
354.6	22	40	1.07	1.99	0.92
29120.4	139	104	36.47	36.76	0.29
10342.6	81	152	13.94	14.05	0.11
4517.5	53	149	5.17	4.81	0.36
756.8	23	40	1.17	2.14	0.97
34636.8	182	150	46.06	46.57	0.51
6148.2	56	75	7.64	7.90	0.26
4712.4	47	92	5.24	4.56	0.68
5308.4	58	144	6.69	6.66	0.27
7401.3	64	76	9.73	10.54	0.81

Table T4.18 cont.

<u>³H SumDiff Quench Correction Results</u>

using Fisofluor II cocktail ($\approx$ 3 years old) (+ mixtures of

b-PBD in xylene and colour quencher in Fisofluor II)

Sample CPM	Ext. std. mean sum	Ext. std mean diff.	True eff. %	Predicted eff. %	Error
2152.1	40	132	2.46	2.18	0.28
21733.5	108	104	24.88	26.26	1.38
32199.6	146	76	36.86	38.89	2.03
3945.8	43	93	4.51	3.55	0.96
22768.9	104	55	26.03	24.82	1.21
3640.9	42	98	4.16	3.29	0.87
7668.2	58	66	8.77	8.65	0.12
2115.8	33	71	2.42	2.73	0.31
2133.2	33	74	2.44	2.69	0.25
1027.2	23	62	1.17	1.99	0.82
2369.0	34	53	2.71	2.92	0.21
8611.2	61	37	9.84	9.59	0.25
4239.4	44	35	4.85	4.05	0.80
2899.7	37	42	3.32	3.12	0.20
2702.0	37	30	3.09	3.09	0.00

REFERENCES

1. Alessio M, Allegri L, Bella F & Improta S, Nucl. Instr. Methods, _138_, 537, (1976)

2. Alessio M, Allegri L, Bella F & Improta S, Nucl. Instr. Methods, _157_, 579, (1978)

3. Annand J R M & Galloway R B, Nucl. Instr. Methods, _201_, 381, (1982)

4. Arnold J R, Science, _119_ , 155, (1954)

5. Assailly J, Bader C, Funck-Brentano J-L & Pavel D, "Liquid Scintillation Counting", Vol. 2, Crook M A & Johnson P (Eds), (Heyden, 1972)

6. Badger B & Brocklehurst B, Nature, _219_, 263, (1968)

7. Baillie L A, Int. J. Appl. Radiat. Isotop., _8_, 1, (1960)

8. Basson J K, Anal. Chem., _28_, 1472, (1956)

9. Basson J K & Steyn J, Proc. Phys. Soc. London Sect. A, _64_, 874, (1951)

10. Bell T K, "Liquid Scintillation Counting Recent Applications and Developments", Vol. 1, Peng C T, Horrocks D L & Alpen E L (Eds), (Academic Press, 1980)

11. Benakis A, "Liquid Scintillation Counting", Vol. 1, Dyer A (Ed), (Heyden, 1971)

12. Berlman I B, J. Chem. Phys., _33_, 1124, (1960)

13. Birks J B, "The Theory and Practice of Liquid Scintillation Counting", Birks J B , (Pergamon Press, 1964)

14. Birks J B, "Current Status in Liquid Scintillation Counting", Bransome E D (Ed), (Grune & Stratton, 1970)

15. Birks J B, "Organic Scintillators and Liquid Scintillation Counting", Horrocks D L & Peng C T (Eds), (Academic Press, 1971)

16. Birks J B, Chem. Phys. Let., $\underline{1}$, 625, (1968)

17. Birks J B, Proc. Phys. Soc. London Sect. A, $\underline{64}$, 874, (1951)

18. Birks J B, "Liquid Scintillation Counting", Vol. 2, Crook M A & Johnson P (Eds), (Heyden, 1972)

19. Birks J B, "Liquid Scintillation Counting - Recent Developments", Stanley P E & Scoggins B A (Eds), (Academic Press, 1974)

20. Birks J B, "Liquid Scintillation Counting", Vol. 4, Crook M A & Johnson P (Eds), (Heyden, 1977)

21. Birks J B, Braga C L & Lumb M D, Proc. Roy. Soc. A, $\underline{283}$, 83, (1965)

22. Birks J B & Christopherou L G, Nature, $\underline{194}$, 442, (1962)

23. Birks J B & Conte J C, Proc. Roy. Soc. A, $\underline{303}$, 85, (1968)

24. Birks J B, Conte J C & Walker G, IEEE Trans. Nucl. Sci., $\underline{NS13(3)}$, 148, (1966)

25. Birks J B, Dyson D J & Munro I H, Proc. Roy. Soc. A, $\underline{275}$, 575, (1963)

26. Birks J B & Kuchela K N, Proc. Phys. Soc., $\underline{77}$, 1083, (1961)

27. Brooks F D, Prog. Nucl. Phys., $\underline{5}$, 284, (1956)

28. Brown L C, Anal. Chem., _43_, 1326, (1971)

29. Bush E T, Anal. Chem., _35_, 1024, (1963)

30. Bush E T, Int. J. Appl. Radiat. Isotop., _19_, 447, (1968)

31. Calf G E, Int. J. Appl. Radiat. Isotop., _20_, 611, (1969)

32. Calf G E, "Organic Scintillators and Liquid Scintillation Counting", Horrocks D L & Peng C T (Eds), (Academic Press, 1971)

33. Calf G E & Polach H A, "Liquid Scintillation Counting – Recent Developments", Stanley P E & Scoggins B A (Eds), (Academic Press, 1974)

34. Cavanaugh R, "Current Status in Liquid Scintillation Counting", Bransome E D (Ed), (Grune & Stratton, 1970)

35. Clausen T, Anal. Biochem., _22_, 70, (1968)

36. Cooper R & Thomas J K, J. Chem. Phys., _48_, 5097, (1968)

37. Crookes J N & Lilley I, Appl. Radiat. Isot., _38_, N° 4, 301, (1987)

38. Davidson J D & Feigelson P, Int. J. Appl. Radiat. Isotop., _2_, 1, (1957)

39. De Bersaques J, Int. J. Appl. Radiat. Isotop., _14_, 173, (1963)

40. De Filippis S J & Everett L J, Trans. Am. Nucl. Soc., _39_, 21, (1981)

41. De Wachter R & Fiers W, Anal. Biochem., _18_, 351, (1967)

42. Dobbs H E, Nature, _200_, 1283, (1963)

43. Dugan M A & Ice R D, "Organic Scintillators and Liquid Scintillation Counting", Horrocks D L & Peng C T (Eds), (Academic Press, 1971)

44. Engstrom R W, "Photomultiplier Handbook", (RCA Corporation, 1980)

45. Erikson K R, Winn R W & Horrocks D L, "Advances in Scintillation Counting", McQuarrie S A, Ediss C & Wiebe L I (Eds), (University of Alberta Press, 1983)

46. Everett L J, Ring J G & Nguyen D C, "Liquid Scintillation Counting", Vol. 3, Crook M A & Johnson P (Eds), (Heyden, 1974)

47. Ewan W D, Technometrics, $\underline{5}$, 1, (1963)

48. Ewer M J & Harding N G L, "Liquid Scintillation Counting", Vol. 3, Crook M A & Johnson P (Eds), (Heyden, 1974)

49. Farmer G C H & Hugget, Lab. Practice, $\underline{30}$, N°5, 488, (1981)

50. Ferziger J H, "Numerical methods for engineering application", (Wiley, 1981)

51. Fleishman D G & Glazunov U V, Instrum. Exp. Tech. (USSR), 472, (1962); Prib. Tekh. Eksp., $\underline{3}$, 55, (1962)

52. Flynn K F, Glendenin L E & Prodi V, "Organic Scintillators and Liquid Scintillation Counting", Horrocks D L & Peng C T (Eds), (Academic Press, 1971)

53. Flynn K F, Glendenin L E, Steinberg E P & Wright P M, Nucl. Instr. Methods, $\underline{27}$, 13, (1964)

54. Furst M & Kallmann H, Phys. Rev., $\underline{85}$, 816, (1952)

55. Furst M & Kallamnn H, Phys. Rev., $\underline{94}$, 503, (1954)

56. Furst M & Kallmann H, Phys. Rev., $\underline{109}$, 646, (1958)

57. Furst M & Kallmann H, "Liquid Scintillation Counting", Bell C G & Hayes F N (Eds), (Pergamon, 1958)

58. Galloway R B, Nucl. Instr. Methods, _172_, 431, (1980)

59. Garfinkel S B, Mann W B, Medlock R W & Yura O, Int. J. Appl. Radiat. Isotopes, _16_, 27, (1965)

60. Gebicki J, Reinschussel W & Rudzinski J, "Liquid Scintillation Counting Recent Applications and Developments", Vol. 1, Peng C T, Horrocks D L & Alpen E L (Eds), (Academic Press, 1980)

61. Gershuni S, Rabinowitz M, Agranat I & Belman I B, "Liquid Scintillation Counting Recent Applications and Developments", Vol. 1, Peng C T, Horrocks D L & Alpen E L (Eds), (Academic Press, 1980)

62. Gibson J A B, "Liquid Scintillation Science and Technology", Noujaim A A, Ediss C & Wiebe L I (Eds), (Academic Press, 1976)

63. Gibson J A B, "Liquid Scintillation Counting", Vol. 2, Crook M A & Johnson P (Eds), (Heyden, 1972)

64. Gibson J A B, "Liquid Scintillation Counting - Recent Developments", Stanley P E & Scoggins B A (Eds), (Academic Press, 1974)

65. Gibson J A B & Gale H J, Int. J. Appl. Radiat. Isotop., _23_, 321, (1972)

66. Gould J M, Cather R & Winget G D, Anal. Biochem., _50_, 540, (1972)

67. Gringorten J L, Int. J. Appl. Radiat. Isotop., part 9, _34_, 1367, (1983)

68. Gusten H & Seitz W, "Liquid Scintillation Counting Recent Applications and Developments", Vol. 1, Peng C T, Horrocks D L & Alpen E L (Eds), (Academic Press, 1980)

69. Harston M & Pyper N, J. Phys. B G.B., 17, part 24, 839, (1972)

70. Hartley P E & Church V E, "Liquid Scintillation Counting - Recent Developments", Stanley P E & Scoggins B A (Eds), (Academic Press, 1974)

71. Haviland R T & Bieber L L, Anal. Biochem., 50, 540, (1972)

72. Hayes F N, Advan. Tracer Methodol., 3, 93, (1966)

73. Hayes F N, Int. J. Appl. Radiat. Isotop., 1, 46, (1956)

74. Hayes F N, Ott D G & Kerr V N, Nucleonics, 14, 42, (1), (1956)

75. Hayes F N, Rogers B S, Sanders R, Schuch R L and Williams D L, Report LA1639, Los Alamos Sciences Lab. (1953)

76. Helf S & White C, Anal. Chem., 29, 13, (1957)

77. Herberg R J, Anal. Chem., 32, 1468, (1960)

78. Hercules D M, "Current Status in Liquid Scintillation Counting", Bransome E D (Ed), (Grune & Stratton, 1970)

79. Hiebert R D & Watts R J, Nucleonics, 11, N° 12, 38, (1953)

80. Hilaire M, Nucl. Instrm. & Methods, 112, 385, (1973)

81. Higashimura T, Yamada O, Nohara N & Shidei T, Int. J. Appl. Radiat. Isotop., 13, 308, (1962)

82. Hoizumi K, "Liquid Scintillation Counting", Vol. 5, Crook M A & Johnson P (Eds), (Heyden, 1978)

83. Horrocks D L, "Applications of Liquid Scintillation Counting", Horrocks D L, (Academic Press, 1974)

84. Horrocks D L, Photochem. & Photobiol., 15, 1083, (1972)

85. Horrocks D L, Prog. Nucl. Energy Ser. 9, 7, 21, (1966)

86. Horrocks D L, "Liquid Scintillation Counting", Vol. 5, Crook M A & Johnson P (Eds), (Heyden, 1978)

87. Horrocks D L, Trans. Am. Nucl. Soc., 45, 24, (1983)

88. Horrocks D L, "Liquid Scintillation Counting", Vol. 3, Crook M A & Johnson P (Eds), (Heyden, 1974)

89. Horrocks D L, J. Chem. Phys., 52, 1566, (1970)

90. Horrocks D L, J. Chem. Phys., 49, 2913, (1968)

91. Horrocks D L, Int. J. Appl. Radiat. Isotop., 36, Part B, 609, (1985)

92. Horrocks D L, Nature, 202, 78, (1964)

93. Horrocks D L, Trans. Am. Nucl. Soc., 39, 39, (1981)

94. Horrocks D L & Studier M H, Anal. Chem., 30, 1747, (1958)

95. Horrocks D L & Studier M H, Anal. Chem., 30, 2077, (1964)

96. Horrocks D L & Wirth H O, J. Chem. Phys., 49, 2907, (1968)

97. Horrocks D L & Wirth H O, "Organic Scintillators", Horrocks D L (Ed), (Gordon & Breach, 1968)

98. Ivanova T V, Mokkeeva G A & Sveshnikov B Ya, Optics and Spectroscopy, 12, 235, (1962)

99. Johanson K J & Lundquist H, Anal. Biochem., $\underline{50}$, 47, (1972)

100. Johnson S M, IEEE Trans. Nucl. Soc., $\underline{NS20}$, N° 1, 113, (1973)

101. Joon K & Deurloo P A, Int. J. Appl. Radiat. Isotop., $\underline{16}$, 334, (1965)

102. Jordan P, Kaczmar U & Koberle P, Nucl. Instr. Methods., $\underline{60}$, 77, (1968)

103. Kaczmarczyk K N, "Organic Scintillators and Liquid Scintillation Counting", Horrocks D L & Peng C T (Eds), (Academic Press, 1971)

104. Kalbhen D A, "Current Status in Liquid Scintillation Counting", Bransome E D (Ed), (Grune & Stratton, 1970)

105. Kallmann H & Furst M, "Liquid Scintillation Counting", Bell C G & Hayes F N (Eds), (Pergamon, 1958)

106. Kallmann H & Furst M, Nucleonics, $\underline{8}$, (3), 32, (1951)

107. Klevans H B & Platt J R, J. Chem. Phys., $\underline{17}$, 470, (1949)

108. King T A & Voltz R, Proc. Roy. Soc. A, $\underline{289}$, 424, (1966)

109. Kolb A J, "Liquid Scintillation Counting Recent Applications and Developments", Vol. 1, Peng C T, Horrocks D L & Alpen E L (Eds), (Academic Press, 1980)

110. Kolb A J & Horrocks D L, Lab. Practice, $\underline{30}$, N° 5, 481, (1981)

111. Kowalski E, Anliker R & Schmid K, "Organic Scintillators", Horrocks D L (Ed), (Gordon & Breach, 1968)

112. Laney B H, "Liquid Scintillation Science and Technology", Noujaim A A, Ediss C & Wiebe L I (Eds), (Academic Press, 1976)

113. Laney B H, "Liquid Scintillation Counting", Vol. 4, Crook M A & Johnson P (Eds), (Heyden, 1977)

114. Laney B H, "Organic Scintillators and Liquid Scintillation Counting", Horrocks D L & Peng C T (Eds), (Academic Press, 1971)

115. Langenscheidt E, "Liquid Scintillation Counting", Vol. 1, Dyer A (Ed), (Heyden, 1971)

116. Laor V & Weinreb A, J. Chem. Phys., 43, 1565, (1965)

117. Laustriat G, Voltz R & Klein J, "Current Status in Liquid Scintillation Counting", Bransome E D (Ed), (Grune & Stratton, 1970)

118. Lawson C W, Hirayama F & Lipsky S, J. Chem. Phys., 51, 1590, (1969)

119. Liberman R & Moghissi A A, Int. J. Appl. Radiat. Isotop., 21, 319, (1970)

120. Malcolm P J & Stanley P E, "Liquid Scintillation Counting - Recent Developments", Stanley P E & Scoggins B A (Eds), (Academic Press, 1974)

121. Malcolm P J & Stanley P E, "Liquid Scintillation Counting", Vol. 4, Crook M A & Johnson P (Eds), (Heyden, 1977)

122. Malcolm P J & Stanley P E, Int. J. Appl. Radiat. Isotop., 27, 415, (1976)

123. Martin H, Electro Optical Systems Design, $\underline{8}$, N⁰ 11, 16, (1976)

124. McQuarrie S A, Ediss C & Weibe L I, Int. J. Appl. Radiat. Isotop., $\underline{34}$, N⁰ 7, 1009, (1983)

125. Moghissi A A, Kelley H L, Reynier J E & Carter M W, Int. J. Appl. Radiat. Isotop., $\underline{20}$, 145, (1969)

126. Mueller E B, "Current Status in Liquid Scintillation Counting", Bransome E D (Ed), (Grune & Stratton, 1970)

127. Murray R B & Manning J J, IRE Trans. Nucl. Sci., Vol. NS7, part2, 80, (1960)

128. Neary M P & Budd A L, "Current Status in Liquid Scintillation Counting", Bransome E D (Ed), (Grune & Stratton, 1970)

129. Nibeck J I, Bares S L & Williams E S, "Liquid Scintillation Counting Recent Applications and Developments", Vol. 1, Peng C T, Horrocks D L & Alpen E L (Eds), (Academic Press, 1980)

130. Noakes J E, "Liquid Scintillation Counting", Vol. 4, Crook M A & Johnson P (Eds), (Heyden, 1977)

131. Noujaim A A, Weibe L I & Ediss C, "Liquid Scintillation Science and Technology", Noujaim A A, Ediss C & Wiebe L I (Eds), (Academic Press, 1976)

132. Okita G T, Spratt J & Leroy G V, Nucleonics, $\underline{14}$, N⁰ 3, 76, (1956)

133. Oster G K & Kallamnn H, Nature, $\underline{194}$, 1033, (1962)

134. Painter K, "Liquid Scintillation Counting - Recent Developments", Stanley P E & Scoggins B A (Eds), (Academic Press, 1974)

135. Painter K & Gezing M, "Liquid Scintillation Counting
     - Recent Developments", Stanley P E & Scoggins B A
     (Eds), (Academic Press, 1974)

136. Paix D, Int. J. Appl. Radiat. Isotop., 19, 162,
     (1968)

137. Parker R P & Elrick R H, "Current Status in Liquid
     Scintillation Counting", Bransome E D (Ed), (Grune &
     Stratton, 1970)

138. Parmentier J H & ten Haaf F E L, Int. J. Appl.
     Radiat. Isotop., 20, 305, (1969)

139. Pazdur M F, Int. J. Appl. Radiat. Isotop., 27, 179,
     (1976)

140. Peng C, Int. J. Nucl. Med. & Biol., 10, part 2-3,
     149, (1983)

141. Peng C, Anal. Chem., 32, 1292, (1960)

142. Peng C, Anal. Chem., 36, 2456, (1964)

143. Peng C, "Organic Scintillators", Horrocks D L (Ed),
     (Gordon & Breach, 1968)

144. Peng C, "Liquid Scintillation Science and
     Technology", Noujaim A A, Ediss C & Wiebe L I (Eds),
     (Academic Press, 1976)

145. Persyck D E & Lewis T T, "Liquid Scintillation
     Counting", Vol. 3, Crook M A & Johnson P (Eds),
     (Heyden, 1974)

146. Prenter P M, "Splines and Variational Methods",
     Wiley, (1975)

147. Price L W, Lab. Practice, 30, N° 5, 489, (1981)

148. Rapkin E, "Liquid Scintillation Counting", Vol. 2,
     Crook M A & Johnson P (Eds), (Heyden, 1972)

149. Rapkin E, "Applications of Liquid Scintillation Counting", p 255, Horrocks D L, (Academic Press, 1974)

150. Reines F & Cowan C L, Nature, 178, 446, (1956)

151. Reuter E & Trefny F, Int. J. Appl. Radiat. Isotop., 28, 539, (1977)

152. Ring J G, Nguyen D C & Everett L J, "Liquid Scintillation Counting Recent Applications and Developments", Vol. 1, Peng C T, Horrocks D L & Alpen E L (Eds), (Academic Press, 1980)

153. Rohde R E, Nucl. Inst. Methods, 34, 109, (1965)

154. Ross H H, Anal. Chem., 37, 621, (1965)

155. Ross H H & Yerick R E, Anal. Chem., 35, 794, (1963)

156. Rummerfield P S & Goldman I H, Int. J. Appl. Radiat. Isotop., 23, 353, (1972)

157. Scales B, Int. J. Appl. Radiat. Isotop., 18, 1, (1967)

158. Scales B, Anal. Biochem., 5, 489, (1963)

159. Schram E, Demulyder F, DeRycker J & Roosens H, "Liquid Scintillation Science and Technology", Noujaim A A, Ediss C & Wiebe L I (Eds), (Academic Press, 1976)

160. Scoggins B A, Butkus A & Coghlan J P, "Liquid Scintillation Counting - Recent Developments", Stanley B E & Scoggins B A (Eds), (Academic Press, 1974)

161. Seliger H H, Int. J. Appl. Radiat. Isotop., 8, 29, (1960)

162. Simon R E & Williams B F, IEEE Trans. Nucl. Sci., NS15, 166, (1968)

163. Skarstad P, Ma R & Lipsky S, "Organic Scintillators", Horrocks D L (Ed), (Gordon & Breach, 1968)

164. Skerbele A & Lassette E N, J. Chem. Phys., 42, 395, (1965)

165. Smith B S W & Hodgson J C, Lab. Practice, 32, N° 10, 90, (1983)

166. Spicer W E & Wooten F, Proc. IEEE, 51, 1119, (1963)

167. Spolders H, "Liquid Scintillation Counting", Vol. 4, Crook M A & Johnson P (Eds), (Heyden, 1977)

168. Stanley P E, "Liquid Scintillation Science and Technology", Noujaim A A, Ediss C & Wiebe L I (Eds), (Academic Press, 1976)

169. Stanley P E, "Liquid Scintillation Counting", Vol. 2, Crook M A & Johnson P (Eds), (Heyden, 1972)

170. Stanley P E, "Liquid Scintillation Counting Recent Applications and Developments", Vol. 1, Peng C T, Horrocks D L & Alpen E L (Eds), (Academic Press, 1980)

171. Stanley P E & Malcolm P J, "Liquid Scintillation Counting", Vol. 4, Crook M A & Johnson P (Eds), (Heyden, 1977)

172. Steyn J, Proc. Phys. Soc. London A, 69, 865, (1956)

173. Stineman R W, Creative Computing, 54, (1980)

174. Takiuie M & Hayashi M, Nucl. Instr. & Methods Phys. Res. Sect. A, 219, 192, (1984)

175. ten Haaf F E L, "Liquid Scintillation Counting", Vol. 2, Crook M A & Johnson P (Eds), (Heyden, 1972)

176. ten Haaf F E L, "Liquid Scintillation Counting", Vol. 5, Crook M A & Johnson P (Eds), (Heyden, 1978)

177. ten Haaf F E L & Vereijke M L, "Liquid Scintillation Counting", Vol. 4, Crook M A & Johnson P (Eds), (Heyden, 1977)

178. Vadergraft J S, "Introduction to Numerical Computation", 2nd Ed., (Academic Press, 1983)

179. Voltz R, Rad. Res. Rev., 1, 301, (1968)

180. Voltz R, Laustriat G & Coche A, C. R. Acad. Sci. Paris, 257, 1473, (1963), {in French}

181. Wang C H, Advan. Tracer Methodol., 1, 285, (1962)

182. Wang C H, "Current Status in Liquid Scintillation Counting", Bransome E D (Ed), (Grune & Stratton, 1970)

183. Ware W R, J. Amer. Chem. Soc., 83, 4374, (1961)

184. Wetherill G B, "Sampling inspection and quality control", (Chapman and Hall, 1977)

185. Whisman M L, Eccleston B H & Armstrong F E, Anal. Chem., 32, 484, (1960)

186. Wirth H O, Proc. Conf. Organic Scintillation Detectors, Univ. New Mexico, 1960, Rep. TID-7612 US AEC

187. Young A T, Appl. Opt., 2, N° 1, 51, (1963)

188. Yura O, Radioisotopes, 20, 383 ff, 493 ff, 610 ff, (1971)

BIBLIOGRAPHY

B1   "Applications of Liquid Scintillation Counting", D L Horrocks, Academic Press, 1974

B2   "Organic Scintillators and Liquid Scintillation Counting", D L Horrocks and C T Peng (Eds), Academic Press, 1971

B3   "Liquid Scintillation Counting", Vol. 1, A Dyer (Ed), Heyden, 1971

B4   "Liquid Scintillation Counting", Vol. 2, M A Crook and P Johnson (Eds), Heyden, 1972

B5   "Liquid Scintillation Counting", Vol. 3, M A Crook and P Johnson (Eds), Heyden, 1974

B6   "Liquid Scintillation Counting", Vol. 4, M A Crook and P Johnson (Eds), Heyden, 1977

B7   "Liquid Scintillation Counting", Vol. 5, M A Crook and P Johnson (Eds), Heyden, 1978

B8   "Current Status in Liquid Scintillation Counting", E D Bransome (Ed), Grune & Stratton, 1970

B9   "Liquid Scintillation Counting - Recent Developments", P E Stanley and B A Scoggins (Eds), Academic Press, 1974

B10   "Liquid Scintillation Science and Technology", A A Noujaim, C Ediss and L I Wiebe (Eds), Academic Press, 1976

B11   "Liquid Scintillation Counting Recent Applications and Developments", Vol. 1, C T Peng, D L Horrocks and E L Alpen (Eds), Academic Press, 1980

B12   "Liquid Scintillation Counting Recent Applications and Developments", Vol. 2, C T Peng, D L Horrocks and E L Alpen (Eds), Academic Press, 1980

B13   "The Theory and Practice of Liquid Scintillation Counting", J B Birks, Pergamon Press, 1964

B14   "Organic Scintillators", D L Horrocks (Ed), Gordon & Breach, 1968

B15   "Handbook of Fluorescence Spectra of Aromatic Molecules", I B Berlman, Academic Press, 1965

B16   "Advances in Scintillation Counting", S A McQuarrie, C Ediss and L I Wiebe (Eds), University of Alberta Press, 1983

B17   "RCA Photomultiplier Handbook", R W Engstrom, RCA Corporation, 1980

B18   "Liquid Scintillation Counting", C G Bell and F N Hayes (Eds), Pergamon, 1958

B19   "Tables of Physical and Chemical Constants", 14th Ed., G W C Kaye and T H Laby, Longman, 1973

B20   "CRC Handbook of Physics and Chemistry", 64th Ed., Robert C Weast (Ed), CRC Press, 1983

Appendix A

DETECTION OF DRIFT IN RADIOACTIVE COUNTING USING THE CUSUM TECHNIQUE

Introduction

The characteristics of a scintillation counter are critically dependent on the stability of the counting conditions. Instabilities in the system produce a drift in the counting efficiency.[139] Such changes are often associated with drift in the EHT supply due to temperature or mains fluctuations or deterioration of the sample in liquid scintillation counting. Unless remedial action is to be taken the source of the drift is not so important. However, it is essential to know the magnitude and time when any drift occurs. The literature shows very little work on the monitoring of counter performance[3,59] and this has used traditional indicators of change in a Poissonian distribution such as standard deviation, skew and kurtosis. Although producing confidence limits, typically 95%, these indicators have been shown to lack the sensitivity of other methods as well as producing no indication of the onset of drift. This work studies the detection of drift using a cusum method[47,104] and compares its scope and sensitivity with the traditional method.

Cusum method

The cumulative sum chart (or cusum chart) is a highly informative means of presenting data that can be ordered into a logical sequence. A detailed exposition of the methodology is given in a British Standard Guide to Data analysis and quality control using cusum techniques (BS 5703, parts 1, 2, 3 and 4). For observations x_1, x_2, ... x_n obtained sequentially having a target value, T, which may be the mean, $\bar{x}$, for retrospective analysis, the cusum is defined as $C_i = \sum_{r=1}^{i} (x_r - T)$. A cusum chart displays C_i against i.

Where the observations are from a population having a mean equal to the target value the graph will generally be horizontal with random fluctuations about the line. A systematic fluctuation from the target value will result in a change in the slope of the chart.

When measuring variability a plot is made of a sample statistic, say sample mean or range, having a standard error, σ_e. If the population standard deviation, σ, is known, or there exists an accurate estimate, we may use the relevant sampling theory to obtain σ_e e.g. $\sigma_e = \sigma/\sqrt{n}$. Generally it is safer to obtain a direct estimate of the standard error. Denoting the values to be plotted y_1, y_2, ...y_m then $\sigma_e = \left(\sum_{i=1}^{m-1} \frac{(y_i - y_{i+1})^2}{2(m-1)} \right)^{\frac{1}{2}}$

An estimate of the local average in a particular segment is given by the slope of the cusum chart. Consider the segment from sample i+1 to j. The relevant change in cusum is from C_i to C_j over i to j. (For the first segment i = 0 and C_0 = 0). Hence the average shift from the target (mean) value for the segment is $(C_j - C_i)/(j - i)$. Thus the local average is $\overline{X}_{i+1,j} = T + (C_j - C_i)/(j - i)$.

The application of the cusum method to the detection of drift in a parameter requires the establishment of decision rules to distinguish between real changes in the cusum slope and the normal variability of the data. The essential features of the cusum chart relevant to the detection of changes in the underlying average level are the steepness of the cusum slope and the number of samples over which the slope persists. When the parameter (e.g. count) is running at the target level, i.e. an acceptable quality level AQL, there will, because of the random nature of counting, inevitably be occasions when the cusum path apparently diverges from the horizontal. The decision rule should not give false alarms that indicate that such sequences represent significant departure from AQL. On the other hand, when the process moves to an unsatisfactory condition, i.e. a rejectable quality level, RQL, the decision rule should give as rapid a response as possible. The number of events between drift occurring and its detection by the cusum indicates the magnitude of the drift. If the true process is at or near AQL, then this number should be large i.e. few false alarms, whereas if it

323

is near RQL, then it should be short i.e. rapid detection.

The detection of drift by use of AQL and RQL can be achieved in various ways. One graphical method employs a truncated V-mask which comprises a datum point, indicated by A in Fig. A1.1 with two sloping arms running from B to D and C to E. The scaling of the mask i.e. h & f, will determine the stringency of the control. The mask is used by placing the datum A over any point on the chart, usually the most recent point plotted. The AF axis is laid parallel to the sample number axis of the chart. If the path of the cusum crosses either of the arms, a significant departure from the target value is signalled. However, if the entire cusum path remains inside the arms, no significant shift is indicated.

Although the V-mask is essentially a manual inspection method it can be computerised, but in both cases it is slow and laborious. An alternative method is entirely numerical in nature and hence much faster to compute. Again the data defines the AQL, μ_a, and there is a deviation from μ_a which is unacceptable and is represented by the RQL, μ_r. A reference level, K, for deviations from the mean is established where $K = T \pm f\sigma_a$. If $f = 0.5$ then the reference level lies midway between μ_a and μ_r. Each count (x_i) is compared with K. If $x_i < K$ then no action is taken. However, if $x_i > K$, then a cusum is commenced of

the algebraic differences from K, i.e. $C = \sum_i^j (x_i - K)$,

where j represents the end point of the cusum determined by one of the following two conditions: a) if C falls to below 0 or b) C > H where $H = h\sigma_w$ is a decision level, typically h = 5. If a) applies then no action is taken until $T - f\sigma_w > x_j > T + f\sigma_w$ again and a new cusum is commenced. If b) applies then drift is deemed to have occurred, i representing the onset of the cusum but not necessarily the onset of drift (since allowance has to be made for statistical fluctuation), and j - i representing the number of samples from onset to detection.

Simulated Data

In order to test the sensitivity of the method and compare it with the traditional methods of analysis for Poissonian fluctuations, sets of data were produced using the random generator of a microcomputer. 100 sets each containing 1000 numbers were examined and satisfied the normality tests using the 95% confidence limits for skew and kurtosis. For a range of values of K the minimum decision level, h_{min} which failed to indicate drift was determined. This produced a 95% confidence limit as shown in Fig. A1.2 and any RQL indicated by a data set lying within this band must be assumed to be normal data. However, where h_{min} is found to lie outside this range, then drift or non-normality of the data is detected.

Having defined the range for acceptable Poissonian data, more data sets were generated with drifts introduced. This allowed an investigation of the size and length of drift detectable using the cusum as opposed to the traditional methods.

The data sets consisted of 1100 numbers; the first 1000 generated with a theoretical mean value of 20,000 and no drift followed by 100 numbers with a uniform positive drift. The various sets generated had drifts ranging from 0.01% per sample to 0.05% per sample.

The statistical analysis of the drift data was performed on batches of 200 and 1000 numbers with various proportions of the drifting data included for each of the simulated data sets. The cusum analysis produced not only the value of h_{min} required to prevent any drift indication but for lesser values of h also determined the onset of drift and the point at which it was detected. For all drift data an RQL of 1 σ_ω was employed.

For batches of 200 taken from the drift data the variation in the value of h_{min} for a range of drifts as well as non-drift was investigated (Fig. A1.3). The analysis of the results shows that for h greater than 1.6, the drift is detected. However, a small proportion of the total indicated non-normality from a study of the kurtosis. The sensitivity of the cusum technique detects drift of 0.015% per sample when the drift length is greater than 20% of the 200 sample total, but failed to detect a 0.01% drift at any point. The investigation demonstrated the superiority of the cusum technique over the more traditional kurtosis.

When considering 1000 points the sensitivity is increased compared with 200 points so that a drift of 0.01% per sample for a duration of 9% of the total sample size is detected. A drift of 0.05% per sample is detected when only representing 2% of the total at a similar level as would be expected.

327

In order to detect the onset and magnitude of drift, a value of h was fixed at 3 representing a value outside the spread of h_{min} derived from normal data sets and allowing for statistical fluctuations. The number of samples was determined between the onset and detection of drift for the various drift sizes (Fig. A1.4). Although subject to quite large fluctuations the trend is as expected and allows the magnitude of drift in an instrument test to be estimated.

Instrument Tests

Experiments were conducted on three instruments, namely, the Nuclear Enterprises SR3 and Packard Auto Gamma counter with NaI crystals and the Packard 300C liquid scintillation counter. A PET microcomputer, connected on-line to each in turn, acquired 1000 counts for various counting configurations. For the γ-detectors the counts across a ^{137}Cs photopeak at optimum EHT produced no detectable drift. Plotted on Fig. A1.2 the h_{min} values lie within the 95% confidence range for 1000 simulated data sets with no drift.

The tests of the liquid scintillation counter were rather more extensive and designed to assess the presence of drift a) while counting a given radionuclide and b) with alternations between two radionuclides. A single ^{14}C source was subjected to 1000 one minute counts with 43s cycle time intervals between each count. The kurtosis was within the 95% confidence levels and an h_{min} value of 2.1 showed a very low degree of drift (Experiment 1, Table TA1.1). Consequently, the instrument produced a high degree of stability for continuous counting of the same radionuclide.
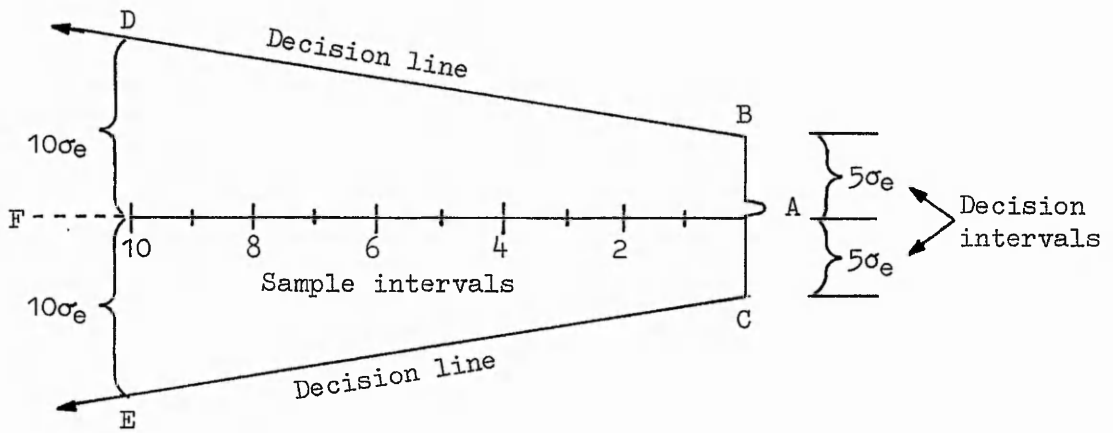
To examine the effect of two radionuclides, single samples of ^{3}H and ^{14}C were counted alternately with the counting conditions varied appropriate to the radionuclide by the automatic programming of the counter. Although only 500

329

counts were taken for each sample in this case, considerable drift was detected by both the kurtosis and cusum techniques (Experiment 2, Table TA1.1). In order to investigate this effect further, rather than single counts of each radionuclide, 25 repeated counts of each i.e. 25 counts of ^{3}H followed by 25 counts of ^{14}C, was performed a total of 40 times. The results showed much less drift. Indeed for both radionuclides the kurtosis values were within the 95% confidence levels. However, the cusum technique demonstrated its better sensitivity and detected some drift for both samples (Experiment 3, Table TA1.1). Hence the test demonstrated that a 'settling down' period follows the changed programme settings between radionuclides to be desirable.

An analysis of the drifts indicated for h = 3 showed that the 10 drifts (7 for ^{14}C and 3 for ^{3}H) ranged from 0.14% per sample to 0.06%, although these readings are subject to quite large errors which are difficult to estimate.

Conclusion

The cusum technique when applied to radioisotope counting is both more sensitive and more informative than the use of kurtosis. A simple computer analysis with a decision level of $3\sigma_{cw}$ determined from theoretical data produced a statement of the instrument behaviour. From the experiments performed using the Packard 300C liquid scintillation counter the stability during long counts of a particular isotope is better than the sensitivity of the cusum technique. However, using the parameters chosen above, drift occurred when alternate single counts of ^{3}H - ^{14}C were made. When the samples were subject to repeated counts during each cycle drift was less severe.

General-purpose truncated V-mask
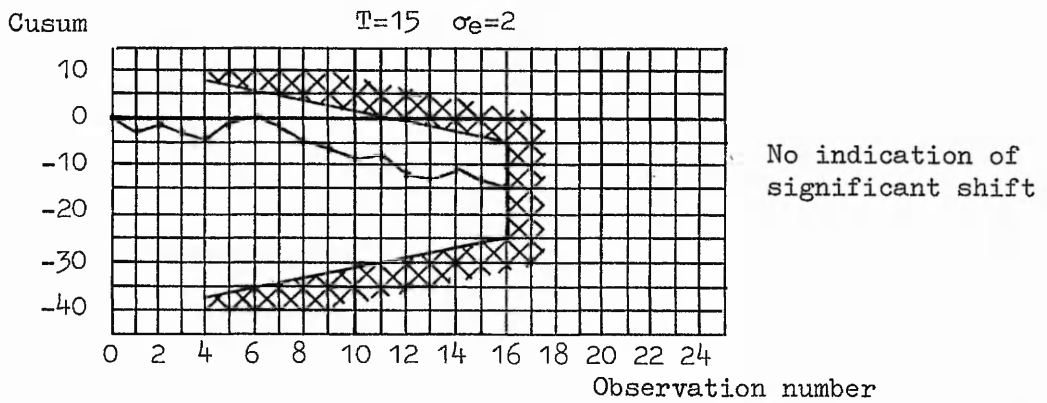
Truncated V-mask applied to cusum chart: no indication of shift

Truncated V-mask applied to cusm chart: indication of shift

Fig. A1.1
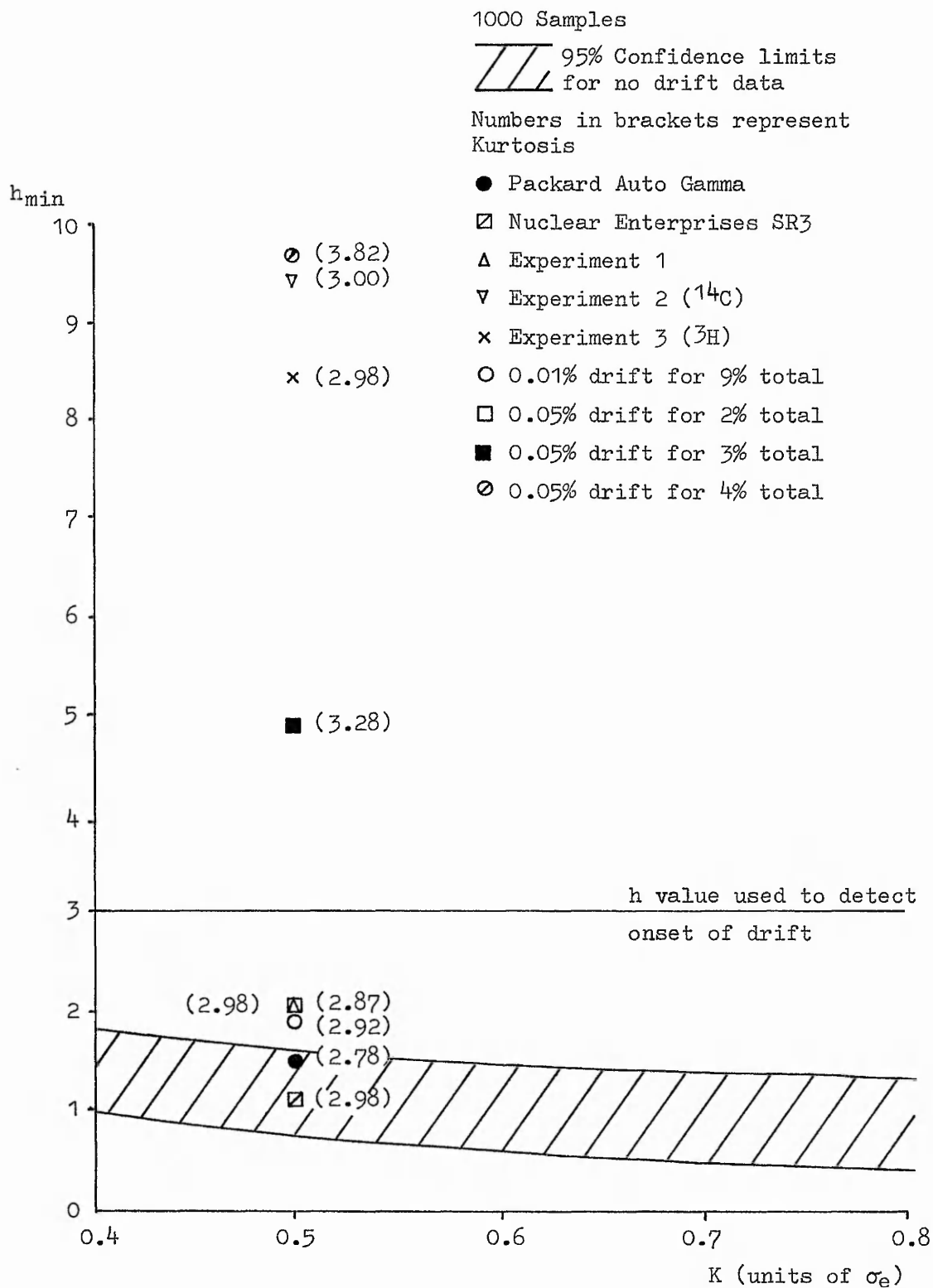
Fig. A1.2 Variation of h_{min}
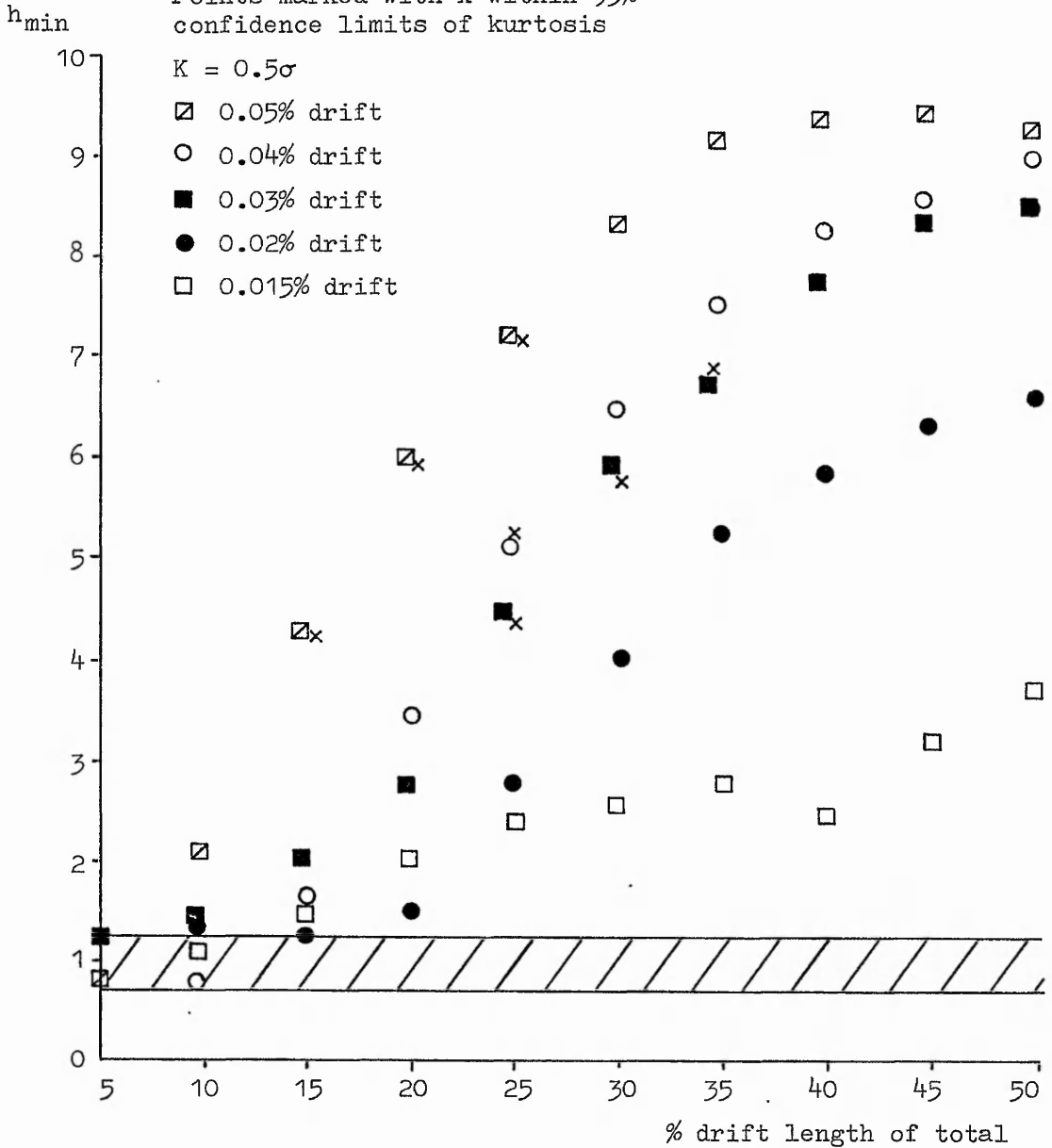
Fig. A1.3 Variation of h_{min} with drift length/total length
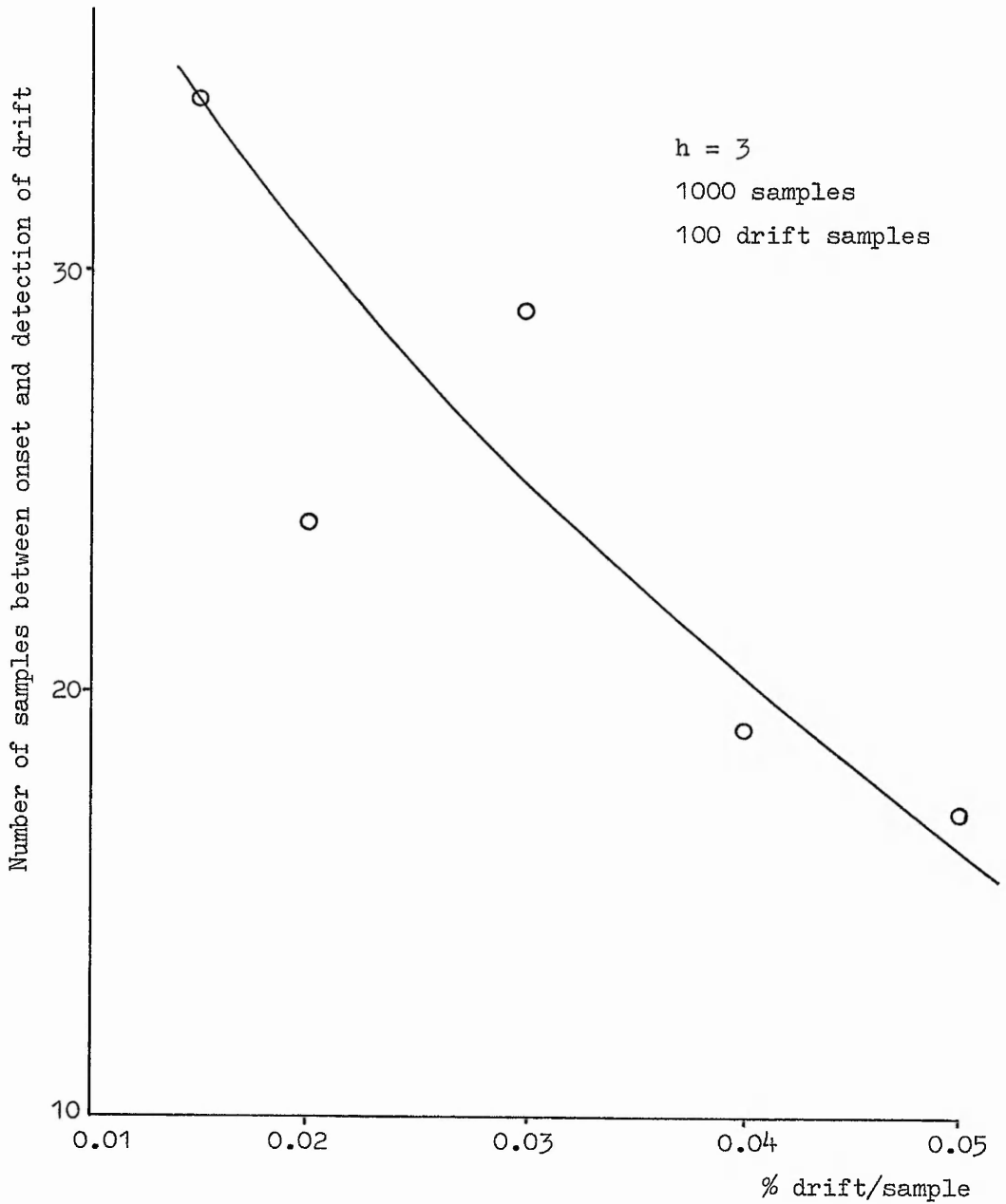
Fig. A1.4 Variation of detection length with % drift

335

Table TA1.1

Results of drift experiments on Packard 300C Liquid Scintillation
Counter

Experiment Number		Kurtosis	Number of drifts detected with h = 3	h_{min}
1		2.98	0	2.1
2*	^{14}C	2.44	11	10
	^{3}H	2.24	11	10
3	^{14}C	3.00	7	9.5
	^{3}H	2.97	3	7.5

* 500 counts of each sample

APPENDIX B

Program Listings

(i) LSC Simulation

M2.2.PAS and M2.2INIT.PAS together comprise the root
version of the LSC Model described in this thesis. The
model simulates the two PMTube Liquid Scintillation Counter
for ^{3}H and ^{14}C counting. Editing of the module
M2.2INIT.PAS enables long sequences of non-interactive
model running.

(ii) Polya Statistics

The program Polya.Pas produces a listing of the compound
poisson (polya) distribution and its two extremes, the
exponential distribution and the poisson distribution. The
polya distribution is used to model PMTube statistics in
the LSC simulation.

(iii) MCA Pulse Height Spectra Transfer and Analysis

The BASIC and 6502 machine code programs listed below
enables the transfer of a pulse height spectrum from a
NE4694 1024 MCA to a PET via a RS232/IEEE interface at 4800
baud; the display of the spectrum on a PET high resolution
graphics screen at variable sensitivity; use of a cursor to
define a region of interest; and calculation of the
integral count and mean pulse height across the region of
interest.

(iv) Fluorescence and Absorption Spectra Capture

The program FLUORESCENCE is written in USCD Pascal as implemented on the Apple IIe microcomputer under the TDI pSystem. It is a program used to capture fluorescence spectra data generated by a Perkin Elmer 3000 Fluorimeter. This is achieved by monitoring two input channels of an attached A/D card. One channel is used for the actual data capture and the other for initiating a run. Initiation of a run results from detection of a 1V signal which goes low when the fluorimeter scan button is depressed. Upon completion of capturing the requested number of samples the data is saved to disk.

(v) Curve Fitting

The program Curfit written in BASIC on a CBM 4000 PET offers a menu of curve fitting routines with screen plotting, screen dumps and printed output. The program requires prior loading of PETGRAPH to enable the graphics function. The printed output is achieved by calling a chained program Curdat.

(vi) Data Capture of 300C Printer Output

LSC1OSHORT, written in BASIC on a CBM 4000 PET is one of a series of programs to capture the printed output of the Packard 300C liquid scintillation counter (LSC). The program is designed to recognise the number of the internal program commenced by the LSC prior to starting any data capture, and subsequent storage of the data on disk.

(i) <u>LSC Simulation - M2.2.PAS</u>

```pascal
PROGRAM LSCMODEL(INPUT,OUTPUT,OUTFILE,OUT1,OUT2,OUT3,
        OUT4,OUT5,OUT6,DATAFILE);
CONST CEFF = 0.85;{ collection eff% }
      PI = 3.14159265;
      PLANCK = 6.6262E-34;
      ECHARGE = 1.60219E-19;
      LIGHTSPEED = 2.997925E8;
TYPE STRING = PACKED ARRAY[1..25] OF CHAR;
     QUENCHREC = RECORD
          QCHEMVAL : REAL;
          QCOLVAL : REAL;
          QMATLS : STRING;
          END;
     CNTSETNGSREC = RECORD
          CNTMODE : CHAR;
          CNTNUM : INTEGER;
          THOLD : INTEGER;
          SCRSETNGS : ARRAY[1..4,1..6] OF INTEGER;
          BSPECSTEP : REAL;
          END;
     LSCGEOMREC= RECORD
          LIQHT : REAL;
          LIQRAD : REAL;
          VIALHT : REAL;
          VIALRAD : REAL;
          VIALOFFSET : REAL;
          CASEHT : REAL;
          CASERAD : REAL;
          END;
     PARAMREC = RECORD
          PMEAN : ARRAY[1..6] OF REAL;
          PMODE : ARRAY[1..6] OF REAL;
          PSCR : ARRAY[1..6] OF REAL;
          PMID : ARRAY[1..6] OF REAL;
          END;
     PULSEREC = RECORD
          PULSENUM : ARRAY[1..2] OF INTEGER;
          END;
     PHOTREC = RECORD
          L1,L2,L3,L4,L5,L6,L7,L8,PNUM:
          INTEGER;
          END;
     CHNLREC = RECORD
          MAXCH : ARRAY[1..6] OF INTEGER;
          END;
MODLREC = RECORD
          RECNUM : [KEY(0)] INTEGER;
          NUCLTYPE : CHAR;
          MODLVERSION : PACKED ARRAY[1..50] OF CHAR;
          QREC : QUENCHREC;
          CREC : CNTSETNGSREC;
          LREC : LSCGEOMREC;
          PREC : PARAMREC;
          PULREC : PULSEREC;
          TLOSS : INTEGER;
```

339

```
                CLOSS : INTEGER;
                QLOSS : INTEGER;
                PHREC : PHOTREC;
                CHREC : CHNLREC;
                END;
     MCAREC = RECORD
                MCARECNUM : [KEY(0)] INTEGER;
                MCADAT : ARRAY[0..4000] OF INTEGER;
                END;
     VAR  {files  records}
          OUTFILE,TMPFILE :FILE OF MODLREC;
          OUT1,OUT2,OUT3,OUT4,OUT5,OUT6 :FILE OF MCAREC;
          DATAFILE :FILE OF INTEGER;
          QREC:QUENCHREC;CREC:CNTSETNGSREC;LREC:LSCGEOMREC;
          MREC:MCAREC;PREC:PARAMREC;PULREC:PULSEREC;
          PHREC:PHOTREC;CHREC:CHNLREC;AREC:MODLREC;
          {real variables}
          QCHEM,QCOL,CRAD,LRAD,ARAD,VRAD,VOS,ESTEP,VHT,LHT,
          AHT,CHT: [GLOBAL] REAL;
          QCHEMVAL,QCOLVAL,EB,PRBMAX,MCPRBMAX,EBSUM,EPOL,
          MCPRB,EP,WPR,PHI,PSI,ANGLINC,ANGLREF,R,Z,VR,VB,VH,
          UA,UB,UC,UD,U,DIST,TEMP,X0,Y0,Z0,X1,Y1,Z1,X2,Y2,Z2,
          XN,ZN,EM,E,SW,RETGAMMA,CRIT,SPLINEX,SPLINEY,NREF,
          EMAX,EBPRBMAX,EVX,EVY,EVZ,WCUTOFF,VIALHT,CASEHT,
          CASERAD,VIALRAD,BSPECSTEP,TEMP1,TEMP2,PHIINC,
          PSIINC,ANGLPOL,XTILT,ZTILT,TILT,NX,NY,NZ,XE,YE,ZE,
          XP,YP,ZP,XL,YL,ZL,VIALOFFSET,LIQHT,LIQRAD : REAL;
          {quadruple reals}
          PMPRBMAX : QUADRUPLE;
          {integer variables}
          IDNUMBER,NDISNTGS,NCOUNTS,DYNUM,THRESHOLD :
          [GLOBAL] INTEGER;
          I,JJ,COUNT,WP,WSTART,WSTOP,ASTART,ASTOP,FSTART,
          SKIP,CHOP,LOOP,II,NFERMI,SEEDVAL,FSTOP,MNUM,K,J,
          PMTMIN,PMTMAX,SUM,DIFF,RATIO,IMCPRB,
          H,W,RND,SPLINESIZE,MAXCHNL,WLOWER,WUPPER,ITEMP,
          COINLOST,THLDLOST,RECNUM,TLOSS,CLOSS,QLOSS,
          QUANTLOST,THOLD,CNTNUM,IEVENTS,MNUMTEMP,FACENUM,
          NFLEC,PARFLAG,L1,L2,L3,L4,L5,L6,L7,L8,RL2,LL2,PNUM,
          MCARECNUM,L1,L2,L3,L4,L5,L6,L7,L8,PNUM :
          INTEGER;
          {boolean  char}
          PHOTONTRACED,OUTWARD,RDO :BOOLEAN;
          STOPFLAG: [GLOBAL] BOOLEAN;
          NUCLIDE,CNTMODE: [GLOBAL] CHAR;
          CNTMODE,NUCLTYPE : CHAR;
          QMATLS :[GLOBAL] PACKED ARRAY[1..25] OF CHAR;
          QMATLS :PACKED ARRAY[1..25] OF CHAR;
          MVERSION:[GLOBAL] PACKED ARRAY[1..50] OF CHAR;
          MODLVERSION :PACKED ARRAY[1..50] OF CHAR;
          {real arrays}
          VV,ZZ,A1,B,C,D1 :ARRAY[0..50] OF REAL;
          P,PP :ARRAY[0..1,0..50] OF REAL;
          SEFF :ARRAY[0..1,0..9] OF REAL;
          MEANENCH,SCR,MODE,MIDNUMCH,PMEAN,PMODE,PSCR,
```

```
                    PMID:ARRAY[1..6] OF REAL;
                    SCRSUM :ARRAY[1..2,1..6] OF REAL;
                    PMPRB :ARRAY[0..1000] OF QUADRUPLE;
                    QI :ARRAY[1..2,0..1000] OF REAL;
                    QP,DYM,BSF : [GLOBAL] ARRAY[1..2] OF REAL;
                    {integer arrays}
                    MCA :ARRAY[1..6,0..4000] OF INTEGER;
                    MCADAT :ARRAY[0..4000] OF INTEGER;
                    FLSWAVE,FLSPROB,ABSPROB,WAVE,PROB,ALABSPROB :
                    ARRAY[0..300] OF INTEGER;
                    SCRSETNGS : ARRAY[1..4,1..6] OF INTEGER;
                    SCRLL, SCRUL : [GLOBAL] ARRAY[1..2,1..6] OF INTEGER;
                    MAXCH :ARRAY[1..6] OF INTEGER;
                    ALAB :ARRAY[0..1,0..11] OF INTEGER;
                    PULSENUM, PULSENUM, PMCOUNT, QIX :
                    ARRAY[1..2] OF INTEGER;
FUNCTION SPLINEINTERP(SPLINEX:REAL) : REAL;
BEGIN
H:=0;W:=0;
WHILE W=0 DO
BEGIN
IF (SPLINEX>=PP[0,H]) AND (SPLINEX<PP[0,H+1])
THEN BEGIN
SPLINEX:=SPLINEX-PP[0,H];
SPLINEY :=A1[H]+B[H]*SPLINEX+C[H]*SPLINEX*SPLINEX;
SPLINEINTERP :=SPLINEY+D1[H]*SPLINEX*SPLINEX*SPLINEX;
W:=1;END;H:=H+1;END;
END;
FUNCTION MAG(X,Y,Z : REAL) : REAL;
BEGIN
  MAG:= SQRT(X*X+Y*Y+Z*Z)
END;
[EXTERNAL,ASYNCHRONOUS] FUNCTION MTH$TAN
(X : REAL) : REAL;
EXTERNAL;
[EXTERNAL,ASYNCHRONOUS] FUNCTION MTH$ASIN
(X : REAL) : REAL;
EXTERNAL;
[EXTERNAL,ASYNCHRONOUS] FUNCTION MTH$ACOS
(X : REAL) : REAL;
EXTERNAL;
[EXTERNAL,ASYNCHRONOUS] FUNCTION MTH$RANDOM
(VAR SEED:INTEGER) : REAL;
EXTERNAL;
[EXTERNAL] PROCEDURE INIT1;
   EXTERN;
FUNCTION LFACT(X:INTEGER) : REAL;
VAR JJJ:INTEGER;
BEGIN
TEMP:=0;IF X>0 THEN BEGIN FOR JJJ:=1 TO X DO
BEGIN TEMP:=TEMP+LN(JJJ);END;END ELSE;
LFACT:=TEMP;
END;
FUNCTION LPOW(X:REAL;Y:INTEGER) : REAL;
BEGIN
```

```
     IF X=0 THEN LPOW:=0 ELSE LPOW:=Y*LN(X);
END;
PROCEDURE RANDOMINT;
BEGIN
   RND:= ROUND(MAXINT*MTH$RANDOM(SEEDVAL))
END;
FUNCTION RAND(LO, HI:INTEGER):INTEGER;
(* GIVES EVEN SPREAD THRO' A RANGE LO TO HI *)
VAR MX, C, D: INTEGER;
PROCEDURE RANDM;
BEGIN
RND:= ROUND(MAXINT*MTH$RANDOM(SEEDVAL))
END;
BEGIN
RAND:=0;
IF LO = HI THEN RAND:= LO ELSE BEGIN
C:= HI - LO + 1;
MX:= (MAXINT - HI + LO) DIV C + 1;
MX:= MX*(HI-LO) + (MX-1);
REPEAT RANDM UNTIL MX>=RND;
RAND:= LO + RND MOD C; END
END;
(* REF INDEX USING CAUCHY EQNS...*)
FUNCTION NPBDXYL(X : INTEGER) : REAL;
 BEGIN
 NPBDXYL:= 1.50675199-1432.37733/X/X-4.12889718E8/X/X/X/X
 END;
FUNCTION NCCL4(X : INTEGER) : REAL;
 BEGIN
 NCCL4:= 1.48042353-5196.90174/X/X-3.92118921E8/X/X/X/X
 END;
FUNCTION NPMTGLS(X : INTEGER) :REAL;
 BEGIN
 NPMTGLS:=1.52
 END;
FUNCTION NVIALGLS(X : INTEGER) :REAL;
 BEGIN
 NVIALGLS:=1.49788933+4061.10397/X/X+5804367.75/X/X/X/X
 END;
FUNCTION NLIQVIAL(X : INTEGER) :REAL;
 BEGIN
 NLIQVIAL:=1
 END;
(* PMT QUANTUM EFF% INTERPOLATED RCA4501/V3 DATA *)
FUNCTION QUANTEFF(X :INTEGER) : REAL;
 BEGIN
 QUANTEFF:= (-8.906E-4*X*X+0.745*X-129.49375)/100;
 (* approx. quadratic 0 to 0.26 efficiency range,
 i.e not normalized *)
 END;
PROCEDURE RANDOMIZE;
BEGIN
SEEDVAL:= CLOCK;
FOR I:= 1 TO 10 DO
TEMP:= MTH$RANDOM(SEEDVAL);
```

```
END;
PROCEDURE H3FERMI;
BEGIN
NFERMI:= 7;EMAX:= 18.6;
FOR I:= 0 TO NFERMI DO BEGIN
P[0,I]:= 511*(SQRT(1+I*I/400)-1);
END;
P[1,0]:= 0;P[1,1]:= 0.00547;P[1,2]:= 0.0153;
P[1,3]:= 0.0302;P[1,4]:= 0.0501;P[1,5]:= 0.0751;
P[1,6]:= 0.105;P[1,7]:= 0.141;
END;
PROCEDURE C14FERMI;
BEGIN
NFERMI:= 20;EMAX:= 156;
FOR I:= 0 TO NFERMI DO BEGIN
P[0,I]:= 511*(SQRT(1+I*I/400)-1);END;
P[1,0]:= 0;P[1,1]:= 0.0162;P[1,2]:= 0.0338;
P[1,3]:= 0.0553;P[1,4]:= 0.0818;P[1,5]:= 0.114;
P[1,6]:= 0.151;P[1,7]:= 0.193;P[1,8]:= 0.240;
P[1,9]:= 0.293;P[1,10]:= 0.351;P[1,11]:= 0.416;
P[1,12]:= 0.485;P[1,13]:= 0.560;P[1,14]:= 0.641;
P[1,15]:= 0.728;P[1,16]:= 0.820;P[1,17]:= 0.918;
P[1,18]:= 1.021;P[1,19]:= 1.131;P[1,20]:= 1.246;
P[1,21]:= 1.494;
END;

PROCEDURE SCINTEFF;
BEGIN
SEFF[0,0]:= 0;SEFF[0,1]:=0.5;SEFF[0,2]:= 1;SEFF[0,3]:= 5;
SEFF[0,4]:= 18.6;SEFF[0,5]:= 50;SEFF[0,6]:= 158;
SEFF[0,7]:= 300;SEFF[0,8]:= 500;SEFF[0,9]:= 1000;
SEFF[1,0]:= 0;SEFF[1,1]:= 0.024;SEFF[1,2]:= 0.031;
SEFF[1,3]:= 0.040;SEFF[1,4]:= 0.047;SEFF[1,5]:= 0.052;
SEFF[1,6]:= 0.058;SEFF[1,7]:= 0.062;
SEFF[1,8]:= 0.062;SEFF[1,9]:= 0.062;
END;

PROCEDURE FSTSPL;
BEGIN
W:=SPLINESIZE;FOR H:=0 TO W DO A1[H]:=PP[1,H];
FOR H:=0 TO W-1 DO D1[H]:= PP[0,H+1]-PP[0,H];
D1[W]:=D1[W-1];D1[W+1]:=D1[0];B[0]:=2*D1[0];
FOR H:=1 TO W-1 DO B[H]:=2*(D1[H]+D1[H-1]);
B[W]:=2*D1[W-1];C[0]:=3*(A1[1]-A1[0]);
FOR H:=1 TO W-1 DO
C[H]:=3*(D1[H-1]*(A1[H+1]-A1[H])/D1[H]+(D1[H]/D1[H-1])
        *(A1[H]-A1[H-1]));
END;

PROCEDURE SECSPL;
BEGIN
C[W]:=3*(A1[W]-A1[W-1]);VV[0]:=B[0];
VV[1]:=B[1]-(D1[1]*D1[W+1]/VV[0]);
FOR H:= 2 TO W DO VV[H]:=B[H]-((D1[H]*D1[H-2])/VV[H-1]);
ZZ[0]:=C[0];FOR H:= 1 TO W DO
```

```
ZZ[H]:=C[H]-(D1[H]*ZZ[H-1]/VV[H-1]);
B[W]:=ZZ[W]/VV[W];
FOR H:=W-1 DOWNTO 1 DO
B[H]:=(ZZ[H]-(D1[H-1]*B[H+1]))/VV[H];
B[O]:=(ZZ[O]-(D1[W+1]*B[1]))/VV[O];
C[O]:=0;C[W]:=0;FOR H:= 1 TO W-1 DO
C[H]:=3*(A1[H+1]-A1[H])/SQR(D1[H])
       -((2*B[H])+B[H+1])/D1[H];
FOR H:=0 TO W-1 DO
D1[H]:=(C[H+1]-C[H])/(3*D1[H]);
END;


PROCEDURE SPLINEFORM;
BEGIN
FSTSPL;
SECSPL;
END;


PROCEDURE INIT2;
BEGIN
PULSENUM[1]:= 0;PULSENUM[2]:= 0;COINLOST:= 0;
THLDLOST:= 0;QUANTLOST:=0;
L1:=0;L2:=0;L3:=0;L4:=0;L5:=0;L6:=0;L7:=0;L8:=0;RL2:=0;
LL2:=0;PNUM:=0;EBSUM:=0;IEVENTS:=0;
FOR I:= 1 TO 6 DO BEGIN
MAXCH[I]:=0;SCRSUM[1,I]:= 0;SCRSUM[2,I]:= 0;
FOR II:= 1 TO 4000 DO MCA[I,II]:=0;END;
TILT:= ARCTAN((CHT/2)/(CRAD-VRAD));XTILT:= COS(TILT);
ZTILT:=SIN(TILT);
IF NUCLIDE = 'H' THEN H3FERMI ELSE C14FERMI;
FOR I:= 0 TO NFERMI DO
BEGIN
PP[0,I]  := P[0,I];PP[1,I]  := P[1,I];
END;
SPLINESIZE:= NFERMI;
SPLINEFORM;
SCINTEFF;
WCUTOFF:= PLANCK*LIGHTSPEED/600/1E-9;
END;(* INIT2 *)
PROCEDURE BSPECMAX;
BEGIN
EM:= 1+EMAX/510.91;PRBMAX:= -999;EB:= ESTEP*EMAX;
{ keV..0==>SW=0}
REPEAT E:= 1+EB/510.91;
SW:=SPLINEINTERP(EB)*E/SQRT(E*E-1)*SQR(EM-E);
IF SW>PRBMAX THEN BEGIN PRBMAX:= SW;EBPRBMAX:= EB;
END;EB:= EB+ESTEP*EMAX;UNTIL SW<PRBMAX;
MCPRBMAX:= PRBMAX*(1+ESTEP);
(* MONTECARLO PROB MAX SLIGHTLY OVERESTIMATES SPECTRUM *)
END;(* BSPECMAX *)
PROCEDURE BETAENERGY;
BEGIN
REPEAT EB:= MTH$RANDOM(SEEDVAL)*EMAX;
E:= 1+EB/510.91;IF SQRT(E*E-1)=0 THEN SW:=0

ELSE BEGIN MCPRB:= MTH$RANDOM(SEEDVAL)*MCPRBMAX;
```

344

```
SW:=SPLINEINTERP(EB)*E*SQR(EM-E)/SQRT(E*E-1);END;
UNTIL MCPRB <= SW;
ITEMP:=0;I:=0;EBSUM:=EBSUM+EB;
REPEAT
IF EB<SEFF[O,I+1] THEN BEGIN TEMP:=SEFF[1,I+1]-SEFF[1,I];
TEMP:=SEFF[1,I]+TEMP*(EB-SEFF[O,I])
                    /(SEFF[O,I+1]-SEFF[O,I]);
EB:= EB*TEMP;ITEMP:=1;END
ELSE;{linear interp of scint effy curve}
I:=I+1;UNTIL ITEMP=1;
EB:= 1000 * EB * ECHARGE;(* KEV TO JOULES *)
END;(*BETAENERGY*)
PROCEDURE CHEMQUENCH;
BEGIN
EB:= (1-QCHEM)*EB;
(*is QCHEM a function of EB ? *)
END;(*CHEMQUENCH*)
PROCEDURE SPECDATA;
VAR DAT, II :INTEGER;
BEGIN
RESET (DATAFILE);
DAT:= DATAFILE;
GET(DATAFILE);
WSTART:= DAT;
DAT:= DATAFILE;
GET(DATAFILE);
WSTOP:= DAT;
LOOP:= WSTOP-WSTART-1;
FOR I:= 0 TO LOOP DO
BEGIN
WAVE[I]:= WSTART+I;DAT:= DATAFILE;
GET(DATAFILE);
PROB[I]:= DAT;
END;
CLOSE (DATAFILE);
END;(*SPECDATA*)
PROCEDURE FLSPEC;
BEGIN
OPEN(DATAFILE,'FLSPEC1.DAT',HISTORY:= OLD);
SPECDATA;
FSTART:= WSTART;FSTOP:= WSTOP;
FOR I:= 0 TO LOOP DO BEGIN
FLSWAVE[I]:= WAVE[I];FLSPROB[I]:= PROB[I];
END;
END;
PROCEDURE ABSPEC;
BEGIN
OPEN(DATAFILE,'O7ABSPEC.DAT',HISTORY:= OLD);
SPECDATA;
ASTART:= WSTART;ASTOP:= WSTOP;
IF FSTART > ASTART THEN SKIP:= (FSTART-ASTART)
ELSE SKIP:=0;
IF FSTOP < ASTOP THEN CHOP:= (ASTOP-FSTOP) ELSE CHOP:= 0;
(* N.B. ABS RANGE DIFFERENT TO FLSPEC *)
FOR I:= 0 TO (LOOP-CHOP-SKIP) DO
```

345

```
BEGIN
ABSPROB[I]:= 1000-PROB[I+SKIP];
END;
END;
PROCEDURE ALABSPEC;
BEGIN
ALAB[0,0]:=295;ALAB[0,1]:=310;ALAB[0,2]:=327;
ALAB[0,3]:=345;ALAB[0,4]:=365;ALAB[0,5]:=388;
ALAB[0,6]:=414;ALAB[0,7]:=443;ALAB[0,8]:=477;
ALAB[0,9]:=517;ALAB[0,10]:=564;ALAB[0,11]:=620;
ALAB[1,0]:=752;ALAB[1,1]:=752;ALAB[1,2]:=753;
ALAB[1,3]:=754;ALAB[1,4]:=755;ALAB[1,5]:=757;
ALAB[1,6]:=759;ALAB[1,7]:=758;ALAB[1,8]:=762;
ALAB[1,9]:=772;ALAB[1,10]:=800;ALAB[1,11]:=852;
FOR I:= 0 TO FSTOP-FSTART-1 DO BEGIN
J:=0;ITEMP:=0;
REPEAT
IF (I+FSTART)<ALAB[0,J+1] THEN BEGIN
TEMP:=ALAB[1,J+1]-ALAB[1,J];
TEMP:=ALAB[1,J]+TEMP*(I+FSTART-ALAB[0,J])
              /(ALAB[0,J+1]-ALAB[0,J]);
ALABSPROB[I]:= ROUND(TEMP*100);ITEMP:=1;END
ELSE;{linear interp of scint effy curve}
J:=J+1;UNTIL ITEMP=1;
END;
END;
PROCEDURE EVENTCOORDS;
BEGIN
REPEAT
EVZ:= (MTH$RANDOM(SEEDVAL)-0.5)*LHT;
UNTIL (EVZ < LHT/2)AND(EVZ > (-LHT/2));
REPEAT
EVX:= (MTH$RANDOM(SEEDVAL)-0.5)*LRAD*2;
EVY:= (MTH$RANDOM(SEEDVAL)-0.5)*LRAD*2;
UNTIL (EVX*EVX+EVY*EVY) < (LRAD*LRAD);
{equi probs for cartesians,
not cylindrical coords,  avoid boundary}
X0:= EVX;Y0:= EVY;Z0:= EVZ;
VR:= LRAD;VH:= LHT/2;VB:= -LHT/2;
END;
PROCEDURE INITPHOTDIR;
BEGIN
PHI:= MTH$RANDOM(SEEDVAL)*2*PI;
PSI:= MTH$RANDOM(SEEDVAL)*2*PI;
X1:= VR*SIN(PSI)*COS(PHI);
Y1:= VR*SIN(PSI)*SIN(PHI);
Z1:= VR*COS(PSI);
EPOL:= MTH$RANDOM(SEEDVAL)*PI/2;{angle of polarization
of E-vector}
{rotate coords to get PE in global coords}
XE:=COS(-PSI)*COS(EPOL)-SIN(-PSI)*SIN(EPOL);
ZE:=SIN(-PSI)*COS(EPOL)+COS(-PSI)*SIN(EPOL);{rot abt
east west}
XE:=COS(-PHI)*XE;YE:=SIN(-PHI)*XE;{rot abt north south}
END;
```

```
PROCEDURE CYLU;
BEGIN
IF (X1=0)AND(Y1=0) THEN UA:= -99999 ELSE BEGIN
TEMP:=XO*X1;
TEMP:=TEMP+YO*Y1;TEMP:=SQR(TEMP);UA:=X1*X1;
UA:=UA+Y1*Y1;TEMP1:=((VR*VR)-(YO*YO+XO*XO));
UA:=UA*TEMP1;{if ua close to zero here then final
result ua=zero is wrong}
{to cater for this rare event (occured after >4hours
cpu time.. event is so close to the wall that certain
P1 vectors cause the error) PICKU must choose CYLU and
cylu must be set to some non-zero value e.g. 1 }
UA:=TEMP+UA;IF UA<0 THEN BEGIN
WRITELN('CYLU',MNUMTEMP,FACENUM,NFLEC,PARFLAG);
WRITELN(XO,YO,ZO,X1,Y1,Z1,X2,Y2,Z2);
IF OUTWARD=FALSE THEN WRITELN('F') ELSE;END ELSE;
UA:=(SQRT(UA)-(XO*X1+YO*Y1))/(X1*X1+Y1*Y1);
IF NFLEC=1 THEN UA:=1 ELSE;{ ..radius reflection
R=XO**2+YO**2 =>UA=0}
IF UA=0 THEN BEGIN
WRITELN('CYLU',MNUMTEMP,FACENUM,NFLEC,PARFLAG);
WRITELN(XO,YO,ZO,X1,Y1,Z1,X2,Y2,Z2);
IF OUTWARD=FALSE THEN WRITELN('F') ELSE;END ELSE;END;
END;
PROCEDURE DISCU;
BEGIN
IF Z1<>0 THEN BEGIN
IF Z1>0 THEN UB:= (VH-ZO)/Z1 ELSE UB:= (VB-ZO)/Z1;END
ELSE UB:= -99999;
END;
PROCEDURE TORU;
BEGIN
IF XO<>0 THEN BEGIN
IF (XO>0)AND(YO>=0) THEN TEMP:=ARCTAN(YO/XO) ELSE;
IF (XO<0)AND(YO>=0) THEN TEMP:=PI-ARCTAN(ABS(YO/XO)) ELSE;
IF (XO<0)AND(YO<0) THEN TEMP:=PI+ARCTAN(ABS(YO/XO)) ELSE;
IF (XO>0)AND(YO<0) THEN TEMP:=2*PI-ARCTAN(ABS(YO/XO))
ELSE;END ELSE BEGIN IF YO>=0 THEN TEMP:=0 ELSE TEMP:=PI
END;IF X1<>0 THEN BEGIN
IF (X1>0)AND(Y1>=0) THEN TEMP1:=ARCTAN(Y1/X1) ELSE;
IF (X1<0)AND(Y1>=0) THEN TEMP1:=PI-ARCTAN(ABS(Y1/X1))
ELSE;
IF (X1<0)AND(Y1<0) THEN TEMP1:=PI+ARCTAN(ABS(Y1/X1)) ELSE;
IF (X1>0)AND(Y1<0) THEN TEMP1:=2*PI-ARCTAN(ABS(Y1/X1))
ELSE;END ELSE BEGIN
IF Y1>0 THEN TEMP1:=0 ELSE TEMP1:=PI;END;
IF OUTWARD=TRUE THEN BEGIN
TEMP:=ABS(PI-ABS(TEMP-TEMP1));TEMP:=COS(TEMP);
UA:=LRAD*LRAD*(TEMP*TEMP-1)+VRAD*VRAD;
UA:=(LRAD*TEMP+SQRT(UA))/MAG(X1,Y1,0);
END ELSE BEGIN
TEMP:=ABS(ABS(TEMP-TEMP1)-PI);TEMP:=COS(TEMP);
UA:=LRAD*LRAD*(TEMP*TEMP-1)+VRAD*VRAD;
UA:=(VRAD*TEMP-SQRT(UA))/MAG(X1,Y1,0);
UA:=1;{for all inwards phots ,no pmt reflection case}
```

```
END;
END;
PROCEDURE PARU;
BEGIN
IF X1>0 THEN UC:=(VRAD-X0)/X1 ELSE UC:=-(VRAD+X0)/X1;
TEMP:=ABS(Z0+UC*Z1)*XTILT/SIN(TILT-ARCTAN(ABS(Z1/X1)))
                        /MAG(X1,0,Z1);
UC:=TEMP+UC;
END;
PROCEDURE PICKU;
BEGIN IF UA=0 THEN BEGIN UA:=1;U:=UA;END
ELSE BEGIN
CASE MNUM OF
1,2,3 : IF ABS(UA) < ABS(UB) THEN U:= UA ELSE U:= UB;
4     : BEGIN IF ABS(UA) < ABS(UB) THEN TEMP1:=UA
 ELSE TEMP1:=UB;IF PARFLAG=0 THEN BEGIN
 IF ABS(UC) < TEMP1 THEN U:=UC ELSE U:=TEMP1;
 END ELSE U:=TEMP1;END;
END;END;X1:=U*X1;Y1:=U*Y1;Z1:= U*Z1;
X2:=X0+X1;Y2:=Y0+Y1;Z2:=Z0+Z1;
{now scale to avoid tolerance errors}
IF MAG(X2,Y2,0)>VR THEN BEGIN
TEMP:=VR/MAG(X2,Y2,0);X2:=X2*TEMP;
Y2:=Y2*TEMP;Z2:=Z2*TEMP;END
ELSE;{chamber done individually}
END;
PROCEDURE EVECTOR;
BEGIN
IF X1<>0 THEN BEGIN
IF (X1>0)AND(Y1>=0) THEN PHI:=ARCTAN(Y1/X1) ELSE;
IF (X1<0)AND(Y1>=0) THEN PHI:=PI-ARCTAN(ABS(Y1/X1)) ELSE;
IF (X1<0)AND(Y1<0) THEN PHI:=PI+ARCTAN(ABS(Y1/X1)) ELSE;
IF (X1>0)AND(Y1<0) THEN PHI:=2*PI-ARCTAN(ABS(Y1/X1)) ELSE;
END ELSE BEGIN IF Y1>0 THEN PHI:=0 ELSE PHI:=PI;
END;IF Z1>=0 THEN PSI:=MTH$ACOS(ABS(Z1)/MAG(X1,Y1,Z1))
ELSE PSI:= -MTH$ACOS(ABS(Z1)/MAG(X1,Y1,Z1));
XE:=COS(-PSI)*COS(EPOL)-SIN(-PSI)*SIN(EPOL);
ZE:=SIN(-PSI)*COS(EPOL)+COS(-PSI)*SIN(EPOL);{rot abt
east west}
XE:=COS(-PHI)*XE;
YE:=SIN(-PHI)*XE;{rot abt north south}
END;
PROCEDURE DISCREFLECT;
BEGIN
Z1:= -Z1;X0:=X2;Y0:=Y2;Z0:=Z2;EVECTOR;
END;
PROCEDURE DISCREFRACT;
BEGIN
X0:=X2;Y0:=Y2;
IF ANGLINC<>0
THEN Z1:=Z1*MTH$TAN(ANGLINC)/MTH$TAN(ANGLREF) ELSE;
IF Z1>0 THEN BEGIN
MNUMTEMP:=2;VH:=AHT/2;VB:= -AHT/2;VR:=ARAD;Z0:=-AHT/2;

MNUMTEMP:=1;VH:=LHT/2;VB:= -LHT/2;VR:=LRAD;Z0:=LHT/2;
```

```
END;EVECTOR;
END;
PROCEDURE CYLREFLECT;
BEGIN
TEMP:= 2*MAG(X1,Y1,Z1)*COS(ANGLINC)/VR;
IF OUTWARD=FALSE THEN TEMP:=-TEMP ELSE;
X1:= X1-X2*TEMP;
Y1:= Y1-Y2*TEMP;
XO:=X2;YO:=Y2;ZO:=Z2;
EVECTOR;
END;
PROCEDURE CYLREFRACT;
BEGIN
IF MTH$TAN(ANGLINC)<>0 THEN BEGIN DIST:= MAG(X1,Y1,Z1);
TEMP:=(1-MTH$TAN(ANGLREF)/MTH$TAN(ANGLINC));
IF OUTWARD=FALSE THEN TEMP:=-TEMP ELSE;
TEMP:=TEMP*COS(ANGLINC)*DIST/VR;
X1:= TEMP*X2+MTH$TAN(ANGLREF)/MTH$TAN(ANGLINC)*X1;
Y1:= TEMP*Y2+MTH$TAN(ANGLREF)/MTH$TAN(ANGLINC)*Y1;
Z1:= MTH$TAN(ANGLREF)/MTH$TAN(ANGLINC)*Z1;END
ELSE;{anglinc=0 ==>leave x1,y1,z1 same}
XO:=X2;YO:=Y2;ZO:=Z2;
EVECTOR;
END;
PROCEDURE PARREFLECT;
BEGIN
TEMP:=2*MAG(X1,Y1,Z1)*COS(ANGLINC);
X1:=X1+TEMP*ZTILT*XN;Z1:=Z1+TEMP*XTILT*ZN;
XO:=X2;YO:=Y2;ZO:=Z2;
EVECTOR;
END;
PROCEDURE LAFACE;
BEGIN
DIST:= MAG(X1,Y1,Z1);
DIST:= MAG(X1,Y1,Z1);
IF DIST=0 THEN BEGIN WRITELN('ZERO P1 VECTOR',U,XO,YO,ZO);
PHOTONTRACED:=TRUE;L4:=L4+1;END ELSE BEGIN
{check colour quench outwards..}
IF OUTWARD=TRUE THEN BEGIN
IF MTH$RANDOM(SEEDVAL) >EXP( -DIST*ABSPROB[W]/1000*QCOL)
THEN BEGIN PHOTONTRACED:= TRUE;L4:=L4+1;END
ELSE;END ELSE;
IF PHOTONTRACED=FALSE THEN BEGIN IF Z1=0
THEN BEGIN NX:=1;NY:=0;NZ:=0;END ELSE BEGIN
NX:= -Y1/Z1;NY:=1;NZ:=0;END;IF (NX<>0)THEN
PHI:=ARCTAN(ABS(NY/NX)) ELSE PHI:=PI/2;
IF (XE<>0) THEN PHIINC:=ABS(PHI-ARCTAN(ABS(YE/XE)))
ELSE PHIINC:=ABS(PHI-(PI/2));
PSIINC:= MTH$ACOS(ABS(ZE)/MAG(XE,YE,ZE));
ANGLPOL:= MTH$ACOS(1/SQRT(1+SQR(MTH$TAN(PHIINC)))

                      /SQRT(1+SQR(MTH$TAN(PSIINC))));
ANGLINC:= MTH$ACOS(ABS(Z1)/DIST);
IF OUTWARD=TRUE THEN BEGIN NREF:=1/NFBDXYL(WP);
CRIT:= MTH$ASIN(NREF);END ELSE BEGIN
NREF:=NFBDXYL(WP);CRIT:=PI/2;END;
```

```
IF ANGLINC < CRIT THEN BEGIN
ANGLREF:=MTH$ASIN(SIN(ANGLINC)/NREF);
IF ANGLINC=0 THEN TEMP:=SQR((NREF-1)/(NREF+1))
ELSE BEGIN
TEMP1:=SQR(SIN(ANGLINC-ANGLREF)/SIN(ANGLREF+ANGLINC));
TEMP2:=SQR(MTH$TAN(ANGLINC-ANGLREF)
            /MTH$TAN(ANGLINC+ANGLREF));
TEMP:=SQR(SIN(ANGLPOL))*TEMP1+SQR(COS(ANGLPOL))*TEMP2;
END;{weighted average of Fresnel paraperp reflectances}
IF MTH$RANDOM(SEEDVAL) <= TEMP THEN DISCREFLECT
ELSE DISCREFRACT;END ELSE DISCREFLECT;
{discface bidirectional}END ELSE;NFLEC:=0;END
END;
PROCEDURE LVFACE;
BEGIN
DIST:= MAG(X1,Y1,Z1);
IF DIST=0 THEN BEGIN WRITELN('ZERO P1 VECTOR',U,X0,Y0,Z0);
PHOTONTRACED:=TRUE;L3:=L3+1;END ELSE BEGIN
{check colour quench outwards..}
IF MNUMTEMP=1 THEN BEGIN
IF MTH$RANDOM(SEEDVAL) > EXP( -DIST*ABSPROB[W]*QCOL)
THEN BEGIN PHOTONTRACED:= TRUE;L6:=L6+1;END ELSE;END ELSE;
IF PHOTONTRACED=FALSE THEN BEGIN
IF ((Y1*X2/Y2-X1)<>0)AND((Y1-X1*Y2/X2)<>0) THEN BEGIN
NX:=Z1/(Y1*X2/Y2-X1);NY:= -Z1/(Y1-X1*Y2/X2);NZ:=1;END
ELSE;{photon parallel to normal =>NX,NY,NZ unchanged}
IF (NX<>0) THEN PHI:=ARCTAN(ABS(NY/NX)) ELSE PHI:=PI/2;
IF (XE<>0) THEN PHIINC:=ABS(PHI-ARCTAN(ABS(YE/XE)))
ELSE PHIINC:=ABS(PHI-(PI/2));
PSIINC:=ABS(MTH$ACOS(ABS(NZ)/MAG(NX,NY,NZ))
            -MTH$ACOS(ABS(ZE)/MAG(XE,YE,ZE)));
ANGLPOL:= MTH$ACOS(1/SQRT(1+SQR(MTH$TAN(PHIINC)))
            /SQRT(1+SQR(MTH$TAN(PSIINC))));
IF (X2<>0) THEN PHI:=ARCTAN(ABS(Y2/X2)) ELSE PHI:=PI/2;
IF (X1<>0) THEN PHIINC:=ABS(PHI-ARCTAN(ABS(Y1/X1)))
ELSE PHIINC:=ABS(PHI-(PI/2));
PSIINC:= PI/2-MTH$ACOS(ABS(Z1)/DIST);
ANGLINC:= MTH$ACOS(1/SQRT(1+SQR(MTH$TAN(PHIINC)))
            /SQRT(1+SQR(MTH$TAN(PSIINC))));
IF MNUMTEMP=1 THEN BEGIN
NREF:=NVIALGLS(WP)/NPBDXYL(WP);CRIT:=PI/2;END ELSE BEGIN
NREF:=NPBDXYL(WP)/NVIALGLS(WP);CRIT:=MTH$ASIN(NREF);
END;IF ANGLINC<CRIT THEN BEGIN
ANGLREF:=MTH$ASIN(SIN(ANGLINC)/NREF);IF ANGLINC=0
THEN TEMP:=SQR((NREF-1)/(NREF+1)) ELSE BEGIN
TEMP1:=SQR(SIN(ANGLINC-ANGLREF)/SIN(ANGLREF+ANGLINC));
TEMP2:=SQR(MTH$TAN(ANGLINC-ANGLREF)

            /MTH$TAN(ANGLINC+ANGLREF));
TEMP:=SQR(SIN(ANGLPOL))*TEMP1+SQR(COS(ANGLPOL))*TEMP2;
END;{weighted average of Fresnel paraperp reflectances}
IF MTH$RANDOM(SEEDVAL) <= TEMP THEN BEGIN CYLREFLECT;
IF OUTWARD=FALSE THEN BEGIN OUTWARD:=TRUE;NFLEC:=1;
VR:=VRAD;END ELSE END ELSE BEGIN CYLREFRACT;
IF OUTWARD=TRUE THEN BEGIN VH:=VHT/2;VB:= -VHT/2;VR:=VRAD;
MNUMTEMP:=3;Z0:=Z0-(VHT-LHT)/2;NFLEC:=0;
```

```
END ELSE BEGIN VH:=LHT/2;VB:= -LHT/2;VR:=LRAD;
MNUMTEMP:=1;NFLEC:=0;OUTWARD:=TRUE;ZO:=ZO+(VHT-LHT)/2;
END;END;END ELSE BEGIN CYLREFLECT;
IF OUTWARD=FALSE THEN BEGIN OUTWARD:=TRUE;NFLEC:=1;
VR:=VRAD;END ELSE END;END ELSE; {photontraced}
END;
END;
PROCEDURE AVFACE;
BEGIN
DIST:= MAG(X1,Y1,Z1);
IF DIST=0 THEN BEGIN
WRITELN('ZERO P1 VECTOR',U,XO,YO,ZO);
PHOTONTRACED:=TRUE;L4:=L4+1;END ELSE BEGIN
IF ((Y1*X2/Y2-X1)<>0)AND((Y1-X1*Y2/X2)<>0)
THEN BEGIN
NX:=Z1/(Y1*X2/Y2-X1);NY:= -Z1/(Y1-X1*Y2/X2);NZ:=1;END
ELSE; {photon parallel to normal =>NX,NY,NZ unchanged}
IF (NX>0) THEN PHI:=ARCTAN(ABS(NY/NX)) ELSE PHI:=PI/2;
IF (XE<>0) THEN PHIINC:=ABS(PHI-ARCTAN(ABS(YE/XE)))
ELSE PHIINC:=ABS(PHI-(PI/2));
PSIINC:=ABS(MTH$ACOS(ABS(NZ)/MAG(NX,NY,NZ))
            -MTH$ACOS(ABS(ZE)/MAG(XE,YE,ZE)));
ANGLPOL:= MTH$ACOS(1/SQRT(1+SQR(MTH$TAN(PHIINC)))
            /SQRT(1+SQR(MTH$TAN(PSIINC))));
IF (X2<>0)THEN PHI:=ARCTAN(ABS(Y2/X2)) ELSE PHI:=PI/2;
IF (X1<>0) THEN PHIINC:=ABS(PHI-ARCTAN(ABS(Y1/X1)))
ELSE PHIINC:=ABS(PHI-(PI/2));
PSIINC:= PI/2-MTH$ACOS(ABS(Z1)/DIST);
ANGLINC:= MTH$ACOS(1/SQRT(1+SQR(MTH$TAN(PHIINC)))
            /SQRT(1+SQR(MTH$TAN(PSIINC))));
NREF:=NPBDXYL(WP);CRIT:= PI/2;
ANGLREF:=MTH$ASIN(SIN(ANGLINC)/NREF);
IF ANGLINC=0 THEN TEMP:=SQR((NREF-1)/(NREF+1)) ELSE BEGIN
TEMP1:=SQR(SIN(ANGLINC-ANGLREF)/SIN(ANGLREF+ANGLINC));
TEMP2:=SQR(MTH$TAN(ANGLINC-ANGLREF)
            /MTH$TAN(ANGLINC+ANGLREF));
TEMP:=SQR(SIN(ANGLPOL))*TEMP1+SQR(COS(ANGLPOL))*TEMP2;
END; {weighted average of Fresnel paraperp reflectances}
IF MTH$RANDOM(SEEDVAL) <= TEMP
THEN BEGIN CYLREFLECT;NFLEC:=1;END ELSE BEGIN
CYLREFRACT;VH:=VHT/2;VB:= -VHT/2;VR:=VRAD;
MNUMTEMP:=3;ZO:=ZO+(VHT-AHT)/2;
END; {no rotate ,but coords-origin z-translates}
{phot lost up vial wall on any reflection in mnum=3}
END;
END;
PROCEDURE VCFACE;
BEGIN
DIST:= MAG(X1,Y1,Z1);
IF DIST=0 THEN BEGIN
WRITELN('ZERO P1 VECTOR',U,XO,YO,ZO);
PHOTONTRACED:=TRUE;L5:=L5+1;END
ELSE BEGIN IF ((Y1*X2/Y2-X1)<>0)AND((Y1-X1*Y2/X2)<>0)
THEN BEGIN
NX:=Z1/(Y1*X2/Y2-X1);NY:= -Z1/(Y1-X1*Y2/X2);NZ:=1;END
```

```pascal
ELSE;{photon parallel to normal =>NX,NY,NZ unchanged}
IF (NX<>0) THEN PHI:=ARCTAN(ABS(NY/NX)) ELSE PHI:=PI/2;
IF (XE<>0) THEN PHIINC:=ABS(PHI-ARCTAN(ABS(YE/XE)))
ELSE PHIINC:=ABS(PHI-(PI/2));
PSIINC:=ABS(MTH$ACOS(ABS(NZ)/MAG(NX,NY,NZ))
       -MTH$ACOS(ABS(ZE)/MAG(XE,YE,ZE)));
ANGLPOL:= MTH$ACOS(1/SQRT(1+SQR(MTH$TAN(PHIINC)))
              /SQRT(1+SQR(MTH$TAN(PSIINC))));
IF (X2<>0)THEN PHI:=ARCTAN(ABS(Y2/X2)) ELSE PHI:=PI/2;
IF (X1<>0) THEN PHIINC:=ABS(PHI-ARCTAN(ABS(Y1/X1)))
ELSE PHIINC:=ABS(PHI-(PI/2));
PSIINC:= PI/2-MTH$ACOS(ABS(Z1)/DIST);
ANGLINC:= MTH$ACOS(1/SQRT(1+SQR(MTH$TAN(PHIINC)))
              /SQRT(1+SQR(MTH$TAN(PSIINC))));
NREF:=1/NPBDXYL(WP);CRIT:= MTH$ASIN(NREF);
IF ANGLINC < CRIT THEN BEGIN IF ANGLINC=0
THEN TEMP:=SQR((NREF-1)/(NREF+1))
ELSE BEGIN
TEMP1:=SQR(SIN(ANGLINC-ANGLREF)/SIN(ANGLREF+ANGLINC));
TEMP2:=SQR(MTH$TAN(ANGLINC-ANGLREF)
     /MTH$TAN(ANGLINC+ANGLREF));
TEMP:=SQR(SIN(ANGLPOL))*TEMP1+SQR(COS(ANGLPOL))*TEMP2;
END;{weighted average of Fresnel paraperp reflectances}
IF MTH$RANDOM(SEEDVAL) <= TEMP
THEN BEGIN CYLREFLECT;OUTWARD:=FALSE;NFLEC:=1;VR:=LRAD;
END ELSE BEGIN CYLREFRACT;TEMP:=-Z1;Z1:=Y1;Y1:=TEMP;
TEMP:=-Z1;ANGLREF:=MTH$ASIN(SIN(ANGLINC)/NREF);
Z2:=Y2;Y2:=TEMP;TEMP:=-Z0;Z0:=Y0;Y0:=TEMP;VR:=CRAD;
VH:=CHT/2;VB:=-CHT/2;MNUMTEMP:=4;FACENUM:=4;NFLEC:=0;
IF ((((Z1/MAG(X1,0,Z1))<-XTILT)AND(Z0>0))
 OR(((Z1/MAG(X1,0,Z1))>XTILT)AND(Z0<0)))
 OR(MAG(X0,Y0,0)>=CRAD) THEN BEGIN
PHOTONTRACED:=TRUE;L8:=L8+1;END;
{a few phots are returned by parmirror to vial}
{chamber doesn't envelop the vial}
END;END ELSE BEGIN
CYLREFLECT;OUTWARD:=FALSE;VR:=LRAD;NFLEC:=1;
END;FACENUM:=4;END;
END;
PROCEDURE PARMIRROR;
BEGIN
IF MTH$RANDOM(SEEDVAL) >= (ALABSPROB[W]/1000000)
THEN BEGIN DIST:= MAG(X1,Y1,Z1);IF DIST=0
THEN BEGIN WRITELN('ZERO P1 VECTOR',U,X0,Y0,Z0);
PHOTONTRACED:=TRUE;L1:=L1+1;END
ELSE BEGIN IF Z0>0 THEN BEGIN
ZN:=1;IF X1>0 THEN XN:= -1 ELSE XN:=1;END ELSE BEGIN
ZN:= -1; IF X1>0 THEN XN:= -1 ELSE XN:=1;
END;PSIINC:= PI/2-TILT+ARCTAN(ABS(Z1/X1));
PHIINC:= MTH$ASIN(ABS(Y1)/DIST);
ANGLINC:=MTH$ACOS(1/SQRT(1+SQR(MTH$TAN(PHIINC)))
              /SQRT(1+SQR(MTH$TAN(PSIINC))));

PARREFLECT END END ELSE BEGIN
PHOTONTRACED := TRUE;L1:=L1+1;END;
FACENUM:=5;PARFLAG:=1;
```

```
{for area of parmirror where PO=CRAD
approx. set nflec as for cylmirror}
IF MAG(XO,YO,O)>=CRAD THEN NFLEC:=1 ELSE NFLEC:=0;
END;
PROCEDURE CYLMIRROR;
BEGIN
IF MTH$RANDOM(SEEDVAL) >= (ALABSPROB[W]/1000000)
THEN BEGIN DIST:= MAG(X1,Y1,Z1);
IF DIST=0 THEN BEGIN
WRITELN('ZERO P1 VECTOR',U,XO,YO,ZO);
PHOTONTRACED:=TRUE;L1:=L1+1;END ELSE BEGIN
IF X2<>0 THEN PHI:=ARCTAN(ABS(Y2/X2)) ELSE PHI:=PI/2;
IF X1<>0 THEN PHIINC:=ABS(PHI-ARCTAN(ABS(Y1/X1)))
ELSE PHIINC:=ABS(PHI-PI/2);
PSIINC:= PI/2-MTH$ACOS(ABS(Z1)/DIST);
ANGLINC:=MTH$ACOS(1/SQRT(1+SQR(MTH$TAN(PHIINC)))
          /SQRT(1+SQR(MTH$TAN(PSIINC))));
CYLREFLECT;NFLEC:=1;END; END ELSE BEGIN
PHOTONTRACED := TRUE;L1:=L1+1;
END;
FACENUM:=6;
END;
PROCEDURE PMTUBE;
BEGIN
IF Z1>0 THEN BEGIN QIX[1]:=QIX[1]+1;
QI[1,QIX[1]]:=QUANTEFF(WP);END
ELSE BEGIN QIX[2]:=QIX[2]+1;
QI[2,QIX[2]]:=QUANTEFF(WP);END;
PHOTONTRACED:=TRUE;
END;
PROCEDURE PMGLASS;
BEGIN
DIST:= MAG(X1,Y1,Z1);
IF DIST=0 THEN BEGIN WRITELN('ZERO P1 VECTOR',U,XO,YO,ZO);
PHOTONTRACED:=TRUE;
IF Z1>0 THEN RL2:=RL2+1 ELSE LL2:=LL2+1;
L2:=L2+1;END ELSE BEGIN IF X1=0 THEN BEGIN
NX:=1;NY:=0;NZ:=0;END ELSE BEGIN
NX:= -Y1/X1;NY:=1;NZ:=0;END;
IF (NX<>0)THEN PHI:=ARCTAN(ABS(NY/NX)) ELSE PHI:=PI/2;
IF (XE<>0) THEN PHIINC:=ABS(PHI-ARCTAN(ABS(YE/XE)))
ELSE PHIINC:=ABS(PHI-(PI/2));
PSIINC:=ABS(MTH$ACOS(ABS(NZ)/MAG(NX,NY,NZ))
            -MTH$ACOS(ABS(ZE)/MAG(XE,YE,ZE)));
ANGLPOL:= MTH$ACOS(1/SQRT(1+SQR(MTH$TAN(PHIINC)))
            /SQRT(1+SQR(MTH$TAN(PSIINC))));
ANGLINC:= MTH$ACOS(ABS(Z1)/DIST);
NREF:=NPMTGLS(WP);CRIT:= PI/2;
ANGLREF:= MTH$ASIN(SIN(ANGLINC)/NREF);
IF ANGLINC=0 THEN TEMP:=SQR((NREF-1)/(NREF+1))

ELSE BEGIN
TEMP1:=SQR(SIN(ANGLINC-ANGLREF)/SIN(ANGLREF+ANGLINC));
TEMP2:=SQR(MTH$TAN(ANGLINC-ANGLREF)
            /MTH$TAN(ANGLINC+ANGLREF));
TEMP:=SQR(SIN(ANGLPOL))*TEMP1+SQR(COS(ANGLPOL))*TEMP2;
```

```
END;{weighted average of Fresnel paraperp reflectances}
IF MTH$RANDOM(SEEDVAL) <= TEMP THEN BEGIN
PHOTONTRACED:=TRUE;
IF Z1>0 THEN RL2:=RL2+1 ELSE LL2:=LL2+1;L2:=L2+1;
END ELSE PMTUBE;END;
END;
PROCEDURE CHAMBERTRACK;
BEGIN
IF X1<>0 THEN BEGIN
IF ARCTAN(ABS(Z1/X1))>=TILT THEN PARFLAG:=1 ELSE;
END ELSE PARFLAG:=1;
CASE FACENUM OF
   4: BEGIN CYLU;DISCU;
      IF PARFLAG=0 THEN PARU ELSE;
      PICKU;
      IF U=UB
      THEN PMGLASS ELSE BEGIN
      IF U=UA THEN CYLMIRROR ELSE PARMIRROR;
      END;
      END;
   5: BEGIN CYLU;DISCU;PICKU;
      IF U=UA THEN CYLMIRROR ELSE PMGLASS;
      END;
   6: BEGIN CYLU;DISCU;
      IF PARFLAG=0 THEN PARU ELSE;
      PICKU;
      IF U=UB THEN PMGLASS ELSE BEGIN
      IF U=UA THEN CYLMIRROR ELSE PARMIRROR;END;
      END;
   END;{case}
END;
PROCEDURE FLASHTRACK;
VAR LOW, HIH:INTEGER;
BEGIN
QIX[1]:=0;QIX[2]:=0;{pmtube arrays initialized
for new photon batch}
WHILE EB > WCUTOFF DO
BEGIN
REPEAT
IF EB < (PLANCK*LIGHTSPEED/340/1E-9)THEN
WLOWER:=TRUNC(PLANCK*LIGHTSPEED/EB/1E-9) ELSE
WLOWER:=FLSWAVE[0];WUPPER:= FLSWAVE[FSTOP-FSTART-1];
WP:= RAND(WLOWER,WUPPER);
IMCPRB:= RAND(1,900);
UNTIL IMCPRB <= FLSPROB[WP-FLSWAVE[0]];
W:= WP-FLSWAVE[0];WPR:= WP*1E-9;(*  REAL NO. NANOMETERS *)
EP:= PLANCK * LIGHTSPEED / WPR;PNUM:= PNUM+1;
INITPHOTDIR;
VR:=LRAD;VH:=LHT/2;VB:=-LHT/2;MNUM:=1;MNUMTEMP:=1;
PHOTONTRACED:=FALSE;OUTWARD:=TRUE;XO:=EVX;YO:=EVY;
ZO:=EVZ;PARFLAG:=0;NFLEC:=0;
REPEAT
CASE MNUM OF
1 : BEGIN PARFLAG:=0;CYLU;DISCU;PICKU;
      IF ABS(UB) <= ABS(UA) THEN BEGIN
```

```
                IF Z1>0 THEN LAFACE ELSE BEGIN
                PHOTONTRACED:= TRUE;
                L3:=L3+1;END END ELSE LVFACE
                END;
        2 : BEGIN CYLU;DISCU;PICKU;
                IF ABS(UB) <= ABS(UA) THEN BEGIN
                IF Z1>0 THEN BEGIN PHOTONTRACED:=TRUE;L4:=L4+1;
                END ELSE LAFACE{shouldn't occur}END
                ELSE AVFACE;
                END;
        3 : BEGIN TORU;DISCU;PICKU;IF ABS(UB) >= ABS(UA)
                THEN BEGIN IF OUTWARD=TRUE THEN VCFACE
                ELSE BEGIN IF Z2>(-0.0035) THEN BEGIN
                PHOTONTRACED:=TRUE;L5:=L5+1;END ELSE LVFACE
                END END ELSE BEGIN PHOTONTRACED:=TRUE;L5:=L5+1;END
                END;
        4 : BEGIN IF MAG(XO,YO,0)>=(CRAD+0.00001) THEN BEGIN
                TEMP:=MAG(XO,YO,0);
                WRITELN('PO>CRAD',MNUMTEMP,FACENUM,XO,YO,ZO);
                WRITELN(X1,Y1,Z1,X2,Y2,Z2,TEMP,VB);END ELSE;
                CHAMBERTRACK END;
        END;{case}
        MNUM:=MNUMTEMP;
        UNTIL PHOTONTRACED = TRUE;
        EB:= EB-EP;(*note.. always leaves residual energy*)
        END;(*while*)
        END;(*FLASHTRACK*)
        PROCEDURE PMSTATS1;
        BEGIN
        {Gives No. of photelectrons produced}
        FOR K:=1 TO 2 DO {k=1 ==> leftpmtube,k=2 ==> rightpmtube}
        BEGIN IF QIX[K]<>0 THEN BEGIN
        REPEAT
        ITEMP:=TRUNC(MTH$RANDOM(SEEDVAL)*(QIX[K]+1));
        UNTIL ITEMP<(QIX[K]+1);
        QP[K]:=QI[K,ITEMP];PMPRBMAX:=0;
        {qp ==> quantum effy picked from qi distribution
        of quantum effy's, trunc used to eliminate end bias}
        FOR J:=0 TO QIX[K] DO BEGIN
        TEMP1:= LPOW(QP[K],J)+LPOW((1-QP[K]),(QIX[K]-J));
        TEMP2:= LFACT(QIX[K])-LFACT(J)-LFACT(QIX[K]-J);
        PMPRB[J]:= QUAD(TEMP1+TEMP2);PMPRB[J]:= EXP(PMPRB[J]);
        IF PMPRB[J] > PMPRBMAX THEN BEGIN
        PMPRBMAX:=PMPRB[J];ITEMP:=J;END ELSE;END;
        {big num phots ==> sparse prob.distribution}
        J:=ITEMP;REPEAT PMTMIN:=J; J:=J-1;
        UNTIL (J=(-1))OR(PMPRB[J+1]<=0.0001);
        J:=ITEMP;REPEAT PMTMAX:=J; J:=J+1;
        UNTIL (J=(QIX[K]+1))OR(PMPRB[J-1]<=0.0001);
        REPEAT
        PMCOUNT[K]:= PMTMIN+TRUNC(MTH$RANDOM(SEEDVAL)
                    *(PMTMAX+1));
        UNTIL PMPRB[PMCOUNT[K]] >=(MTH$RANDOM(SEEDVAL)*PMPRBMAX);
        END ELSE PMCOUNT[K]:=0;{no phots=>no count}
        END;{k loop}
```

```
END;{pmstats1}
PROCEDURE PMSTATS2;
BEGIN
{Apply collection efficiency of PMT electron optics}
FOR K:=1 TO 2 DO BEGIN ITEMP:=0;IF PMCOUNT[K]<>0
THEN BEGIN FOR I:=1 TO PMCOUNT[K] DO BEGIN
IF MTH$RANDOM(SEEDVAL)<CEFF THEN ITEMP:=ITEMP+1 ELSE;
END;PMCOUNT[K]:= ITEMP;END ELSE;END;
{Now gives No. of secondary electrons
from dynode using Polya distribution}
FOR JJ:=1 TO DYNUM DO{ number of dynode stages}
BEGIN
TEMP2:=1+BSF[JJ]*DYM[JJ];
FOR K:=1 TO 2 DO{left  right tubes}
BEGIN IF PMCOUNT[K]<>0 THEN BEGIN SUM:=0;
FOR J:=1 TO PMCOUNT[K] DO BEGIN
REPEAT
ITEMP:= RAND(1,12);{i.e. range of probs
includes all but 0.001 of total}
TEMP1:=1;IF ITEMP>=2 THEN BEGIN
FOR I:=1 TO ITEMP-1 DO BEGIN TEMP1:=TEMP1*(1+I*BSF[JJ]);
END;END ELSE;
TEMP:=LPOW(DYM[JJ],ITEMP)-LFACT(ITEMP)
                    -(ITEMP+1/BSF[JJ])*LN(TEMP2);
TEMP:=TEMP+LN(TEMP1);
TEMP:=EXP(TEMP);{itemp=no. 2ndry's per single primary}
UNTIL MTH$RANDOM(SEEDVAL)<TEMP;
SUM:=SUM+ITEMP;END;
PMCOUNT[K]:=SUM;{Re-use count arrays for next dynode}
END ELSE;END;{leftright}
END;{dynodes}
END;
PROCEDURE MULTIMCA;
BEGIN
IF(PMCOUNT[1]=0)AND(PMCOUNT[2]=0)
THEN QUANTLOST:=QUANTLOST+1 ELSE BEGIN
IF PMCOUNT[1]>THRESHOLD THEN
PMCOUNT[1]:=PMCOUNT[1]-THRESHOLD ELSE PMCOUNT[1]:= 0;
IF PMCOUNT[2]>THRESHOLD THEN
PMCOUNT[2]:=PMCOUNT[2]-THRESHOLD ELSE PMCOUNT[2]:= 0;
IF (PMCOUNT[1]=0)AND(PMCOUNT[2]=0)
THEN THLDLOST:= THLDLOST+1 ELSE BEGIN
SUM:= PMCOUNT[1]+PMCOUNT[2];
DIFF:= ABS(PMCOUNT[1]-PMCOUNT[2]);
IF NUCLIDE="H" THEN RATIO:=(500*PMCOUNT[1]) DIV SUM
ELSE RATIO:=(4000*PMCOUNT[1]) DIV SUM;
{non-coincidence spectra}
MCA[1,SUM]:= MCA[1,SUM]+1;MCA[2,DIFF]:= MCA[2,DIFF]+1;
MCA[3,RATIO]:= MCA[3,RATIO]+1;
PULSENUM[1]:= PULSENUM[1]+1;{total accumulated pulses}
IF SUM > MAXCH[1] THEN MAXCH[1]:= SUM;
IF DIFF > MAXCH[2] THEN MAXCH[2]:= DIFF;
IF RATIO > MAXCH[3] THEN MAXCH[3]:= RATIO;
{max channel markers}
IF ((PMCOUNT[1] > THRESHOLD) AND
```

```
(PMCOUNT[2] > THRESHOLD)) = TRUE THEN BEGIN
MCA[4,SUM]:= MCA[4,SUM]+1;MCA[5,DIFF]:= MCA[5,DIFF]+1;
MCA[6,RATIO]:= MCA[6,RATIO]+1;{coincidence spectra}
PULSENUM[2]:= PULSENUM[2]+1;
IF SUM > MAXCH[4] THEN MAXCH[4]:= SUM;
IF DIFF > MAXCH[5] THEN MAXCH[5]:= DIFF;
IF RATIO > MAXCH[6] THEN MAXCH[6]:= RATIO;END
ELSE COINLOST:= COINLOST+1;END;{thldlost}
END;{quantlost}
END;{multimca}

PROCEDURE SPECALYSIS;
VAR RNE, RSUM :REAL;
    NE, SUM :INTEGER;
BEGIN
FOR II:= 1 TO 6 DO BEGIN
NE:= 0;SUM:= 0;MODE[II]:= 0;WP:=0;ITEMP:=0;
IF II > 3 THEN W:= 2 ELSE W:= 1;
MAXCHNL:= MAXCH[II];WRITELN('MAXCH=',MAXCHNL);
FOR I:= 0 TO MAXCHNL DO BEGIN SUM:= SUM+MCA[II,I];
NE:= NE+I*MCA[II,I];
IF SUM >= (PULSENUM[W] DIV 2) THEN BEGIN
IF ITEMP=0 THEN MIDNUMCH[II]:= I;ITEMP:=1;END
ELSE;IF MCA[II,I] > WP THEN BEGIN
WP:= MCA[II,I];MODE[II]:= I END ELSE;
FOR H:= 1 TO 2 DO BEGIN
IF (I>SCRLL[H,II]) AND (I<SCRUL[H,II])
THEN SCRSUM[H,II]:= SCRSUM[H,II]+1 ELSE;END;END;
RSUM:= SUM;RNE:= NE;IF RSUM >= 1
THEN MEANENCH[II]:= RNE/RSUM ELSE MEANENCH[II]:= 0;
IF SCRSUM[2,II] >= 1
THEN SCR[II]:= SCRSUM[1,II]/SCRSUM[2,II] ELSE SCR[II]:= 0;
END;
END;
PROCEDURE DATASAVE;
BEGIN
OPEN (OUTFILE,'LSCM22.DAT',HISTORY:= UNKNOWN,
ACCESSMETHOD:= KEYED,ORGANIZATION:= INDEXED);
FINDK(OUTFILE,0,IDNUMBER);
IF UFB(OUTFILE) THEN BEGIN
WITH AREC DO
BEGIN
RECNUM:= IDNUMBER;MODLVERSION:= MVERSION;
NUCLTYPE:= NUCLIDE;
WITH QREC DO
BEGIN
QCHEMVAL:= QCHEM;QCOLVAL:= QCOL;QMATLS:= QMATLS;
END;
WITH CREC DO
BEGIN
CNTMODE:= CNTMODE;
IF CNTMODE='D' THEN CNTNUM:= NDISNTGS
ELSE CNTNUM:= NCOUNTS;
THOLD:= THRESHOLD;FOR I:= 1 TO 2 DO BEGIN
FOR II:= 1 TO 6 DO BEGIN
```

```
SCRSETNGS[I,II]:= SCRLL[I,II];
SCRSETNGS[I+2,II]:= SCRUL[I,II];END;END;
DSPECSTEP:= ESTEP;
END;
WITH LREC DO
BEGIN
LIQHT:=LHT;LIQRAD:=LRAD;VIALHT:= VHT;
VIALRAD:= VRAD;VIALOFFSET:=VOS;
CASEHT:= CHT;CASERAD:= CRAD;
END;
WITH PREC DO
BEGIN
FOR I:= 1 TO 6 DO BEGIN
PMEAN[I]:= MEANENCH[I];PMODE[I]:= MODE[I];
PSCR[I]:= SCR[I];PMID[I]:= MIDNUMCH[I];END;
END;
WITH PULREC DO
BEGIN
FOR I:=1 TO 2 DO
BEGIN PULSENUM[I]:=PULSENUM[I];END;
END;
WITH PHREC DO
BEGIN
L1:=L1;L2:=L2;L3:=L3;L4:=L4;L5:=L5;L6:=L6;
L7:=L7;L8:=L8;PNUM:=PNUM;
END;
WITH CHREC DO
BEGIN
FOR I:=1 TO 6 DO BEGIN MAXCH[I]:=MAXCH[I];END;END;
TLOSS:= THLDLOST;CLOSS:= COINLOST;QLOSS:= QUANTLOST;
END;
WRITE(OUTFILE, AREC);FOR J:=1 TO 6 DO BEGIN
WITH MREC DO
BEGIN
MCARECNUM:=IDNUMBER;FOR I:= 0 TO 4000 DO BEGIN
MCADAT[I]:= MCA[J,I];END;
END;
CASE J OF
1 : BEGIN OPEN (OUT1,'MCA1.DAT',HISTORY:= UNKNOWN,
    ACCESSMETHOD:= KEYED,ORGANIZATION:= INDEXED);
    FINDK(OUT1,0,IDNUMBER);
    IF UFB(OUT1) THEN WRITE(OUT1, MREC) ELSE;
    CLOSE(OUT1);END;
2 : BEGIN OPEN (OUT2,'MCA2.DAT',HISTORY:=UNKNOWN,
    ACCESSMETHOD:= KEYED,ORGANIZATION:= INDEXED);
    FINDK(OUT2,0,IDNUMBER);
    IF UFB(OUT2) THEN WRITE(OUT2, MREC) ELSE;
    CLOSE(OUT2);END;
3 : BEGIN OPEN (OUT3,'MCA3.DAT',HISTORY:= UNKNOWN,
    ACCESSMETHOD:= KEYED,ORGANIZATION:= INDEXED);
    FINDK(OUT3,0,IDNUMBER);
    IF UFB(OUT3) THEN WRITE(OUT3, MREC) ELSE;
    CLOSE(OUT3);END;
4 : BEGIN OPEN (OUT4,'MCA4.DAT',HISTORY:= UNKNOWN,
    ACCESSMETHOD:= KEYED,ORGANIZATION:= INDEXED);
```

```
            FINDK(OUT4,0,IDNUMBER);
            IF UFB(OUT4) THEN WRITE(OUT4, MREC) ELSE;
            CLOSE(OUT4);END;
   5 :  BEGIN OPEN (OUT5,'MCA5.DAT',HISTORY:= UNKNOWN,
            ACCESSMETHOD:= KEYED,ORGANIZATION:= INDEXED);
            FINDK(OUT5,0,IDNUMBER);
            IF UFB(OUT5) THEN WRITE(OUT5, MREC) ELSE;
            CLOSE(OUT5);END;
   6 :  BEGIN OPEN (OUT6,'MCA6.DAT',HISTORY:= UNKNOWN,
            ACCESSMETHOD:= KEYED,ORGANIZATION:= INDEXED);
            FINDK(OUT6,0,IDNUMBER);
            IF UFB(OUT6) THEN WRITE(OUT6, MREC) ELSE;
            CLOSE(OUT6);END;
END;{case}
END;{mrec}
END ELSE WRITELN('FILE NOT STORED ..IDNUMBER',
IDNUMBER,'ALREADY EXISTS');
CLOSE(OUTFILE);
END;
[EXTERNAL] PROCEDURE MAINDO;
   EXTERN;
[EXTERNAL] PROCEDURE MAININIT;
   EXTERN;
(*..MAIN PROGRAM..*)
BEGIN
MAININIT;INIT1;FLSPEC;ABSPEC;ALABSPEC;RANDOMIZE;
REPEAT
MAINDO;INIT2;BSPECMAX;
IF CNTMODE= 'D' THEN BEGIN
FOR IEVENTS:=1 TO NDISNTGS DO BEGIN
EVENTCOORDS;BETAENERGY;CHEMQUENCH;FLASHTRACK;
PMSTATS1;PMSTATS2;MULTIMCA;END
END
ELSE BEGIN
IEVENTS:=0;
REPEAT
EVENTCOORDS;BETAENERGY;CHEMQUENCH;FLASHTRACK;
PMSTATS1;PMSTATS2;MULTIMCA;
IEVENTS:=IEVENTS+1;
UNTIL (IEVENTS-QUANTLOST-THLDLOST-COINLOST)=NCOUNTS;
END;
SPECALYSIS;
TEMP:=EBSUM/IEVENTS;
WRITELN('Mean E-beta was ',TEMP,' keV');
DATASAVE;
UNTIL STOPFLAG=TRUE;
END.
```

```
MODULE M2INIT;
VAR        QCHEM, QCOL, VOS, VHT, LHT, AHT, VRAD, LRAD, ARAD, CHT,
  CRAD, ESTEP: [EXTERNAL] REAL;
  IDNUMBER, NDISNTGS, NCOUNTS, DYNUM, THRESHOLD:
          [EXTERNAL] INTEGER;
  STOPFLAG: [EXTERNAL] BOOLEAN;
  NUCLIDE, CNTMODE: [EXTERNAL] CHAR;
  MVERSION: [EXTERNAL] PACKED ARRAY[1..50] OF CHAR;
  QMATLS: [EXTERNAL] PACKED ARRAY[1..25] OF CHAR;
  SCRLL, SCRUL: [EXTERNAL] ARRAY[1..2,1..6]
          OF INTEGER;
  QP, BSF, DYM: [EXTERNAL] ARRAY[1..2] OF REAL;
[GLOBAL] PROCEDURE INIT1;
BEGIN
MVERSION:=
'XM22 SE=CURVE QE=26                          ';
NUCLIDE:='C';
CNTMODE:='C';
NDISNTGS:=1000;NCOUNTS:=1000;
QMATLS:=' CCL4 AND DISPERSE 07 DYE';
SCRLL[1,1]:=0;SCRUL[1,1]:=4000;
SCRLL[2,1]:=10;SCRUL[2,1]:=4000;
SCRLL[1,2]:=0;SCRUL[1,2]:=4000;
SCRLL[2,2]:=5;SCRUL[2,2]:=4000;
SCRLL[1,3]:=0;SCRUL[1,3]:=4000;
SCRLL[2,3]:=50;SCRUL[2,3]:=4000;
SCRLL[1,4]:=0;SCRUL[1,4]:=4000;
SCRLL[2,4]:=10;SCRUL[2,4]:=4000;
SCRLL[1,5]:=0;SCRUL[1,5]:=4000;
SCRLL[2,5]:=5;SCRUL[2,5]:=4000;
SCRLL[1,6]:=0;SCRUL[1,6]:=4000;
SCRLL[2,6]:=50;SCRUL[2,6]:=4000;
BSF[1]:=0.2;BSF[2]:=0.2;DYM[1]:=3.94;
DYM[2]:=3.94;DYNUM:=2;
VOS:=0;VHT:=0.047+VOS;VRAD:=0.0147;
CHT:=0.04374;CRAD:=0.02286;
{..thick wall includes gaps in chamber around vial..}
LHT:=0.02+VOS;LRAD:=0.0125;AHT:=0.027+VOS;ARAD:=0.0125;
ESTEP:=0.001;
THRESHOLD:=50;
END;
[GLOBAL] PROCEDURE MAININIT;
BEGIN
STOPFLAG:=FALSE;
IDNUMBER:= 0;
END;
[GLOBAL] PROCEDURE MAINDO;
BEGIN
IDNUMBER:=IDNUMBER+1;
{IF IDNUMBER=240 THEN IDNUMBER:=251 ELSE;}
CASE IDNUMBER OF
1 : BEGIN QCOL:=0;QCHEM:=0;END;
2 : BEGIN QCOL:=0;QCHEM:=0.3;END;
3 : BEGIN QCOL:=0;QCHEM:=0.5;END;
4 : BEGIN QCOL:=0;QCHEM:=0.7;END;
```

```
5 : BEGIN QCOL:=0;QCHEM:=0.9;END;
6 : BEGIN QCOL:=0.05;QCHEM:=0;END;
7 : BEGIN QCOL:=0.5;QCHEM:=0;END;
8 : BEGIN QCOL:=5;QCHEM:=0;END;
9 : BEGIN QCOL:=50;QCHEM:=0;END;
END;
IF IDNUMBER=9 THEN STOPFLAG:=TRUE ELSE;
END;
END.
```

(ii) <u>Polya Statistics</u> - Polya.Pas

```pascal
PROGRAM POLYA(INPUT,OUTPUT);
VAR M,B,LP,LF,PROD,SUM:REAL;
    I,X:INTEGER;
    P:ARRAY[0..80] OF REAL;
PROCEDURE POISSON;
BEGIN
I:= -1;SUM:=0;
REPEAT
I:=I+1;LF:=0;
IF I>1 THEN BEGIN
FOR X:=1 TO I DO
BEGIN LF:=LF+LN(X);END;END ELSE;
LP:=I*LN(M)-M-LF;
P[I]:=EXP(LP);SUM:=SUM+P[I];
WRITELN('Probability of obtaining ',I,' is ',P[I]);
UNTIL P[I]<0.001;
WRITELN('                          Sum = ',SUM);
END;
PROCEDURE POL;
BEGIN
I:= -1;SUM:=0;
REPEAT
I:=I+1;LF:=0;PROD:=1;
IF I>=2 THEN BEGIN FOR X:=1 TO I DO
BEGIN LF:=LF+LN(X);END;
FOR X:=1 TO I-1 DO
BEGIN PROD:=PROD*(1+X*B);END;END ELSE;
LP:=I*LN(M)-LF-(I+1/B)*LN(1+B*M)+LN(PROD);
P[I]:=EXP(LP);SUM:=SUM+P[I];
WRITELN('Probability of obtaining ',I,' is ',P[I]);
UNTIL P[I]<0.001;
WRITELN('                          Sum = ',SUM);
END;
PROCEDURE EXPO;
BEGIN
I:= -1;SUM:=0;
REPEAT
I:=I+1;
LP:=I*LN(M)-(I+1)*LN(1+M);
P[I]:=EXP(LP);SUM:=SUM+P[I];
WRITELN('Probability of obtaining ',I,' is ',P[I]);
UNTIL P[I]<0.001;
WRITELN('                          Sum = ',SUM);
END;
{MAIN PROGRAM}
BEGIN
WRITELN('Shape factor B <0=poisson,1=exponential,
0.2=50/50each>');
READLN(B);
WRITELN('Required mean, >= 1, (e.g.
dynode yield=3.04 for LSC) ');
READLN(M);
IF B=0 THEN POISSON ELSE BEGIN IF B=1 THEN EXPO
ELSE POL;END;
END.
```

362

BASIC Program

```
1 OPEN1,5:PRINT#1,CHR$(255);"JE2GA":CLOSE1
5 POKE53,95
6 POKE52,255
7 SYS29760
10 REM DISPLAY WHOLE SPECTRUM AT MINIMUM SENSITIVITY
15 SYS25317:REM CLEAR
19 POKE24969,1
20 POKE24968,0:REM AVOIDS INTEGRATION
21 POKE24964,4
22 POKE24982,0:POKE24983,0:REM START CH =0
24 POKE24984,3:POKE24985,252
25 POKE24963,8:REM MIN SENS
27 SYS25344
30 PRINT""
40 POKE49151,3
50 PRINT"DOUBLE SENSITIVITY(Y/N)?"
60 GETA$:IFA$=""THEN60
61 IFA$="Y"THEN70
65 GOTO270
70 POKE24963,4
72 SYS25317
75 POKE24982,0:POKE24983,0
80 SYS25344
90 PRINT""
100 POKE49151,3
110 PRINT"DOUBLE SENS(Y/N)?"
120 GETA$:IFA$=""THEN120
121 IFA$="Y"THEN140
130 GOTO270
140 POKE24963,2
142 SYS25317
145 POKE24982,0:POKE24983,0
150 SYS25344
160 PRINT""
170 POKE49151,3
180 PRINT"DOUBLE SENS(Y/N)?"
190 GETA$:IFA$=""THEN190
200 IFA$="Y"THEN220
210 GOTO270
220 POKE24963,1
230 SYS25317
250 POKE24982,0:POKE24983,0
260 SYS25344
270 PRINT""
280 POKE49151,3
290 PRINT"WHICH HALF OF SPECTRUM(U/L)?"
300 GETA$:IFA$=""THEN300
310 IFA$="U"THEN350
320 POKE24982,0:POKE24983,0
330 POKE24984,1:POKE24985,254
```

```
340 GOTO370
350 POKE24982,2:POKE24983,Ø
360 POKE24984,3:POKE24985,254
370 SYS25317
375 POKE24964,2
380 SYS25344
390 PRINT""
400 POKE49151,3
410 PRINT"DEFINE REQUIRED 256 CHANNELS"
420 INPUT"LOWEST CHANNEL";L1
430 U=L1+255
440 X=L1/256
450 UL=INT(X)
460 LL=(X-UL)*256
470 POKE24982,UL
480 POKE24983,LL
490 X=U/256
500 UU=INT(X)
510 LU=(X-UU)*256
520 POKE24984,UU
530 POKE24985,LU
540 POKE24964,1
550 SYS25317
555 PRINT""
560 SYS25344
570 POKE49151,3
580 PRINT"INTEGRATION LIMITS"
590 PRINT"LOWER CHANNEL"
592 GOSUB2000
594 L=X+L1
600 PRINT"UPPER CHANNEL"
602 GOSUB2000
604 U=X+L1
610 X=L/256
620 UL=INT(X)
630 LL=(X-UL)*256
640 POKE24982,UL
650 POKE24983,LL
660 X=U/256
670 UU=INT(X)
680 LU=(X-UU)*256
690 POKE24984,UU
700 POKE24985,LU
710 POKE24968,1
720 PRINT""
730 SYS25344
740 X=PEEK(24944)
750 Y=X/16:Z=INT(Y)
760 TE=(Y-Z)*16+1Ø*Z
770 X=PEEK(24945)
780 Y=X/16:Z=INT(Y)
790 TH=((Y-Z)*16+1Ø*Z)*100
800 X=PEEK(24946)
810 Y=X/16:Z=INT(Y)
820 HT=((Y-Z)*16+1Ø*Z)*10000
```

```
830  X=PEEK(24947)
840  Y=X/16:Z=INT(Y)
850  TM=((Y-Z)*16+10*Z)*1000000
860  TT=TE+TH+HT+TM
870  PRINT"SUM FROM CH ";L;" TO CH ";U;" = ";TT
880  V=PEEK(25852)
890  W=PEEK(25853)*256
900  X=PEEK(25854)*256*256
910  Y=PEEK(25855)*256*256*256
915  YY=PEEK(25999)*256*256*256*256
920  Z=V+W+X+Y+YY
930  EN=Z/TT
940  PRINT"MEAN ENERGY BETWEEN CH";L;"AND CH";U;"=";INT(EN
);"KEV"
950  END
2000  PRINT"CURSOR MOVE RIGHT(R),LEFT(L),STEP(S),END(E)"
2005  FORI=1TO3000:NEXTI
2010  Y=10
2020  X=0
2030  POKE24969,1:POKE25007,X
2032  PRINT""
2033  GOSUB2500
2035  PRINT"CH:";X+L1,,"COUNTS:";NU
2040  SYS26880
2050  GETA$:IFA$=""THEN2050
2055  POKE24969,0:SYS26880
2060  IFA$="R"THEN2090
2070  IFA$="L"THEN2110
2075  IFA$="S"THEN2130
2080  RETURN
2090  X=X+Y:IFX>255THENX=255
2100  GOTO2030
2110  X=X-Y:IFX<0THENX=0
2120  GOTO2030
2130  INPUT"STEP SIZE";Y
2140  GOTO2030
2500  F=X+L1
2505  G=F/256
2510  A=INT(G)
2515  B=(G-A)*256
2520  POKE24982,A
2530  POKE24983,B
2540  SYS24640
2550  SYS24734
2560  C=PEEK(24948)
2570  D=C/16:E=INT(D)
2580  NE=(D-E)*16+10*E
2590  C=PEEK(24949)
2600  D=C/16:E=INT(D)
2610  NF=((D-E)*16+10*E)*100
2620  C=PEEK(24950)
2630  NG=10000*C
2640  NU=NE+NF+NG
2650  RETURN
```

```
6000  A9 00      LDA #$00          Rem:  6000 - 6032
6002  8D 70 61   STA $6170               Initializes program
6005  8D 71 61   STA $6171
6008  8D 72 61   STA $6172
600B  8D 73 61   STA $6173
600E  20 40 60   JSR $6040
6011  20 A0 60   JSR $60A0
6014  20 40 61   JSR $6140
6017  AD 97 61   LDA $6197
601A  CD 99 61   CMP $6199
601D  D0 08      BNE $6027
601F  AD 96 61   LDA $6196
6022  CD 98 61   CMP $6198
6025  F0 0B      BEQ $6032
6027  EE 97 61   INC $6197
602A  D0 E2      BNE $600E
602C  EE 96 61   INC $6196
602F  4C 0E 60   JMP $600E
6032  60         RTS


6040  18         CLC               Rem:  6040 - 6096
6041  AD 97 61   LDA $6197               Calculates 2n + X + 2
6044  69 01      ADC #$01                where X = int(n/2)
6046  8D 9B 61   STA $619B
6049  AD 96 61   LDA $6196
604C  69 00      ADC #$00
604E  8D 9A 61   STA $619A
6051  0E 9A 61   ASL $619A
6054  18         CLC
6055  0E 9B 61   ASL $619B
6058  AD 9A 61   LDA $619A
605B  69 00      ADC #$00
605D  8D 9A 61   STA $619A
6060  AD 97 61   LDA $6197
6063  4A         LSR
6064  8D 9D 61   STA $619D
6067  18         CLC
6068  AD 96 61   LDA $6196
606B  4A         LSR
606C  8D 9C 61   STA $619C
606F  90 09      BCC $607A
6071  18         CLC
6072  AD 9D 61   LDA $619D
6075  69 80      ADC #$80
6077  8D 9D 61   STA $619D
607A  18         CLC
607B  AD 9D 61   LDA $619D
607E  6D 9B 61   ADC $619B
6081  8D 9F 61   STA $619F
```

```
6084 AD 9C 61    LDA $619C
6087 6D 9A 61    ADC $619A
608A 8D 9E 61    STA $619E
608D 18          CLC
608E AD 9E 61    LDA $619E
6091 69 76       ADC #$76
6093 8D 9E 61    STA $619E
6096 60          RTS


609E A0 00       LDY #$00
60A0 AD 9E 61    LDA $619E
60A3 85 09       STA $09
60A5 AD 9F 61    LDA $619F
60A8 85 08       STA $08
60AA A9 01       LDA #$01
60AC 2C 97 61    BIT $6197
60AF D0 54       BNE $6105
60B1 A0 00       LDY #$00
60B3 B1 08       LDA ($08),Y
60B5 29 F0       AND #$F0
60B7 4A          LSR
60B8 4A          LSR
60B9 4A          LSR
60BA 4A          LSR
60BB 8D 74 61    STA $6174
60BE A5 08       LDA $08
60C0 D0 02       BNE $60C4
60C2 C6 09       DEC $09
60C4 C6 08       DEC $08
60C6 B1 08       LDA ($08),Y
60C8 29 0F       AND #$0F
60CA 0A          ASL
60CB 0A          ASL
60CC 0A          ASL
60CD 0A          ASL
60CE 18          CLC
60CF 6D 74 61    ADC $6174
60D2 8D 74 61    STA $6174
60D5 B1 08       LDA ($08),Y
60D7 29 F0       AND #$F0
60D9 4A          LSR
60DA 4A          LSR
60DB 4A          LSR
60DC 4A          LSR
60DD 8D 75 61    STA $6175
60E0 A5 08       LDA $08
60E2 D0 02       BNE $60E6
60E4 C6 09       DEC $09
60E6 C6 08       DEC $08
60E8 B1 08       LDA ($08),Y
60EA 29 0F       AND #$0F
60EC 0A          ASL
60ED 0A          ASL
60EE 0A          ASL
```

Rem: 609E – 6126
Prepares next number for
addition and stores in
s6176,5,4

367

```
60EF  0A           ASL
60F0  18           CLC
60F1  6D 75 61      ADC $6175
60F4  8D 75 61      STA $6175
60F7  B1 08         LDA ($08),Y
60F9  29 F0         AND #$F0
60FB  4A            LSR
60FC  4A            LSR
60FD  4A            LSR
60FE  4A            LSR
60FF  8D 76 61      STA $6176
6102  4C 26 61      JMP $6126
6105  B1 08         LDA ($08),Y
6107  8D 74 61      STA $6174
610A  A5 08         LDA $08
610C  D0 02         BNE $6110
610E  C6 09         DEC $09
6110  C6 08         DEC $08
6112  B1 08         LDA ($08),Y
6114  8D 75 61      STA $6175
6117  A5 08         LDA $08
6119  D0 02         BNE $611D
611B  C6 09         DEC $09
611D  C6 08         DEC $08
611F  B1 08         LDA ($08),Y
6121  29 0F         AND #$0F
6123  8D 76 61      STA $6176
6126  60            RTS


6140  F8           SED
6141  18           CLC
6142  AD 74 61      LDA $6174
6145  6D 70 61      ADC $6170
6148  8D 70 61      STA $6170
614B  AD 75 61      LDA $6175
614E  6D 71 61      ADC $6171
6151  8D 71 61      STA $6171
6154  AD 76 61      LDA $6176
6157  6D 72 61      ADC $6172
615A  8D 72 61      STA $6172
615D  A9 00         LDA #$00
615F  6D 73 61      ADC $6173
6162  8D 73 61      STA $6173
6165  D8           CLD
6166  60           RTS
```

Rem: 6140 - 6166
Addition of 6176,5,4 to
running total in 6173,2,1,0
in decimal mode.

```
61ED  A9 ØØ       LDA  #$ØØ
61EF  8D A1 61    STA  $61A1
61F2  AD 81 61    LDA  $6181
61F5  C9 C8       CMP  #$C8
61F7  9Ø Ø5       BCC  $61FE
61F9  A9 C7       LDA  #$C7
61FB  8D 81 61    STA  $6181
61FE  A9 Ø2       LDA  #$Ø2
62ØØ  8D FF BF    STA  $BFFF
62Ø3  AD 87 61    LDA  $6187
62Ø6  8D AF 61    STA  $61AF
62Ø9  AD 81 61    LDA  $6181
62ØC  8D AE 61    STA  $61AE
62ØF  38          SEC
621Ø  A9 C7       LDA  #$C7
6212  ED AE 61    SBC  $61AE
6215  8D AD 61    STA  $61AD
6218  A9 ØØ       LDA  #$ØØ
621A  8D AØ 61    STA  $61AØ
621D  AD AD 61    LDA  $61AD
622Ø  ØA          ASL
6221  8D AC 61    STA  $61AC
6224  9Ø Ø9       BCC  $622F
6226  18          CLC
6227  AD AØ 61    LDA  $61AØ
622A  69 Ø2       ADC  #$Ø2
622C  8D AØ 61    STA  $61AØ
622F  AD AC 61    LDA  $61AC
6232  ØA          ASL
6233  8D AC 61    STA  $61AC
6236  AD AØ 61    LDA  $61AØ
6239  69 ØØ       ADC  #$ØØ
623B  8D AB 61    STA  $61AB
623E  18          CLC
623F  AD AC 61    LDA  $61AC
6242  6D AD 61    ADC  $61AD
6245  8D AA 61    STA  $61AA
6248  AD AB 61    LDA  $61AB
624B  69 ØØ       ADC  #$ØØ
624D  8D A9 61    STA  $61A9
625Ø  AD AA 61    LDA  $61AA
6253  ØA          ASL
6254  8D A2 61    STA  $61A2
6257  9Ø Ø6       BCC  $625F
6259  A9 Ø4       LDA  #$Ø4
625B  8D A1 61    STA  $61A1
625E  18          CLC
625F  AD A2 61    LDA  $61A2
6262  ØA          ASL
6263  8D A2 61    STA  $61A2
6266  9Ø ØA       BCC  $6272
6268  18          CLC
6269  A9 Ø2       LDA  #$Ø2
626B  6D A1 61    ADC  $61A1
626E  8D A1 61    STA  $61A1
6271  18          CLC
```

Rem: 61ED - 62DE
     Plots point on HRG screen

369

```
6272 AD A2 61  LDA $61A2
6275 ØA        ASL
6276 8D A2 61  STA $61A2
6279 A9 ØØ     LDA #$ØØ
627B 6D A1 61  ADC $61A1
627E 8D A1 61  STA $61A1
6281 AD A9 61  LDA $61A9
6284 ØA        ASL
6285 ØA        ASL
6286 ØA        ASL
6287 6D A1 61  ADC $61A1
628A 8D A3 61  STA $61A3
628D 18        CLC
628E AD AF 61  LDA $61AF
6291 4A        LSR
6292 4A        LSR
6293 4A        LSR
6294 8D A4 61  STA $61A4
6297 18        CLC
6298 6D A2 61  ADC $61A2
629B 8D A5 61  STA $61A5
629E AD A3 61  LDA $61A3
62A1 69 ØØ     ADC #$ØØ
62A3 8D A6 61  STA $61A6
62A6 69 9Ø     ADC #$9Ø
62A8 8D A6 61  STA $61A6
62AB AD AF 61  LDA $61AF
62AE 29 Ø7     AND #$Ø7
62BØ 8D A7 61  STA $61A7
62B3 38        SEC
62B4 A9 Ø7     LDA #$Ø7
62B6 ED A7 61  SBC $61A7
62B9 8D A8 61  STA $61A8
62BC A9 Ø1     LDA #$Ø1
62BE 8D BØ 61  STA $61BØ
62C1 AD A8 61  LDA $61A8
62C4 FØ ØB     BEQ $62D1
62C6 ØE BØ 61  ASL $61BØ
62C9 CE A8 61  DEC $61A8
62CC FØ Ø3     BEQ $62D1
62CE 4C C6 62  JMP $62C6
62D1 AD A5 61  LDA $61A5
62D4 85 Ø8     STA $Ø8
62D6 AD A6 61  LDA $61A6
62D9 85 Ø9     STA $Ø9
62DB 2Ø DB 68  JSR $68DB
62DE 6Ø        RTS


62E5 A9 9Ø     LDA #$9Ø      Rem:  62E5 - 62FE
62E7 85 Ø9     STA $Ø9             Clears HRG screen
62E9 A9 ØØ     LDA #$ØØ
62EB 85 Ø8     STA $Ø8
62ED AØ ØØ     LDY #$ØØ
62EF A9 ØØ     LDA #$ØØ
```

370

```
62F1  91 Ø8      STA  ($Ø8),Y
62F3  C8         INY
62F4  DØ F9      BNE  $62EF
62F6  E6 Ø9      INC  $Ø9
62F8  A5 Ø9      LDA  $Ø9
62FA  C9 BØ      CMP  #$BØ
62FC  DØ F1      BNE  $62EF
62FE  6Ø         RTS


63ØØ  A9 ØØ      LDA  #$ØØ
63Ø2  2Ø 83 65   JSR  $6583
63Ø5  8D 71 61   STA  $6171
63Ø8  8D 72 61   STA  $6172
63ØB  8D 73 61   STA  $6173
63ØE  8D 87 61   STA  $6187
6311  8D FC 64   STA  $64FC
6314  8D FD 64   STA  $64FD
6317  8D FE 64   STA  $64FE
631A  8D FF 64   STA  $64FF
631D  2Ø 4Ø 6Ø   JSR  $6Ø4Ø
632Ø  2Ø AØ 6Ø   JSR  $6ØAØ
6323  AD 88 61   LDA  $6188
6326  FØ ØC      BEQ  $6334
6328  2Ø 4Ø 61   JSR  $6140
632B  2Ø FD 65   JSR  $65FD
632E  2Ø ØØ 65   JSR  $65ØØ
6331  4C 4Ø 63   JMP  $6340
6334  2Ø 75 63   JSR  $6375
6337  2Ø 6Ø 64   JSR  $6460
633A  2Ø ED 61   JSR  $61ED
633D  EE 87 61   INC  $6187
634Ø  AD 97 61   LDA  $6197
6343  CD 99 61   CMP  $6199
6346  DØ Ø8      BNE  $6350
6348  AD 96 61   LDA  $6196
634B  CD 98 61   CMP  $6198
634E  FØ 12      BEQ  $6362
635Ø  18         CLC
6351  AD 97 61   LDA  $6197
6354  6D 84 61   ADC  $6184
6357  8D 97 61   STA  $6197
635A  DØ C1      BNE  $631D
635C  EE 96 61   INC  $6196
635F  4C 1D 63   JMP  $631D
6362  6Ø         RTS
```

Rem: 6300 - 6445
      Main routine which displays,
      integrates and averages
      spectrum between limits
      determined by cursor
      positions.

```
6375 A9 00      LDA #$00
6377 8D 7C 61   STA $617C
637A 8D 7A 61   STA $617A
637D 8D 82 61   STA $6182
6380 18         CLC
6381 AD 76 61   LDA $6176
6384 0A         ASL
6385 0A         ASL
6386 8D 78 61   STA $6178
6389 0A         ASL
638A 0A         ASL
638B 0A         ASL
638C 8D 79 61   STA $6179
638F 8D 7B 61   STA $617B
6392 90 0B      BCC $639F
6394 18         CLC
6395 A9 02      LDA #$02
6397 8D 7C 61   STA $617C
639A A9 01      LDA #$01
639C 8D 7A 61   STA $617A
639F 0E 7B 61   ASL $617B
63A2 EA         NOP
63A3 EA         NOP
63A4 EA         NOP
63A5 90 09      BCC $63B0
63A7 18         CLC
63A8 A9 01      LDA #$01
63AA 6D 7C 61   ADC $617C
63AD 8D 7C 61   STA $617C
63B0 18         CLC
63B1 AD 78 61   LDA $6178
63B4 6D 79 61   ADC $6179
63B7 8D 7D 61   STA $617D
63BA AD 7A 61   LDA $617A
63BD 69 00      ADC #$00
63BF 8D 7E 61   STA $617E
63C2 AD 7D 61   LDA $617D
63C5 6D 7B·61   ADC $617B
63C8 8D 7D 61   STA $617D
63CB AD 7C 61   LDA $617C
63CE 6D 7E 61   ADC $617E
63D1 8D 7E 61   STA $617E
63D4 18         CLC
63D5 AD 75 61   LDA $6175
63D8 29 F0      AND #$F0
63DA 4A         LSR
63DB 4A         LSR
63DC 4A         LSR
63DD 4A         LSR
63DE 8D 80 61   STA $6180
63E1 0A         ASL
63E2 8D 81 61   STA $6181
63E5 90 06      BCC $63ED
63E7 A9 02      LDA #$02
63E9 8D 82 61   STA $6182
63EC 18         CLC
```

```
63ED  AD 81 61   LDA  $6181
63F0  0A          ASL
63F1  8D 81 61   STA  $6181
63F4  AD 82 61   LDA  $6182
63F7  69 00       ADC  #$00
63F9  8D 82 61   STA  $6182
63FC  AD 80 61   LDA  $6180
63FF  6D 81 61   ADC  $6181
6402  8D 81 61   STA  $6181
6405  AD 82 61   LDA  $6182
6408  69 00       ADC  #$00
640A  8D 82 61   STA  $6182
640D  0A          ASL
640E  8D 82 61   STA  $6182
6411  AD 81 61   LDA  $6181
6414  0A          ASL
6415  8D 81 61   STA  $6181
6418  AD 82 61   LDA  $6182
641B  69 00       ADC  #$00
641D  8D 82 61   STA  $6182
6420  AD 75 61   LDA  $6175
6423  29 0F       AND  #$0F
6425  6D 81 61   ADC  $6181
6428  8D 81 61   STA  $6181
642B  AD 82 61   LDA  $6182
642E  69 00       ADC  #$00
6430  8D 82 61   STA  $6182
6433  AD 81 61   LDA  $6181
6436  6D 7D 61   ADC  $617D
6439  8D 81 61   STA  $6181
643C  AD 82 61   LDA  $6182
643F  6D 7E 61   ADC  $617E
6442  8D 82 61   STA  $6182
6445  60          RTS


6460  AD 83 61   LDA  $6183          Rem:  6460 - 64B0
6463  C9 01       CMP  #$01                Sets verical scaling factor
6465  F0 49       BEQ  $64B0                on spectrum display.
6467  AD 81 61   LDA  $6181
646A  4A          LSR
646B  8D 81 61   STA  $6181
646E  18          CLC
646F  AD 82 61   LDA  $6182
6472  4A          LSR
6473  8D 82 61   STA  $6182
6476  90 09       BCC  $6481
6478  18          CLC
6479  AD 81 61   LDA  $6181
647C  69 80       ADC  #$80
647E  8D 81 61   STA  $6181
6481  AD 83 61   LDA  $6183
6484  C9 02       CMP  #$02
6486  F0 28       BEQ  $64B0
6488  AD 81 61   LDA  $6181
```

373

```
648B 4A          LSR
648C 8D 81 61    STA $6181
648F 18          CLC
6490 AD 82 61    LDA $6182
6493 4A          LSR
6494 8D 82 61    STA $6182
6497 90 09       BCC $64A2
6499 18          CLC
649A AD 81 61    LDA $6181
649D 69 80       ADC #$80
649F 8D 81 61    STA $6181
64A2 AD 83 61    LDA $6183
64A5 C9 04       CMP #$04
64A7 F0 07       BEQ $64B0
64A9 AD 81 61    LDA $6181
64AC 4A          LSR
64AD 8D 81 61    STA $6181
64B0 60          RTS


64FD 50 3F       BVC $653E          Rem:  64FD - 6599
64FF 05 AD       ORA $AD                  Multiplies number in
6501 96 61       STX $61,Y                64F8,9,A,(B) by number
6503 8D F7 64    STA $64F7                in 64F6,7 and stores in
6506 AD 97 61    LDA $6197                64FC,D,E,F.
6509 8D F6 64    STA $64F6
650C A2 0A       LDX #$0A
650E A9 00       LDA #$00
6510 8D FB 64    STA $64FB
6513 AD F6 64    LDA $64F6
6516 29 01       AND #$01
6518 C9 01       CMP #$01
651A D0 2C       BNE $6548
651C 18          CLC
651D AD FC 64    LDA $64FC
6520 6D F8 64    ADC $64F8
6523 8D FC 64    STA $64FC
6526 AD FD 64    LDA $64FD
6529 6D F9 64    ADC $64F9
652C 8D FD 64    STA $64FD
652F AD FE 64    LDA $64FE
6532 6D FA 64    ADC $64FA
6535 8D FE 64    STA $64FE
6538 20 90 65    JSR $6590
653B EA          NOP
653C EA          NOP
653D EA          NOP
653E EA          NOP
653F EA          NOP
6540 AD 8F 65    LDA $658F
6543 69 00       ADC #$00
6545 8D 8F 65    STA $658F
6548 18          CLC
6549 0E FB 64    ASL $64FB
654C 0E FA 64    ASL $64FA
```

```
654F AD FB 64  LDA $64FB
6552 69 00      ADC #$00
6554 8D FB 64  STA $64FB
6557 0E F9 64  ASL $64F9
655A AD FA 64  LDA $64FA
655D 69 00      ADC #$00
655F 8D FA 64  STA $64FA
6562 0E F8 64  ASL $64F8
6565 AD F9 64  LDA $64F9
6568 69 00      ADC #$00
656A 8D F9 64  STA $64F9
656D 4E F6 64  LSR $64F6
6570 18         CLC
6571 4E F7 64  LSR $64F7
6574 90 09      BCC $657F
6576 18         CLC
6577 AD F6 64  LDA $64F6
657A 69 80      ADC #$80
657C 8D F6 64  STA $64F6
657F CA         DEX
6580 D0 91      BNE $6513
6582 60         RTS


6583 8D 8F 65  STA $658F
6586 8D 70 61  STA $6170
6589 60         RTS


6590 AD FF 64  LDA $64FF
6593 6D FB 64  ADC $64FB
6596 8D FF 64  STA $64FF
6599 60         RTS


65FD A9 00      LDA #$00
65FF 8D D2 64  STA $64D2
6602 8D E2 64  STA $64E2
6605 8D E4 64  STA $64E4
6608 8D E6 64  STA $64E6
660B 8D B9 64  STA $64B9
660E 8D DB 64  STA $64DB
6611 18         CLC
6612 AD 76 61  LDA $6176
6615 0A         ASL
6616 0A         ASL
6617 0A         ASL
6618 0A         ASL
6619 8D E0 64  STA $64E0
661C 0A         ASL
661D 8D E1 64  STA $64E1
6620 AD E2 64  LDA $64E2
6623 69 00      ADC #$00
6625 8D E2 64  STA $64E2
6628 18         CLC
6629 0E E2 64  ASL $64E2
```

Rem: 65FD - 6892
       Converts 5 digit decimal
       number to 3 bytes of
       hexadecimal.

375

```
662C  ØE E1 64  ASL  $64E1
662F  AD E2 64  LDA  $64E2
6632  69 ØØ     ADC  #$ØØ
6634  8D E2 64  STA  $64E2
6637  18        CLC
6638  ØE E2 64  ASL  $64E2
663B  ØE E1 64  ASL  $64E1
663E  AD E2 64  LDA  $64E2
6641  69 ØØ     ADC  #$ØØ
6643  8D E2 64  STA  $64E2
6646  18        CLC
6647  ØE E2 64  ASL  $64E2
664A  ØE E1 64  ASL  $64E1
664D  AD E2 64  LDA  $64E2
665Ø  69 ØØ     ADC  #$ØØ
6652  8D E2 64  STA  $64E2
6655  18        CLC
6656  AD E2 64  LDA  $64E2
6659  ØA        ASL
665A  8D E3 64  STA  $64E3
665D  AD E4 64  LDA  $64E4
666Ø  69 ØØ     ADC  #$ØØ
6662  8D E4 64  STA  $64E4
6665  18        CLC
6666  AD E3 64  LDA  $64E3
6669  ØA        ASL
666A  8D E5 64  STA  $64E5
666D  AD E6 64  LDA  $64E6
667Ø  69 ØØ     ADC  #$ØØ
6672  8D E6 64  STA  $64E6
6675  18        CLC
6676  AD E6 64  LDA  $64E6
6679  ØA        ASL
667A  8D E8 64  STA  $64E8
667D  AD E5 64  LDA  $64E5
668Ø  ØA        ASL
6681  8D E7 64  STA  $64E7
6684  AD E8 64  LDA  $64E8
6687  69 ØØ     ADC  #$ØØ
6689  8D E8 64  STA  $64E8
668C  18        CLC
668D  ØE E8 64  ASL  $64E8
669Ø  ØE E7 64  ASL  $64E7
6693  AD E8 64  LDA  $64E8
6696  69 ØØ     ADC  #$ØØ
6698  8D E8 64  STA  $64E8
669B  18        CLC
669C  ØE E8 64  ASL  $64E8
669F  ØE E7 64  ASL  $64E7
66A2  AD E8 64  LDA  $64E8
66A5  69 ØØ     ADC  #$ØØ
66A7  8D E8 64  STA  $64E8
66AA  18        CLC
66AB  AD 75 61  LDA  $6175
66AE  29 FØ     AND  #$FØ
66BØ  4A        LSR
```

```
66B1  8D B7 64   STA $64B7
66B4  ØA          ASL
66B5  ØA          ASL
66B6  8D B8 64   STA $64B8
66B9  AD B9 64   LDA $64B9
66BC  69 ØØ       ADC #$ØØ
66BE  8D B9 64   STA $64B9
66C1  18          CLC
66C2  AD B9 64   LDA $64B9
66C5  ØA          ASL
66C6  8D BB 64   STA $64BB
66C9  AD B8 64   LDA $64B8
66CC  ØA          ASL
66CD  8D BA 64   STA $64BA
66DØ  AD BB 64   LDA $64BB
66D3  69 ØØ       ADC #$ØØ
66D5  8D BB 64   STA $64BB
66D8  18          CLC
66D9  AD BB 64   LDA $64BB
66DC  ØA          ASL
66DD  8D BC 64   STA $64BC
66EØ  AD BA 64   LDA $64BA
66E3  ØA          ASL
66E4  8D BD 64   STA $64BD
66E7  AD BC 64   LDA $64BC
66EA  69 ØØ       ADC #$ØØ
66EC  8D BC 64   STA $64BC
66EF  18          CLC
66FØ  AD BC 64   LDA $64BC
66F3  ØA          ASL
66F4  8D BE 64   STA $64BE
66F7  AD BD 64   LDA $64BD
66FA  ØA          ASL
66FB  8D BF 64   STA $64BF
66FE  AD BE 64   LDA $64BE
67Ø1  69 ØØ       ADC #$ØØ
67Ø3  8D BE 64   STA $64BE
67Ø6  18          CLC
67Ø7  AD BE 64   LDA $64BE
67ØA  ØA          ASL
67ØB  8D FØ 64   STA $64FØ
67ØE  AD BF 64   LDA $64BF
6711  ØA          ASL
6712  8D F1 64   STA $64F1
6715  AD FØ 64   LDA $64FØ
6718  69 ØØ       ADC #$ØØ
671A  8D FØ 64   STA $64FØ
671D  18          CLC
671E  AD 75 61   LDA $6175
6721  29 ØF       AND #$ØF
6723  ØA          ASL
6724  ØA          ASL
6725  8D DØ 64   STA $64DØ
6728  ØA          ASL
6729  ØA          ASL
672A  ØA          ASL
```

```
672B  8D D1 64   STA $64D1
672E  AD D2 64   LDA $64D2
6731  69 ØØ      ADC #$ØØ
6733  8D D2 64   STA $64D2
6736  AD D2 64   LDA $64D2
6739  ØA         ASL
673A  8D D4 64   STA $64D4
673D  AD D1 64   LDA $64D1
674Ø  ØA         ASL
6741  8D D3 64   STA $64D3
6744  AD D4 64   LDA $64D4
6747  69 ØØ      ADC #$ØØ
6749  8D D4 64   STA $64D4
674C  EA         NOP
674D  EA         NOP
674E  EA         NOP
674F  18         CLC
675Ø  AD DØ 64   LDA $64DØ
6753  6D D1 64   ADC $64D1
6756  8D D5 64   STA $64D5
6759  AD D2 64   LDA $64D2
675C  69 ØØ      ADC #$ØØ
675E  8D D6 64   STA $64D6
6761  2Ø 8Ø 68   JSR $688Ø
6764  EA         NOP
6765  EA         NOP
6766  EA         NOP
6767  18         CLC
6768  AD 74 61   LDA $6174
676B  29 FØ      AND #$FØ
676D  4A         LSR
676E  4A         LSR
676F  8D D7 64   STA $64D7
6772  4A         LSR
6773  4A         LSR
6774  8D D8 64   STA $64D8
6777  6D D7 64   ADC $64D7
677A  8D D9 64   STA $64D9
677D  ØA         ASL
677E  8D DA 64   STA $64DA
6781  AD DB 64   LDA $64DB
6784  69 ØØ      ADC #$ØØ
6786  8D DB 64   STA $64DB
6789  AD 74 61   LDA $6174
678C  29 ØF      AND #$ØF
678E  8D DC 64   STA $64DC
6791  18         CLC
6792  AD EØ 64   LDA $64EØ
6795  6D E1 64   ADC $64E1
6798  8D CØ 64   STA $64CØ
679B  AD E2 64   LDA $64E2
679E  69 ØØ      ADC #$ØØ
67AØ  8D C1 64   STA $64C1
67A3  6D E3 64   ADC $64E3
67A6  8D C1 64   STA $64C1
67A9  AD E4 64   LDA $64E4
```

```
67AC  69  ØØ      ADC  #$ØØ
67AE  8D  C2  64  STA  $64C2
67B1  AD  E5  64  LDA  $64E5
67B4  6D  C1  64  ADC  $64C1
67B7  8D  C1  64  STA  $64C1
67BA  AD  C2  64  LDA  $64C2
67BD  6D  E6  64  ADC  $64E6
67CØ  8D  C2  64  STA  $64C2
67C3  AD  E7  64  LDA  $64E7
67C6  6D  C1  64  ADC  $64C1
67C9  8D  C1  64  STA  $64C1
67CC  AD  E8  64  LDA  $64E8
67CF  6D  C2  64  ADC  $64C2
67D2  8D  C2  64  STA  $64C2
67D5  AD  B7  64  LDA  $64B7
67D8  6D  B8  64  ADC  $64B8
67DB  8D  C3  64  STA  $64C3
67DE  AD  B9  64  LDA  $64B9
67E1  69  ØØ      ADC  #$ØØ
67E3  8D  C4  64  STA  $64C4
67E6  AD  BA  64  LDA  $64BA
67E9  6D  C3  64  ADC  $64C3
67EC  8D  C3  64  STA  $64C3
67EF  AD  BB  64  LDA  $64BB
67F2  6D  C4  64  ADC  $64C4
67F5  8D  C4  64  STA  $64C4
67F8  AD  BD  64  LDA  $64BD
67FB  6D  C3  64  ADC  $64C3
67FE  8D  C3  64  STA  $64C3
68Ø1  AD  BC  64  LDA  $64BC
68Ø4  6D  C4  64  ADC  $64C4
68Ø7  8D  C4  64  STA  $64C4
68ØA  AD  BF  64  LDA  $64BF
68ØD  6D  C3  64  ADC  $64C3
681Ø  8D  C3  64  STA  $64C3
6813  AD  BE  64  LDA  $64BE
6816  6D  C4  64  ADC  $64C4
6819  8D  C4  64  STA  $64C4
681C  AD  F1  64  LDA  $64F1
681F  6D  C3  64  ADC  $64C3
6822  8D  C3  64  STA  $64C3
6825  AD  FØ  64  LDA  $64FØ
6828  6D  C4  64  ADC  $64C4
682B  8D  C4  64  STA  $64C4
682E  AD  DC  64  LDA  $64DC
6831  6D  DA  64  ADC  $64DA
6834  8D  F8  64  STA  $64F8
6837  AD  DB  64  LDA  $64DB
683A  69  ØØ      ADC  #$ØØ
683C  8D  F9  64  STA  $64F9
683F  AD  D5  64  LDA  $64D5
6842  6D  F8  64  ADC  $64F8
6845  8D  F8  64  STA  $64F8
6848  AD  D6  64  LDA  $64D6
684B  6D  F9  64  ADC  $64F9
684E  8D  F9  64  STA  $64F9
```

```
6851 AD C3 64  LDA $64C3
6854 6D F8 64  ADC $64F8
6857 8D F8 64  STA $64F8
685A AD C4 64  LDA $64C4
685D 6D F9 64  ADC $64F9
6860 8D F9 64  STA $64F9
6863 AD C0 64  LDA $64C0
6866 6D F8 64  ADC $64F8
6869 8D F8 64  STA $64F8
686C AD C1 64  LDA $64C1
686F 6D F9 64  ADC $64F9
6872 8D F9 64  STA $64F9
6875 AD C2 64  LDA $64C2
6878 69 00     ADC #$00
687A 8D FA 64  STA $64FA
687D 60        RTS


6880 AD D5 64  LDA $64D5
6883 6D D3 64  ADC $64D3
6886 8D D5 64  STA $64D5
6889 AD D4 64  LDA $64D4
688C 6D D6 64  ADC $64D6
688F 8D D6 64  STA $64D6
6892 60        RTS


68DB A0 00     LDY #$00       Rem:  68DB - 68F2
68DD AD 89 61  LDA $6189            Subroutine of point
68E0 F0 0B     BEQ $68ED            plotting.
68E2 B1 08     LDA ($08),Y
68E4 9D 00 5F  STA $5F00,X
68E7 0D B0 61  ORA $61B0
68EA 91 08     STA ($08),Y
68EC 60        RTS
68ED BD 00 5F  LDA $5F00,X
68F0 91 08     STA ($08),Y
68F2 60        RTS


6900 A9 03     LDA #$03       Rem:  6900 - 6918
6902 8D FF BF  STA $BFFF            Positions cursor.
6905 A2 C7     LDX #$C7
6907 8A        TXA
6908 8D AE 61  STA $61AE
690B A9 00     LDA #$00
690D 8D A1 61  STA $61A1
6910 20 0F 62  JSR $620F
6913 CA        DEX
6914 E0 FF     CPX #$FF
6916 D0 EF     BNE $6907
6918 60        RTS
```

```
7440  A9 76       LDA #$76
7442  85 09       STA $09
7444  A9 00       LDA #$00
7446  85 08       STA $08
7448  A0 00       LDY #$00
744A  98          TYA
744B  8D FE 75    STA $75FE
744E  8D FA 75    STA $75FA
7451  A9 80       LDA #$80
7453  8D FD 75    STA $75FD
7456  A9 09       LDA #$09
7458  8D FC 75    STA $75FC
745B  A9 06       LDA #$06
745D  8D FB 75    STA $75FB
7460  20 E0 74    JSR $74E0
7463  A2 01       LDX #$01
7465  20 B0 75    JSR $75B0
7468  AD FC 75    LDA $75FC
746B  18          CLC
746C  E9 08       SBC #$08
746E  F0 42       BEQ $74B2
7470  AD FB 75    LDA $75FB
7473  18          CLC
7474  E9 05       SBC #$05
7476  F0 3A       BEQ $74B2
7478  A5 02       LDA $02
747A  49 30       EOR #$30
747C  8D FF 75    STA $75FF
747F  AD FA 75    LDA $75FA
7482  C9 00       CMP #$00
7484  D0 06       BNE $748C
7486  20 50 75    JSR $7550
7489  4C 9D 74    JMP $749D
748C  AD FF 75    LDA $75FF
748F  18          CLC
7490  71 08       ADC ($08),Y
7492  91 08       STA ($08),Y
7494  C8          INY
7495  CE FE 75    DEC $75FE
7498  A9 00       LDA #$00
749A  8D FA 75    STA $75FA
749D  CA          DEX
749E  D0 C5       BNE $7465
74A0  AD FA 75    LDA $75FA
74A3  D0 0D       BNE $74B2
74A5  AD FE 75    LDA $75FE
74A8  D0 08       BNE $74B2
74AA  A0 00       LDY #$00
74AC  98          TYA
74AD  8D FE 75    STA $75FE
74B0  E6 09       INC $09
74B2  20 20 75    JSR $7520
74B5  20 80 75    JSR $7580
74B8  A9 04       LDA #$04
74BA  0D 40 E8    ORA $E840
74BD  8D 40 E8    STA $E840
```

Rem: 7440 - 75EA
       Transfers spectrum via
       IEEE port and stores the
       5k digits in 2½k of
       memory from 7600 to 7FFF
       ignoring channel numbers
       and spaces.
       i.e. channel n stored in
       locations s7600 + 2n + X
       to s7600 + 2n + X + 2
       where X = int(n/2)

```
74CØ  CE FB 75  DEC  $75FB
74C3  DØ 9B     BNE  $746Ø
74C5  CE FC 75  DEC  $75FC
74C8  DØ 91     BNE  $745B
74CA  CE FD 75  DEC  $75FD
74CD  DØ 87     BNE  $7456
74CF  6Ø        RTS
74DØ  DØ 8A     BNE  $745C
74D2  CE FD 75  DEC  $75FD
74D5  DØ 8Ø     BNE  $7457
74D7  6Ø        RTS


74EØ  A9 FB     LDA  #$FB
74E2  2D 4Ø E8  AND  $E84Ø
74E5  8D 4Ø E8  STA  $E84Ø
74E8  A9 25     LDA  #$25
74EA  85 Ø1     STA  $Ø1
74EC  2Ø 8Ø 75  JSR  $758Ø
74EF  A9 Ø8     LDA  #$Ø8
74F1  85 Ø1     STA  $Ø1
74F3  2Ø 8Ø 75  JSR  $758Ø
74F6  A9 46     LDA  #$46
74F8  85 Ø1     STA  $Ø1
74FA  2Ø 8Ø 75  JSR  $758Ø
74FD  A9 FD     LDA  #$FD
74FF  2D 4Ø E8  AND  $E84Ø
75Ø2  8D 4Ø E8  STA  $E84Ø
75Ø5  A9 F7     LDA  #$F7
75Ø7  2D 21 E8  AND  $E821
75ØA  8D 21 E8  STA  $E821
75ØD  A9 Ø4     LDA  #$Ø4
75ØF  ØD 4Ø E8  ORA  $E84Ø
7512  8D 4Ø E8  STA  $E84Ø
7515  6Ø        RTS


752Ø  A9 FB     LDA  #$FB
7522  2D 4Ø E8  AND  $E84Ø
7525  8D 4Ø E8  STA  $E84Ø
7528  A9 Ø2     LDA  #$Ø2
752A  ØD 4Ø E8  ORA  $E84Ø
752D  8D 4Ø E8  STA  $E84Ø
753Ø  A9 Ø8     LDA  #$Ø8
7532  ØD 21 E8  ORA  $E821
7535  8D 21 E8  STA  $E821
7538  A9 5F     LDA  #$5F
753A  85 Ø1     STA  $Ø1
753C  6Ø        RTS
```

```
7550 AD FF 75  LDA $75FF
7553 ØA        ASL
7554 ØA        ASL
7555 ØA        ASL
7556 ØA        ASL
7557 91 Ø8     STA ($Ø8),Y
7559 A9 Ø1     LDA #$Ø1
755B 8D FA 75  STA $75FA
755E 6Ø        RTS


7580 AD 4Ø E8  LDA $E84Ø
7583 29 4Ø     AND #$4Ø
7585 FØ F9     BEQ $758Ø
7587 A5 Ø1     LDA $Ø1
7589 49 FF     EOR #$FF
758B 8D 22 E8  STA $E822
758E A9 F7     LDA #$F7
759Ø 2D 23 E8  AND $E823
7593 8D 23 E8  STA $E823
7596 AD 4Ø E8  LDA $E84Ø
7599 29 Ø1     AND #$Ø1
759B FØ F9     BEQ $7596
759D A9 Ø8     LDA #$Ø8
759F ØD 23 E8  ORA $E823
75A2 8D 23 E8  STA $E823
75A5 A9 FF     LDA #$FF
75A7 8D 22 E8  STA $E822
75AA 6Ø        RTS


75BØ A9 Ø2     LDA #$Ø2
75B2 ØD 4Ø E8  ORA $E84Ø
75B5 8D 4Ø E8  STA $E84Ø
75B8 AD 4Ø E8  LDA $E84Ø
75BB 29 8Ø     AND #$8Ø
75BD DØ F9     BNE $75B8
75BF AD 2Ø E8  LDA $E82Ø
75C2 49 FF     EOR #$FF
75C4 85 Ø2     STA $Ø2
75C6 A9 FD     LDA #$FD
75C8 2D 4Ø E8  AND $E84Ø
75CB 8D 4Ø E8  STA $E84Ø
75CE A9 Ø8     LDA #$Ø8
75DØ ØD 21 E8  ORA $E821
75D3 8D 21 E8  STA $E821
75D6 AD 4Ø E8  LDA $E84Ø
75D9 29 8Ø     AND #$8Ø
75DB FØ F9     BEQ $75D6
75DD A9 F7     LDA #$F7
75DF 2D 21 E8  AND $E821
75E2 8D 21 E8  STA $E821
75E5 A9 FF     LDA #$FF
75E7 8D 22 E8  STA $E822
75EA 6Ø        RTS
```

```
         2    1     1:D      1 PROGRAM FLUORESCENCE;
         3    1     1:D      3 (* PROGRAM TO GET FLUORESCENCE SPE
CTRA DATA ONTO DISK IN A SERIAL FILE
         4    1     1:D      3    USING XAD1 CARD IN SLOTS 1..5.C
HART/DRIVE IS SCANNED FOR START
         5    1     1:D      3    DATA READ EVERY 1 SECOND USING
XAD1 CLOCK AND 12 BIT CONVERSION*)
         6    1     1:D      3 VAR DATAFILE: FILE OF INTEGER;
         7    1     1:D    304   DAT : ARRAY [Ø..3ØØ] OF INTEGER;
         8    1     1:D    6Ø5   FL : STRING;
         9    1     1:D    646   A : CHAR;
        1Ø    1     1:D    647   FS, LL, XS, MS :INTEGER;
        11    1     1:D    651   L, LØ, L1, SF, SS, I, J, K, CLKØ,
CLK1, CLK2, C, CC, SLOT, S, S1, S2: INTEGER;
        12    1     1:D    668 (*------------------------
---*)
        13    1     2:D      3 FUNCTION PEEK(K: INTEGER): INTEGER
;
        14    1     2:D      4 EXTERNAL;
        15    1     2:D      4 (*-----------------------
---*)
        16    1     3:D      1 PROCEDURE POKE(I: INTEGER;J: INTEG
ER);
        17    1     3:D      3 EXTERNAL;
        18    1     3:D      3 (*-----------------------
---*)
        19    1     4:D      1 PROCEDURE INIT;
        2Ø    1     4:Ø      Ø BEGIN
        21    1     4:1      Ø WRITELN;WRITE ('ENTER START WAVELE
NGTH IN NM: ');
        22    1     4:1     5Ø READLN (LØ);
        23    1     4:1     69 WRITELN;WRITE ('ENTER  STOP WAVELE
NGTH IN NM: ');
        24    1     4:1    119 READLN (L1);
        25    1     4:1    138 WRITELN;WRITE ('ENTER SCAN SPEED I
N NM/MIN: ');
        26    1     4:1    186 READLN (SS);
        27    1     4:1    2Ø5 WRITELN;WRITE ('ENTER EXCITATION S
LIT WIDTH');
        28    1     4:1    252 READLN (XS);
        29    1     4:1    271 WRITELN;WRITE ('ENTER EMISSION SLI
T WIDTH');
        3Ø    1     4:1    316 READLN (MS);
        31    1     4:1    335 SF:= 1;FS:= 1;
        32    1     4:1    343 IF SS = 15 THEN SF:= 4 ELSE
        33    1     4:2    356 IF SS = 3Ø THEN SF:= 2 ELSE
        34    1     4:3    369 IF SS = 6Ø THEN SF:= 1 ELSE
        35    1     4:4    382 IF SS = 12Ø THEN FS:= 2 ELSE
        36    1     4:5    395 IF SS = 24Ø THEN FS:= 4 ELSE FS:=
8;
        37    1     4:1    414 WRITELN ('TYPE XAD1 SLOT NUMBER');
        38    1     4:1    455 READLN (SLOT);
```

```
39    1    4:Ø    474 END;
40    1    4:Ø    486 (*--------------------------------
----*)
41    1    5:D      1 PROCEDURE SCANSTART;
42    1    5:D      1 VAR X : INTEGER;
43    1    5:Ø      Ø BEGIN
44    1    5:1      Ø X:= Ø;
45    1    5:1      3 REPEAT
46    1    5:2      3 POKE (1,S);
47    1    5:2      9  REPEAT
48    1    5:2      9  UNTIL PEEK (S) < 128;
49    1    5:2     22   IF PEEK (S1) < 4Ø THEN X := 1
50    1    5:2     33    ELSE X := Ø;
51    1    5:1     41 UNTIL X = 1;
52    1    5:1     46 WRITELN ('SCANSTART DONE');
53    1    5:Ø     80 END;
54    1    5:Ø     96 (*--------------------------------
----*)
55    1    6:D      1 PROCEDURE SETCLOCK;
56    1    6:D      1 VAR CLKI, CS :INTEGER;
57    1    6:Ø      Ø BEGIN
58    1    6:1      Ø POKE (Ø,CLK1);
59    1    6:1      6 POKE (1,CLKØ);POKE (Ø,CLKØ);
60    1  · 6:1     18 FOR I:= Ø TO 1Ø DO
61    1    6:2     32   BEGIN
62    1    6:3     32     CLKI:= 3 + I - 16384 + 256 * SLO
T;
63    1    6:3     51    POKE (Ø,CLKI);
64    1    6:2     55   END;
65    1    6:1     65 WRITELN ('SETCLOCK DONE');
66    1    6:Ø     98 END;
67    1    6:Ø    112 (*--------------------------------
----*)
68    1    7:D      1 PROCEDURE STARTCLOCK;
69    1    7:Ø      Ø BEGIN
70    1    7:1      Ø POKE (Ø,CLKØ);POKE (1,CLKØ);
71    1    7:Ø     12 END;
72    1    7:Ø     24 (*--------------------------------
----*)
73    1    8:D      1 PROCEDURE READCLOCK;
74    1    8:Ø      Ø BEGIN
75    1    8:1      Ø C:= PEEK (CLK2);
76    1    8:Ø     10 END;
77    1    8:Ø     22 (*--------------------------------
----*)
78    1    9:D      1 PROCEDURE DISKSTORE;
79    1    9:Ø      Ø BEGIN
80    1    9:1      Ø WRITELN ('TYPE FULL DISK:FILE.NAME
');
81    1    9:1     44 READLN (FL);
82    1    9:1     64 REWRITE (DATAFILE, FL);
83    1    9:1     76 DATAFILE^ := LØ;
84    1    9:1     81 PUT (DATAFILE);
85    1    9:1     88 DATAFILE^ := L1;
```

385

```
86    1    9:1     93  PUT (DATAFILE);
87    1    9:1    100  DATAFILE^ := SS;
88    1    9:1    105  PUT (DATAFILE);
89    1    9:1    112  DATAFILE^ := XS;
90    1    9:1    117  PUT (DATAFILE);
91    1    9:1    124  DATAFILE^ := MS;
92    1    9:1    129  PUT(DATAFILE);
93    1    9:1    136  J:= Ø;
94    1    9:1    140  FOR J := Ø TO L DO
95    1    9:2    156    BEGIN
96    1    9:3    156    DATAFILE^ := DAT [J] ;
97    1    9:3    172    PUT(DATAFILE)
98    1    9:2    179    END;
99    1    9:1    189  CLOSE (DATAFILE,LOCK);
100   1    9:Ø    197  END;
101   1    9:Ø    212  (*-----------MAIN PROGRAM--------
----*)
102   1    1:Ø      Ø  BEGIN
103   1    1:1      Ø  INIT;
104   1    1:1     13  S:= SLOT * 16 -16256;
105   1    1:1     25  S1:= S + 1;
106   1    1:1     33  S2:= S + 2;
107   1    1:1     41  CLK1:= SLOT * 256 -16384;
108   1    1:1     55  CLK2:= CLK1 + 2;
109   1    1:1     63  CLKØ:= CLK1 + 14;
110   1    1:1     71  SETCLOCK;
111   1    1:1     73  SCANSTART;
112   1    1:1     75  STARTCLOCK;
113   1    1:1     77  REPEAT
114   1    1:2     77    C:= PEEK (CLK2);
115   1    1:1     87    UNTIL (C MOD 16) <> 15;
116   1    1:1     96  CC:= C ;L:= Ø;
117   1    1:1    106  LL:= ((L1 - LØ) * SF) DIV FS;
118   1    1:1    124    WRITELN (LL);
119   1    1:1    144    REPEAT
120   1    1:2    144    POKE (8,S);
121   1    1:2    150    REPEAT
122   1    1:2    150    UNTIL PEEK (S) < 128;
123   1    1:2    163    WRITELN (L);
124   1    1:2    183    DAT [L] := PEEK (S1) * 16 + PEEK
(S2) DIV 16;
125   1    1:2    216    WRITELN (DAT [L] );
126   1    1:2    247      REPEAT
127   1    1:3    247      REPEAT
128   1    1:4    247      C:= PEEK (CLK2)
129   1    1:3    250      UNTIL (C MOD 16) <> 15
130   1    1:2    262      UNTIL (ABS(C-CC)) MOD 2 = 1;
131   1    1:2    280    CC:= C;
132   1    1:2    286    L:= L+1
133   1    1:1    289  UNTIL L = LL;
134   1    1:1    303  WRITELN ('DISK STORAGE (Y/N)');
135   1    1:1    341  READLN (A);
136   1    1:1    360  IF A = 'Y' THEN DISKSTORE;
137   1    1:Ø    369  END.
```

```
 50 REM MAIN
 51 REM ****
 60 POKE52,0:POKE53,109
 70 S$="0":R$="0":OP=0:C=0:Z=0:M=0:EC=0
100 PRINT"                          "
110 PRINT"              CURVE-FITTER"
120 PRINT"                          "
130 FORI=1TO800:NEXT:PRINT""
140 PRINT" THIS PROGRAM WILL FIT ONE OF SEVERAL TYPES OF
APPROXIMATION TO A";
142 PRINT" GIVEN FUNCTION OR DATA"
143 INPUT"FUNCTION(=F) OR DATA(=D) FIT";D$
147 PRINT:PRINT"SELECT THE FIT REQUIRED BY TYPING THE APP
ROPRIATE NUMBER:-"
148 PRINT"    ... 1 = NEWTON'S POLYNOMIAL"
150 PRINT"    ... 2 = ORTHOGONAL POLYNOMIAL"
152 PRINT"    ... 3 = LEAST SQUARES "
154 PRINT"    ... 4 = CUBIC SPLINE INTERPOLATION"
155 PRINT"    ... 5 = TENSION SPLINE INTERPOLATION"
156 PRINT"    ... 6 = STINEMAN INTERPOLATION"
158 PRINT"    ... 7 = BEZIER BLENDING"
160 PRINT"    ... 8 = QUADRATIC SPLINE"
162 PRINT"    ... 9 = PIECEWISE LINEAR (SPLINE)"
180 PRINT:INPUT"FIT TYPE NUMBER IS.......";FT
190 IFFT=1THENGOSUB10000
192 IFFT=2THENGOSUB20000
194 IFFT=3THENGOSUB30000
196 IFFT=4THENGOSUB40000
198 IFFT=5THENGOSUB41000
200 IFFT=6THENGOSUB50000
202 IFFT=7THENGOSUB60000
204 IFFT=8THENGOSUB42000
206 IFFT=9THENGOSUB43000
215 GOSUB5000
216 POKE49151,3
220 GOSUB1000:REM PLOT IT
222 IFD$="D"THEN310
230 PRINT"          PRINTOUT FOLLOWS":PRINT""
240 DOPEN#10,"CURDAT",W
250 PRINT#10,FT:PRINT#10,FU:PRINT#10,EC:PRINT#10,LS$
252 PRINT#10,WT:PRINT#10,C:PRINT#10,Z:PRINT#10,OP:PRINT#1
0,M
255 PRINT#10,S$:PRINT#10,R$:PRINT#10,NN:PRINT#10,OO
260 FORI=0TONN:PRINT#10,X(I):PRINT#10,Y(I):NEXT
270 FORI=0TOOO:PRINT#10,XX(I):PRINT#10,G(I):PRINT#10,P(I)
:NEXT
275 IFWT=0THEN280
```

```
 278 FORI=ØTONN:PRINT#1Ø,WT(I):NEXT
 28Ø DCLOSE#1Ø
 3ØØ CLR:DLOAD"CURPRINT"
 31Ø OPEN4,4:PRINT#4:PRINT#4
 311 PRINT#4,"STANDARDS FOR EFFICIENCY CURVE TAKEN FROM FI
LE ";FL$
 312 PRINT#4,"FIT TYPE=";
 32Ø IFFT=1THENPRINT#4,"NEWTON'S INTERPOLATION"
 33Ø IFFT=2THENPRINT#4,"ORTHOG. POLYNOMIAL INTERPOLATION"
 34Ø IFFT=3THENPRINT#4,"LINEAR LEAST SQUARES"
 342 IFFT=6THENPRINT#4,"STINEMAN INTERPOLATION"
 344 IFFT=9THENPRINT#4,"PIECEWISE LINEAR"
 348 IFFT<4THEN4ØØ
 349 IFFT>5THEN37Ø
 35Ø IFFT=4THENPRINT#4,"CUBIC SPLINE INTERPOLATION"
 351 IFFT=5THENPRINT#4,"TENSION SPLINE INTERPOLATION"
 352 PRINT#4,"SPLINE END CONDITONS ARE ";
 353 IFEC=1THENPRINT#4,"NATURAL"
 354 IFEC=2THENPRINT#4,"PARABOLIC"
 355 IFEC=3THENPRINT#4,"CANTILEVER..WITH END LOAD CONSTANT
=";CC
 356 IFEC=4ANDS$="C"ANDR$="A"THENPRINT#4,"SWARTZ & VARGA'S
"
 357 IFEC>=4ANDS$="C"ANDR$="E"THENPRINT#4,"CUBIC LAGRANGE'
S EULER"
 358 IFEC>=4ANDS$="C"ANDR$="C"THENPRINT#4,"CUBIC LAGRANGE'
S COMPOUND EULER"
 359 IFEC>=4ANDS$="Q"ANDR$="C"THENPRINT#4,"QUADRATIC LAGRA
NGE'S COMPOUND EULER"
 36Ø IFEC>=4ANDS$="Q"ANDR$="A"THENPRINT#4,"QUADRATIC LAGRA
NGE'S ANALYTIC"
 361 IFEC>=4ANDS$="Q"ANDR$="E"THENPRINT#4,"QUADRATIC LAGRA
NGE'S EULER"
 362 IFEC>=4ANDS$="L"THENPRINT#4,"LINEAR LAGRANGE'S"
 363 IFEC=5THENPRINT#4,"FORSYTHE'S"
 364 IFEC=6THENPRINT#4,"CUBIC LAGRANGE'S 2ND DERIV=SPLINE'
S 2ND DERIV."
 365 IFFT=5THENPRINT#4,"TENSION PARAMETER = ";Z
 37Ø IFFT<>8THEN4ØØ
 371 PRINT#4,"QUADRATIC SPLINE"
 372 PRINT#4,"SPLINE END CONDITONS ARE ";
 373 IFEC=1THENPRINT#4,"LINEAR SLOPE"
 374 IFEC=2THENPRINT#4,"SPLINE SLOPE=QUAD.LAGRANGE SLOPE"
 375 IFEC=3THENPRINT#4,"SPLINE 2ND DERIV.=QUAD.LAGRANGE 2N
D.DERIV"
 4ØØ PRINT#4
 41Ø DATA 671,177,2.44,361Ø,235,1.Ø5,62Ø8,272,.8Ø,38Ø63,59
3,.32,351Ø9,6Ø9,.34
 411 UN=5:FORIJ=ØTOUN-1
 412 IFMD$<>"Y"THEN414
 413 READ CPM,QIP,CM:OO=Ø:GOTO42Ø
 414 IFGF$<>"Y"THEN413
 415 INPUT#1Ø,DUMMY,CPM,DUMMY,DUMMY,XX(Ø):XX(Ø)=XX(Ø)/1ØØØ
:OO=Ø
 42Ø QE=Ø.ØØØ17:XX(Ø)=QIP/1ØØØ
 421 IFTC=2THEN424
 422 BKG=8.2222189+33.212264*XX(Ø)+59.4222547*XX(Ø)^2-68.5
823397*XX(Ø)^3
```

388

```
 423 GOTO425
 424 BKG=-27.1258658+353.96925*XX(Ø)-568.797189*XX(Ø)^2+3Ø
3.356678*XX(Ø)^3
 425 CPM=CPM-BKG      .
 429 IFFT=1THENGOSUB1Ø1ØØ
 43Ø IFFT=2THENGOSUB2Ø17Ø
 44Ø IFFT=3THENGOSUB3Ø355
 45Ø IFFT=4THENGOSUB4Ø115
 46Ø IFFT=5THENGOSUB41155
 47Ø IFFT=6THENGOSUB5Ø12Ø
 48Ø REM FT=7
 49Ø IFFT=8THENGOSUB42Ø8Ø
 5ØØ IFFT=9THENGOSUB43Ø4Ø
 5Ø2 E2=2*QE*SL/P(Ø)*1ØØ:REM STDS QIP ERROR & UNKNOWNS QIP
ERROR
 5Ø4 REM STDS %CPMERROR=CM
 5Ø6 REM %STDS DPMERROR=Ø.Ø15%
 5Ø8 E4=SQR(E2*E2+CM*CM+Ø.Ø15*Ø.Ø15):REM TOTAL EFFIC%. %ER
R
 51Ø DPM=CPM/P(Ø):P(Ø)=P(Ø)*1ØØ
 515 DM=SQR(CM*CM+E4*E4):REM %ERR IN DPM
 52Ø PRINT#4,"CPM=";INT(CPM);CHR$(141);
 521 PRINT#4,"          QIP=";XX(Ø)*1ØØØ;CHR$(141);
 524 PRINT#4,"                    %EFFICIENCY=";P(
Ø);CHR$(141);
 525 PRINT#4,"
          DPM=";DPM
 53Ø PRINT#4,"+/-%";CM;CHR$(141);
 531 PRINT#4,"          +/-%";QE/XX(Ø)*1ØØ;CHR$(141);
 534 PRINT#4,"                    +/-%";E4
;CHR$(141);
 535 PRINT#4,"
          +/-%";DM
 541 PRINT#4,"          +/- ";Ø.5;CHR$(141);
 544 PRINT#4,"                    +/- ";E4
*P(Ø)/1ØØ;CHR$(141);
 545 PRINT#4,"
          +/- ";
 546 PRINT#4,DPM*DM/1ØØ
 548 PRINT#4
 55Ø NEXT
 56Ø CLOSE4:IFMD$="Y"THEN6ØØ
 57Ø DCLOSE
 6ØØ END
1ØØØ REM PLOTIT USING PETGRAPH
1ØØ1 REM ********************
1ØØ5 REM AXES
1ØØ6 CLEAR
1ØØ8 FORI=ØTON:X(I)=X(I)*(UL-LL)+LL:NEXT
1ØØ9 FORL=ØTOOO:XX(L)=XX(L)*(UL-LL)+LL:NEXT
1Ø1Ø SETL(27,12,27,191):SETL(24,188):SETL(27,191,3Ø,188)
1Ø15 Y=Ø:IFPN>YTHENY=PN
1Ø16 GOSUB3ØØØ
1Ø2Ø SETL(27,Y1,295,Y1):SETL(292,Y1+3):SETL(295,Y1,292,Y1
-3)
1Ø3Ø A$="X"
```

```
1040  TEXT(296,Y1-4,A$)
1050  B$="Y"
1060  TEXT(X1,192,B$)
1070  REM AXIS NICKS
1080  X1=24:X2=27:FORY=PNTOPXSTEP(PX-PN)/10:GOSUB3000:SETL
(X1,Y1,X2,Y1)
1090  T$=STR$(Y):TEXT(0,Y1-4,MID$(T$,2,3)):NEXT
1095  Y=0:IFPN>YTHENY=PN
1099  GOSUB3000
1100  SET(27,Y1):Y2=Y1-3:Y3=Y1
1110  FORX=XNTOXMSTEPABS((XM-XN)/10):GOSUB3050:SETL(X1,Y2,
X1,Y3)
1120  T$=STR$(X):TEXT(X1-15,Y1-12,MID$(T$,1,4)):NEXT
1180  REM ORIGINAL DATA PLOT
1190  FORI=0TONN:X=X(I):Y=Y(I):GOSUB3000:GOSUB3050:TEXT(X1
-4,Y1-4,"+"):NEXT
1200  REM APPROXIMATION PLOT
1210  MM=0:FORI=0TOOO:X=XX(I):Y=P(I):MM=MM+1:GOSUB3000:GOS
UB3050
1220  IFMM<>1THEN1240
1230  SET(X1,Y1):GOTO1250
1240  DOTL(X1,Y1)
1250  NEXT
1260  IFD$="D"THEN1400
1300  REM EXACT FUNCTION PLOT
1310  MM=0:FORI=0TOOO:X=XX(I):Y=G(I):MM=MM+1:GOSUB3000:GOS
UB3050
1320  IFMM<>1THEN1340
1330  SET(X1,Y1):GOTO1350
1340  SETL(X1,Y1)
1350  NEXT
1400  REM LABELS
1410  L$="N"
1420  IF L$="N"THEN1450
1430  INPUT"START COORDINATES ...(X,Y)";XL,YL
1440  TEXT(XL,YL,L$):GOTO1410
1450  RETURN
3000  REM Y-AXIS SCALE
3001  REM ***********
3010  Y1=12+Y*179/(PX-PN)-179*PN/(PX-PN)
3020  RETURN
3050  REM X-AXIS SCALE
3051  REM ***********
3060  X1=27+X*268/(XM-XN)
3064  X1=X1-XN*268/(XM-XN)
3070  RETURN
5000  REM MAX&MIN FINDER
5001  REM *************
5002  IFD$<>"F"THEN5008
5003  DIMG(OO)
5004  FORI=0TOOO:X=XX(I)*(UL-LL)+LL:G(I)=FN F1(X):NEXT
5007  GX=G(0):GN=G(0)
5008  PX=P(0):PN=P(0):YX=Y(0):YN=Y(0)
5009  IFD$="D"THEN5014
5010  FORI=0TOOO-1
5011  IFG(I+1)<GNTHENGN=G(I+1)
5012  IFG(I+1)>GXTHENGX=G(I+1)
```

```
5013 NEXT
5014 FORI=ØTOOO-1
5015 IFP(I+1)<PNTHENPN=P(I+1)
5016 IFP(I+1)>PXTHENPX=P(I+1)
5017 NEXT
5020 FORI=1TON
5022 IFY(I)>YXTHENYX=Y(I)
5025 IFY(I)<YNTHENYN=Y(I)
5026 NEXT
5030 IFYX>PXTHENPX=YX
5033 IFYN<PNTHENPN=YN
5034 IFD$="D"THEN5040
5035 IFGX>PXTHENPX=GX
5036 IFGN<PNTHENPN=GN
5040 RETURN
8000 N=1Ø
8001 N=N-1:MD$="N"
8002 DIMVS(N),BKG(N),X(N),Y(N):IFMD$="Y"THEN8040
8004 GF$="N":REM INPUT"GETCPM FILE(Y/N)";GF$
8006 IFGF$="Y"THEN8030
8011 FL=33:FL$="H3CHM33"
8012 DOPEN#Ø+FL,""+FL$
8014 FORI=ØTON:INPUT#Ø+FL,Y(I),X(I),VS(I):NEXT:GOTO8069
8031 DOPEN#10,"DPMDAT10",D1
8032 FORI=NTOØSTEP-1:INPUT#10,DUMMY,Y(I),DUMMY,DUMMY,X(I)
:NEXT:GOTO8069
8040 FORI=ØTON:INPUT"CPM,QIP,ACTIVITY";Y(I),X(I),VS(I):NE
XT
8069 NN=N
8070 VV=N+UN:NN=N
8080 INPUT"TRIT/C14(1/2)";TC
8082 FORI=ØTON:X(I)=X(I)/1000
8083 IFTC=2THEN8088
8084 BKG(I)=8.2222189+33.212264*X(I)+59.4222547*X(I)^2-68
.5823397*X(I)^3-30
8086 GOTO8090
8088 BKG(I)=-27.1258658+353.96925*X(I)-568.797189*X(I)^2+
303.356678*X(I)^3-40
8090 NEXT
8120 FORI=ØTON:Y(I)=(Y(I)-BKG(I))/VS(I):NEXT
8155 LL=Ø:UL=1:REM NOW SORT DATA TO ASCENDING ORDER
8160 RETURN
9000 REM INITIAL (FUNCTION) DATA INPUT
9001 REM ****************************
9010 INPUT"NUMBER DATA POINTS=";N:N=N-1
9015 INPUT"TYPE 1 FOR WEIGHTS Ø OTHERWISE";WT
9016 IFWT=ØTHEN9020
9017 DIMWT(N)
9020 DIMX(N),Y(N):NN=N
9022 FORI=1TON:X(I)=Ø:Y(I)=Ø:NEXT
9030 PRINT"FUNCTION TYPES ARE %V/V(=1),SCR(=2),QIPSIE(=3)
,QIPC14(=4),SINE";
9031 PRINT"(=5),EXP(X)(=6)"
9040 INPUT"FUNCTION TYPE NUMBER=";FUT
9050 FORI=ØTON:INPUT"...X=";SS:X(I)=SS
9060 IF FUT=1THEN DEF FN F1(SS)=Ø.4064*EXP(-Ø.458145*SS)+
Ø.Ø1
```

391

```
 9070 IF FUT=2THEN DEF FN F1(SS)=0.4*EXP(-0.02*(0.2*SS-168
)^1.8)+SS/10000-0.05
 9072 F5=.4*.25/12
 9074 F6=16/495
 9076 F7=.51515
 9080 IFFUT=3THEN DEF FN F1(SS)=F5*(F6*SS+F7)^2*EXP(-.1*(F
6*SS+F7))
 9081 IF FUT=4THEN DEF FN F1(SS)=1.24-1.24*EXP(-SS*SS/3990
0)-0.305
 9082 IF FUT=6THEN DEF FN F1(SS)=EXP(SS)
 9083 IF FUT=5THEN DEF FN F1(SS)=SIN(SS)
 9085 Y(I)=FN F1(SS)
 9090 PRINT"...Y=";Y(I):NEXTI
 9092 IFWT=0THEN9100
 9093 FORI=0TON:INPUT"..WEIGHT=";SS
 9094 WT(I)=SS:NEXT
 9100 LL=X(0):UL=X(N)
 9110 FORI=0TON:X(I)=(X(I)-LL)/(UL-LL):NEXT
 9199 RETURN
 9200 REM DATA INPUT FOR PLOT OF FITTING FUNCTION
 9201 REM *********************************
 9205 XN=100
 9206 XM=900
 9210 OO=6
 9215 DIMXX(OO):XN=XN/1000:XM=XM/1000
 9220 FORI=0TOOO:XX(I)=((XM-XN)/OO)*I+XN:NEXT
 9230 FORI=0TOOO:XX(I)=((XX(I)-LL))/(UL-LL):NEXT
 9240 RETURN
10000 REM NEWTON'S POLYNOMIAL INTERPOLATION (FAST LAGRANG
IAN)
 10001 REM ********************************************
***
 10010 REM FIND DIVIDED DIFFERENCES
 10020 IFD$="F"THENGOSUB9000
 10025 IFD$="D"THENGOSUB8000
 10030 DIMD(N+1)
 10040 FORJ=1TON+1
 10041 D(J)=Y(J-1)
 10043 NEXTJ
 10050 FORK=1TON
 10060 FORJ=N+1TOK+1STEP-1:D(J)=(D(J)-D(J-1))/(X(J-1)-X(J-
K-1)):NEXTJ
 10070 NEXTK
 10080 REM CALCULATE NEWTONS FORMULA
 10090 GOSUB9200
 10095 DIMP(OO)
 10100 FORL=0TOOO
 10110 P(L)=D(N+1)
 10112 FORI=N+1TO1STEP-1:P(L)=P(L)*(XX(L)-X(I-1))+D(I):NEX
T:NEXT
 10140 RETURN
 20000 REM ORTHOGONAL POLYNOMIAL FIT
 20001 REM ************************
 20010 INPUT"TYPE 1 FOR TCHEBYCHEV,2 FOR LEGENDRE";OP
 20012 INPUT"NO. BASIS FNCTNS=";M
 20015 IFD$="F"THENGOSUB9000
 20025 IFD$="D"THENGOSUB8000
 20030 DIMA(M),T(M),XR(N)
```

```
20040 FORI=0TON:XR(I)=2*(X(I)-X(0))/(X(N)-X(0))-1:NEXT
20050 FORK=1TOM:A=0
20060 FORI=0TON:X=XR(I)
20080 IFOP=1THENGOSUB20500
20090 IFOP=2THENGOSUB20600
20095 IFI<>0ORI<>NTHEN20100
20096 A=A+Y(I)*Z/2:GOTO20120
20100 A=A+Y(I)*Z
20120 NEXTI
20130 A(K)=A*2/N
20140 NEXTK
20150 REM GOT ALL A'S.NOW CALCULATE APPROX Y(I)
20160 GOSUB9200
20165 DIMP(OO),X2R(OO)
20166 FORL=0TOOO:P(L)=0:NEXT
20170 FORL=0TOOO
20175 X2R(L)=2*(XX(L)-XN)/(XM-XN)-1
20180 X=X2R(L):FORK=1TOM
20190 IFOP=1THENGOSUB20500
20200 IFOP=2THENGOSUB20600
20205 IFK<>1THEN20210
20206 P(L)=P(L)+A(K)*Z/2:GOTO20215
20210 P(L)=P(L)+A(K)*Z
20215 NEXTK:NEXTL
20220 RETURN
20500 REM TCHEBYCHEV FUNCTIONS
20501 REM *********************
20510 FORJJ=1TOK
20520 IFJJ=1THEN20550
20530 IFJJ=2THEN20560
20540 T(JJ)=2*T(JJ-1)*X-T(JJ-2)
20545 GOTO20570
20550 T(1)=1:GOTO20570
20560 T(2)=X
20570 NEXTJJ:Z=T(K)
20580 RETURN
20600 REM LEGENDRE FUNCTIONS
20601 REM ******************
20610 FORJJ=1TOK
20620 IFJJ=1THEN20650
20630 IFJJ=2THEN20660
20640 T(JJ)=(2*JJ-1)/JJ*X*T(JJ-1)-(JJ-1)*T(JJ-2)/JJ
20645 GOTO20670
20650 T(1)=1:GOTO20670
20660 T(2)=X
20670 NEXTJJ:Z=T(JJ-1)
20680 RETURN
30000 REM LINEAR LEAST SQUARES
30001 REM ********************
30010 REM FIRST COMPUTE NORMAL EQNS
30020 IFD$="F"THENGOSUB9000
30021 IFD$="F"THENGOTO30025
30022 GOSUB8000
30023 DIMWT(N):FORI=0TON:WT(I)=1:NEXT
30025 INPUT"NO. OF BASIS FNCTNS";M
30030 DIMA(M,M),B(M),S(M),SUB(M)
30040 FORK=1TOM:FORJ=KTOM:A(K,J)=0
```

```
30045 FORI=0TON
30050 H=X(I):GOSUB30500
30060 A(K,J)=A(K,J)+S(K)*S(J)
30070 NEXTI:A(J,K)=A(K,J):NEXTJ
30080 B(K)=0:FORI=0TON
30085 H=X(I):GOSUB30500
30090 B(K)=B(K)+S(K)*Y(I)
30100 NEXTI:NEXTK
30120 REM NOW USE GAUSS ELIMINATION & BACKSOLVING
30130 FORI=1TOM:SUB(I)=I:NEXTI
30140 FORK=1TOM-1:MAX=0:FORI=KTOM
30150 IFMAX>=ABS(A(SUB(I),K))THEN30156
30155 MAX=ABS(A(SUB(I),K)):INDX=I
30156 NEXTI
30160 IFMAX<>0THENGOTO30180
30170 PRINT"ERROR":END
30180 J=SUB(K):SUB(K)=SUB(INDX):PIVOT=A(SUB(K),K):SUB(IND
X)=J
30190 FORI=K+1TOM
30200 A(SUB(I),K)=-A(SUB(I),K)/PIVOT
30210 FORJ=K+1TOM
30220 A(SUB(I),J)=A(SUB(I),J)+A(SUB(I),K)*A(SUB(K),J):NEX
TJ
30230 B(SUB(I))=B(SUB(I))+A(SUB(I),K)*B(SUB(K)):NEXTI
30240 NEXTK
30250 REM NOW BACKSOLVE THE UPPER TRIANGULAR MATRIX
30260 DIMAA(M)
30270 AA(M)=B(SUB(M))/A(SUB(M),M)
30280 FORK=M-1TO1STEP-1:AA(K)=B(SUB(K))
30290 FORI=K+1TOM
30300 AA(K)=AA(K)-A(SUB(K),I)*AA(I)
30310 NEXTI:AA(K)=AA(K)/A(SUB(K),K)
30320 NEXTK
30330 REM AA FUNCTION COEFFS FOUND
30340 REM NOW EVALUATE LST SQS FUNCTION
30345 GOSUB 9200
30350 DIMP(OO)
30355 FORL=0TOOO:P(L)=0
30360 FORK=1TOM:X=XX(L)
30370 H=XX(L):GOSUB30500
30380 P(L)=P(L)+AA(K)*S(K)
30385 SL=SL+AA(K)*K*S(K-1):REM SLOPE
30386 NEXTK
30390 NEXTL
30400 RETURN
30500 REM LEAST SQUARES FUNCTION INPUT
30501 REM ***************************
30510 REM N.B.   INPUT FUNCTION VIA POKE TO DEF FN( ) COMM
AND IS CLEVEREST
30520 REM HERE MAKE DO WITH RE-TYPES
30530 S(1)=1
30531 S(2)=H
30532 S(3)=H*H
30533 S(4)=H*H*H
30534 REMS(5)=H*H*H*H
30535 REM S(6)=H*H*H*H*H
30540 LS$="1    X    X*X    X*X*X"
30599 RETURN
```

```
40000 REM CUBIC SPLINE
40001 REM ************
40003 IFD$="F"THENGOSUB9000
40004 IFD$="D"THENGOSUB8000
40005 DIMAA(N),E(N),S2(N),H(N),A(N),C(N)
40010 FORI=0TON-1
40020 H(I)=X(I+1)-X(I):NEXT
40025 GOSUB40300
40030 FORI=1TON-1
40040 C(I)=H(I-1)/6:A(I)=H(I)/6
40060 AA(I)=(H(I-1)+H(I))/3-C(I-1)*A(I)/AA(I-1)
40070 E(I)=Y(I+1)/H(I)-Y(I)/H(I)-Y(I)/H(I-1)+Y(I-1)/H(I-1
)-E(I-1)*A(I)/AA(I-1)
40080 NEXTI
40085 S2(N)=E(N)/AA(N)
40090 FORI=N-1TO0STEP-1
40095 S2(I)=(E(I)-C(I)*S2(I+1))/AA(I)
40097 NEXTI
40100 GOSUB9200
40111 DIMP(OO)
40115 FORL=0TOOOO
40120 GOSUB40200
40130 S1=(Y(K+1)-Y(K))/H(K)-S2(K+1)*H(K)/6-S2(K)*H(K)/3
40140 P(L)=Y(K)+S1*(XX(L)-X(K))+S2(K)*(XX(L)-X(K))^2/2
40150 P(L)=P(L)+(S2(K+1)-S2(K))*(XX(L)-X(K))^3/(6*H(K))
40160 NEXTL:SL=S1
40170 RETURN
40200 REM INTERVAL SEARCH
40201 REM ***************
40205 IFXX(L)<=X(N)THEN40220
40206 K=N-1:GOTO40270
40220 FORK=0TON-2
40230 IFXX(L)<X(K+1)THEN40270
40250 NEXTK
40270 RETURN
40300 REM SPLINE END CONDITIONS
40301 REM *********************
40310 PRINT"SEVERAL END CONDITIONS ARE AVAILABLE FOR SPLI
NE FIT"
40320 PRINT"TYPE 1 FOR NATURAL (S''=0 ATBOTH ENDS)
40322 PRINT"TYPE 2 FOR PARABOLIC (S''(0)=S''(1) & S''(N)=
S''(N-1))"
40324 PRINT"TYPE 3 FOR CANTILEVER (S''(0)=CONST*S''(1) &
S''(N)=C*S''(N-1))"
40326 PRINT"TYPE 4 FOR VARGA'S TYPE (S'(0)=L'(0) & S'(N)=
L'(N))"
40327 PRINT"TYPE 5 FOR FORSYTHE'S TYPE (S'''(0)=L'''(0) &
S'''(N)=L'''(N))"
40328 PRINT"TYPE 6 FOR IAN'S TYPE (S''(0)=L''(0) & S''(N)
=L''(N))"
40330 INPUT"TYPE NUMBER=";EC
40335 IFEC=6THEN40602
40340 IFEC=5THEN40602
40350 IFEC=4THEN40415
40360 IFEC=3THEN40400
40370 IFEC=2THEN40390
40380 AA(0)=1:C(0)=0:E(0)=0
```

```
40381 AA(N)=1:A(N)=Ø:E(N)=Ø
40382 IFFT=4THEN40387
40384 E(Ø)=Z*Z*Y(Ø)
40386 E(N)=Z*Z*Y(N)
40387 GOTO40999
40390 AA(Ø)=1:C(Ø)=-1:E(Ø)=Ø
40391 AA(N)=1:A(N)=-1:E(N)=Ø
40392 IFFT=4THEN40397
40394 E(Ø)=Z*Z*(Y(Ø)-Y(1))
40396 E(N)=Z*Z*(Y(N)-Y(N-1))
40397 GOTO40999
40400 INPUT"CONSTANT(Ø<=C<=1) =";C
40403 AA(Ø)=1:C(Ø)=-C:E(Ø)=Ø
40404 AA(N)=1:A(N)=-C:E(Ø)=Ø
40405 IFFT=4THEN40411
40406 E(Ø)=Z*Z*(Y(Ø)-C*Y(1))
40408 E(N)=Z*Z*(Y(N)-C*Y(N-1))
40411 GOTO40999
40415 INPUT"LINEAR,QUADRATIC OR CUBIC SLOPE APPROX? (L/Q/
C)";S$
40421 IFS$="Q"THEN40500
40422 IFS$="C"THEN40600
40425 G1=(Y(1)-Y(Ø))/(X(1)-X(Ø))
40426 GN=(Y(N)-Y(N-1))/(X(N)-X(N-1)):GOTO40800
40500 INPUT"ANALYTIC,EULER OR COMPOUND EULER SLOPE REQD.
(A/E/C)";R$
40502 DIMLA(2),LY(2)
40505 MM=Ø:FORJ=ØTONSTEPN
40510 IFJ=NTHENMM=N-2
40515 FORI=ØTO2:LX(I)=X(I+MM):LY(I)=Y(I+MM):NEXTI
40520 AØ=LY(Ø)/((LX(Ø)-LX(1))*(LX(Ø)-LX(2)))
40525 A1=LY(1)/((LX(1)-LX(Ø))*(LX(1)-LX(2)))
40530 A2=LY(2)/((LX(2)-LX(Ø))*(LX(2)-LX(1)))
40536 A=AØ+A1+A2
40537 IFEC=4THEN40540
40538 IFJ=ØTHENB1=A
40539 GOTO40770
40540 BØ=AØ*(LX(1)+LX(2))
40545 B1=A1*(LX(Ø)+LX(2))
40550 B2=A2*(LX(Ø)+LX(1))
40556 B=BØ+B1+B2
40560 CØ=AØ*LX(1)*LX(2)
40565 C1=A1*LX(Ø)*LX(2)
40570 C2=A2*LX(Ø)*LX(1)
40576 C=CØ+C1+C2
40578 IFR$<>"A"THEN40584
40579 GN=2*X(J)*A-B
40580 IFJ=NTHEN40770
40581 G1=GN
40582 GOTO40770
40584 IFJ=ØTHENGX=LX(Ø)-(LX(1)-LX(Ø))
40585 IFJ=NTHENGX=LX(2)+(LX(2)-LX(1))
40586 GY=A*GX*GX-B*GX+C
40587 IFR$="C"THEN40591
40588 IFJ=ØTHENG1=(LY(1)-GY)/(LX(1)-GX)
40589 IFJ=NTHENGN=(GY-LY(1))/(GX-LX(1))
40590 GOTO40770
```

```
40591 IFJ=ØTHENG1=((LY(Ø)-GY)/(LX(Ø)-GX)+(LY(1)-LY(Ø))/(L
X(1)-LX(Ø)))/2
40592 IFJ=NTHENGN=((GY-LY(2))/(GX-LX(2))+(LY(2)-LY(1))/(L
X(2)-LX(1)))/2
40593 GOTO4077Ø
40600 INPUT"ANALYTIC,EULER OR COMPOUND EULER SLOPE REQD.
(A/E/C)";R$
40602 DIMLA(3),LY(3)
40605 MM=Ø:FORJ=ØTONSTEPN
40610 IFJ=NTHENMM=N-3
40615 FORI=ØTO3:LX(I)=X(I+MM):LY(I)=Y(I+MM):NEXTI
40620 AØ=LY(Ø)/((LX(Ø)-LX(1))*(LX(Ø)-LX(2))*(LX(Ø)-LX(3))
)
40625 A1=LY(1)/((LX(1)-LX(Ø))*(LX(1)-LX(2))*(LX(1)-LX(3))
)
40630 A2=LY(2)/((LX(2)-LX(Ø))*(LX(2)-LX(1))*(LX(2)-LX(3))
)
40635 A3=LY(3)/((LX(3)-LX(Ø))*(LX(3)-LX(1))*(LX(3)-LX(2))
)
40636 A=AØ+A1+A2+A3
40638 IFJ=ØTHENAZ=A
40639 IFEC=5THEN4077Ø
40640 BØ=AØ*(LX(1)+LX(2)+LX(3))
40645 B1=A1*(LX(Ø)+LX(2)+LX(3))
40650 B2=A2*(LX(Ø)+LX(1)+LX(3))
40655 B3=A3*(LX(Ø)+LX(1)+LX(2))
40656 B=BØ+B1+B2+B3
40658 IFJ=ØTHENBZ=B
40659 IFEC=6THEN4077Ø
40660 CØ=AØ*(LX(1)*LX(2)+LX(2)*LX(3)+LX(1)*LX(3))
40665 C1=A1*(LX(Ø)*LX(2)+LX(2)*LX(3)+LX(Ø)*LX(3))
40670 C2=A2*(LX(Ø)*LX(1)+LX(1)*LX(3)+LX(Ø)*LX(3))
40675 C3=A3*(LX(Ø)*LX(1)+LX(1)*LX(2)+LX(Ø)*LX(2))
40676 C=CØ+C1+C2+C3
40678 IFR$<>"A"THEN407ØØ
40680 GN=3*X(J)*X(J)*A-2*X(J)*B+C
40685 IFJ=NTHEN4077Ø
40690 G1=GN
40695 GOTO4077Ø
40700 DØ=LX(1)*LX(2)*LX(3)*AØ
40705 D1=LX(Ø)*LX(2)*LX(3)*A1
40710 D2=LX(Ø)*LX(1)*LX(3)*A2
40715 D3=LX(Ø)*LX(1)*LX(2)*A3
40720 D=DØ+D1+D2+D3
40725 IFJ=ØTHENGX=LX(Ø)-(LX(1)-LX(Ø))
40730 IFJ=NTHENGX=LX(3)+(LX(3)-LX(2))
40735 GY=A*GX*GX*GX-B*GX*GX+C*GX-D
40740 IFR$="C"THEN4075Ø
40745 IFJ=ØTHENG1=(LY(1)-GY)/(LX(1)-GX)
40746 IFJ=NTHENGN=(GY-LY(2))/(GX-LX(2))
40748 GOTO4077Ø
40750 IFJ=ØTHENG1=((LY(Ø)-GY)/(LX(Ø)-GX)+(LY(1)-LY(Ø))/(L
X(1)-LX(Ø)))/2
40755 IFJ=NTHENGN=((GY-LY(3))/(GX-LX(3))+(LY(3)-LY(2))/(L
X(3)-LX(2)))/2
40760 GOTO4077Ø
40770 NEXTJ
```

```
40775  IFFT=5THEN40855
40779  IFEC=6THEN40845
40780  IFEC=4THEN40800
40782  AA(Ø)=-1:C(Ø)=1:E(Ø)=6*AZ*H(Ø)
40784  AA(N)=1:A(N)=-1:E(N)=6*A*H(N-1)
40786  GOTO40999
40800  AA(Ø)=H(Ø)/3:C(Ø)=H(Ø)/6:E(Ø)=(Y(1)-Y(Ø))/H(Ø)-G1
40820  AA(N)=H(N-1)/3:A(N)=H(N-1)/6
40830  E(N)=GN-(Y(N)-Y(N-1))/H(N-1)
40840  GOTO40999
40845  AA(Ø)=H(Ø)/6-1:C(Ø)=-H(Ø)/6:E(Ø)=6*X(Ø)*AZ-2*BZ
40846  AA(N)=1-H(N-1)/6:A(N)=H(N-1)/6:E(N)=6*X(N)*A-2*B
40848  GOTO40999
40850  IFEC=6THEN40890
40855  IFEC=4THEN40880
40860  AA(Ø)=-1:C(Ø)=1:E(Ø)=Z*Z*(Y(1)-Y(Ø))+6*AZ*H(Ø)
40865  AA(N)=1:A(N)=-1:E(N)=Z*Z*(Y(N)-Y(N-1))+6*A*H(N-1)
40870  GOTO40999
40880  AA(Ø)=H(Ø)/3:C(Ø)=H(Ø)/6
40882  E(Ø)=(Y(1)-Y(O))/H(Ø)-G1+Z*Z*H(Ø)*(Y(Ø)/3+Y(1)/6)
40885  AA(N)=H(N-1)/3:A(N)=H(N-1)/6
40886  E(N)=GN-(Y(N)-Y(N-1))/H(N-1)+Z*Z*H(N-1)*(Y(N)/3+Y(N
-1)/6)
40888  GOTO40999
40890  AA(Ø)=H(Ø)/6-1:C(Ø)=-H(Ø)/6
40891  E(Ø)=6*X(Ø)*AZ-2*BZ+Z*Z*H(Ø)*(Y(Ø)-Y(1))/6-Z*Z*Y(Ø)
40892  AA(N)=1-H(N-1)/6:A(N)=H(N-1)/6
40893  E(N)=6*X(N)*A-2*B+Z*Z*H(N-1)*(Y(N-1)-Y(N))/6+Z*Z*Y(
N)
40999  RETURN
41000  REM TENSION SPLINE
41001  REM **************
41010  IFD$="F"THENGOSUB9000
41011  IFD$="D"THENGOSUB8000
41015  INPUT"TENSION PARAMETER,Z =";Z
41020  DIMAA(N),E(N),S2(N),H(N),A(N),C(N)
41030  FORI=ØTON-1:H(I)=X(I+1)-X(I):NEXT
41040  GOSUB40300
41050  FORI=1TON-1
41060  TS=Z*(EXP(Z*H(I-1))+EXP(-Z*H(I-1)))/(EXP(Z*H(I-1))-
EXP(-Z*H(I-1)))
41061  TS=TS-1/H(I-1)
41062  TS=TS+Z*(EXP(Z*H(I))+EXP(-Z*H(I)))/(EXP(Z*H(I))-EXP
(-Z*H(I)))
41063  AA(I)=(TS-1/H(I))/Z/Z
41070  C(I)=-(Z*2/(EXP(Z*H(I))-EXP(-Z*H(I)))-1/H(I))/Z/Z
41071  A(I)=-(Z*2/(EXP(Z*H(I-1))-EXP(-Z*H(I-1)))-1/H(I-1))
/Z/Z
41075  AA(I)=AA(I)-C(I-1)*A(I)/AA(I-1)
41085  E(I)=Y(I+1)/H(I)-Y(I)/H(I)-Y(I)/H(I-1)+Y(I-1)/H(I-1
)-E(I-1)*A(I)/AA(I-1)
41090  NEXTI
41100  S2(N)=E(N)/AA(N)
41110  FORI=N-1TOØSTEP-1
41120  S2(I)=(E(I)-C(I)*S2(I+1))/AA(I)
41130  NEXTI
41140  GOSUB9200
```

```
41150 DIMP(OO)
41155 FORL=ØTOOO:GOSUB40200
41160 P=S2(K)*(EXP(Z*(X(K+1)-XX(L)))-EXP(-Z*(X(K+1)-XX(L)
)))
41170 P=P+S2(K+1)*(EXP(Z*(XX(L)-X(K)))-EXP(-Z*(XX(L)-X(K)
)))
41180 P=P/(Z*Z*(EXP(Z*H(K))-EXP(-Z*H(K))))
41185 PP=(Y(K)-S2(K)/Z/Z)*(X(K+1)-XX(L))+(Y(K+1)-S2(K+1)/
Z/Z)*(XX(L)-X(K))
41186 P(L)=P+PP/H(K)
41190 NEXTL
41200 RETURN
42000 REM QUADRATIC SPLINE
42001 REM ****************
42003 IFD$="F"THENGOSUB9000
42004 IFD$="D"THENGOSUB8000
42005 DIMS1(N)
42010 PRINT:PRINT"   END CONDITION AT R.H.S MAY BE ....."
42012 PRINT"     1...LINEAR SLOPE "
42013 PRINT"     2... S' = LAGRANGIAN QUADRATIC SLOPE
   (L')"
42014 PRINT"     3...S'' = LAGRANGIAN QUADRATIC 2ND
   DERIVATIVE (L'')"
42016 INPUT"TYPE OF END CONDITION=";EC
42018 IFEC=1THEN42029
42019 A3=Y(N)/(X(N)-X(N-2))/(X(N)-X(N-1))
42020 A2=Y(N-1)/(X(N-1)-X(N-2))/(X(N-1)-X(N))
42021 A1=Y(N-2)/(X(N-2)-X(N-1))/(X(N-2)-X(N))
42022 A=A1+A2+A3:B=A1*(X(N)+X(N-1))+A2*(X(N)+X(N-2))+A3*(
X(N-1)+X(N-2))
42024 IFEC=2THEN42027
42025 S1(N)=A*(X(N)-X(N-1))+(Y(N)-Y(N-1))/(X(N)-X(N-1)):G
OTO42030
42027 S1(N)=2*A*X(N)-B:GOTO42030
42029 S1(N)=(Y(N)-Y(N-1))/(X(N)-X(N-1))
42030 FORI=N-1TOØSTEP-1
42040 S1(I)=2*(Y(I+1)-Y(I))/(X(I+1)-X(I))-S1(I+1)
42050 NEXT
42060 GOSUB9200
42070 DIMP(OO)
42080 FORL=ØTOOO
42090 GOSUB40200
42100 P(L)=S1(K+1)/(X(K+1)-X(K))*(XX(L)-X(K))^2
42102 P(L)=(P(L)+(S1(K)*(XX(L)-X(K+1))^2)/(X(K)-X(K+1))+S
1(K)*(X(K+1)-X(K)))/2
42105 P(L)=P(L)+Y(K)
42110 NEXTL:SL=S(K)
42120 RETURN
43000 REM PIECEWISE LINEAR
43001 REM ***************
43003 IFD$="F"THENGOSUB9000
43004 IFD$="D"THENGOSUB8000
43020 GOSUB9200
43030 DIMP(OO)
43040 FORL=ØTOOO:GOSUB40200
43050 P(L)=(Y(K+1)*(XX(L)-X(K))-Y(K)*(XX(L)-X(K+1)))/(X(K
+1)-X(K))
```

```
43060 NEXT:SL=(Y(K+1)-Y(K))/(X(K+1)-X(K)):REM SLOPE
43070 RETURN
50000 REM STINEMAN INTERPOLATION
50001 REM ***********************
50010 IFD$="F"THENGOSUB9000
50015 IFD$="D"THENGOSUB8000
50020 DIM C(N)
50040 Z=Y(1)-Y(0):X=X(1)-X(0):FORJ=1TON-1:Y=Z:Z=Y(J+1)-Y(
J):W=X:X=X(J+1)-X(J)
50050 U=X*X+Z*Z:V=W*W+Y*Y:C(J)=(Y*U+Z*V)/(W*U+X*V):NEXT
50060 U=(Y(1)-Y(0))/(X(1)-X(0)):V=(Y(N)-Y(N-1))/(X(N)-X(N
-1))
50070 IFU=0ANDC(1)=0THENC(0)=0:GOTO50100
50080 IF(U>0ANDU>C(1))OR(U<0ANDU<C(1))THENC(0)=U+U-C(1):G
OTO50100
50090 C(0)=C(1)+ABS(U)*(U-C(1))/(ABS(U)+ABS(U-C(1)))
50100 IFV=0ANDC(N-1)=0THENC(N)=0:GOTO50115
50110 C(N)=C(N-1)+ABS(V)*(V-C(N-1))/(ABS(V)+ABS(V-C(N-1))
)
50115 GOSUB9200
50117 DIMP(OO)
50120 FORL=0TOOO
50122 GOSUB40200
50130 UU=(Y(K+1)-Y(K))/(X(K+1)-X(K)):V=Y(K)+UU*(XX(L)-X(K
))
50140 Z0=Y(K)+C(K)*(XX(L)-X(K))-V:Z1=Y(K+1)+C(K+1)*(XX(L)
-X(K+1))-V:Z2=Z0*Z1
50150 IFZ2=0THENP(L)=V:GOTO50180
50160 IFZ2>0THENP(L)=V+Z0*Z1/(Z0+Z1):GOTO50180
50170 P(L)=V+Z2*(XX(L)-X(K)+XX(L)-X(K+1))/((Z0-Z1)*(X(K+1
)-X(K)))
50180 NEXT:SL=UU
50190 RETURN
60000 REM BEZIER BLENDING
60001 REM ***************
60010 IFD$="F"THENGOSUB9000
60015 IFD$="D"THENGOSUB8000
60020 GOSUB9200
60022 DIMU(OO),P(OO)
60025 FORJ=0TOOO
60028 U(J)=J/OO:XSUM=0:YSUM=0:T=0
60030 FORI=0TON
60035 IFI=0THEN60046
60040 K=N:GOSUB60200:T=F
60042 K=I:GOSUB60200:T=T/F
60044 K=N-I:GOSUB60200:T=T/F:GOTO60050
60046 T=1
60050 T=T*U(J)^I*(1-U(J))^(N-I)
60060 XSUM=XSUM+T*X(I):YSUM=YSUM+T*Y(I)
60070 NEXTI
60075 IFJ<>0THEN60080
60076 XSUM=X(0):YSUM=Y(0)
60080 XX(J)=XSUM:P(J)=YSUM:NEXTJ
60090 RETURN
60200 REM FACTORIALS
60210 F=1:FORG=1TOK:F=F*G:NEXT
60220 RETURN
```

```
2 DOPEN#1,"BKGBLURB",D1,W
3 DOPEN#10,"BKGDAT10",D1,W
4 DOPEN#11,"BKGDAT11",D1,W
5 PRINT#1
6 PRINT#10
7 PRINT#11
8 DCLOSE#10:DCLOSE#11:DCLOSE#1
9 INPUT"NUMBER OF PROGRAMS....1...OR...2";NP
10 INPUT"FIRST PROGRAM NUMBER=";P1
15 INPUT"NUMBER IN FIRST SAMPLE=";S1
17 INPUT"NUMBEROF REPEAT COUNTS/VIAL";R1
20 INPUT"NUMBER OF CYCLES OF FIRST SAMPLE=";C1
25 IF NP=1THEN55
30 INPUT"SECOND PROGRAM NUMBER=";P2
35 INPUT"NUMBER IN SECOND SAMPLE=";S2
36 INPUT"NUMBEROF REPEAT COUNTS/VIAL";R2
40 INPUT"NUMBER OF CYCLES OF SECOND SAMPLE=";C2
55 OPEN1,5:PRINT#1,CHR$(255);"FE2GA":CLOSE1
56 OPEN2,6
57 APPEND#10,"BKGDAT10",D1
58 APPEND#11,"BKGDAT11",D1
59 IFNP=1THEN70
60 D=C1-C2
63 IFD<0THEN65
64 CC=C2:GOTO70
65 CC=C1
70 FORC=1TOC1
75 GOSUB7000
110 IF NP=1THEN GOTO310
150 GOSUB8000
310 NEXTC
315 IF NP=1THEN330
318 IFD=0THEN330
320 FOR G=1TOABS(D)
325 IFCC=C1THEN GOSUB8000
328 IFCC=C2THEN GOSUB7000
329 NEXT G
330 DCLOSE#10:DCLOSE#11
350 PRINT"DONE"
400 END
1000 GET#2,A$:IFST=2THEN1000
1010 RETURN
2000 IF MARK=1THEN2010
2005 PRINT#10,VAL(X$)
2007 GOTO2020
2010 PRINT#11,VAL(X$)
2020 RETURN
3000 APPEND#1,"BKGBLURB",D1
3001 REM ROLLING STRING LOOKS FOR "PROG" TO IDENTIFY A PR
OGRAM START
3003 AA$="":Z$=""
3005 FORI=1TO4:GOSUB1000
```

```
3006 AA$=AA$+A$:NEXTI
3007 IFAA$="PROG"THEN3019
3010 GOSUB1000:AA$=AA$+A$
3012 AA$=RIGHT$(AA$,4):GOTO3007
3018 REM Z$ LOOKS FOR CORRECT PROGRAM NUMBER
3019 FORI=1TO10:GOSUB1000
3020 Z$=Z$+A$:NEXTI
3021 IF VAL(RIGHT$(Z$,2))=P1THEN3100
3024 GOTO3003
3100 PRINT#1,AA$+Z$
3115 FORI=1TO5:GOSUB1000:NEXTI
3116 FORI=1TO68:GOSUB1000:PRINT#1,A$;
3118 NEXTI:PRINT#1
3120 FORI=1TO5:GOSUB1000:NEXTI
3122 FORI=1TO68:GOSUB1000:PRINT#1,A$;
3130 NEXTI:PRINT#1
3135 FORI=1TO5:GOSUB1000:NEXTI
3140 FORI=1TO68:GOSUB1000:PRINT#1,A$;
3141 NEXTI:PRINT#1
3143 FORI=1TO5:GOSUB1000:NEXTI
3145 FORI=1TO47:GOSUB1000:PRINT#1,A$;
3148 NEXTI:PRINT#1
3150 FORI=1TO4:GOSUB1000:NEXTI
3155 FORI=1TO76:GOSUB1000:PRINT#1,A$;
3158 NEXTI:PRINT#1
3160 FORI=1TO11:GOSUB1000:NEXTI
3170 DCLOSE#1
3205 RETURN
4000 P$="":S$="":CT$="":CA$="":IA$=""
4002 CB$="":IB$="":CC$="":IC$="":QIP$=""
4004 SC$="":RT$=""
4006 GOSUB1000
4008 IFASC(A$)=18THEN4012
4010 GOTO4006
4012 GOSUB1000
4016 FORI=1TO2
4018 GOSUB1000:P$=P$+A$
4020 NEXTI:X$=P$
4024 FORI=1TO5
4026 GOSUB1000:S$=S$+A$
4028 NEXTI:X$=S$
4032 FORI=1TO7
4034 GOSUB1000:CT$=CT$+A$
4036 NEXTI:X$=CT$
4038 GOSUB2000
4040 FORI=1TO8
4042 GOSUB1000:CA$=CA$+A$
4044 NEXTI:X$=CA$:GOSUB2000
4046 FORI=1TO5
4048 GOSUB1000:IA$=IA$+A$
4050 NEXTI:X$=IA$
4052 FORI=1TO8
4054 GOSUB1000:CB$=CB$+A$
4056 NEXTI:X$=CB$:GOSUB2000
4058 FORI=1TO5
4060 GOSUB1000:IB$=IB$+A$
4062 NEXTI
4064 FORI=1TO8
```

```
4066 GOSUB1000:CC$=CC$+A$
4068 NEXTI:X$=CC$:GOSUB2000
4070 FORI=1TO5
4072 GOSUB1000:IC$=IC$+A$
4074 NEXTI
4076 FORI=1TO6
4078 GOSUB1000:QIP$=QIP$+A$
4080 NEXTI:X$=QIP$
4082 GOSUB2000
4084 FORI=1TO7:GOSUB1000
4086 NEXTI
4088 FORI=1TO7
4090 GOSUB1000:SC$=SC$+A$
4092 NEXTI:X$=SC$
4096 FORI=1TO5
4098 GOSUB1000:RT$=RT$+A$
4100 NEXTI:X$=RT$
4106 FORI=1TO6
4108 GOSUB1000
4110 NEXTI
4150 RETURN
6000 AA$="":Z$=""
6005 FORI=1TO4:GOSUB1000
6006 AA$=AA$+A$:NEXTI
6007 IFAA$="PROG"THEN6019
6009 GOSUB1000:AA$=AA$+A$
6011 AA$=RIGHT$(AA$,4):GOTO6007
6019 FORI=1TO10:GOSUB1000
6020 Z$=Z$+A$:NEXTI
6021 IF VAL(RIGHT$(Z$,2))=P1THEN6100
6025 IF VAL(RIGHT$(Z$,2))=P2THEN6100
6034 GOTO6000
6100 RETURN
7000 MARK=0
7010 IFC>1THEN7040
7020 GOSUB3000
7030 GOTO 7060
7040 GOSUB6000
7060 FORS=1TOS1
7062 IFR1=1THEN7070
7064 FORR=1TOR1
7066 GOSUB4000:PRINT#10
7067 NEXT
7068 GOSUB9000:GOTO7090
7070 GOSUB4000
7080 PRINT#10
7090 NEXTS
7100 RETURN
8000 MARK=1
8010 IFC>1THEN8040
8020 GOSUB3000
8030 GOTO8060
8040 GOSUB6000
8060 FOR SS=1TOS2
8062 IFR1=1THEN8070
8064 FORR=1TOR1
8066 GOSUB4000:PRINT#11
8067 NEXT
```

```
8068  GOSUB9000:GOTO8090
8070  GOSUB4000
8080  PRINT#11
8090  NEXTSS
8100  RETURN
9000  FORI=1TO81
9010  GOSUB1000
9020  NEXT
9030  RETURN
```

Abstract

QUENCH CORRECTION IN LIQUID SCINTILLATION COUNTING

I. Lilley

Quench correction in liquid scintillation counting has been
investigated. A detailed comparison of the curve fitting
routines compatible with a microcomputer has been made for
the quench calibration curve and concludes that a cubic
spline with natural end conditions is most suitable.   The
effect of colour/chemical quenching on the calibration
curve and the choice of regions for dual and triple radio-
nuclide counting is studied.

A new computer simulation of the LS counter has been
created and proven to be a useful tool in LS counting.
Modelling of the LSC has led to the invention of several
novel quench correction techniques which are independent of
colour and/or chemical quench for homogeneous solutions. A
fully worked example of the use of one of the techniques
(the SumDiff quench correction method) is presented. The
successful application and modular design of the simulation
has established a LS research program from which future
discoveries are anticipated.

A STUDY OF CURVE FITTING TO LIQUID SCINTILLATION COUNTER CALIBRATION DAT

J.N. CROOKES and I. LILLEY

Department of Physical Sciences, Trent Polytechnic, Clifton Lane, Nottingham, England

A comprehensive study is made of the various curve fitting procedures available for representing the calibration data used i dpm assay of LSC samples and compatible with the limited memory storage available in modern instruments. The output data the LSC are echoed to a microcomputer allowing the utilisation of user developed algorithms for data processing and analysis. evidence shows that the normal practice of the machine selecting a curve without choice by the user may not produce the best re In general the cubic spline interpolation with natural end conditions is found to give the best representation for standards invo errors of less than 1.5% for ^{3}H and ^{14}C. However, for ^{14}C and higher energy β-emitters there is strong evidence for the u Stineman interpolation.

A STUDY OF CURVE FITTING TO LIQUID SCINTILLATION COUNTER CALIBRATION DATA

J.N. CROOKES and I. LILLEY

Department of Physical Sciences, Trent Polytechnic, Clifton Lane, Nottingham, England

A comprehensive study is made of the various curve fitting procedures available for representing the calibration data used in th dpm assay of LSC samples and compatible with the limited memory storage available in modern instruments. The output data from the LSC are echoed to a microcomputer allowing the utilisation of user developed algorithms for data processing and analysis. Th evidence shows that the normal practice of the machine selecting a curve without choice by the user may not produce the best result In general the cubic spline interpolation with natural end conditions is found to give the best representation for standards involvin errors of less than 1.5% for ^{3}H and ^{14}C. However, for ^{14}C and higher energy β-emitters there is strong evidence for the use c Stineman interpolation.

1. Introduction

Modern liquid scintillation counters (LSCs) allow many useful functions, such as batch handling of samples, counting efficiency vs quench calibration and multilabelled radioassay, to be performed automatically. However, the advances in machine design which have led to the provision of such facilities tend to remove the user from the analysis of the basic data which are obtained and the results are presented as a fait accompli. The most important stage in the analysis of results is the generation of the standards' counting efficiency vs quench calibration curves from which the activity of subsequently counted samples can be calculated. This applies whichever parameter is used to indicate the degree of quench in a sample, whether it is based on internal or external standards, H$^\#$ numbers [1] or spectral indices [2], and whether the quenching is colour or chemical [3] in nature.

Since different curve fitting routines are better matched to some data sets than others, the fitting of curves through efficiency vs quench calibration data should be dependent on the form of the data set for best results. This availability of a choice of curve fitting routines is not provided on commercial liquid scintillation counters with manufacturers choosing one particular procedure, e.g. Packard use double fixed point least-squares quadratic interpolations and Beckman use cubic spline with natural end conditions. This is reasonable with the good and almost equispaced data provided by commercial calibration standards but the more frequently produced inhouse standards are often less regular.

There are a multitude of algorithms to which re-

course may be made in order to fit a curve to LS(efficiency vs quench calibration data. In this work restriction is made to those algorithms which could b installed in a modern stand-alone counter and/or dedi cated microcomputer operating in a real time mode.

2. Experimental

All samples were counted with a United Technolo gies Packard 300C model liquid scintillation counte and the data were stored on disk via a 3D GPIB, Serie 4000 CBM microcomputer and CBM 4022 disk drive Data were obtained on this equipment through use of BASIC program which recognised the number of th internal program commenced by the LSC and begar data capture on identification of the correct batch o samples. Disk storage of results allowed repeated use o data sets for comparison purposes.

Postcounting analysis was performed by a BASI(and 6502 machine code program offering a menu o curve fitting routines with screen plotting, screen dump and printed output. When fitting to experimenta calibration data the program allowed comparisons o the resulting assayed activities with samples of knowr dispensed activity. The types of curve fitting offered by the program are:
1) Lagrangian polynomial (using Newton's method) [4]
2) Piecewise linear (piecewise polynomials of degre $\geqslant 2$ unsuitable).
3) Quadratic splines (end conditions linear, spline slop = Lagrangian quadratic slope, or spline 2nd deriva tive = Lagrangian quadratic 2nd derivative).
4) Cubic splines (end conditions natural, parabolic

cantilever, Forsythe's, Swartz and Varga's, or spline 2nd derivative ≡ Lagrangian cubic 2nd derivative) [5,6].

5) Tension (cubic) spline.
6) Stineman interpolation [7].
7) Bezier blending.

Table 1
Comparison of calculated and dispensed DPM for ^{3}H single label

Sample No. [a]	QIP	Dispensed DPM	Piecewise linear DPM ± ΔDPM	Lst-squares °3 polynomial	Lst-squares °4 polynomial	Quadratic spline natural EC
A1	177	69691	58429 ± 2161	49439 ± 11394	71956 ± 12395	54789 ± 1891
A2	235	86294	83320 ± 1327	69691 ± 4694	85248 ± 3625	90245 ± 1340
A3	272	87006	83646 ± 1006	76781 ± 3727	84816 ± 2441	79972 ± 905
A4	593	96780	97470 ± 446	96304 ± 1150	95658 ± 713	95382 ± 713
A5	609	86128	87213 ± 423	85609 ± 1107	85598 ± 710	85237 ± 410
B1	130	78102	×	×	×	×
B2	235	86294	83320 ± 1327	73463 ± 6117	85164 ± 2952	86401 ± 1283
B3	272	87006	83646 ± 1006	76513 ± 4353	85029 ± 2061	83211 ± 942
B4	593	96780	96512 ± 442	96746 ± 1326	95809 ± 645	96628 ± 438
B5	655	82244	82249 ± 398	80882 ± 1093	81883 ± 589	81519 ± 392
C1	269	89800	83197 ± 1644	81376 ± 1583	67638 ± 6378	77712 ± 1429
C2	534	99801	99127 ± 518	98534 ± 505	101374 ± 1402	97193 ± 495
C3	562	80162	80645 ± 453	80244 ± 462	82363 ± 1201	79208 ± 437
C4	622	102579	103317 ± 473	102627 ± 520	104015 ± 1421	103631 ± 469
C5	815	90829	91341 ± 376	91616 ± 429	89479 ± 979	91341 ± 375
D1	219	93827	100601 ± 3675	118035 ± 7356	×	83028 ± 2677
D2	256	85400	81874 ± 1805	82286 ± 2623	70185 ± 10648	93330 ± 1980
D3	534	99801	98789 ± 517	98465 ± 505	100766 ± 1696	99420 ± 506
D4	669	89202	89535 ± 409	88377 ± 401	88652 ± 1176	89844 ± 407
D5	865	82009	82304 ± 350	82445 ± 356	82257 ± 923	82304 ± 349

Quadratic spline L′ = S′	Cubic spline natural	Cubic spline parabolic	Cubic spline Swartz S′ = L′	Cubic spline Forsythe S‴ = L‴	Stineman
59526 ± 2054	65104 ± 2321	64343 ± 2304	64383 ± 2305	64448 ± 2306	63940 ± 2395
87628 ± 1301	84744 ± 1326	84775 ± 1326	84774 ± 1326	84771 ± 1326	84470 ± 1348
82118 ± 929	84798 ± 1013	84775 ± 1013	84777 ± 1013	84779 ± 1013	85099 ± 1026
96575 ± 437	96764 ± 443	96764 ± 443	96859 ± 444	96759 ± 443	96551 ± 442
86365 ± 415	86509 ± 420	86509 ± 420	86611 ± 421	86504 ± 420	86329 ± 419
×	×	×	×	×	×
88630 ± 1316	84888 ± 1325	84720 ± 1326	84687 ± 1327	84661 ± 1327	86401 ± 1283
81267 ± 920	84692 ± 1013	84816 ± 1013	84841 ± 1013	84860 ± 1013	83211 ± 941
96246 ± 436	96350 ± 442	96350 ± 442	96348 ± 442	96352 ± 442	96628 ± 438
82027 ± 395	81945 ± 397	81945 ± 397	81959 ± 397	81934 ± 397	81519 ± 392
79379 ± 1459	85168 ± 1646	84976 ± 1648	84978 ± 1647	84946 ± 1648	84758 ± 1679
97785 ± 495	98814 ± 517	98812 ± 518	98816 ± 517	98813 ± 517	98842 ± 516
79648 ± 439	80262 ± 451	80261 ± 451	80266 ± 451	80262 ± 451	80329 ± 451
103168 ± 467	102836 ± 473	102836 ± 473	102827 ± 473	102835 ± 473	102974 ± 472
90854 ± 373	90945 ± 375	90945 ± 375	90664 ± 374	90902 ± 375	91310 ± 376
86956 ± 2804	96188 ± 3359	90386 ± 3031	86769 ± 2856	89257 ± 2974	102119 ± 3743
90070 ± 1910	86294 ± 1884	87616 ± 1889	88554 ± 1896	87899 ± 1891	82644 ± 1823
99071 ± 505	98671 ± 516	98672 ± 516	98672 ± 516	98673 ± 516	98685 ± 516
89378 ± 405	89007 ± 407	89007 ± 407	88961 ± 407	88996 ± 407	88938 ± 406
82116 ± 349	82177 ± 350	82177 ± 350	82018 ± 349	82139 ± 350	82314 ± 350

[a] A and B groups are two chemically quenched calibration curves with different standards. C and D groups are two colour quenched calibration curves with different standards.

8) Linear least-squares polynomials of degree 2, 3, 4 or 5 [4].

Standards were prepared by accurately weighing out quantities of a 10 gl^{-1} solution of b-PBD in pXylene (Fisons "Scintran" grade), and quantities of CCl_4 or disperse Orange-7 as chemical and colour quenchers respectively. Weights were taken to ± 0.0002 g. All liquids and glassware were first purged of oxygen using a vacuum and freezing degassing technique. The dye was recrystallised from acetone and dried prior to dissolving in the same batch of b-PBD/pXylene solution used throughout the sample preparation.

3. Results and discussion

Tables 1 and 2 give the results for the standards and samples prepared experimentally. Those entries marked $\times$ were not computed because of the observed occurrence of grossly inaccurate results. Chemically quenched and colour quenched tritium standards and/or samples of known activity range from SIE of 865 down to an SIE of 130 corresponding to ^3H detection efficiencies of approximately 55% to 0.1%. The ^{14}C samples were taken only from the region of rapid change of the efficiency curve gradient and the region of very high quench, SIE < 500 (fig. 1). The calculation of the error bounds associated with each curve-generated dpm value is based on the errors in the count, the SIE and the dispensed DPM of the standards used for calibration curve production and the errors in the count and the SIE of the samples (of supposedly unknown activity). The experimental procedure used resulted in error bounds of $\pm 0.06\%$ and $\pm 0.02\%$ for the dispensed DPMs of ^3H and ^{14}C respectively with the manufacturers' absolute uncertainties of $\pm 3\%$ and $\pm 1.5\%$ being con-
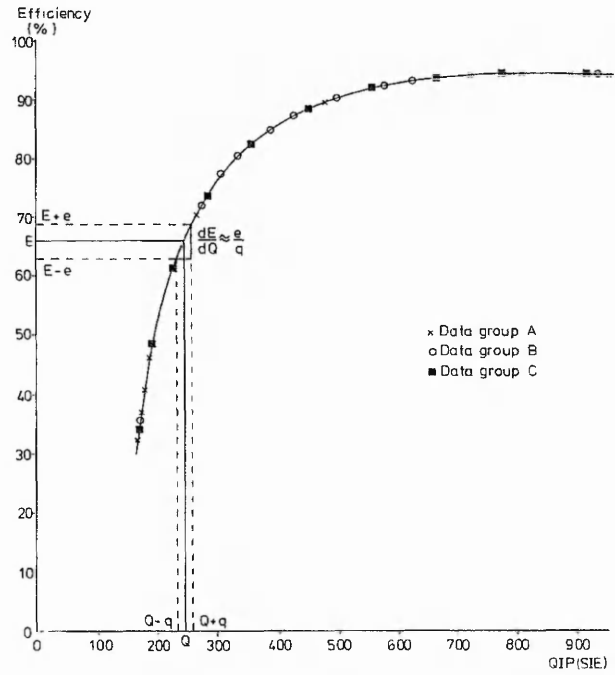
Fig. 1. Typical ^{14}C efficiency vs QIP curve showing data group types.

stant throughout the samples. Coupled with these is the error due to the counting statistics with the percent deviation automatically calculated and printed by the Packard 300C. The SIE values were assumed to be correct to the nearest integer value (error range of ± 0.5, and letting $3\sigma = 100\%$ of range then $\sigma \simeq 0.17$ for SIE number probability constant from $X - 0.5$ to $X + 0.5$), but the effect of this error on the efficiency value is dependent on the slope/form of the calibration curve. The efficiency error $e \simeq q\, dE/dQ$, where q is the error

Table 2

Comparison of calculated and dispensed DPM for ^{14}C single label

Sample no.	QIP	Dispensed DPM	Piecewise linear	Least-squares 3° polynomial	Least-squares 4° polynomial	Quadratic spline natural
1	175	120543	121240 ± 786	129332 ± 10168	131056 ± 7801	120771 ± 513
2	329	96384	97406 ± 321	93724 ± 3410	93999 ± 2500	95843 ± 312
3	426	75413	75747 ± 268	75147 ± 2772	71638 ± 1911	75549 ± 267

Quadratic spline $L' = S'$	Cubic spline natural	Cubic spline parabolic	Cubic spline Swartz	Cubic spline Forsythe	Stineman
120791 ± 513	119705 ± 916	119454 ± 893	120026 ± 887	120080 ± 882	120477 ± 779
95797 ± 312	96294 ± 321	96236 ± 322	96219 ± 322	96206 ± 322	46228 ± 317
25585 ± 267	75342 ± 268	75356 ± 268	75360 ± 268	75362 ± 268	75449 ± 267

Table 3
Summary of errors for ^{3}H and ^{14}C for curve fitting routines

	Piecewise linear	Least squares 3° polynomial	Quadratic spline	Quadratic spline	Cubic spline	Cubic spline	Cubic spline	Cubic spline	Stineman
End conditions			Natural	$L' = S'$	Natural	Parabolic	Swartz	Forsythe	
^{3}H mean error [%]	2.95	8.10	4.37	3.21	1.48	1.70	1.96	1.77	2.11
^{14}C mean error [%]	0.69	5.41	0.30	0.34	0.30	0.25	0.23	0.22	0.08
Mean of ^{3}H and ^{14}C	1.82	6.76	2.34	1.78	0.89	0.97	1.10	1.00	1.10

in the SIE value and dE/dQ is the rate of change of efficiency with respect to SIE at an SIE value of Q (fig. 1). These errors are all combined using the expression:

Fractional dpm$_{unknown}$ error,

$$d_u = \left\{ \left(\frac{\%dev_{unk}}{100} \right)^2 + \left(\frac{\%dev_{stds}}{100} \right)^2 \right.$$
$$\left. + \left(\frac{\%DPM_{error}}{100} \right)^2 + 2 \times \frac{\%(SIE \times slope_{error})}{100} \right\}^{1/2}.$$

The listed values of average percentage differences refer to the differences between the dispensed dpms and calculated dpms.

Selection of the best curve fitting routine for LSC efficiency vs quench calibration data depends on the judgement criteria used. For example, if the resultant curve is to be smooth (with continuous first derivatives) then piecewise linear fitting is ruled out. Calibration curves are normally based on ten reasonably well spaced standards, and so the results of the routines presented in tables 1 and 2 are taken to be suitable judgement criteria.

4. Conclusion

It may be concluded that cubic spline interpolation with natural end conditions is the best of the LSC efficiency vs quench curve fitting routines tested, but also noted that cubic splines with Forsythe's or parabolic end conditions and Stineman interpolation give good results for tritium and carbon-14 efficiency curves respectively. This assertion follows from the rankings of the routines (see table 3). Indeed, Stineman interpolation has an additional advantage of being more robust

and better at fitting curves with sharply changing gradients, i.e. ^{14}C and more energetic β-sources.

Not all the routines tested are displayed in tables 1 and 2 due to their total inadequacy. For example, the Lagrangian polynomial produced large oscillations due to the experimental errors in the standards.

The currently used LSC machine routines are therefore found to be acceptable, but it should be emphasised that if calibration standards are poorly spaced then curve fitting by interpolation introduces large errors (even with perfect standards) and visual display of the resultant calibration curve is essential unless some mechanism for rejecting the fit is triggered. This may be accomplished by setting a data spacing tolerance limit or switching to a generally less accurate but more universally applicable least-squares fitting routine as a backup.

References

[1] D.L. Horrocks, Liquid Scintillation Science and Technology, eds., A.A. Noujaim et al. (Academic Press, New York, 1976).
[2] J.G. Ring, D.C. Nguyen and L.J. Everett, Liquid Scintillation Counting, Recent Applications and Development, vol. 1, eds., C.T. Peng et al. (Academic Press, New York, 1980).
[3] S.A. McQuarrie, C. Edisse and L.I. Wiebe, Int. J. Appl. Radiat. Isot. 34 (1983) 1009.
[4] J.S. Vandergraft, Introduction to numerical computations, 2nd ed. (Academic Press, New York, 1983).
[5] P.M. Prenter, Splines and variational methods (Wiley, New York, 1975).
[6] J.H. Ferziger, Numerical methods for engineering application (Wiley, New York, 1981).
[7] R.W. Stineman, Creative Computing (1980) 54.

Detection of Drift in Radioactive Counting Using the Cusum Technique

J. N. CROOKES and I. LILLEY

Physical Science Department, Trent Polytechnic, Clifton, Nottingham NG11 8NS, England

A comparison of the cusum method and kurtosis as the indicator of drift in radioactive counting is made.

Modern programmable counters are tested and interesting features are observed with alternate counting of different radionuclides. Patterns of repeated counts suggest that an initial "settling" period is advisable following a change of radionuclide.

Introduction

The characteristics of a scintillation counter are critically dependent on the stability of the counting conditions. Instabilities in the system produce a drift in the counting efficiency.[1] Such changes are often associated with drift in the EHT supply due to temperature or mains fluctuations or deterioration of the sample in liquid scintillation counting. Unless remedial action is to be taken the source of the drift is not so important. However, it is essential to know the magnitude and time when any drift occurs. The literature shows very little work on the monitoring of counter performance[2,3] and this has used traditional indicators of change in a Poissonian distribution such as standard deviation, skew and kurtosis. Although producing confidence limits, typically 95%, these indicators have been shown to lack the sensitivity of other methods as well as producing no indication of the onset of drift. This work studies the detection of drift using a cusum method[4,5] and compares its scope and sensitivity with the traditional method.

Cusum Method

The cumulative sum chart (or cusum chart) is a highly informative means of presenting data that can be ordered into a logical sequence. A detailed exposition of the methodology is given in a British Standard Guide to data analysis and quality control using cusum techniques (BS 5703, parts, 1, 2, 3, 4). For observations $x_1, x_2, \ldots, x_n$ obtained sequentially having a target value, T, which may be the mean, $\bar{X}$, for retrospective analysis, the cusum is defined as

$$C_i = \sum_{r=1}^{i} (x_r - T).$$

A cusum chart displays C_i against i.

Where the observations are from a population having a mean equal to the target value the graph will generally be horizontal with random fluctuations about the line. A systematic fluctuation from the target value will result in a change in the slope of the chart.

An estimate of the local average in a particular segment is given by the slope of the cusum chart. Consider the segment from sample $i + 1$ to j. The relevant change in cusum is from C_i to C_j over i to j. (For the first segment $i = 0$ and $C_o = 0$). Hence the average shift from the target (mean) value for the segment is

$$\frac{C_j - C_i}{j - i}.$$

Thus the local average is

$$\bar{X}_{i+1,j} = T + \frac{C_j - C_i}{j - i}.$$

The application of the cusum method to the detection of drift in a parameter requires the establishment of decision rules to distinguish between real changes in the cusum slope and the normal variability of the data. The essential features of the cusum chart relevant to the detection of changes in the underlying average level are the steepness of the cusum slope and the number of samples over which the slope persists. When the parameter (e.g. count) is running at the target level, i.e. an acceptable quality level AQL, there will, because of the random nature of counting, inevitably be occasions when the cusum path apparently diverges from the horizontal. The decision rule should not give false alarms that indicate that such sequences represent significant departure from AQL. On the other hand, when the process moves to an unsatisfactory condition, i.e. a rejectable quality level, RQL, the decision rule should give as rapid a response as possible. The number of events between drift occurring and its detection by the cusum indicate the magnitude of the drift. If the true process is at or near the AQL, then this number should be large i.e. a few false alarms, whereas if it is near the RQL, then it should be short i.e. rapid detection.

Decision Interval Scheme

The method adopted in this study is entirely numerical in nature and hence readily computed. A reference level, K, for deviations from the mean is established where $K = T \pm f\sigma_e$ where

$$\sigma_e = \left(\sum_{i=1}^{m-1} \frac{(X_i - X_{i+1})^2}{2(m-1)} \right)^{1/2}$$

for m samples. If $f = 0.5$ then the reference level lies midway between AQL and RQL. Each count (x_i) is compared with K. If x_i is within the limits defined by K then no action is taken. However, if x_i lies outside the K limits, then a cusum is commenced of the algebraic differences from the appropriate K, i.e.

$$C = \sum_{i}^{j} (x_i - K)$$

where j represents the end point of the cusum determined by one of the following two conditions: (a) if C falls to below

Table 1. Results of drift experiments on Packard 300C liquid scintillation counter

Experiments Number		Kurtosis	Number of drifts detected with $h = 3$	h_{min}
1		2.98	0	2.1
2*	^{14}C	2.44	11	>10
	^{3}H	2.24	11	>10
3	^{14}C	3.00	7	9.5
	^{3}H	2.97	3	7.5

* 500 counts of each sample.

zero or (b) $C > H$ where $H = h\sigma_e$ is a decision level, typically $h = 5$. If (a) applies then no action is taken until $T - f\sigma_e > x_i > T > f\sigma_e$ again and a new cusum is commenced. If (b) applies then drift is deemed to have occurred, i representing the onset of the cusum but not necessarily the onset of drift, since allowance has to be made for statistical fluctuation, $j - i$ representing the number of samples from onset to detection.

In order to detect the onset and magnitude of drift, a value of $h = 3$ was fixed representing a value outside the spread of h_{min} derived from normal data sets and allowing for statistical fluctuations.

Instrument Tests

Experiments were conducted on three instruments, namely, the Nuclear Enterprises SR3 and Packard auto gamma counter with NaI crystals and the Packard 300C liquid scintillation counter. A PET microcomputer, connected on-line to each in turn, acquired 1000 counts for various counting configurations. For the gamma-detectors the counts across a ^{137}Cs photopeak at optimum EHT produced no detectable drift. The h_{min} values lie within the 95% confidence range for 1000 simulated data sets with no drift.

The tests on the liquid scintillation counter were rather more extensive and designed to assess the presence of drift (a) while counting a given radionuclide and (b) with alternations between two radionuclides. A single ^{14}C source was subjected to 1000 one minute counts with 43 s cycle time intervals between each count. The kurtosis was within the 95% confidence levels and an h_{min} value of 2.1 showed a very low degree of drift (Experiment 1, Table 1). Consequently, the instrument produced a high degree of stability for continuous counting of the same radionuclide.

To examine the effect of two radionuclides, single samples of ^{3}H and ^{14}C were counted alternately with the counting conditions varied appropriate to the radionuclide by the automatic programming of the counter. Although only 500 counts were taken for each sample in this case, considerable drift was detected by both the kurtosis and cusum tech-

niques (Experiment 2, Table 1). In order to investigate this effect further, rather than single counts of each radionuclide, 25 repeated counts of each i.e. 25 counts of ^{3}H followed by 25 counts of ^{14}C, was performed a total of 40 times. The results showed much less drift. Indeed for both radionuclides the kurtosis values were within the 95% confidence levels. However, the cusum technique demonstrated its better sensitivity and detected some drift for both samples (Exeriment 3, Table 1). Hence the test demonstrated that a "settling down" period following the changed programme settings between radionuclides to be desirable.

An analysis of the drifts indicated for $h = 3$ showed that the 10 drifts (7 for ^{14}C and 3 for ^{3}H) ranged from 0.14% per sample to 0.06%, although these readings are subject to quite large errors which are difficult to estimate.

Conclusion

The cusum technique when applied to radioisotope counting is both more sensitive and more informative than the use of kurtosis. A simple computer analysis with a decision level of $3\sigma_e$ determined from theoretical data produced a statement of the instrument behaviour. From the experiments performed using the Packard 300C liquid scintillation counter the stability during long counts of a particular isotope is better than the sensitivity of the cusum technique. However, using the parameters chosen above, drift occurred when alternate single counts of ^{3}H–^{14}C were made. When the samples were subject to repeated counts during each cycle drift was less severe.

References

1. Pazdur M. F. *Int. J. Appl. Radiat. Isot.* **27**, 179 (1976).
2. Galloway R. B. *Nucl. Instrum. Methods* **172**, 431 (1980).
3. Annand J. R. M. and Galloway R. B. *Nucl. Instrum. Methods* **201**, 381 (1982).
4. Ewan W. D. *Technometrics* **5**, 1 (1963).
5. Wetherill G. B. *Sampling Inspection and Quality Control.* (Chapman and Hall, London, 1977).